STRUCTURAL IDENTIFICATION AND VIBRATION-BASED DAMAGE DETECTION USING INTERVAL ARITHMETIC AND CONTRACTOR PROGRAMMING

by

Timothy Philip Kernicky

A dissertation submitted to the faculty of
The University of North Carolina at Charlotte
in partial fulfillment of the requirements
for the degree of Doctor of Philosophy in
Infrastructure and Environmental Systems

Charlotte

2018

Approved by:

_____
Dr. Matthew J. Whelan

_____
Dr. Ehab Al-Shaer

_____
Dr. David C. Weggel

_____
Dr. David T. Young

_____
Dr. Tara Cavalline

©2018
Timothy Philip Kernicky
ALL RIGHTS RESERVED

ABSTRACT

TIMOTHY PHILIP KERNICKY. Structural Identification and Vibration-Based Damage Detection Using Interval Arithmetic and Contractor Programming. (Under the direction of DR. MATTHEW J. WHELAN)

Structural identification continues to gain increased attention as an applied technique for structural health monitoring and condition assessment. However, methods for structural identification through finite element model updating that have been developed over the last several decades fail to completely address pertinent challenges including computational efficiency, solution uniqueness, and the ability to incorporate measurement and modeling uncertainties in parameter identification and confidence quantification. To address many of the difficulties of past model updating approaches, this dissertation explores using constraint satisfaction with interval arithmetic and contractor programming for vibration-based model updating to facilitate the advancement of structural identification as a viable tool for performance-based condition assessment. The work presented within develops, verifies, and validates methodologies for parameter identification of continuous and multiple degree-of-freedom system models using a novel interval-based approach capable of structuring partially described and incompletely measured inverse eigenvalue problems as nonlinear constraint satisfaction problems and propagating measurement uncertainties to the parameter space. A methodology based on the Set Inversion Via Interval Arithmetic algorithm is first developed for determining the internal axial force and boundary restraints within in-service prismatic beam elements, including short cables, struts, bracing, and tie-rods, where bending stiffness and boundary conditions significantly affect natural frequencies. The framework offers the ability to completely enclose the feasible solution space

for the unknown axial force and boundary restraints in prismatic beam and cable elements using a set of natural frequencies obtained from measurements of a single transducer with specified measurement uncertainties. The methodology is first demonstrated and verified on a numerical model and subsequently experimentally validated using dynamic measurements obtained from an axially loaded rod with progressively increased end restraint at one end. A second methodology is then developed for model updating of multiple degree-of-freedom system models that is based on formulating the structured inverse eigenvalue problem as a Constraint Satisfaction Problem. The approach of contractor programming with interval arithmetic is demonstrated to offer unique capabilities to fully enclose the feasible parameter space given specified measurement uncertainties as well as solve non-unique constructions of the inverse eigenvalue problem. These capabilities are first demonstrated and verified using synthetic data for a numerical six degree-of-freedom mass-spring model. The method is then experimentally validated using vibration measurements obtained from a laboratory shear building model and, furthermore, contrasted with probabilistic model updating to illustrate the unique capabilities of addressing the effects of measurement uncertainty on the parameter estimation. Subsequent extension of the methodology is then introduced to address challenges associated with scaling from small multiple degree-of-freedom models to much larger structures with significantly more uncertain parameters. Specifically, modifications to the methodology are developed to address the computational challenges resulting from the dramatic increase in dimensionality of the parameter space and the enforcement of eigenvalue inclusion constraints. The extended methodology is verified on a 45 degree-of-freedom, 45 member, 2D Pratt truss using partially described and incompletely measured modal properties acquired through hybrid testing. To demonstrate

the vibration-based damage detection capabilities of the methodology, realistic damage, in the form of fracture and crack propagation in the net section rupture limit state is progressively introduced to the experimental member in the hybrid simulations. Through a matrix of experimental validation tests, the methodology is shown to be successful at not only identifying the damaged members of the truss in the presence of measurement uncertainty, but also capable of correctly quantifying the severity of damage, which provides an important contribution to damage diagnosis and prognostication.

ACKNOWLEDGMENTS

Writing this short note of thanks does not even scratch the surface of the incomparable support I have received over the many years I have dedicated to the works contained within this dissertation.

First, I would like the gratefully thank my advisor Dr. Matthew Whelan. Over the past seven years, it has been an absolute pleasure studying under Dr. Whelan. I am overwhelmingly appreciative for the opportunities that he has afforded me. His patience, knowledge, and guidance have been nothing short of superlative. In addition to the detailed vision developed for the works contained within this dissertation, I am immensely grateful for the assistance provided in revising this document. Gratitude is also given to the rest of my committee for their valuable recommendations for strengthening this research.

Secondly, I want to thank my wife Ashley for standing by me and unselfishly supporting our young family throughout my studies. I am incredibly grateful for her love and understanding and for helping me get through many difficult times. I am also thankful for my two loving children Kai Julian and Ianna Mae who have given me the strength to push forward. I would also like to express my gratitude for the unequivocal support shown by the rest of my family.

Finally, I need to thank God who has gracefully orchestrated all of the events that have brought me to this point and for giving me the ability to undertake this endeavor.

TABLE OF CONTENTS

LIST OF FIGURES xiii

LIST OF TABLES xx

NOMENCLATURE xxii

CHAPTER 1: INTRODUCTION 1

1.1. Introduction 1

1.2. Overview of Research Effort 2

1.3. Expected Contribution 7

1.4. Dissertation Outline 9

CHAPTER 2: LITERATURE REVIEW 12

2.1. Structural Identification 12

2.2. Structural Identification Process 15

2.2.1. Establish Need for Application 15

2.2.2. Formulation of Initial FE Model 15

2.2.3. Experimental Regimen 17

2.2.4. Feature Extraction Through System Identification 19

2.2.5. Model Updating 21

2.2.6. Utilization of Results 21

2.3. Challenges in Structural Identification 22

2.3.1. Physical Knowledge Gap 22

2.3.2. Measurement Limitations 23

2.3.3. FE Model Updating Challenges 24

2.4. Model Updating Techniques 26

2.4.1. Heuristic Model Updating 29

2.4.2. Sensitivity-based Methods 30

2.4.3. Computational Intelligence Methods 34

2.4.4. Probabilistic Model Updating 42

2.4.5. Interval Methods 47

2.5. Concluding Remarks 52

CHAPTER 3: INTERVAL ANALYSIS AND CONSTRAINT PROGRAMMING 53

3.1. Introduction 53

3.2. Interval Analysis 54

3.2.1. Intervals 54

3.2.2. Interval Arithmetic 55

3.2.3. Set Operations 56

3.2.4. Interval Vectors 57

3.2.5. Interval Functions 58

3.2.6. Inclusion Functions 58

3.3. Set Characterization 61

3.3.1. Subpavings 61

3.4. Constraint Satisfaction Programming 62

3.4.1. Systematic Search 67

3.4.2. Arc Consistency 68

3.4.3. Hull Consistency 69

3.5. Contractor Programming 71

3.5.1. HC4 Contractor 72

3.5.2. Interval Hull 79

3.6. Structural Identification Using Nonlinear Constraint Satisfaction 80

3.6.1. Illustrative Example on a 3DOF Shear Building Model 82

3.7. Extensions to Different Systems Models and Structural Health Monitoring Applications 84

CHAPTER 4: DYNAMIC IDENTIFICATION OF AXIAL FORCE AND BOUNDARY RESTRAINTS IN TIE RODS AND CABLES WITH UNCERTAINTY QUANTIFICATION USING SET INVERSION VIA INTERVAL ANALYSIS 86

4.1. Introduction 87

4.2. Theoretical Basis and Formulation 91

4.3. Set Inversion Via Interval Analysis 96

4.3.1. Accounting for Measurement Uncertainty Using Interval Constraint Equations 102

4.3.2. Simple Illustrative Example of the Application of SIVIA 104

4.4. Methodology For Parameter Estimation With Uncertainty Quantification 107

4.4.1. Demonstration and Verification for Axial Force and Rotational Boundary Restraints 108

4.4.2. Demonstration and Verification for Axial Force and Translational and Rotational Boundary Restraints 113

4.5. Experimental Application of the Methodology 121

4.6. Determination of Scale Factors, γ_T and γ_R 126

4.7. Conclusion 128

CHAPTER 5: STRUCTURAL IDENTIFICATION USING A NONLINEAR CONSTRAINT SATISFACTION PROCESSOR WITH INTERVAL ARITHMETIC AND CONTRACTOR PROGRAMMING 130

5.1. Introduction 131

5.2. Nonlinear Constraint Satisfaction With Contractor Programming and Interval Analysis 135

5.2.1. Contractor Programming 138

5.2.2. Illustrative Example Using Cross-in-Tray Function 140

5.3. Formulation of Interval Constraint Equations for the Structured Inverse Eigenvalue Problem 141

5.4. Numerical Verification of Methodology 147

5.4.1. Application to a Well-Posed Problem 148

5.4.2. Application to an Ill-Posed Problem 150

5.5. Experimental Application on a Shear Building Model 156

5.5.1. Vibration Testing and System Identification 157

5.5.2. Experimental Application to a Well-Posed Problem 158

5.5.3. Experimental Application to an Ill-Posed Problem 161

5.6. Comparison to Bayesian Model Updating Approaches 163

5.7. Conclusion 170

CHAPTER 6: Vibration-based Damage Detection with Uncertainty Quantification by Structural Identification using Nonlinear Constraint Satisfaction with Interval Arithmetic 173

6.1. Introduction 174

6.2. Finite Element Model Updating Using Nonlinear Constraint Satisfaction 180

6.2.1. Constraint Satisfaction with Interval Arithmetic 184

6.2.2. Contractor Programming 186

6.2.3. Illustrative Example on a 3DOF Shear Building Model 188

6.2.4. Issues with Scalability 190

6.3. Details of Experimental Program for Validation of the Methodology 195

6.3.1. Details on the Experimental Substructure and Hybrid Simulation 196

6.3.2. Damage Prescription and Progression 199

6.3.3. System Identification 202

6.4. Structural Identification 203

6.4.1. Parameter Selection and Sensor Layout 204

6.4.2. Identification of the Undamaged Case Using the Interval Hull 206

6.4.3. Identification of the Damaged Cases Using the Interval Hull 208

6.5. Conclusion 213

CHAPTER 7: CONCLUSION 215

7.1. Summary and Concluding Remarks 215

7.2. Recommendations for Future Work 219

REFERENCES 222

APPENDIX A: CABLE FORCE NATURAL FREQUENCIES 236

A.1. Generation of Synthetic Frequencies For the Two Spring Analytical Example 236

A.2. Generation of Synthetic Frequencies For the Four Spring Analytical Example 237

A.3. Two Spring Experimental Validation 238

APPENDIX B: EXPERIMENTAL MODAL ANALYSIS DATA FOR SIX DOF SYSTEM MODEL 239

APPENDIX C: EXPERIMENTAL MODAL PROPERTIES ESTIMATES OF THE TRUSS 240

APPENDIX D: SUPPLEMENTAL MATLAB/C++ CODES 263

D.1. MATLAB C++ Code Generation For Two Spring Identification 263

D.2. MATLAB Script For Three DOF Example 271

LIST OF FIGURES

FIGURE 1.1: Prismatic beam element with elastic rotational and translational end restraints under axial loading 4

FIGURE 1.2: Six degree-of-freedom mass-spring system 6

FIGURE 1.3: Forty-five degree-of-freedom Pratt truss used for validating the extended constraint programming methodology for structural identification and damage detection 7

FIGURE 2.1: Flow of the structural identification process 16

FIGURE 2.2: a) Deterministic approaches with the assumption of correctly identified modal parameters, b) propagation of measurement uncertainties to the parameter space to quantify the confidence in the parameter estimates 28

FIGURE 2.3: a) Three degree-of-freedom mass-spring system for illustrating the effectiveness of some of the most prominent model updating methods, b) Natural frequencies and corresponding mode shapes for the system (measured components are colored blue) 29

FIGURE 2.4: Sensitivity-based model updating example: Starting point (1.5,1.5,1.5) with 500 iterations (red) resulting in a single solution (blue) 34

FIGURE 2.5: Multi-start sensitivity-based model updating example: a) Initial 500 starting points, b) Solution space for the different starting points 34

FIGURE 2.6: Flowchart of genetic algorithm process (Mares and Surace, 1996) (reproduced) 36

FIGURE 2.7: Genetic algorithm model updating example: Populations for the first generation (black), 10th generation (red), 20th generation (green), and best solution (blue) 42

FIGURE 2.8: Multi-start genetic algorithm model updating example: Solution space for the genetic algorithm updating procedure for 500 different starting populations 42

FIGURE 2.9: Samples for the posterior distribution obtained from Bayesian model updating of three degree of freedom model: a) mode shape correlation over-expressed in the measure of fit, b) natural frequencies over-expressed in the measure of fit, c) balanced expression of natural frequencies and mode shapes in the measure of fit 48

FIGURE 2.10: Parameter domain for the three degree-of-freedom interval finite element model update depicting all boxes evaluated as well as the solutions (blue) 51

FIGURE 3.1: The Cartesian product of three intervals creates box $[\boldsymbol{x}] \in \mathbb{IR}^3$. 57

FIGURE 3.2: Images of $[\boldsymbol{x}]$ by f for a pessimistic inclusion function, $[f]([\boldsymbol{x}])$ and a minimal inclusion function, $[f]^{min}([\boldsymbol{x}])$ 59

FIGURE 3.3: Pessimistic vs. exact image representations of example functions that would otherwise be equivalent under ordinary real arithmetic. 60

FIGURE 3.4: Branch and Prune Algorithm 66

FIGURE 3.5: Set inversion problem mapping modal property measurements, $\mathbb{Y}$, to structural parameters, $\mathbb{X}$ 67

FIGURE 3.6: a) Entire search tree, b) Checking consistency of the arcs in the constraint graph and removing assignments from the variable domains until all arcs are consistent for a subset of the entire problem 70

FIGURE 3.7: HC4 algorithm (Benhamou et al., 1999) 73

FIGURE 3.8: HC4Revise algorithm (Benhamou et al., 1999) 73

FIGURE 3.9: First forward-backward contraction for $y^2 - 5y + 2x^2 - 3 = [0, 0]$ with $x, y \in [-10, 10]$. a) Forward evaluation, b) Backward contraction w.r.t x, c) Backward contraction w.r.t. y. 75

FIGURE 3.10: Second forward-backward contraction for $y^2 - 5y + 2x^2 - 3 = [0, 0]$ with $x, y \in [-10, 10]$. a) Forward evaluation, b) Backward contraction w.r.t x, c) Backward contraction w.r.t. y. 76

FIGURE 3.11: Forward-backward contraction for $(y-2.5)^2+2x^2-9.25 = [0, 0]$ with $x, y \in [-10, 10]$. a) Forward evaluation, which exactly bounds the image without pessimism, b) Backward contraction w.r.t x, c) Backward contraction w.r.t. y. 78

FIGURE 3.12: Three degree-of-freedom mass-spring system for demonstrating structural identification using nonlinear constraint satisfaction with interval arithmetic and contractor programming 83

FIGURE 3.13: Subpaving of all feasible solutions to the inverse eigenvalue problem for the three degree-of-freedom system 84

FIGURE 4.1: (a) Conventional deterministic approach to parameter identification of axial force and boundary restraints using inverse methods applied to vibration measurements without uncertainty estimates; (b) Objective of the proposed methodology for inversely propagating measurement uncertainties to the parameter space to quantify confidence in the parameter estimates. 91

FIGURE 4.2: A prismatic beam element with elastic rotational end restraints under axial loading 94

FIGURE 4.3: Inclusion tests applied to determine whether the box being tested lies within the solution set ($\boldsymbol{x_i}$), on the boundary ($\boldsymbol{x_b}$), or outside the solution set ($\boldsymbol{x_o}$) 99

FIGURE 4.4: A set inversion $f(x) \in [y]$ with (a) $f(x) = (\frac{x_1}{4})^2 + (\frac{x_2}{2})^2 - 1$ and $[y] \in [-1, 1]$. (b) The initial box, $[\boldsymbol{x}] = [-10, 10] \times [-10, 10]$. (c) Subpavings from the set inversion using the classic branch and bound SIVIA algorithm. (d) Subpavings from the set inversion using SIVIA with inner and outer contractors. 101

FIGURE 4.5: Illustration of how inequality constraints developed using the characteristic equation with lower and upper bound natural frequency estimates are utilized to form inclusion functions for the inner and outer contractors for the first natural frequency. 104

FIGURE 4.6: Illustration of contractor programming for axial force determination in the presence of measurement uncertainty over a two dimensional search space: (a) Noise-free intersection of constraint equations; (b) Constraint equations in the presence of measurement error; (c) Specifying constraint equations with measurement uncertainty of ±0.05 Hz; (d) Subpaving of solutions space displaying inner, outer, and boundary boxes generated with an interval precision of 0.0005; (e) Inner approximation of the feasible parameter set shown with constraint equations; (f) Further pruning of solution space by inclusion of addition constraint equations (additional natural frequency measurement) 105

FIGURE 4.7: Sets of subpavings developed across the discrete set of values for N using the first eight natural frequencies in the parameter identification and an interval uncertainty of $\frac{1}{2}\sigma$ 111

FIGURE 4.8: Interpolation of continuous basins for feasible parameter space for interval uncertainty of $\pm\frac{1}{2}\sigma$ on natural frequencies with four, six, or eight natural frequencies included in parameter identification. 112

FIGURE 4.9: Sensitivity of the identified parameter uncertainty with measurement uncertainty; shown for interval uncertainties of $\pm\frac{1}{2}\sigma$, $\pm\sigma$, and $\pm 2\sigma$ using the first eight natural frequencies in the parameter identification 114

FIGURE 4.10: Verification of extended methodology: (a) sampling of real-valued parameter assignments for verification; (b) maximum residual errors computed for the sampled verification points 114

FIGURE 4.11: Extension of methodology to the identification of rotational boundary restraints, translational boundary restraints, and internal axial force with uncertainty quantification; confidence intervals of $\pm\frac{1}{2}\sigma$ using either 6, 8, 10, or 12 natural frequencies in the parameter identification 117

FIGURE 4.12: Verification of methodology: (a) sampling of discrete parameter set from the subpavings; (b) maximum residual relative to standard deviation of measurements computed by the forward solution with sampled points. 118

FIGURE 4.13: Illustration of the solution time for the entire discrete range of axial forces for 6, 8, 10, and 12 frequencies included in the parameter identification with confidence intervals of $\pm\frac{1}{2}\sigma$ 121

FIGURE 4.14: (a) Photograph of experimental rod subjected to constant tension using a MTS load frame; (b) photograph of ball joint rod end connection to end gusset plates; (c) photograph of introduced rotational restraint through taut wires at rod end 123

FIGURE 4.15: Representative frequency response functions obtained through impulse testing of the experimental specimen for each of the four cases 124

FIGURE 4.16: Interpolation of continuous basins for the feasible parameter space for all four experimental cases using the first eight natural frequencies 125

FIGURE 4.17: Feasible parameter space for all four experimental cases with fixed axial force of 2.5kN using the first eight natural frequencies 126

FIGURE 4.18: Histograms for the posterior probability distributions of the identified parameters generated from the subpavings 127

FIGURE 4.19: Determining suitable values for γ_R and γ_T to ensure that the generalized equation is uniform across the entire range of fixity. 128

FIGURE 5.1: a) An interval vector, or box, generated from the product of two intervals. b) contraction of an interval vector on a system of constraints 138

FIGURE 5.2: a.) Cross-in-Tray Function, b.) Set of satisfiable solutions produced with relaxed inequality constraint using contractor programming (all boxes shown represent interval vectors after subsequent contractions and shaded boxes indicate satisfiable solutions) 141

FIGURE 5.3: Six degree-of-freedom mass-spring system considered in numerical verification 148

FIGURE 5.4: Feasible solutions for a well-posed analytical case of model updating with increasing uncertainty on the measured components of the mode shapes 151

FIGURE 5.5: Complete set of feasible solutions for non-unique model updating problem with numerical data: a.) Basins of feasible stiffness assignments; b.) Natural frequencies associated with the feasible solutions; c.) Comparison of reconstructed mode shapes to the complete analytical modes from the reference structure 154

FIGURE 5.6: Laboratory six-story shear building model: a.) photograph of instrumented test structure, b.) structural geometry and thickness of aluminum sheet columns, c.) frequency response functions obtained from impact excitation at elevation of first story mass 157

FIGURE 5.7: Undamped natural frequency and mode shape estimates of the test structure obtained through system identification 158

FIGURE 5.8: Feasible solutions for a well-posed experimental case of model updating with increasing uncertainty on the measured components of the mode shapes 161

FIGURE 5.9: Complete set of feasible solutions for non-unique model updating problem with experimental data: a.) Basins of feasible stiffness assignments; b.) Natural frequencies associated with the feasible solutions; c.) Comparison of reconstructed mode shapes to the complete experimental measurements 164

FIGURE 5.10: Samples of the posterior distribution obtained from Bayesian model updating of two degree of freedom model with uncertain stiffness parameters: a) mode shapes over-expressed in the measure of fit; b) natural frequencies over-expressed in the measure of fit; c) balanced model class 168

FIGURE 5.11: Subpavings of feasible solution space for parameters in two degree of freedom model: a) using only the mode shape measurements in the constraint equations; b) using only the natural frequency measurements in the constraint equations; c) using both the mode shape and natural frequency measurements 170

FIGURE 6.1: An interval vector, or box, generated from the product of three intervals 186

FIGURE 6.2: Three degree-of-freedom mass-spring model used to demonstrate structural identification using nonlinear constraint satisfaction with interval arithmetic and contractor programming 188

FIGURE 6.3: Subpavings of the feasible parameter space for the inverse eigenvalue problem subject to partially described, incomplete, and uncertain modal parameters of the three degree-of-freedom system (synthetic measurements of natural frequencies and mode shape coordinates highlighted in bold) 190

FIGURE 6.4: Illustration of the use of the interval hull to enclose the feasible parameter space as an alternative to subpavings 192

FIGURE 6.5: a) Schematic of the hybrid simulation applied in the current study, b) details of the experimental substructure and instrumentation 196

FIGURE 6.6: a) Forty-five degree-of-freedom Pratt truss used in hybrid testing program for structural identification and damage detection, b) First eight natural frequencies and mode shapes of the truss 197

FIGURE 6.7: a) Force-elongation curve for the first two damage scenarios of specimen one, b) crack initiation on one side of a bolt hole (specimen one) , c) cracking on both sides of bolt hole (specimen one), and d) net section rupture of one bar (specimen two) 200

FIGURE 6.8: Force-elongation histories for healthy and damage cases for the experimental substructure 202

FIGURE 6.9: a) Sensor layout chosen to identify all of the diagonal members of the truss b)Determination of identifiable diagonal and horizontal members based on the interval hull 206

FIGURE 6.10: Interval hull solution for the stiffness scalars with member 27 as the experimental substructure and tested in the healthy condition 209

FIGURE 6.11: Interval hull solutions for the stiffness scalars with member 31 as the experimental substructure and in the healthy condition 209

FIGURE 6.12: Interval hull solutions for the stiffness scalars with the experimental substructure representing member 27 a) damage case D1, b) damage case D2, c) damage case D3, and d) damage case D4, where member 5 was subjected to a 25% stiffness reduction in the analytical model 211

FIGURE 6.13: Interval hull solutions for the stiffness scalars with the experimental substructure representing member31 a) damage case D1, b) damage case D2, c) damage case D3, and d) damage case D4, where members 8 and 9 were subjected to 25% stiffness reductions in the analytical model 212

LIST OF TABLES

TABLE 3.1: Endpoint formulas for binary arithmetic operations 55

TABLE 3.2: Comparison of forward-backward contractor operations on different functional forms of an inclusion function 79

TABLE 4.1: Application of Equilibrium Conditions to Generalized Beam Model 95

TABLE 4.2: Interval hull of feasible parameters obtained with a confidence interval of $\frac{1}{2}\sigma$ for the natural frequency measurements and interval precision of 1e-3 112

TABLE 4.3: Interval hull of feasible parameters obtained with a confidence interval of $\pm\frac{1}{2}\sigma$ for the natural frequency measurements and interval precision of 1e-3 119

TABLE 5.1: Comparison of stiffness estimates to experimental results obtained using three incompletely measured eigenpairs 162

TABLE 5.2: Comparison between experimental modal estimates and updated model 162

TABLE 6.1: Summary of damage cases investigated (*represents reduction in analytical portion of hybrid test) 201

TABLE 6.2: Comparison between modal parameter estimates of the healthy structure to each damage case where member 27 was the experimental substructure 203

TABLE 6.3: Comparison between modal parameter estimates of the healthy structure to each damage case where member 31 was the experimental substructure 204

TABLE 6.4: Comparison between experimental natural frequencies and interval natural frequencies of the identified model for case 1 208

TABLE 6.5: Comparison between expected stiffness parameter estimates to those identified by the interval hull for both experimental substructures and all damage cases (* represents the cases with significant nonlinearity in the force-elongation response) 210

TABLE A.1: Average natural frequencies and standard deviations for the first eight natural frequencies of the two spring problem where k_A=0.70, k_B=0.30, and $k_C = k_D$=0.70 and the applied force was $581kN$. 236

TABLE A.2: Average natural frequencies and standard deviations for the first twelve natural frequencies of the four spring problem where k_A=0.70, k_B=0.30, k_C=0.75, and k_D=0.45 237

TABLE A.3: Average natural frequencies for the first eight natural frequencies of the two spring problem with $k_C = k_D = 1$ and $N = 2.5kN$ 238

TABLE B.1: Average natural frequencies and corresponding mode shapes for the six degree-of-freedom experimental shear structure in Chapter 5 239

TABLE C.1: Average natural frequencies and standard deviations for the first eight natural frequencies for all states of damage where the experimental substructure represented member 27 240

TABLE C.2: Average of the measured mode shape components for all cases of damage where the experimental substructure represented member 27 241

TABLE C.3: Standard deviations of the measured mode shape components for all cases of damage where the experimental substructure represented member 27 246

TABLE C.4: Average natural frequencies and standard deviations for the first eight natural frequencies for all states of damage where the experimental substructure represented member 31 251

TABLE C.5: Average of the measured mode shape components for all cases of damage where the experimental substructure represented member 31 252

TABLE C.6: Standard deviations of the measured mode shape components for all cases of damage where the experimental substructure represented member 31 257

NOMENCLATURE

Ω^2	eigenvalue matrix
Φ	eigenvector matrix
Ctc	contractor
K	structural stiffness matrix
M	structural mass matrix
CP	constraint programming
CSP	constraint satisfaction problem
MAC	modal assurance critereon
SIVIA	set inversion via interval analysis
St-Id	structural identification

Intervals

$[x]$	scalar interval
$[\boldsymbol{x}]$	interval vector (or box)
$f([\boldsymbol{x}])$	image of $[\boldsymbol{x}]$
$\underline{x}$	lower bound of $[x]$
$\overline{x}$	upper bound of $[x]$
$w([x])$	width of $[x]$
$m([x])$	midpoint of $[x]$
ϵ	prescribed interval precision

Sets

$\emptyset$:	empty set

$\mathbb{S}$	generic set
$\underline{\mathbb{S}}$	inner approximation of $\mathbb{S}$
$\overline{\mathbb{S}}$	outer approximation of $\mathbb{S}$
$\delta\mathbb{S}$	boundary of $\mathbb{S}$
$[\mathbb{S}]$	interval hull of $\mathbb{S}$
$\mathbb{IR}$	set of all interval real numbers
$\mathbb{R}$	set of all real numbers
$\forall$	for all
$\in$	is a set element of

Symbols

$\cap$	intersection
$\cup$	union
$\sqcup$	interval union
$\subset$	subset
χ	measurement uncertainty
$\supset$	superset
N	axial force
σ	standard deviation
α	stiffness modifier

CHAPTER 1: INTRODUCTION

1.1 Introduction

One the main challenges facing the civil engineering field, especially in the United States of America, is the maintenance of a failing infrastructure system. In 2017, the American Society of Civil Engineers reported an overall grade of D+ for America's infrastructure (ASCE, 2017). Specifically, the report stated that almost 40% of America's 614,387 bridges are at least 50 years old, with just nearly 25% being rated structurally deficient or obsolete. The total cost for rehabilitation of existing bridges is estimated at over $120 billion. Structural failures may be life-threatening and costly to both the infrastructure managers and end-users. For instance, the collapse of the I-35 bridge in 2007 dramatically altered the surrounding transportation system, causing congestion and leading to economic losses, for road-users and areas businesses alike, anywhere from $71,000-220,000 a day (Xie and Levinson, 2011). In addition to economic impacts, bridge closures adversely affect the daily lives of users. For example, the sudden closure of the Lake Champlain Bridge in 2009, due to rapid deterioration, forced users to commute an additional 85 miles as an alternative route (NYSDOT, 2012). These astounding results highlight the growing necessity to deploy approaches aimed at determining the in-service behavior of structures to better inform decision making for repair and replacement of critical infrastructure components.

In the past few decades, numerous techniques have been proposed for structural iden-

tification (St-Id) using modal parameter estimates obtained from either experimental or operational modal analysis. St-Id has typically been performed by updating finite element models through modification of structural stiffness and mass matrices such that the differences between experimentally measured modal properties and those of an analytical finite element model are minimized with the end goal being utilization of the calibrated model to determine the in-service behavior of the structure to support performance-based civil engineering. Applications for structural identification are wide-ranging and include design verification, improved structural analysis, damage detection, structural health monitoring, and long-term performance assessment. Although structural identification originated as a means to determine the performance of as-built structures through higher fidelity simulations, it has also been heavily pursued as a method for vibration-based damage detection. Despite the plentiful library of analytical and experimental case studies performed to date, there exists a great need to address many of the pitfalls plaguing current model updating methods. Specifically, techniques for model updating that fully incorporate the effects of measurement and modeling uncertainties on the identified structural parameters are necessary in order to produce confidence bounds on the parameter estimates to ensure informed decision making and minimize false positives and false negatives in damage diagnosis and prognostication.

1.2 Overview of Research Effort

The aim of this dissertation is to explore alternative methods for structural identification that may overcome several of the difficulties of past model updating strategies. These challenges include computability, feasibility, and uniqueness, which are inherent when only

a limited number of degrees of freedom and eigeninformation pairs can actually be measured. To address these issues this work presents a new paradigm for model updating that is based on casting the inverse eigenvalue problem as one of constraint satisfaction. As illustrated in the next chapter, the most predominantly applied methods for model updating are only capable of providing a single solution and, while some tout the ability to determine alternative solutions, none are capable of producing the set of *all* feasible solutions to the inverse eigenvalue problem. In addition, many of the methods examined are theoretically capable of finding the global minimum, but given the effects of measurement and modeling uncertainties, the global optimum may not represent the most physically meaningful solution from an engineering standpoint. In contrast, the methodologies presented in this work employ interval arithmetic, which naturally handles uncertainties, and contractor programming to generate the complete set of possible solutions to the inverse eigenvalue problem rather than optimizing a single objective function that necessarily aggregates model correlations into a single measure of fit.

Application of the proposed approach will be demonstrated through several case studies, encompassing both continuous system model representations as well as multiple degree of freedom system models. A methodology is first developed for determining estimates of the internal axial force and boundary restraints within in-service prismatic beam elements such as short cables, struts, bracing, and tie-rods, using uncertain natural frequency measurements. The methodology proposed provides a new technique for approaching this challenging inverse problem using the Set Inversion Via Interval Analysis (SIVIA) algorithm as an alternative to optimization schemes. The framework offers the ability to completely enclose the feasible solution space for the unknown axial force and boundary restraints

in prismatic beam and cable elements (Figure 1.1) and, unlike existing approaches, is applicable to members with any degree of non-dimensional bending stiffness since it adopts no assumptions in the solution of the natural frequencies of a Timoshenko beam. The methodology is first demonstrated and validated using synthetically generated data. Subsequently, an experiment is conducted on an axially loaded rod with progressively increased end restraint at one end to experimentally validate the application of the approach on a real structural member.

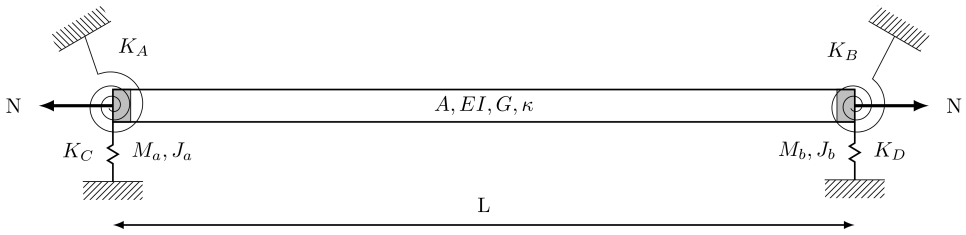


FIGURE 1.1: Prismatic beam element with elastic rotational and translational end restraints under axial loading

The techniques within the general methodology are then extended from the continuous system model to finite element model updating of multiple degree-of-freedom system models using partially described and incompletely measured natural frequencies and mode shape data. The methodology formulates the structured inverse eigenvalue problem as a Constraint Satisfaction Problem and uses interval arithmetic and contractor programming to solve for the complete feasible parameter space for uncertain stiffness parameters in the model. The approach offers the unique capabilities of fully enclosing the feasible parameter space given specified measurement uncertainties as well as solving non-unique constructions of the inverse eigenvalue problem. Instead of the traditional approach of solving

the forward eigenvalue problem and then comparing the analytical modal properties to the experimental, this problem is formulated using matrix-based constraints coupled with additional mechanics-based constraints over a bounded search space. The formulation of the constraint equations using intervals lends to the inclusion of measurement uncertainty, which is necessary for the quantification of uncertainty in the parameter assignments. The approach is capable of mapping the entire solution space in contrast to traditional updating techniques or emerging probabilistic methods. In addition, the use of interval arithmetic allows for the relaxation of constraint equations for identifying solutions other than the global optimum, which lends to practitioner involvement for evaluation of alternative solutions. These capabilities are first demonstrated and verified using synthetic data for a numerical six degree-of-freedom indeterminate mass-spring model (Figure 1.2). The method is then experimentally validated using vibration measurements obtained from a laboratory shear building model that is an analog to the mass-spring system. The acquired natural frequencies and mode shapes are then utilized to determine the relative stiffness of the aluminum walls between each floor by casting the updating problem as one of constraint satisfaction. The methodology is applied to well-posed and ill-posed cases for both the numerical and experimental cases. Lastly, the methodology is contrasted with probabilistic model updating to illustrate the unique capabilities for completely addressing the effects of measurement uncertainty on the parameter estimation and avoiding challenges associated with the determination of relative weighting factors in the modal measure of fit function that is necessary to aggregate model correlation residuals in this approach, which represents the current state-of-the-art in this field.

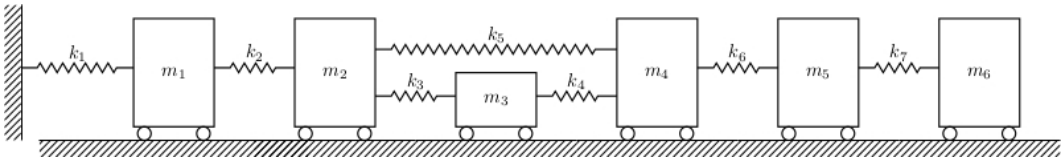


FIGURE 1.2: Six degree-of-freedom mass-spring system

The scalability of the methodology developed for small multiple degree-of-freedom system models to much larger structures with significantly more uncertain parameters is subsequently addressed. However, due to the dramatic increase in dimensionality of the search space, modifications to the methodology are presented such that the problem remains computationally tractable and retains enforcement of the eigenvalue inclusion constraints. Instead of determining the set of all feasible solutions, the methodology developed contracts the initial search domain to a single interval solution, called the interval hull, that is guaranteed to contain the set of all feasible solutions. Additionally, a response surface methodology is introduced to provide a means of approximating the interval natural frequencies associated with interval stiffness matrices and retain the ability to perform interval contractions on the eigenvalue inclusion constraints. The extended methodology is verified on a 45 degree-of-freedom, 45 member, 2D Pratt truss (Figure 1.3). As an alternative to full-scale vibration testing, hybrid testing is utilized for acquisition of experimental modal testing data. In this hybrid testing approach, only a portion of the structure is physically tested while the remainder interacts with the experimental member through a substructured form of the dynamic equation of motion. This approach uniquely permits for evaluation of a large matrix of experimental validation tests where both realistic damage is incorporated in the testing and the actual effect of the damage on the stiffness reduction of the member is well quantified. To demonstrate the vibration-based damage detection capabilities of the

methodology, realistic damage, in the form of fracture and crack propagation in the net section rupture limit state, is progressively introduced to the experimental member in the hybrid simulations. Through the matrix of experimental validation tests, the methodology is shown to be successful not only for identifying the damaged members of the truss in the presence of measurement uncertainties, but also capable of correctly quantifying the severity of damage, which provides an important contribution to damage diagnosis and prognostication.

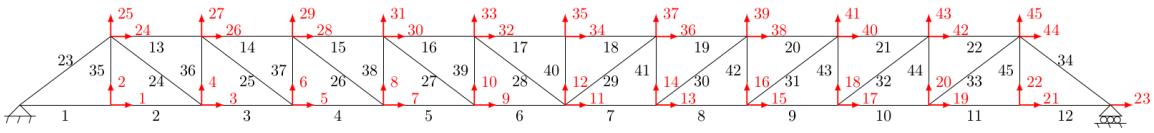


FIGURE 1.3: Forty-five degree-of-freedom Pratt truss used for validating the extended constraint programming methodology for structural identification and damage detection

1.3 Expected Contribution

This dissertation provides methodologies that are attractive alternatives to traditional and emerging model updating techniques by addressing several of the shortcomings inherent in those methods. Although many methods have been proposed and pursued over the last several decades for structural identification, the two most prevalent are deterministic and probabilistic. Deterministic methods attempt to minimize the difference between experimentally measured and analytical modal properties by identifying a set of uncertain parameters in the model that optimize a particular measure of the correlation between the modal parameters of the model and those measured experimentally. However there are numerous difficulties with such methods including: computational efficiency, ill-conditioning,

solution uniqueness, and the selection of appropriate uncertain parameters (Friswell et al., 2001). In addition, the objective function utilized for the optimization is generally aggregated across all modal correlations without taking into consideration the uncertainty associated with individual modal parameter estimates. Furthermore, some optimization schemes, while offering the ability to find the global minimum to the objective function, may not actually provide the most physically meaningful solution. Probabilistic approaches attempt to combat some of these pitfalls, but introduce several additional difficulties. Although probabilistic model updating methods have the ability to incorporate model and measurement uncertainties to determine the most probable solution, the methods rely on assumed probability density function estimates to drive the update and require computationally expensive simulations such as Markov Chain Monte Carlo methods (Marwala, 2010). Similar to the deterministic methods, probabilistic model updating also relies on an aggregation of modal correlations. In addition, the objective function employs weighting factors to emphasize certain modal parameter correlations, which can be difficult to determine and may greatly affect the performance of the identification. Although probabilistic model updating has the benefit of generating a family of potential solutions to the inverse eigenvalue problem, it is not capable of determining the entire set of feasible solutions.

The methodologies developed in this dissertation seek to address many of the underlying challenges within model updating, condition assessment, and damage identification by formulating the structural identification problem as one of constraint satisfaction with interval arithmetic and contractor programming and will ultimately facilitate the advancement of St-Id as a viable tool for performance-based condition assessment. In the formulations, measurement uncertainties, in the form of intervals, are naturally accounted for within

physics-based constraint equations to define a guaranteed complete feasible solution space within a bounded region. The ability to propagate measurement uncertainty into the parameter space is critical towards quantifying the confidence in the individual parameter estimates to inform decision-making within structural health diagnosis and prognostication applications.

1.4 Dissertation Outline

The outline of this dissertation is as follows:

- Chapter 2 provides an overview of traditional structural identification techniques for model updating along with a survey of applications of those methods for structural identification of civil structures. Each of the methods discussed are applied to a small three degree-of-freedom system model to demonstrate the performance capabilities and shortcomings of each technique. Limitations in the ability to accurately identify the behavior of in-service structures in the presence of measurement and modeling uncertainties are also discussed.

- Chapter 3 provides an brief primer on interval arithmetic and interval analysis followed by an overview of the theory behind the methods ultimately utilized to cast the structural identification problem as one of constraint satisfaction with interval arithmetic and contractor programming.

- Chapter 4 details the formulation of a methodology that leverages the Set Inversion Via Interval Analysis algorithm to determine the unknown axial forces and end restraints within in-service prismatic axial force members of structural systems using

natural frequency measurements. The framework is applied to both numerical problems, with synthetic data, as well as an experimental problem, with measured natural frequencies acquired from impulse response modal testing of an axially loaded steel rod with progressively increased end restraint at one end. In each case, the ability to completely enclose the feasible solutions to the parameter identification problem, given specified measurement uncertainties for the natural frequencies, is demonstrated. This chapter has been prepared as a journal manuscript and the final definitive version has been published in *Journal of Sound and Vibration* by Elsevier Limited. It is available at https://www.journals.elsevier.com/journal-of-sound-and-vibration.

- Chapter 5 details the methodology for model updating of multiple degree-of-freedom system models that is based on formulating the structured inverse eigenvalue problem as a Constraint Satisfaction Problem. Background information on interval arithmetic and contractor programming is presented followed by application of the methodology to a numerical six degree-of-freedom mass-spring model and subsequently on an experimental analog of the same system model. Results for both applications demonstrate the unique advantages of the methodology, which are favorably contrasted with the emerging probabilistic model updating approach. This chapter has been prepared as a journal manuscript and the final definitive version has been published in *Computers and Structures* by Elsevier Limited. It is available at https://www.journals.elsevier .com/computers-and-structures.

- Chapter 6 introduces techniques and modifications for scaling the methodology pre-

sented in Chapter 5 to much larger structures with significantly more uncertain parameters. This extended methodology is first applied to modal data acquired though hybrid testing of a 45 degree-of-freedom, 45 member, 2D Pratt truss, where the experimental substructure is undamaged and subsequently to several cases where realistic damage is applied to the substructure through overloading. The results in all cases demonstrate that the method is capable of determining both the location and severity of realistic structural damage, while also being able to quantify the uncertainty in the parameter estimates by providing a single interval vector solution to the inverse eigenvalue problem with partially described and incompletely measured modal information. This chapter has been prepared in the format of a journal manuscript and has been submitted for peer review.

- Chapter 7 provides an overview of the contributions of this dissertation and discusses potential avenues for future work.

CHAPTER 2: LITERATURE REVIEW

2.1 Structural Identification

Structural identification (St-Id), which stems from system identification, aims to analytically model physical behavior based on experimental measurements. The concept was first introduced in the late 1970s (Liu and Yao, 1978) and has since continued to be an active area of research, especially with advances in modern computing. The technique most often employed is finite element (FE) model updating, in which an analytical model is developed and subsequently calibrated based on experimentally measured response information with an emphasis on faithfully maintaining the physical plausibility of updated parameters in the model. To date, methods for calibrating initial FE models have been largely iterative and, while St-Id has been pursued in several fields other than civil engineering such as aerospace and manufactured systems (Zimmerman, 2000), widespread use has yet to be realized. However, in recent years a wide range of case studies have piqued interest in this burgeoning field, further bridging the gap between physical systems and analytical models. In addition, advancements in computing technology have enriched this field by offering means to develop and update higher fidelity models that better represent actual in-service behavior (Ribeiro et al., 2012; Cheung and Bansal, 2017; Whelan et al., 2018).

The success or failure of a St-Id endeavor hinges heavily on the model updating strategy employed as well as quality and richness of the experimental data and the uncertain param-

eters chosen for the updating process. Since the overarching goal of structural identification is to reduce the discrepancies between the experimental measurements and analytical model, the strategy employed must be capable of handling a reasonably large number of uncertain parameters as well account for the effect of measurement uncertainties in the parameter identification. In addition, the parameters that are updated must maintain physical plausibility in order to be meaningful for decision making purposes. Common choices for uncertain parameters have been member properties, material properties, boundary conditions, and connectivity assignments (Mottershead et al., 2011). Since the majority of St-Id applications have been based on the measured modal response of a structure, the process involves full-scale vibration testing of a structure to acquire dynamic response measurements, typically in the form of accelerations. The testing program may either be output-only, where the excitation is ambient, or input-output where controlled excitation is prescribed and also measured. For large civil structures, output-only vibration testing is more routinely employed due to the difficulties in prescribing and measuring controlled excitation to such large structures as well as the advantage of requiring interruption of regular service when performing ambient vibration monitoring (Wenzel and Pichler, 2005). Modal properties in the form of undamped natural frequencies, f_n, mode shapes, ϕ, and relative damping factors, ξ, are extracted through system identification using the acquired structural responses. An initial finite element model of the structure is then created and calibrated by adjusting the set of uncertain modeling parameters to reduce the discrepancies between the experimentally measured modal properties and those of the analytical model.

Past calibration approaches can be largely classified into one of two categories: direct or iterative. Updating of structural matrices via direct methods has been long pursued for the

potential benefit of ease of application relative to iterative methods (Baruch, 1978; Zimmerman and Kaouk, 1992; Friswell et al., 1998a; Carvalho et al., 2007; Yang and Chen, 2009). However, direct methods have only been successfully applied to small systems and, in such cases, the experimental measurements have been well replicated by the updated model, but the physically meaningfulness of the mass and stiffness matrix solutions are not guaranteed (Friswell et al., 1998a; Marwala, 2010; Ahmadian et al., 1997). Most critically with respect to civil infrastructure, the successful application of such methods on larger models or complex structures has yet to be demonstrated. In contrast, iterative optimization schemes have demonstrated more promising results for the application of St-Id to in-service structures, including buildings (Moaveni et al., 2013; Boscato et al., 2015) and bridges (Brownjohn and Xia, 2000; Teughels and DeRoeck, 2004; Schlune et al., 2009; Wang et al., 2010; Ribeiro et al., 2012; Jung and Kim, 2013). While successful in many aspects, iterative methods have been fraught with numerous persistent issues including: computational inefficiency, solution uniqueness, and challenges related to parameter selection. One of the main drawbacks of these methods is that the global solution, while optimal in that it reduces the differences in modal parameters, may not be physically significant. The reason for this is that uncorrected uncertainties in the model and measurement uncertainties can lead to the correct physical solution being a local minimum rather than the global minimum. Additionally, iterative methods aggregate the model correlations with the experimental measures into a single objective function so the choice of the objective function and relative weighting of the residuals affects the inverse solution. As such, methods for model updating need to be capable of mapping or bounding the range of feasible solutions given prescribed measures of uncertainty. Additionally, alternatives to optimization

techniques that require the use of objective functions should be explored to overcome the associated drawbacks of these model correction techniques that aggregate the residuals into a common function.

2.2 Structural Identification Process

The ASCE/SEI report on structural identification (ASCE-SEI, 2011) states that the St-Id process may be divided into six distinct stages, which are summarized below. The main steps are also visually depicted in Figure 2.1 for an experimental application investigated in Chapter 5.

2.2.1 Establish Need for Application

The first stage in process is recognizing the need for performing a structural identification. There are many situations where an asset manager may wish to pursue structural identification including: load capacity testing, design verification, establishing a baseline for future assessment, evaluating the cause for deterioration/damage, and assessing the impact of retrofit actions (ASCE-SEI, 2011). Each of these tasks is based on the underlying need to understand the actual in-service performance of a particular structure.

2.2.2 Formulation of Initial FE Model

Once the key mechanisms and complexity of the structure under test have been throughly examined, an *a priori* finite element model is created taking into account concerns such as geometry, proper element selection, sufficient discretization, idealized or approximated boundary conditions, and connectivity between substructures. Inappropriately simplifying the structure will lead to poor model performance and the uncorrected errors in the model will continue to propagate through the St-Id process. These errors can lead to poor corre-

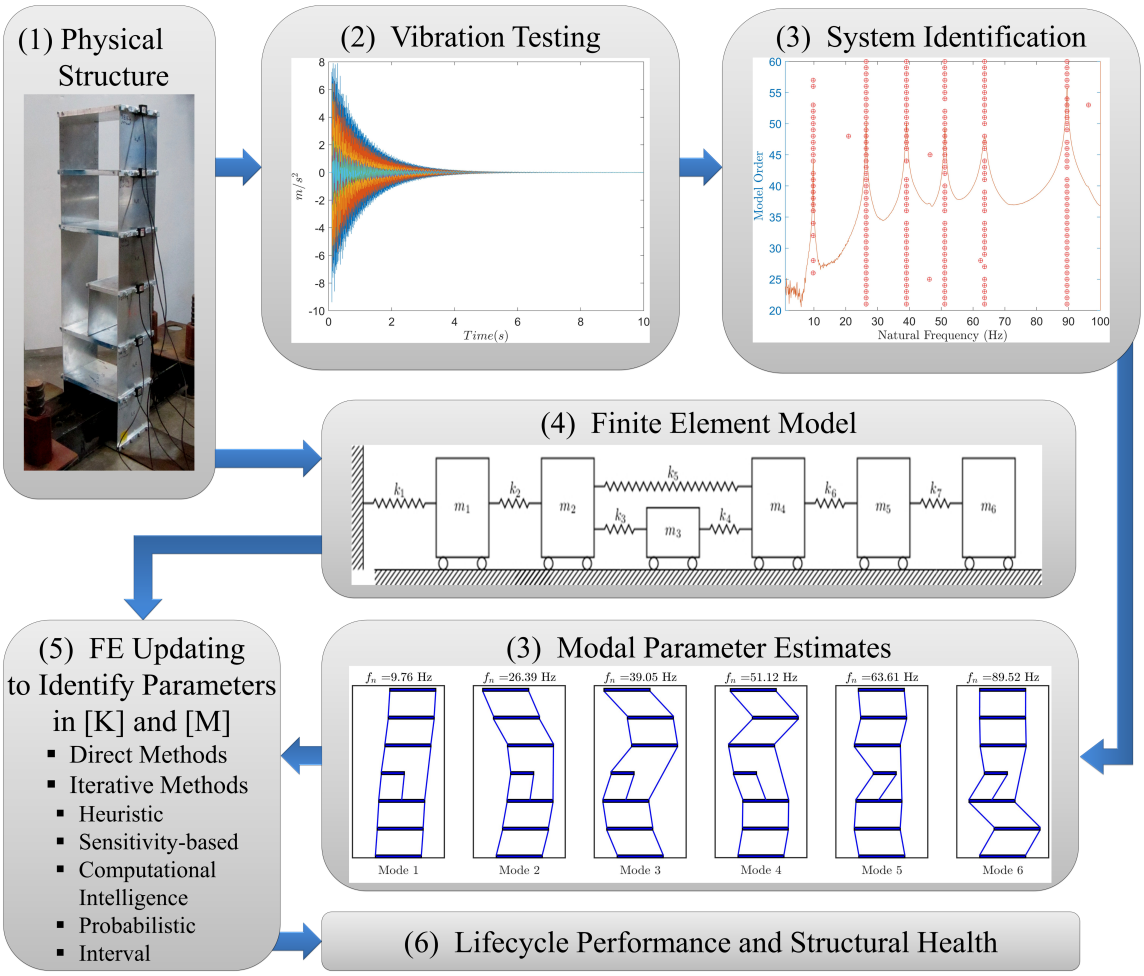


FIGURE 2.1: Flow of the structural identification process

lations between the calibrated model and the experimental measurements and can distort or bias the physical meaningfulness of the identified parameters as the changes in the parameters may be more influenced by attempts to compensate for modeling errors than to correct uncertainties in the initial parameter assumptions. This stage is also when experimental concerns such as sensor layout for the vibration test, required frequency bandwidth of the sensors and data acquisition system, and excitation regimen are formulated using the analytical model as a basis for understanding the expected modal parameters of the structure.

2.2.3 Experimental Regimen

The third stage in the St-Id process deals with application of the developed experimental regimen. Extracting quality experimental modal parameter estimates hinges on acquiring meaningful data and is directly affected by the experimental setup including: instrumentation, sampling rate, data acquisition, pre-processing and storage of data, and thorough documentation of the entire experiment (ASCE-SEI, 2011). Excitation of structures for vibration-based testing may be either ambient or controlled. Ambient excitations (wind, traffic, waves, etc.) cannot be directly measured in a meaningful way and therefore result in output-only measurement sets, while controlled, or forced excitations, can be directly measured to create input-output measurement sets. One of the main benefits of forced excitation testing is the improved signal-to-noise ratio compared to ambient vibration monitoring, which lends to easier and more accurate identification of an often larger set of experimental modal parameter estimates (Brownjohn et al., 2011). Application of ambient vibration monitoring is typically reserved for larger structures, where forced input is generally barred by logistics, cost, and/or equipment limitations. Wind is the dominant ambient source of vibration excitation for structures with low natural frequencies, such as cables and tall buildings. Highway bridges are rarely closed for testing, so traffic contributes to the ambient excitation in such cases. Smaller structures and structural components are more suitable candidates for forced vibration testing. The most common methods used to excite such structures are impulse and shaker excitation. Impulse response testing is a widely used method for forced excitation and also fairly simple to perform. An instrumented hammer capable of measuring impact force is used to excite the structure with a fixed duration

impulse (Peeters, 2000). The duration, amplitude, and quality of the impulse determines the bandwidth of structural frequencies that are excited and how well. Interchangeable hammer tips of varying hardness may be used to spread the energy of the impulse over a wide frequency bandwidth or concentrate the energy over a lower frequency bandwidth. The output response of the structure, typically measured as accelerations, may be used in conjunction with the input to develop transfer function estimates. These estimates take discrete time-domain input-output data and transform it into frequency response functions (FRFs), which provide a measure of the relative response of the system as a function of excitation. Input-output measurements provide for greater flexibility in the permitted system identification techniques, as either the input-output time histories or FRFs can be fit to provide experimental estimates of the modal parameters. One of the main advantages of using impulse excitation is the ease of deployment, since the structure does not need to be loaded by a large shaker (Reynolds and Pavic, 2000). In addition, a roving hammer technique may be used to reduce the setup and test times due to the reduced number of output sensors required (Brandt, 2011). One of the main disadvantages of this technique is that the use of an instrumented hammer relies heavily on the experience and skill of the operator. Successful testing requires repeatable, high quality impacts without double hits and without exceeding the limits of the force transducer. Also, in many cases the operator has to stand on the structure under test, which may affect modal properties due to the human structure interaction (Dougill et al., 2006). Larger civil structures that are difficult to excite with a hammer may benefit from shaker excitation, which provides several advantages including an improved signal-to-noise ratio. This is due to the fact that the excitation force occurs for a longer duration of the measurement than impact testing (Brandt, 2011). While shaker

excitation has many advantages over impact testing, there are several disadvantages. The cost of the shaker with reaction masses, power amplifiers, signal generators, and other acquisition equipment is much higher than the cost of the equipment required for an impulse hammer. Shaker excitation typically has a comparatively longer setup time as the shaker, which may be very heavy, is often repositioned throughout the test and also a larger array of accelerometers is typically used with such tests since the roving excitation technique is often impractical with a shaker.

2.2.4 Feature Extraction Through System Identification

The fourth step is post-processing of data and modal feature extraction through system identification of the acquired vibration test data. During this stage, the data is thoroughly cleansed through numerous processes, often including: filtering, averaging, windowing, and downsampling. System identification has its roots in electrical engineering and numerous algorithms are available that are either non-parametric, such as frequency domain decomposition (Brincker et al., 2001b), or physics-based. Examples of physics-based system identification techniques are the Eigensystem Realization Algorithm (ERA) (Juang and Pappa, 1985), which derives a state-space model from impulse response measurements, or subspace identification methods, such as the stochastic subspace indentification (SSI) algorithm developed by VanOverschee and DeMoor (1996). Physics-based parametric methods fit the measurement data to models based on the governing equation for dynamic motion of linear time-invariant multiple degree of freedom systems. The matrix equation is typically restated in the state-space representation and regression techniques are used to estimate the state-space model across a range of model orders. The modal properties of the system,

specifically the natural frequencies, relative damping factors, and mode shapes, may be extracted from the parametric model through eigenvalue decomposition of the state matrix. Physics-based system identification techniques have been found to yield higher quality sets of experimental modal parameter estimates than non-parametric methods when employed on civil structures (Whelan et al., 2009).

Changes in system matrices are reflected by alterations in modal properties, which allows for the modal parameters to serve as dynamic properties of the system with intrinsic value for describing the structural performance. Aktan et al. (1997) stated that if quality estimates of modal properties are extracted from experimental measurements, they have greatest potential to describe the mechanics of a system, even over static tests. This is because a modal test may yield a large number of natural frequency and mode shape estimates with corresponding measurements at each sensor location, whereas a static test provides only a single result for each sensor location. As a result, modal parameters have been extensively researched as a direct means to provide indication of damage in structures without the use of structural models. Cawley and Adams (1979), Vandiver (1975), and Coppolino and Rubin (1980) studied damage detection in structures based on changes in measured natural frequencies. However, it is generally accepted that such changes may be useful for indicating the onset of structural damage, but taken by themselves they are not appropriate for determining the location or severity of the damage (Salawu, 1997). Moreover, Catbas and Aktan (2002) stated that natural frequencies may change drastically due to changes in ambient temperature and wind, which may lead to a false indication of damage. Other studies have attempted to utilize changes in mode shape curvature for determining the presence and location of damage (Pandey et al., 1991; Wahab and Roeck, 1999; Zhong

and Yang, 2016; Roy, 2017). Although many of those attempts have proven capable of detecting damage, determining the extent of the damage in meaningful engineering units has proven difficult.

2.2.5 Model Updating

Calibration of the initial physics-based finite element model using the identified modal properties is the fifth stage of the process and the main focus of this dissertation. During this stage, multiple models should be generated as possible candidates for calibration given that modeling assumptions and engineering judgment are often insufficient to develop a single best preliminary model (ASCE-SEI, 2011). Once the set of uncertain parameters is established, the models are then calibrated by optimizing the set of those parameters such that the discrepancies between the analytical and experimentally measured modal properties is minimized. There are numerous approaches for model calibration and several of the most prominent ones are reviewed in Section 2.4.

2.2.6 Utilization of Results

The final stage in the St-Id process is the utilization of the calibrated model for decision making. Since St-Id has not transitioned into routine engineering practice, most studies thus far have stopped short of being able to affect decision making processes, with the majority culminating with a calibrated model that, again, may not be the most physically meaningful representation of the in-service structure. However, having a properly calibrated model for applications such as life-cycle analysis, health monitoring, and design verification, is paramount for advancing performance-based maintenance of civil infrastructure (ASCE-SEI, 2011).

2.3 Challenges in Structural Identification

Despite decades of research on structural health monitoring and performance of as-built structures, there are many difficulties that restrict the use of structural identification in routine engineering practice. The following subsections will outline a few of these challenges.

2.3.1 Physical Knowledge Gap

There are several issues inherent to performing a successful structural identification. As opposed to manufactured systems and aerospace structures that are often well characterized through extensive physical testing (Lo et al., 2001; Zimmerman, 2000), there are extensive uncertainties in the actual mechanical characteristics of constructed systems and components, many of which are outlined by Aktan et al. (1998b). Often boundary conditions are generalized when in reality most are neither completely free nor fixed, but have some degree of partial fixity that significantly influences the structural response. Catbas et al. (2007) stated that idealized analytical models may produce errors in structural characteristics in excess of 10 times the in-service response. The initial state and properties of as-built structures are also largely unknown, including stress/strain distributions and how these quantities vary over time (Aktan et al., 1998b). Loading conditions are also an issue of concern since they are affected by construction, traffic (Zhang et al., 2000), and environmental conditions and change over time due to settlement, deterioration, and damage. Most common applications of structural identification also assume linearity (Mottershead et al., 2011) when real constructed systems exhibit numerous mechanics of nonlinear behavior such as cracking, yielding, connection movement, or large displacements. Environmental changes also greatly affect structural behavior (Brownjohn and Xia, 2000), both over daily

temperature variations and, in particular, over seasonal changes. Furthermore, since not all structures reside in the same environment, generalizations about the effects of environmental changes on a particular type of structure are difficult to develop. Another challenge facing the field is simply the uniqueness of constructed systems since most structures are designed for specific applications. Consequently, the value proposition for St-Id is limited to the specific structure as many application-specific tasks are necessary to conduct the full process.

2.3.2 Measurement Limitations

Even with rapid advances in sensing technology, there are still several limitations related to the instrumentation of civil infrastructure for model updating. One of the most important aspects for successful model updating is deployment of a sensor network that captures a meaningful representation of the system behavior either locally, globally, or both which is why it is crucial to create an initial FE model prior to conducting any type of vibration measurements (Catbas et al., 2007). However, the measurement bandwidth of vibration transducers is limited such that often only a small portion of the eigenproperties of the analytical model can be physically obtained, thus providing partially described eigeninformation pairs (Chu and Golub, 2005). In addition to bandwidth limitations, it is not feasible to completely measure all of the corresponding degrees of freedom of a properly discretized analytical model. For models of even modest size structures, the number of sensors required to measure every degree of freedom in a sufficiently discretized finite element model is generally prohibitive. Furthermore, the direct measurement of some rows of the eigenvector, such as those associated with the rotational degrees of freedom, is not even

possible with conventional transducers (Avitabile and O'Callahan, 2003). Consequently, the experimental mode shape estimates are incomplete measurements of the eigenvectors. Given the incomplete nature of the eigenvectors, optimization of the sensor layout is important to ensure that the information obtained from the modal parameter estimates is maximized for the model calibration (Papadimitriou, 2004). This is especially true on large, complex structures due to the labor and cost associated with deployment of a dense array (Zhang et al., 2017).

2.3.3 FE Model Updating Challenges

In addition to the challenges associated with experimental modal analysis, development of the initial finite element model presents its own difficulties including: simplifying assumptions, discretization considerations, elements types, and boundary constraints (Friswell and Mottershead, 1995). Simoen et al. (2015) provides several errors that initial finite element models suffer from including:

- Uncertainties in assignments in the model. These are caused by unknown physical characteristics of the as-built structure, such as material properties and geometries. In addition, the appropriate selection of element type is a potential source of error affecting the fidelity of the model.

- Idealization errors may cause significant discrepancies between the predicted and physical behavior of the structure. Examples of this type of error are incorrect boundary conditions, lumped mass formulations, external loading assumptions, mesh connectivity, joint fixity, and non-linear mechanisms and behaviors being simplified as linear (Mottershead et al., 2011).

- Discretization/model order errors. These assumptions may be either intentional, where the practitioner makes simplifications for sake of complexity, or unintentional, where there is a lack of knowledge about the structural system. A simple example of a discretization error is the use of a coarse mesh that results in an overly stiff approximation of the structural response.

- Computational uncertainties arise from numerical approximations that are inherent in computer modeling of real-world structures. In the context of FE model updating, these result from approximations and simplifications adopted in the formation of the finite elements. However, Kennedy and O'Hagan (2001) states that this type of uncertainty should be lumped under modeling assumptions.

Traditional approaches for FE model updating have employed global optimization techniques such as those reviewed in next section. However, due to the combined influence of measurement and modeling uncertainties, the global solution may not actually be the most physically meaningful representation of the structure. Several techniques have been proposed to address this challenge by extending optimization techniques to determine alternative solutions (Beck and Au, 2002; Zárate and Caicedo, 2008; Jin et al., 2014). However, existing methods are incapable of determining *all* feasible solutions to the inverse eigenvalue problem and completely propagating measurement uncertainties to the parameter space. Other methods have been based on running multiple deterministic FE model updates to provide alternative solutions (Zárate and Caicedo, 2008) and then employing engineering judgment to determine the most plausible solution. However, such approaches can be time consuming and fail to guarantee that the alternatives found are the most meaningful and

accurate representation of the physical structure. Therefore, alternative methodologies that may be capable of determining all potential solutions satisfying a prescribed measurement confidence should be explored. In addition, the determination of the set of all plausible solutions for uncertain parameters would have the advantages of facilitating risk analysis and practitioner input for decision making. Aside from modeling uncertainties, determining the set of parameters to update in the model can be a particularly difficult challenge that affects how well the updated finite element model correlates with the measured modal properties. Improper selection of parameters to update may lead to an updated model that does not correlate well with the experimental measurements no matter what traditional updating technique is employed (Kim and sik Park, 2008). Whenever possible, ill-conditioning of the FE model updating problem should be avoided by choosing a parameter set that is sensitive to the limited vibration data available and also robust to inherent measurement uncertainty (Wan and Ren, 2015). In addition, given limited mode shape measurement, some parameters in the model may be simply unidentifiable and engineering judgment should be used in such cases to determine suitable values for those parameters.

2.4 Model Updating Techniques

Traditional model calibration techniques fall into two categories: direct and iterative. Direct methods are capable of reproducing the measured dynamic properties exactly, but the updated structural matrices are not physically meaningful for parameter identification. Since models calibrated with such methods are consequently limited in their usefulness for decision making, direct methods will not be included in the following review. Iterative methods, however, seek to update the initial model, while also retaining the matrix

structure, connectivity, and physical meaning of the parameters in the model. Under such constraints, measurement data is not reproduced exactly, but only to a certain degree of accuracy. A significant advantage of iterative approaches over direct methods is that iterative schemes are suitable for damage detection applications, since physical meaning is retained. However, it should be stated that just because parameters in the updated model have physical meaning does not necessarily mean that they are physically meaningful from a decision making point of view. This is because the inverse solution may not best represent the actual properties of the in-service structure in the presence of measurement uncertainties and modeling errors. Figure 2.2a graphically depicts the deterministic inverse identification process through which most classical approaches address model updating, wherein the measured modal properties are assumed to be correct and a single optimal solution to the inverse eigenvalue problem is sought. However, in reality experimental measurements have associated uncertainty and, furthermore, there are inherent errors in the analytical model that cannot be completely addressed by parameter calibration. Consequently, a more complete approach is sought to determine the uncertainty in the parameter space, including potential multiple solution basins, by projecting the measurement uncertainty in the inverse eigenvalue problem (Figure 2.2b).

The following subsections will provide overviews of the some of the most utilized optimization schemes employed in FE model updating and each will be applied to a small three degree-of-freedom shear building model displayed in Figure 2.3 to illustrate the effectiveness and shortcomings associated with existing techniques for structural identification. For the baseline model, the stiffnesses were assigned as $k_1 = k_2 = k_3 = 1$. Elemental contributions to the stiffness matrix from each linear elastic spring are explicitly defined in the

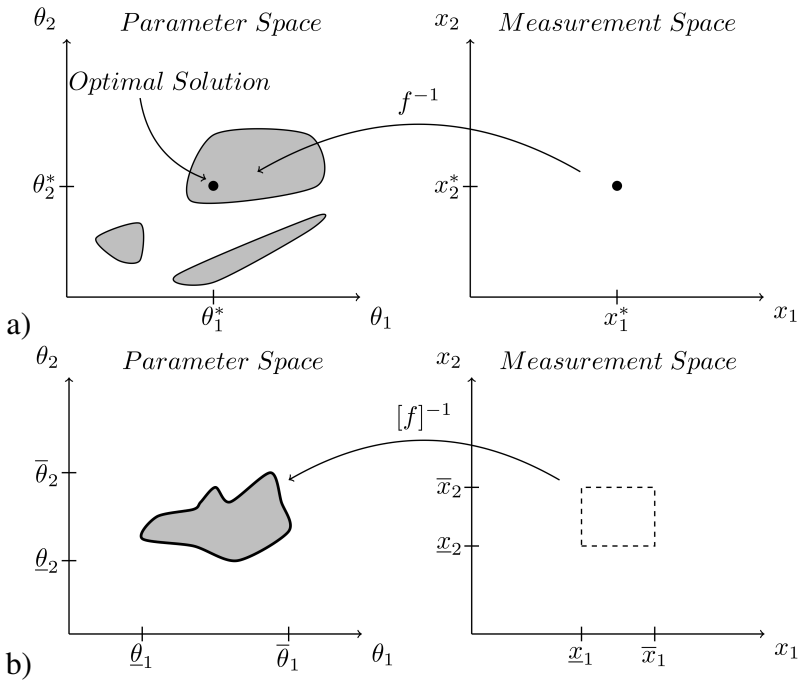


FIGURE 2.2: a) Deterministic approaches with the assumption of correctly identified modal parameters, b) propagation of measurement uncertainties to the parameter space to quantify the confidence in the parameter estimates

structural matrices. To add uncertainty to the model, 15 sets of synthetic modal parameter estimates with a standard deviation of 0.01 were generated around the natural frequencies and mode shapes corresponding to the baseline model. For each model updating scheme, it is assumed that only the first two modes of the structure are measured and that mode shape measurement is limited to degrees of freedom u_2 and u_3. Therefore, in addition to the three unknown stiffness parameters, k_1 through k_3, there are two unknown mode shape components, $\phi_{1,1}$ and $\phi_{1,2}$ for a total of five unknowns in the partially described and incompletely measured inverse eigenvalue problem. In the absence of measurement noise, there is a single unique solution to this problem since there are more equations than unknowns. However, uncertainties in the measurements, which propagate to the parameter space, can yield basins of alternative solutions.

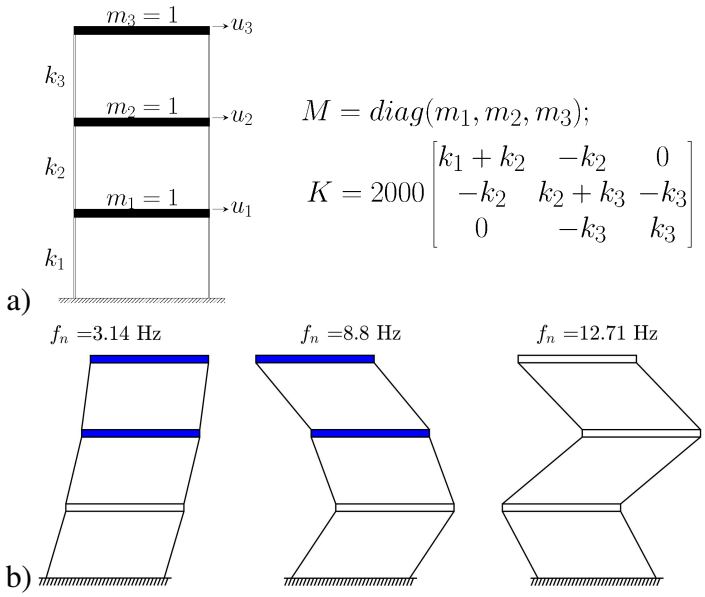


FIGURE 2.3: a) Three degree-of-freedom mass-spring system for illustrating the effectiveness of some of the most prominent model updating methods, b) Natural frequencies and corresponding mode shapes for the system (measured components are colored blue)

2.4.1 Heuristic Model Updating

Manual or heuristic model updating is the most basic approach for calibrating initial finite element models to produce better agreement with experimental measurements. The first step in most heuristic model updating approaches is to determine a limited set of parameters in the model that have the greatest effect on the modal parameters. This step is particularly critical for manual updating since the time associated with manual iterations generally precludes updating more than a few parameters in the model. This step is also useful for determining upper and lower plausible bounds for the unknown parameter assignments. The main drawback of this method is that once the sensitive parameters are selected, they are manually tuned in an attempt to reduce discrepancies between the analytical and experimentally measured modal parameters. This is especially cumbersome when

the number of uncertain parameters is large and exploration of the entire search space is impossible. While this method of calibration may produce a model that better correlates with the measured response (Catbas et al., 2007), there is no guarantee that the error will be minimized to the fullest extent possible or that the parameter identification will reflect the actual structural properties. Generally, this method has been deemed impractical for St-Id and may result in a calibrated model that is physically meaningless (Aktan et al., 1998a).

2.4.2 Sensitivity-based Methods

Several shortcomings of heuristic updating were addressed with the advent of sensitivity-based updating. In manual updating, a single parameter is perturbed at a time, which decreases the feasible domain of the search space that can be explored while increasing the amount of time necessary for calibration. With the sensitivity-based approach, multiple variables may be simultaneously updated, which drastically decreases the time needed for calibration and permits for expansion of the domain of the of search space explored. This method is based on an approximate linearization of the nonlinear relationships between parameter changes in the model and eigenproperties by first-order Taylor series expansion (Friswell and Mottershead, 1995). In short, the sensitivity-based method works by locally approximating the gradients of the modal properties in the FE model as a function of the uncertain parameters. Using this gradient, which is updated at each iteration, sensitivity-based methods can converge on an optimal solution using nonlinear optimization techniques for differentiable functions, such as Newton's method.

Mottershead et al. (2011) provides a concise overview of the sensitivity-based model updating method. The first step in this iterative method is defining the objective function,

which is formulated as an aggregated correlation of the error between the eigenproperties predicted by the model and those obtained through experimental measurements. A typical objective function can be defined using the natural frequency and mode shape residuals as:

$$J(\theta) = \sum_{r=1}^{N_m} \left[\alpha_r \left(\frac{\omega_r - \hat{\omega}_r}{\hat{\omega}_r} \right) + \beta_r \left(1 - \frac{(\hat{\phi}_r^T \phi_r)^2}{(\hat{\phi}_r^T \hat{\phi}_r) * (\phi_r^T \phi_r)} \right) \right] \tag{2.1}$$

where N_m is the number of experimental modes included in the updating scheme, $\hat{\omega}_r$ and $\hat{\phi}_r$ are the experimental natural frequency and mode shape estimates, respectively, for the r-th mode, and ω_r and ϕ_r are the corresponding natural frequency and mode shape predicted by the model with parameter assignments, θ. Additionally, α_r and β_r are weighting factors used to place significance on certain natural frequency and mode shape correlations. Note that the second term employs the popular Modal Assurance Criterion (MAC) (Allemang, 2003) for the eigenvector residuals. The frequency residuals are typically weighted more than the eigenvector residuals since greater confidence is generally placed on those in system identification, but doing so may affect the solution accuracy and uniqueness (Friswell and Mottershead, 1995). A study by Zhang et al. (2000) demonstrated that careful selection of weighting matrices may increase the accuracy of particular modes. However, there is no definitive method for choosing weighting matrices as they are largely problem dependent. After the objective function is defined, the set of parameters in the model subject to updating must be selected. The number of parameters included in the set is an important consideration, as more parameters will allow for greater correlation of the model, but leads to a more challenging optimization problem. Furthermore, having more parameters than measurements produces an underdetermined system, where the solution will be inherently non-unique. Therefore, it is wise to utilize more measurements than the number of param-

eters to produce overdetermined systems for sensitivity-based model updating. Choosing a subset of model parameters is generally aided by sensitivity analysis with the aim being to select parameters that are most uncertain by engineering judgment or knowledge and lead to the greatest changes in the modal parameters of the model (Brownjohn and Xia, 2000). Convergence on a globally optimal or even unique solution cannot be guaranteed using gradient-based optimization algorithms, such as Newton's method, so assessment of the model after updating is necessary in order to provide a minimum level of confidence before using it for simulations to inform decision making (Mottershead et al., 2011). An additional drawbacks of this method is that it can be computationally expensive as the sensitivity matrix is numerically computed using the first derivative of the eigenvalues for each parameter. Therefore, it is beneficial for the initial finite element model to be as close to the in-service structure as possible to alleviate both of these concerns (Brownjohn et al., 2001; Marwala, 2010). For cases that are ill-conditioned due to noise, a regularization parameter may need to be introduced to perturb parameters based on their sensitivities, but this places an additional layer of complexity on the problem by having to choose the regularization term (Mottershead et al., 2011). Despite its limitations, the sensitivity-based optimization method has been employed in several applications including scaled structures (Zhang et al., 2000; Moaveni et al., 2013), full-scale bridges (Teughels and DeRoeck, 2004; Brownjohn et al., 2003; Brownjohn and Xia, 2000), and damage detection (Moaveni et al., 2013).

2.4.2.1 Illustrative Example

For illustration, the technique outlined by Mottershead et al. (2011) was applied to the three degree-of-freedom example previously described. The modal parameter estimates

employed were taken as the means of the 15 sets of synthetic data to facilitate deterministic model updating. The objective function employed during the update was the same as that shown in Equation 2.1, which is a combination of the error between the analytical and experimental eigenvalues and the correlation between the eigenvectors in the form of the Modal Assurance Criterion (MAC) with equal weighting given to both residuals. In conventional sensitivity-based model updating, only a single starting point, which represents the initial best guess for the parameters, is typically used due to the computational burden of updating large FE models. This leads to a single deterministic solution, which in this case is shown to not be exactly the actual solution for the parameters, even when an initial starting point relatively close to the solution is used (Figure 2.4). Sensitivity-based model updates with a single starting point provide no indication of the confidence in the parameter estimates or the quality of the deterministic solution obtained relative to alternatives that may lie in the nearby search space. One computationally intensive approach that has been proposed to address this shortcoming is multi-start sensitivity-based model updating, where the optimization process is repeated many times using different starting points (Martí, 2003). To extend this example, 500 potential parameter sets were generated via Latin Hypercube Sampling for the three-dimensional space with lower bound, $LB = [0, 0, 0]$ and upper bound, $UB = [3, 3, 3]$. Figure 2.5a displays the starting points, which, due to the effect of measurement uncertainty, converge across a volume that reflects the apparent confidence in the individual parameters identified. Although 500 potential solutions could be mapped in a relatively short computation time of approximately 3 minutes for this very small example problem, this method lacks the ability to explicitly account for measurement uncertainties, is not capable of determining all feasible solutions to the

inverse problem, and can be very computationally expensive with larger FE models.

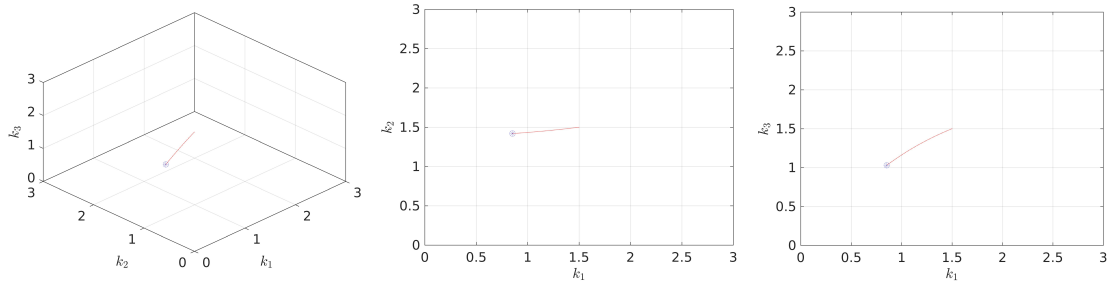


FIGURE 2.4: Sensitivity-based model updating example: Starting point (1.5,1.5,1.5) with 500 iterations (red) resulting in a single solution (blue)

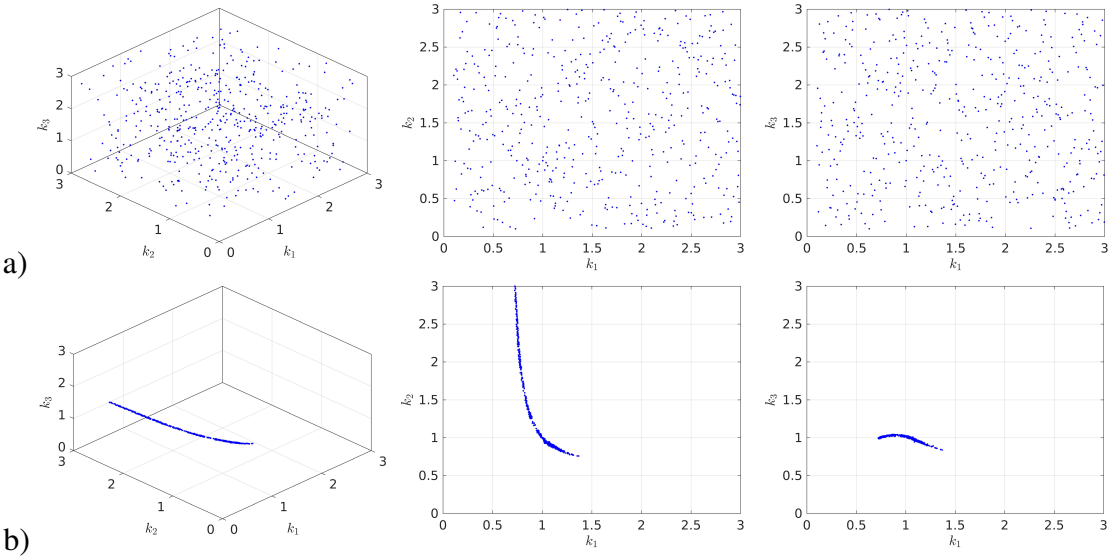


FIGURE 2.5: Multi-start sensitivity-based model updating example: a) Initial 500 starting points, b) Solution space for the different starting points

2.4.3 Computational Intelligence Methods

Modern advancements in computing have fostered the introduction of FE model updating methods aimed at more thoroughly examining the search space to encourage global optimization instead of premature convergence on a local minimum to address one of the key shortcomings of the sensitivity-based method. There are two main categories for compu-

tational intelligence techniques: machine learning and evolutionary algorithms. Machine learning includes model updating by methods such as artificial neural networks (Zapico et al., 2008) and pattern recognition (Zhu and Zhang, 2009). Despite the significance of machine learning approaches, this section will focus mainly on evolutionary strategies since they have been more commonly used in full-scale case studies (Perera and Ruiz, 2008; Ribeiro et al., 2012; Whelan et al., 2018).

Evolutionary search techniques have the ability to theoretically determine the global minimum of the objective function as opposed to previous gradient-based approaches that are prone to converging on local minima. The most prominent of these methods for FE model updating are genetic algorithms, which stems from the concepts of "survival" of the fittest and evolutionary processes proposed by Charles Darwin (Darwin, 1909). The procedure was originally presented by Holland (1975) and is formulated on the processes of natural selection, genetic inheritance, and random mutations. Over the past few decades, genetic algorithms have been used extensively to address applications in model updating and damage detection (Mares and Surace, 1996; Chou and Ghaboussi, 2001; Lu and Tu, 2005; Jung and Kim, 2013). One of the main advantages of this method as well as other computational intelligence techniques over sensitivity-based updating is that the search space does not need to be continuous because calculations of gradients are not necessary to inform the search. In addition, instead of relying on continuously optimizing a single point in the design space, genetic algorithms (along with other evolutionary-based searches) deploy a large population of plausible points that each have a fitness score computed from the objective function that are used to direct the search. Although a variety of fitness/objective functions have been proposed, a typical one takes the same form of Equation 2.1 and has

been used for FE model updating of civil structures using genetic algorithms (Caicedo and Yun, 2011; Ribeiro et al., 2012; Kernicky et al., 2014).

Figure 2.6 displays the basic algorithm for genetic algorithm processes. Typically, the initial population is stochastically generated between the provided lower and upper bounds for each uncertain parameter. Subsequent populations are generated from the previous generations based on the natural processes of reproduction, crossover, and mutation of the previous population (Mitchell, 1995). A certain number of "elite individuals," which are the parameter sets with the lowest fitness scores across the population, are chosen to automatically survive to the next generation the ensure improvement in model correlation over each generation. The algorithm continues to create new generations until the fitness of an individual parameter set satisfies a given convergence criterion, usually based on a stall in the improvement of the best fitness score or the total number of generations evaluated.

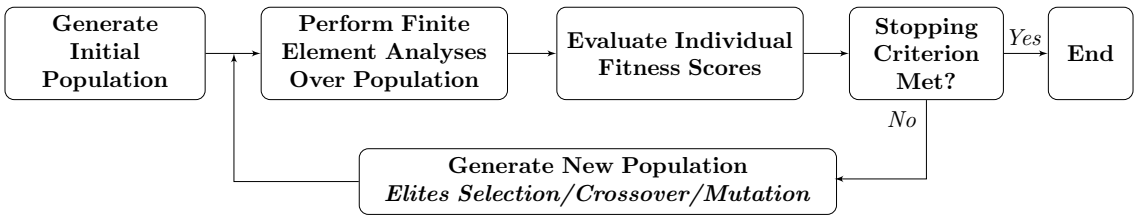


FIGURE 2.6: Flowchart of genetic algorithm process (Mares and Surace, 1996) (reproduced)

The past several decades have seen widespread application of genetic algorithms, as well as other computational intelligence methods, for St-Id. In the early 1990's, genetic algorithms were first applied to finite element model updating by Larson and Zimmerman (1993). Mares and Surace (1996) extended the use of genetic algorithms to successfully locate and quantify damage in numerical truss and beam structures and indicated that the

ability of genetic algorithms to comb the search space through parallel evaluations of the individuals in the population make it an attractive alternative to previous methods, especially if the number of uncertain parameters is significant. Friswell et al. (1998b) demonstrated the robustness of the search capabilities of genetic algorithms for detecting and locating damage in a simulated beam as well as an experimental plate using vibration data. The authors of that study performed a sensitivity-based analysis to estimate the extent of the damage and stated that, while the genetic algorithm approach is robust to errors in measurement, the populations became less diverse as the number of generations increased, which may indicate convergence on a local minimum. They also indicated that genetic algorithms tend to be very slow and should only be utilized for highly complex problems. Lu and Tu (2005) presented a case of updating a six story sway frame using a genetic algorithm combined with a sensitivity-based method to improve the accuracy of the genetic algorithm. The study included weighting matrices on the natural frequencies as well as the mode shapes and the authors stressed that the success of the parameter identification was largely dependent on the weighting factors chosen. Higher weights are generally placed on the natural frequency residuals, while lower weights are given to the mode shape residuals and, if utilized, the lowest weighting is placed on modal flexibility residuals (Li et al., 2009). Lu and Tu (2005) concluded that genetic algorithms provide a robust method for parameter identification, especially in cases such as seismic damage where parameter ranges may vary significantly since the global optimization capabilities overcome the requirement in sensitivity-based methods that the starting model is relatively close to the actual structure.

Perera and Ruiz (2008) provided a procedure to improve damage identification based

on a multi-objective genetic algorithm as opposed to traditional updating methods that define the objective function as the combined weighted error between natural frequencies and mode shapes. Two objective functions were developed using the modal flexibility matrix in conjunction with the modified total modal assurance criterion. Defining two objective functions led to the development of alternative solutions in the form of a Pareto-front instead of a single optimum. One of the main benefits of defining a multi-objective function is that choosing proper weighting factors is assisted by the information contained in the Pareto-front. Although utilizing two objective functions may be an improvement over a single function, the model correlations are still aggregated within each function. Other methods aimed at generating alternative solutions have been developed, including those that combine the computational efficiency of modern computing with so-called "human-in-the-loop" strategies. One such example is the Modeling to Generate Alternatives (MGA) approach proposed by Zárate and Caicedo (2008). The basis of the method presented is that an initial solution can be determined through genetic algorithm and then a search perpendicular to that solution can be performed by minimizing a secondary objective function to find alternative solutions with similar performance characteristics. In that study, the authors contend that the global solution may not be the best representation of the physics of a structure due to parameter uncertainty, modeling and numerical errors, and sensing limitations.

Franco et al. (2004) proposed an alternative to genetic algorithm called evolutionary strategy and stated that it may be superior based on its "self-adaptation" ability. Whereas individuals in genetic algorithms are characterized by a set of parameters, individuals in evolutionary strategy have a secondary set of values defined as the standard deviation of

the parameters of each individual. This second characteristic vector controls the evolution of the associated parameters and may speed up convergence. The study concluded that evolutionary strategy tends to outperform genetic algorithm in cases with reasonable noise, but may not perform as well when the number of outputs is relatively small and the measurements are corrupted by a significant amount of noise. The authors also indicated that genetic algorithm may find the region of the global minimum more easily than evolutionary strategy, but that once the region is established, evolutionary strategy is able to approach the global minimum more accurately. However, they also state that genetic algorithm may be better suited for escaping local minima, whereas evolutionary strategy may be more prone to convergence on a local minimum.

One of the biggest complications with evolutionary optimization strategies is that the search space is directly linked to the number of selected unknown parameters as well as the bounds chosen over those variables. The larger the search space, the longer it takes for the model to converge to the global solution. Given this fact, several studies have attempted to develop ways to adaptively reduce the search space over time in order to focus on more favorable parameter sets. The idea is that if the deviation of a parameter over all individuals in a population is relatively small, then the bounds on that variable may be reduced allowing for faster convergence (Perry et al., 2006). Other researchers have implemented parallel genetic algorithms to address the computational time with increased computational power (Whelan et al., 2018). In addition to genetic and evolutionary strategy algorithms, other methods that mimic natural processes have been proposed for model updating including particle swarm (Marwala, 2010), artificial bee colony (Sun et al., 2013; Ding et al., 2016), simulated annealing (Marwala, 2010), and fish school search optimization (Boulk-

abeit et al., 2013). The use of genetic algorithms for St-Id continues to remain as one of the most commonly used techniques for producing calibrated models with good agreement between the analytical and experimental results. It is still an active area of research and has been applied in recent years to model updating of railway bridges (Ribeiro et al., 2012), scaled bridge structures (Jung and Kim, 2013), railway vehicles (Ribeiro et al., 2013), and damage detection in buildings subject to extreme loads (Kernicky et al., 2014). Despite the increasingly large set of case studies supporting the use of computational intelligence strategies for structural identification, persistent challenges remain related to the computational efficiency, efficient and complete generation of alternative solutions, and ability to account for measurement uncertainties and model errors. These shortcomings will be illustrated in the following example.

2.4.3.1 Illustrative Example

For illustration, a genetic algorithm was applied to the three degree-of-freedom example first using only a single starting population and then with 500 separate starting populations. In both analyses, the populations consisted of 50 individuals each with 5 elites surviving over the course of 200 generations with a crossover fraction of 0.8. For both cases, the fitness value was calculated for each individual in the population using a combination of the residual of the experimental and analytical eigenvalues and the correlation of the eigenvectors through Equation 2.1. Note that equal weights were given to the natural frequency and mode shape correlations. Again, the modal parameter estimates were taken as the mean across the 15 sets of synthetic data for the first two modes and the eigenvector measurement was limited to degrees of freedom u_2 and u_3. For simplicity, direct pairing of the

modes was forced. For the first case, where only a single genetic algorithm was employed, several intermediate generations as well as the final result are presented in Figure 2.7. It is apparent that even with the benefit of evaluating more than a single point for optimization, the final result is highly dependent on the initial starting population. The initial population shrinks as the number of generations increases and finally clusters around the final solution, which does not, however, represent the actual parameters used to generate the noisy synthetic data. To extend the genetic algorithm to a multi-start implementation, the second case employed 500 separate genetic algorithm optimizations. Figure 2.8 displays the optimal solution for each of the 500 separate genetic algorithm optimizations. While the results agree well with the sensitivity-based approach previously shown in Figure 2.5, the genetic algorithm updating approach is not capable of determining every feasible solution while explicitly accounting for measurement uncertainty across the 15 sets of synthetic data.

The results of this example demonstrate several of the shortcomings of using genetic algorithms for structural identification in the presence of measurement uncertainty. For the single genetic algorithm optimization, the population lost diversity as the number of generations increased and mutation did not yield adequate searching outside of the local minimum. Furthermore, while it is theoretically possible to determine the global solution, the time required to reach the global minimum is dependent on several parameters including: population size and diversity, number of elite individuals chosen to survive to the next generation, crossover fraction to generate new individuals from the elites, and random mutation to foster diversity and prevent convergence to a local minimum. In addition, the objective function used to evaluate the fitness of each individual aggregates model correlations as in the sensitivity-based method. Also, while the computational time was relatively

short for this example, employing genetic algorithms to larger FE models can be cumbersome.

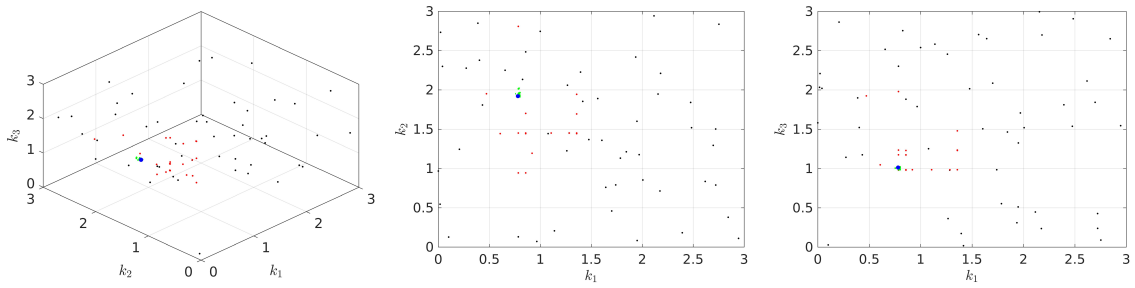


FIGURE 2.7: Genetic algorithm model updating example: Populations for the first generation (black), 10th generation (red), 20th generation (green), and best solution (blue)

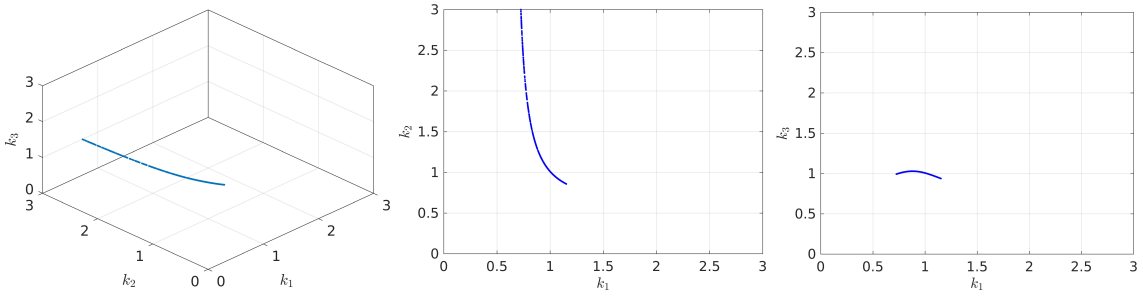


FIGURE 2.8: Multi-start genetic algorithm model updating example: Solution space for the genetic algorithm updating procedure for 500 different starting populations

2.4.4 Probabilistic Model Updating

The model updating methods previously discussed typically use nominal or single values for parameter assignments without regard to the confidence that may be placed on the final determination of the parameters to use in the calibrated model. Introducing probabilistic analysis into the updating scheme reduces the amount of engineering judgment and subjectivity that is necessary when addressing difficulties such as selection of uncertain parameters, defining satisfactory stopping criterion, and interpretation of final results (Dascotte, 2003). The main benefit of probabilistic approaches is that instead of determining

a single best solution, statistical methods are employed to provide a family of potential structural models (Beck and Au, 2002). One of the most popular methods for probabilistic model updating is the Bayesian inference approach, which combines prior knowledge of the structure with observed vibration data through statistical analysis. In this method, models are described based on probability distributions of the uncertain parameters along with some prediction error. The foundation of the Bayesian method is stated as

$$P(\{E\}|[D]) = \frac{P([D]|\{E\})P(\{E\})}{P([D])} \tag{2.2}$$

where $P(\{E\})$, known as the prior distribution, is the probability distribution function (PDF) of the set of updating parameters, E, without regards to the measurement data, $P([D]|\{E\})$ is the likelihood distribution function with regards to the measurement data, $[D]$, $P([D])$ is a normalization factor, and $P(\{E\}|[D])$ is the posterior distribution function with regards to the measurement data. Bayesian model updating approaches rely on a likelihood function to quantify model correlation. When modal data is used, the likelihood function includes a modal measure of fit function that incorporates an objective function for the natural frequencies and an objective function for the partially described mode shapes. For illustration, a commonly used modal measure of fit, provided by Vanik et al. (2000), is:

$$J(\theta) = \sum_{r=1}^{N_m} \sum_{j=1}^{N_s} \left[\left(\frac{(1 - \hat{\omega}_{r,j}^2/\omega_r^2)^2}{\epsilon^2} \right) + \left(\frac{\phi_r^T (I - \hat{\phi}_{r,j}\hat{\phi}_{r,j}^T)\phi_r}{\delta^2 ||\phi_r||^2} \right) \right] \tag{2.3}$$

where N_m is the number of modes included in the identification, N_s is the number of sets of modal data, $\hat{\omega}_{r,j}$ and $\hat{\phi}_{r,j}$ are the experimental natural frequency and incomplete mode shape, respectively, for the r-th mode of the j-th data set, ω_r and ϕ_r are the corresponding

natural frequency and incomplete mode shape for the model with parameter assignments θ, and ϵ and δ are parameters that reflect the uncertainty in the experimentally measured natural frequencies and mode shapes, respectively.

Since probabilistic model updating is capable of providing an optimal set of updated model parameters along with their distributions to quantify uncertainty, it has been heavily pursued in recent years. Beck and Katafygiotis (1998) first presented a general framework for Bayesian model updating for a relatively small number of uncertain parameters that was later extended by Beck and Au (2002) to include sampling techniques such as Markov Chain Monte Carlo (MCMC). Vanik et al. (2000) demonstrated that the method is capable of providing updated probability distributions of uncertain model parameters in addition to damage identification for structural health monitoring purposes. While the approach has also been successfully employed for damage detection on benchmark structures, it may lead to unidentifiable solutions when the data is limited (Yuen et al., 2004). Marwala et al. (2007) provided a study comparing the Maximum-likelihood method using a genetic algorithm with the Bayesian inference method using MCMC and concluded that, while both methods had the same computational efficiency, the Bayesian method provided a more accurate representation of the modal properties. A new Gibbs sampling method was presented by Ching et al. (2006) and later extended by Bansal (2015) for model updating linear systems using real valued modal data. Zhang et al. (2013) utilized an advanced Markov Chain Monte Carlo approach combined with a Delayed Rejection Adaptive Metropolis algorithm for model updating of a grid structure and concluded that the success of Bayesian inference relies heavily on choosing appropriate stochastic simulation methods. The work by Ching et al. (2006) was expanded by Cheung and Bansal (2017) to include incomplete complex

modal data and was applied to a 120 degree-of-freedom structure with 614 uncertain parameters. However, it was stressed that the use of Gibbs sampling does not lead to locally identifiable solutions where the sample models may get trapped in the neighborhood of a single optimal point. Hybrid techniques using computational intelligence based optimizations have also been developed to side step the need for directly computing the PDFs (Sun and Betti, 2015). Behmanesh et al. (2015) applied a Hierarchical Bayesian framework to predict total parameter uncertainty, which includes a measure of parameter estimation uncertainty and a measure of the inherent structural parameter variability.

Despite the numerous applications to a wide range of problems with varying sampling techniques, there are several major drawbacks associated with the use of the modal measure of fit in Bayesian model updating. An example in Chapter 5 will illustrate that the calibration results tend to be very sensitive to the weighting coefficients, ϵ^2 and δ^2, that express the relative importance of the modal frequency and partially described mode shape correlations to the objective function (Goller et al., 2012). In addition, direct matching of modes is required, which Sun and Büyüköztürk (2016) indicates can be challenging with incompletely measured mode shapes. Finally, the modal measure of fit function aggregates the model correlations in the same manner as the sensitivity-based method and computational intelligence techniques outlined previously. In this way, it can not ensure that each of the individual modal parameters of the identified model are consistent with the experimental measurements within prescribed uncertainty bounds. Additional challenges associated with Bayesian model updating stem from the need to solve multidimensional integrals that cannot be solved analytically, which increases computational cost. A favored approach, particularly for models with many parameters, has been to leverage stochastic

simulation methods, such as Metropolis-Hastings or Gibbs sampling, to develop the posterior probability density functions for the uncertain parameters. However, leveraging these approaches introduces an additional challenges. Since the parameter space is evaluated by discrete sampling, the development of posterior joint probability distribution functions can be computationally intensive, particularly if either the size of the model or the uncertainty in the prior distributions is large. Second, the specification of the prior distributions influences the development and accuracy of the posterior probability distribution functions (Beck and Au, 2002). Transitional, or adaptive, methods have been introduced to address this later challenge by converging on the posterior distribution through intermediate probability distribution functions (Ching and Chen, 2007). However, these methods introduce additive complexity and computational cost. Lastly, stochastic simulation methods are sensitive to user specified settings, such as the number of iterations before adaptation of the intermediate probability distribution functions, and cannot guarantee complete exploration of the parameter search space and complete mapping of feasible solutions.

2.4.4.1 Illustrative Example

To illustrate the use of Bayesian model updating, the three degree of freedom system displayed in Figure 2.3 will again be utilized. However, unlike the previous illustrations, the entire set of 15 modal parameter estimates is employed in the modal measure of fit. For Bayesian model updating, an adaptive Metropolis-Hastings Markov Chain Monte Carlo method was used to sample posterior probability distribution functions with a likelihood function incorporating the modal measure of fit function, used by Vanik et al. (2000), presented in Equation 2.3.

A uniform prior distribution was assigned to the three uncertain parameters in the model over the range [0,3]. To demonstrate the how the relative weighting terms affect the solution space, three separate cases were examined. For the first case, the relative weighting coefficients were prescribed such that the mode shape correlations were weighed greater than the natural frequency correlations. The posterior distribution for this probabilistic update is displayed in Figure 2.9a. Conversely, the relative weighting coefficients were prescribed in the second case such that the natural frequency correlations were weighed greater than the mode shape correlations (Figure 2.9b). Lastly, the third case provided a balanced weighting of natural frequency and mode shape correlation terms in the modal measure of fit function, which is more representative of the multi-start solutions obtained by the optimization schemes employed in the prior subsections. This case yields the posterior distribution illustrated in Figure 2.9c. The Metropolis-Hastings Markov Chain Monte Carlo method used to perform the updating took approximately 14 seconds to converge on the posterior distribution presented in Figure 2.9c using 20,000 sample parameter contributions. However, this computational time does not include the time required to choose appropriate weighting factors for the modal fit. The advantage over the previous illustrations is clear as the method is capable of providing a more complete definition of the uncertain parameter space, but the ability to map out *all* feasible solutions is still lacking and the approach is still disadvantaged by the reliance on an aggregated objective function.

2.4.5 Interval Methods

An alternative to probabilistic methods for accounting for structural uncertainties is to use interval methods (Köylüoğlu et al., 1995). Interval arithmetic and interval analysis

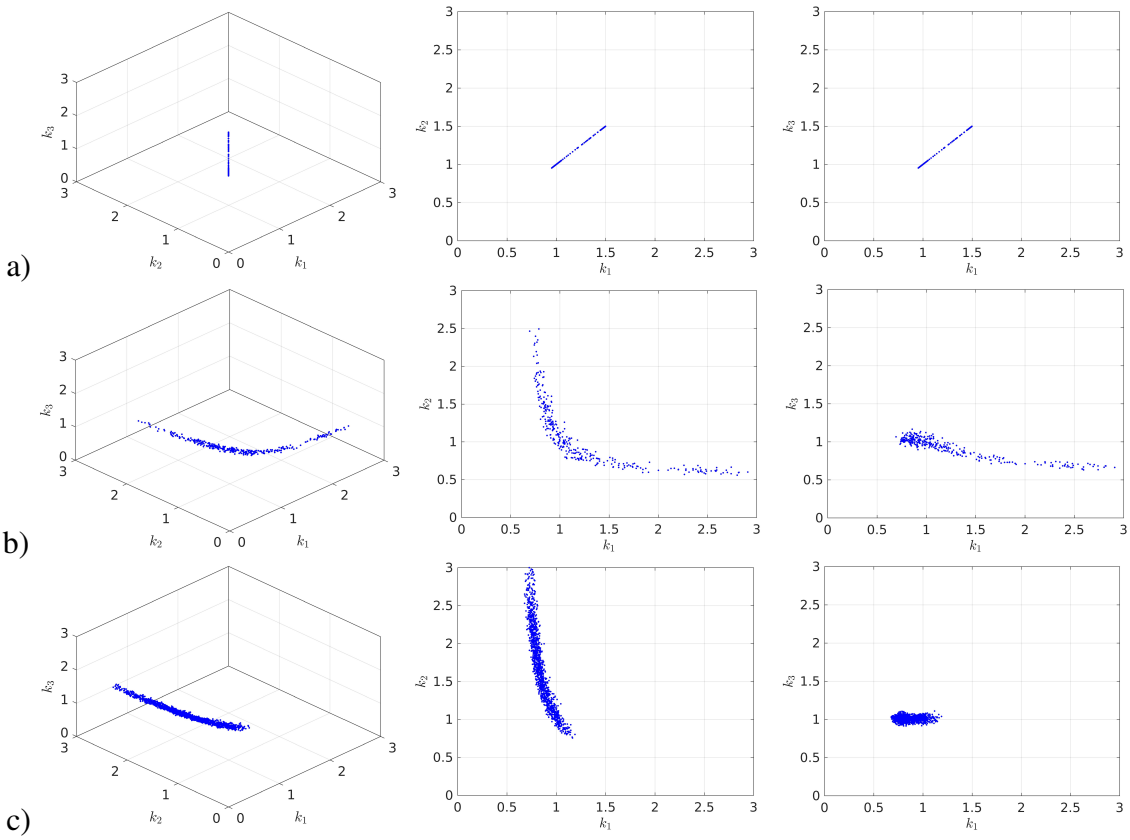


FIGURE 2.9: Samples for the posterior distribution obtained from Bayesian model updating of three degree of freedom model: a) mode shape correlation over-expressed in the measure of fit, b) natural frequencies over-expressed in the measure of fit, c) balanced expression of natural frequencies and mode shapes in the measure of fit

techniques will be extensively reviewed in Chapter 3. Interval analysis techniques have an advantage over probabilistic methods in that they do not require information about the probability density functions of uncertain parameters. Thus, interval methods have been pursued as a way to combat measurement and modeling uncertainties. However, a survey of non-probabilistic approaches by Moens and Vandepitte (2005) investigated interval finite element analysis and indicated that non-probabilistic approaches disregard statistical analyses and may present an overly conservative estimation of the solution set. The authors also suggested that non-probabilistic methods be used in conjunction with proba-

bilistic methods. García et al. (2008) developed a technique for combining interval analysis with constraint propagation for condition assessment of a full-scale bridge with static test data. In addition, Wang et al. (2012) employed interval analysis for damage detection using static displacement measurements and, in a subsequent study, (Wang et al., 2013b) included measured natural frequencies as well for damage detection using a membership-set identification (MSI) method. The authors of the latter study indicated that the MSI method is superior to the overly-conservative interval analysis method. In addition to measured natural frequencies, Wang et al. (2013a) also included uncertain acceleration responses for damage detection and determined that the addition of the dynamic response improved the accuracy of the damage identification. Khodaparast et al. (2011) explored replacing the FE model with a meta-model using the Kriging predictor for model updating, which was implemented successfully for interval model updating of a three degree-of-freedom mass-spring system. The authors of that study stated that the use of meta-models has a distinct advantage over traditional probabilistic methods in that it does not require an exorbitant amount of simulations. One limitation of the study was that mode shapes were not taken into account. However, Fang et al. (2015) presented a stochastic model updating method that adopted the use of eigenvalues as well as eigenvectors. The authors of that study indicated that the proposed interval response surface method (IRSM) provided higher precision than the Kriging predictor and that it was more computationally efficient given that interval arithmetic operations are easily performed on the response surface model.

While the above studies have been instrumental in addressing the uncertainties associated with model updating, the work presented by Gabriele and Valente (2009) is most closely related to the methods employed in this dissertation. In that study, modal proper-

ties were prescribed as intervals and the updating was performed using branch and bound processes until the prescribed modal intervals were encompassed by the interval modal properties (Modares et al., 2006) of the interval FE model. Gabriele (2011) extended the interval intersection method for model updating to include mode shape comparisons through the modal assurance criterion (MAC). The updating was again based on branch and bound techniques and, while successful, the authors concluded that the convergence is slow compared to sensitivity-based optimization techniques.

2.4.5.1 Illustrative Example

The interval updating process outlined by Gabriele (2011) was applied to the selected three degree of freedom example where the problem was to find k_1, k_2, and k_3 such that the measured interval natural frequencies were contained within those of the interval FE model. The interval natural frequencies applied were developed around the mean of the 15 synthetic measurements as $f_i = [f_i^{avg} - \sigma_i, f_i^{avg} + \sigma_i]$. As in the previous examples, only the first two modes of the system are employed such that $f_1 = [3.1393, 3.2099]$ and $f_2 = [8.7961, 8.9941]$. In addition, the synthetic measurement of the mode shapes was limited to only degrees of freedom u_2 and u_3. The branch and bound process was applied recursively starting with an initial parameter space, $[\boldsymbol{k}] = k_1 \times k_2 \times k_3 = [0, 3] \times [0, 3] \times [0, 3]$, which was branched into sub-domains that were retained if the interval natural frequencies of the finite element model fully encompassed the experimental ones, exhibited high MAC correlations (≥ 99.99), and also met the prescribed interval precision of 0.01 on the stiffness terms. If the first two conditions held, but the precision had not been met, the sub-domain was bisected along the dimension with the greatest width and the process continued. How-

ever, if the sub-domain did not exhibit the inclusion of the frequencies or did not have an acceptable MAC, it was discarded. Figure 2.10 displays the obtained interval solutions, which agree well with the results of the previously applied methods. In all, 2,829 solutions were generated from a total of 191,525 box evaluations in approximately 4.5 minutes. It should be noted that, while this branch and bound technique is capable of including uncertainty in the measurement and parameter spaces to completely map the feasible solution set through the use of intervals, it is much slower than the other methods reviewed and would be computationally inefficient with increases in problem dimensionality.

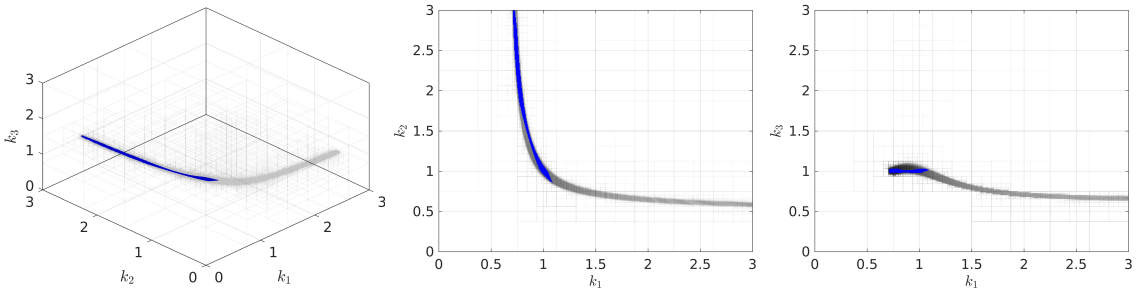


FIGURE 2.10: Parameter domain for the three degree-of-freedom interval finite element model update depicting all boxes evaluated as well as the solutions (blue)

One of the main challenges posed by constraint satisfaction problems is that they are generally non-polynomial and the computational complexity to solve them is NP-hard. NP or *nondeterministic polynomial time* problems do not run in polynomial time on a standard computer meaning that the *brute force* method of trying all possible combinations of parameters is virtually impossible. However, solutions to NP problems can be checked in polynomial time. NP-hard is a class of problems which are at least as hard as NP problems. A classic NP-hard example is the traveling salesman problem. Much research has been performed to decrease the computational burden of NP problems. One such effort is

the *backtrack algorithm* outlined by Golomb and Baumert (1965). It is the most common search in practice and aims to lessen computational effort with the added benefit of being exhaustive. Backtracking performs a depth-first search where one variable is assigned at a time and the algorithm backtracks up the search tree when a variable assignment violates some constraint(s). This type of search differs from other learning programs or hill-climbing search methods which simply move to another vector adjacent to the most recent in order to improve the solution. Although backtracking provides significant speed up compared to generating and checking all possible solutions with the brute force method, it has been shown to exhibit *thrashing* behavior or repeated searching of failing subtrees of the search space (Rossi et al., 2006) which drastically affects runtime.

2.5 Concluding Remarks

Rapid advancements in computing have fostered increased attention on structural identification for the development of high-fidelity analytical models calibrated with experimental measurements. Many case studies have applied numerous model updating strategies in attempts to determine the actual in-service performance of structures, but most case studies have failed to completely address many of the inherent challenges associated with model updating that have been summarized, which has hampered the transition of St-Id into everyday engineering practice. To facilitate the advancement of St-Id as a viable tool for performance-based condition assessment, this dissertation will develop methodologies for parameter identification of continuous and multiple degree-of-freedom system models using constraint programming with interval arithmetic to address many of the underlying challenges within model updating, condition assessment, and damage identification.

CHAPTER 3: INTERVAL ANALYSIS AND CONSTRAINT PROGRAMMING

3.1 Introduction

In the engineering sciences, experimental computations are rarely exact, especially when data is corrupted with noise. Furthermore, the finite element model updating problem introduces additional errors in the form of modeling uncertainties and idealizations. As outlined in Chapter 2, many of the traditional updating techniques do not account for such uncertainties and culminate with a single solution to the inverse problem. Although it may be much "nicer" to state the solution set for the parameters as exact values, doing so provides no information on the overall confidence in the individual parameter estimates and gives no means for examining alternative solutions that may be more physically meaningful than the global minimum to an objective function. In this dissertation, interval analysis is used to bound measurement uncertainties and interval set inversion methods are applied to propagate these uncertainties to the parameter space of the partially described and incompletely measured inverse eigenvalue problem central to FE model updating. This chapter provides an overview of interval analysis, which is based on the idea of representing numbers as intervals and sets as interval vectors or boxes, and the preliminaries necessary to understand techniques for solving inverse problems through set inversion using interval methods. A brief primer on intervals and interval arithmetic will be presented followed by a discussion of the methods utilized to cast the structural identification problem as one of constraint

satisfaction with interval arithmetic and contractor programming.

3.2 Interval Analysis

Interval analysis in the modern era was first introduced by Moore (1962) to place strict bounds on digital computations and avoid computationally expensive analysis of errors accumulated during computation. The advantage being that by employing intervals instead of finite numbers, both the computation and error bounds are computed at the same time. The following subsections provide a short synopsis of the theory of interval analysis necessary to understand the contribution of the dissertation, but the interested reader is referenced to foundational work by Moore (1966) and his most recent textbook (Moore et al., 2009), which provides the basics of interval analysis with emphasis on modern applications.

3.2.1 Intervals

An interval, $[x]$, is a subset of the real numbers, $\mathbb{R}$, that can be represented using a pair of real numbers $[x_1, x_2]$ to denote the set of all real numbers within the range, $x_1 \leq x \leq x_2$ (Moore, 1966). In set notation, an interval is defined as

$$[x_1, x_2] = \{x \in \mathbb{R} : x_1 \leq x \leq x_2\} \tag{3.1}$$

The endpoints, or lower and upper bounds, of an interval are represented as $\underline{x}$ and $\overline{x}$, respectively, such that $[x] = [\underline{x}, \overline{x}]$. If the endpoints of an interval are equal, the interval is known as *degenerate* and may be represented as a single real number. In this sense, interval arithmetic is an extension of real arithmetic. Although there exist many applications in mathematics where open or half-open intervals are of importance, all intervals referred to herein will be closed and connected. Connected means that the interval does not contain

gaps between the lower and upper bounds and closed means that the interval contains its endpoints (Lipschutz, 1965). The set of all such intervals over the real numbers will be denoted by $\mathbb{IR}$. For example, while $[1, 5] \cup [10, 13]$ is a subset of $\mathbb{R}$, it is not connected.

3.2.2 Interval Arithmetic

The basic operations performed in real arithmetic may be expanded to include intervals such that arithmetic operations performed on intervals create sets (Moore et al., 2009). A simple example is the addition of two intervals, which yields a set that contains the sums of all pairs from the initial intervals. Generally speaking interval operations may be expressed as

$$[x] \odot [y] = \{x \odot y : x \in [x], y \in [y]\} \tag{3.2}$$

where $\odot$ represents the binary operations of multiplication, division, addition, and subtraction. The definitions for the endpoints of the interval developed by each binary operation are listed in Table 3.1 for two intervals, $[x] = [\underline{x}, \overline{x}]$ and $[y] = [\underline{y}, \overline{y}]$. Note that for division it is required that $0 \notin [y]$. The derivations of these endpoint formulas for each operation may be found in Moore et al. (2009).

Table 3.1: Endpoint formulas for binary arithmetic operations

Operation	Lower Bound	Upper Bound
$[x] + [y]$	$\underline{x} + \underline{y}$	$\overline{x} + \overline{y}$
$[x] - [y]$	$\underline{x} - \overline{y}$	$\overline{x} - \underline{y}$
$[x] \cdot [y]$	$min\{\underline{x}\underline{y},\ \overline{x}\underline{y},\ \underline{x}\overline{y},\ \overline{x}\overline{y}\}$	$max\{\underline{x}\underline{y},\ \overline{x}\underline{y},\ \underline{x}\overline{y},\ \overline{x}\overline{y}\}$
$[x]/[y]$	$\underline{x} \cdot 1/\overline{y}$	$\overline{x} \cdot 1/\underline{y}$

3.2.3 Set Operations

Since intervals are simply sets of real numbers, traditional set operations may be performed. Suppose we have two intervals, $[x]$ and $[y]$. The *union* of these two intervals, $[x] \cup [y]$, is defined as the set of all elements that belong to either interval:

$$[x] \cup [y] = \{z \in \mathbb{R} \mid z \in [x] \; or \; z \in [y]\} \tag{3.3}$$

However, the resulting set is not guaranteed to be closed and connected. To ensure that the union of two intervals is closed and connected, the *interval hull* is defined as the smallest interval that contains both intervals such that

$$[x] \sqcup [y] = [min\{\underline{x}, \underline{y}\}, max\{\overline{x}, \overline{y}\}] \tag{3.4}$$

It is therefore easy to see that the union of two intervals is a subset of the interval hull of the two intervals. The *intersection* of two intervals, $[x] \cap [y]$, is the set of all elements that belong to both intervals:

$$[x] \cap [y] = \{z \in \mathbb{R} \mid z \in [x] \; and \; z \in [y]\} \tag{3.5}$$

If the intervals $[x]$ and $[y]$ are closed and connected, their intersection is also guaranteed to be closed and connected. In such cases, the intersection of two closed intervals may be represented by the interval endpoints as

$$[x] \cap [y] = [max\{\underline{x}, \underline{y}\}, min\{\overline{x}, \overline{y}\}] \tag{3.6}$$

In application, set operations on intervals along with interval function operations provide the basis for generating solution sets for mathematical problems solved through interval

analysis.

3.2.4 Interval Vectors

The Cartesian product of intervals creates an n-dimensional box, or interval vector, that belongs to the set $\mathbb{IR}^n$ (Jaulin et al., 2001) . This product is defined as

$$[\boldsymbol{x}] = [x_1] \times [x_2] \times \cdots \times [x_n] \tag{3.7}$$

and is visually illustrated in Figure 3.1 as a three dimensional box created by the product of three intervals $[x_1], [x_2]$, and $[x_3]$. In the same way that set operations were defined for ordinary intervals, many of the same operations may be extended to interval vectors. For example, the intersection of two interval vectors $[\boldsymbol{x}]$ and $[\boldsymbol{y}]$ may be expressed as

$$[\boldsymbol{x}] \cap [\boldsymbol{y}] = ([x_1] \cap [y_1], \ldots, [x_n] \cap [y_n]) \tag{3.8}$$

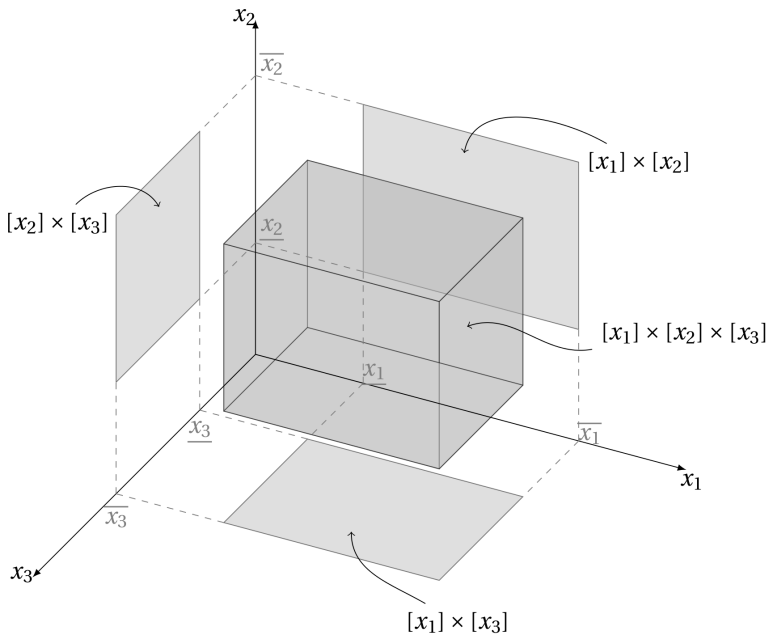


FIGURE 3.1: The Cartesian product of three intervals creates box $[\boldsymbol{x}] \in \mathbb{IR}^3$.

The *width* of a box, or interval vector, is defined as the length of the longest edge of the box, $w([\boldsymbol{x}]) = max(\overline{x_i} - \underline{x_i})$ and the *midpoint* is defined as $m([\boldsymbol{x}]) = [m(x_1), m(x_2), ..., m(x_n)] = \left[\frac{\underline{x_1}+\overline{x}_1}{2}, \frac{\underline{x_2}+\overline{x}_2}{2}, \frac{\underline{x_3}+\overline{x}_3}{2}, ..., \frac{\underline{x_n}+\overline{x}_n}{2}\right]$.

3.2.5 Interval Functions

In addition to elementary interval operations, functions may also be applied to intervals and interval vectors by replacing each variable with an interval and each operation by its interval extension (Moore et al., 2009). This is important for understanding the basis of interval analysis and its extension to constraint satisfaction. A function may be applied to an interval or box such that

$$f([\boldsymbol{x}]) = \{f(x) : x \in [\boldsymbol{x}]\} \tag{3.9}$$

Essentially, a function, f, maps every component of the interval to its image, $f([\boldsymbol{x}])$. However, applying functions to intervals and interval vectors must be done carefully and, unlike real arithmetic, the functional form affects the resulting image. These considerations will be illustrated in the following subsection.

3.2.6 Inclusion Functions

The image of a box, $f([\boldsymbol{x}])$, may take any shape and even be disconnected as seen in Figure 3.2. Consequently, the exact volume represented by the image, $f([\boldsymbol{x}])$, can often not be strictly defined by an interval vector since all interval vectors are strictly boxes. To deal with this fact, the concept of an *inclusion function* is introduced which computes a box, $[f]([\boldsymbol{x}])$, guaranteed to contain $f([\boldsymbol{x}])$ (Ratz, 1996). This inclusion function allows

for the box to serve as a conservative estimate of the image, $f([\boldsymbol{x}])$, and further allows for the representation of the image to be manipulated via the arithmetic and set operations of interval analysis. Formally, given a function f from $\mathbb{R}^n$ to $\mathbb{R}^m$, the inclusion function for f is a box, $[f]$, from $\mathbb{IR}^n$ to $\mathbb{IR}^m$ that ensures

$$\forall [\boldsymbol{x}] \in \mathbb{IR}^n, f([\boldsymbol{x}]) \subset [f]([\boldsymbol{x}]) \tag{3.10}$$

The main advantage of inclusion functions is that they essentially wrap generic set images into outer approximations allowing for quick evaluation for many different classes of functions (Jaulin et al., 2001). However, when the functions involve multiple instances of the same variable, the interval computation may result in an overly conservative or pessimistic representation of the actual set image. This pessimism may be reduced by carefully transforming the function to reduce the number of occurrences of each variables. A minimal inclusion function, $[f]^{min}([\boldsymbol{x}])$, is one that provides the most compact estimate of the image and is formulated by reducing the number of occurrences of each variable in a continuous function as much as possible.

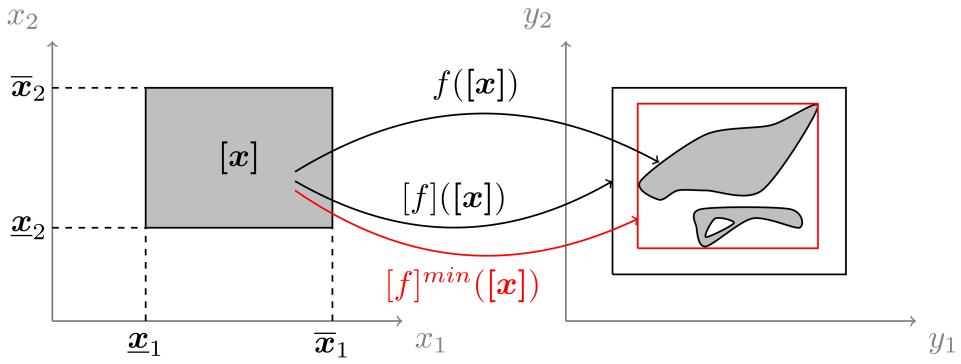


FIGURE 3.2: Images of $[\boldsymbol{x}]$ by f for a pessimistic inclusion function, $[f]([\boldsymbol{x}])$ and a minimal inclusion function, $[f]^{min}([\boldsymbol{x}])$

For example, while $y^2-5y+2x^2-3$ and $(y-2.5)^2+2x^2-9.25$ are mathematically equivalent

functions when using ordinary real arithmetic, the interval evaluations of these functions are not. For $x, y \in [-10, 10]$, applying interval arithmetic using the first expression equals $[-53, 347]$, while using the second equals $[-9.25, 347]$. Figure 3.3 illustrates that the latter (represented by the red bounding box) is the smallest interval vector capable of completely enclosing the function, while the former expression overestimates the function evaluation by the additional gray bounding box. As demonstrated by this example, the number of occurrences of each variable should be reduced as much as possible in order to reduce pessimism in function evaluations. If each variable occurs only once in the functional form and the function is continuous, then the inclusion function is guaranteed to be minimal (Jaulin et al., 2001). Simplifying interval operations such that the resulting equation is minimal (or such that it produces the least pessimistic estimate of the image possible) is also important for the contraction processes, which will be demonstrated in Section 3.5.1.

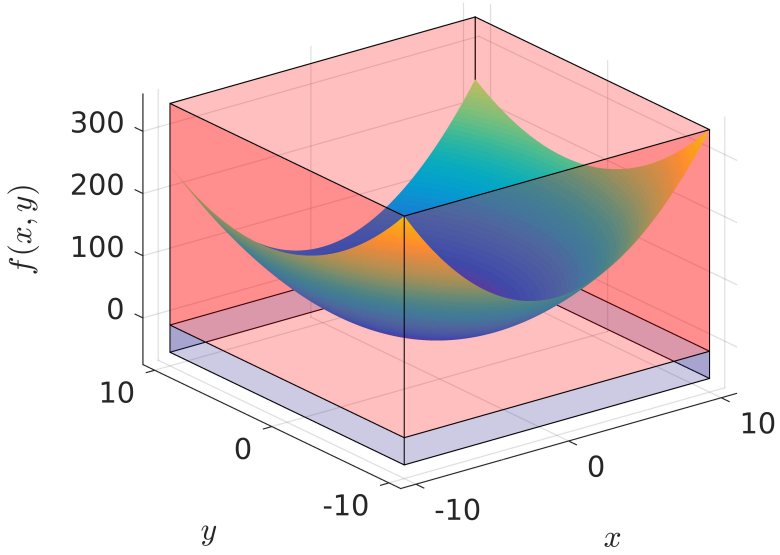


FIGURE 3.3: Pessimistic vs. exact image representations of example functions that would otherwise be equivalent under ordinary real arithmetic.

3.3 Set Characterization

3.3.1 Subpavings

While the use of intervals and boxes is useful, they often provide a poor description of an image with inadequate precision by themselves if the image has a complex shape or discontinuous volume. However, an improved interval characterization of a set $f([\boldsymbol{x}])$ may by performed by covering the set with subsets of non-overlapping boxes called *subpavings* (Kieffer et al., 2001). Subpaving a set can be performed by simply bisecting $[f]([\boldsymbol{x}])$ into a finite number of smaller boxes and then evaluating each of these smaller interval vectors by the inclusion function to test for solution acceptance or rejection. The principal benefit of a subpaving is that it may be used to characterize sets and subsets to any desired degree of precision. In other words, by controlling the size of the smallest boxes in the subpaving, the subpaving may either be limited to a coarse approximation to provide advantages in computational speed or to a fine approximation to more precisely define the boundary of the solution space. Note that using subpavings to characterize sets may in some cases be too computationally expensive, especially with increases in set dimensionality. An application-based example is presented in this research within Chapter 6. Moreover, a subpaving describing a set $\mathbb{X}$ may also be broken down into inner and outer approximations, $\underline{\mathbb{X}}$ and $\overline{\mathbb{X}}$, respectively (Jaulin and Walter, 1993). The difference between the inner and outer approximations is that the inner contains only boxes that wholly satisfy the inclusion functions, whereas the outer approximation contains boxes that may contain solutions, but further bisection and evaluation of the boxes on the boundary of the set has been terminated since the prescribed interval precision has been satisfied. The use of inclusion functions in

conjunction with inclusion tests and subpavings forms the basis for addressing constraint satisfaction problems within this work.

3.4 Constraint Satisfaction Programming

Now that the basics of interval analysis have been presented, the rest of this chapter will be focused on the primary tools necessary for casting the structural identification problem as one of constraint satisfaction using interval arithmetic and contractor programming to incorporate measurement uncertainty and yield all feasible solution sets to reflect the confidence in the parameter estimates given the specified measurement data.

As previously stated, St-Id has traditionally relied on optimization schemes to determine plausible values for a set of independent, unknown parameters of an analytical model using physical measurements obtained from the structure. A drawback of many of the existing methods is that they often find a single solution, which may or may not be the optimum solution, and no information is provided on the certainty with which the parameters are identified in the model. Numerous methods have been developed in recent years that are capable of determining potential alternative solutions, but these methods are not capable of completely determining *all* possible solutions. Likewise, methods have been developed to probabilistically assess the uncertainty in the identified parameters, but these methods rely on assumed probabilistic distribution functions. Furthermore, nearly all existing methods for iterative FE model updating are rooted in optimization techniques that rely on use of a single objective function that aggregates eigenvalue and eigenvector residuals. The various functional forms of these objective functions are regularly criticized since they influence the parameter identification and the use of relative weighting within the objective function

presents another set of challenges associated with measurement confidence and solution uniqueness. In contrast to existing methods, the framework of this dissertation attempts to determine for several classes of inverse eigenvalue problem, all potential solutions that satisfy some set of prescribed constraint equations over real numbers formed from the underlying physics of the model and the physical measurements. This type of problem is called a Constraint Satisfaction Problem (CSP) (Dechter, 2003; Rossi et al., 2006; Hentenryck, 1999) and it differs from conventional imperative programming since, rather than defining the flow of the program in sequential steps, it describes a set of criteria to which all feasible solutions must adhere. One of the main challenges posed by constraint satisfaction problems is that they are generally non-polynomial and the computational complexity to solve them is NP-hard. NP or *nondeterministic polynomial time* problems do not run in polynomial time on a standard computer meaning that the *brute force* method of trying all possible combinations of parameters is virtually impossible (Woeginger, 2003). However, solutions to NP problems can be checked in polynomial time. NP-hard is a class of problems that are at least as hard as NP problems. The following discussion provides basic details on CSPs essential for the understanding the rest of the dissertation.

Ghedira and Dubuisson (2013) defines a CSP as a *4-tuple <V,D,C,L>* where;

- $V = \{v_1, v_2, ..., v_n\}$ *is a set of variables*
- $D = \{d_1, d_2, ..., d_n\}$ *is a set of domains for the prospective variables*
- $C = \{c_1, c_2, ..., c_n\}$ *is a set of constraints over the variables*
- *L is a set of labels that maps constraints to the pair of variables and corresponding domains, formally;* $L : C_i \rightarrow (v_i, d_i)$

Each variable v_i can assume any value in the corresponding non-empty domain d_i. The constraint $c_i \in C$ is defined over a pair (v_i, d_i) through a label function $l_i \subset L$. In the process of finding a satisfiable solution, different values are assigned to the variable (in set V) from domain set (D) through constraint propagation algorithms (also called filtering/contraction algorithms). The evaluation of the label (true/false) determines whether the corresponding assignments to variables for a given constraint lead to a satisfiable solution or not. While assigning values to different variables (through a "systematic search process"), consistency algorithms take into account whether any violation of constraints has occurred during any assignment (Hyvnen, 1992). Likewise, the paradigm for solving CSPs through integration of Systematic Search and Arc Consistency techniques is called Constraint Programming (CP). The main challenges in CSPs are to guarantee correctness and completeness along with the assurance of termination of the solving procedure. In most state-of-the-art approaches for solving CSPs, the most critical aspect of the framework is generally the branch and prune algorithm, which only requires initial ranges of the variables and constraints over them as inputs. Typically, a branch and prune algorithm is a recursion over two steps:

- Pruning the search space
- Making a choice to generate two or more sub-problems

Pruning checks that some local consistency holds (Hentenryck et al., 1997) and, in simpler terms, reduces/contracts/filters a box or interval vector only when it can be proven that the upper bound and lower bound of a box does not satisfy some given constraints.

A sub-domain of constraint programming that integrates interval arithmetic, called Interval Constraint Programming, offers unique advantages for developing solutions to the

inverse eigenvalue problem with experimental data. As previously discussed, interval arithmetic allows for variables as well as constraint relationships among variables to be defined using intervals and mathematical operations can be applied using principles of interval arithmetic (Alefeld and Claudio, 1998). As stated in the beginning of this chapter, interval analysis offers a means of placing bounds on round off errors in numerical calculations, measurement uncertainties, and uncertain parameters in physics-based models. Therefore, rather than defining the exact value of a variable or constraint, it can be defined over an interval, which implies that it may take any value within that interval. In an interval constraint programming problem, the objective is to completely and correctly identify all interval vectors, to a specified interval precision, that satisfy the set of constraint equations within the bounded domains for each set of interval variables. Applied to an interval constraint programming problem, the branch and prune process may be defined by Figure 3.4. The process begin with an initial box and evaluation of its the image. If the image is non-empty, the box is either stored as a solution if its width meets some criteria, or bisected to generate two subproblems. The bisection process is dictated by two parameters: the bisector and the bisection point. Two of the simplest bisectors are largest first, where the dimension bisected is the largest width of the interval, and round robin, where each dimension if the interval is bisected in turn (Granvilliers, 2012). The bisection point defines the point at which the dimension is split defined as some ratio of the interval width. Note that ϵ is a user provided precision that establishes a stopping criteria for termination of the algorithm. If the evaluation of the box is empty, the box is pruned, or discarded, from the stack of boxes. This process of image evaluation continues until there are no more boxes left on the stack.

Stack← {[$\boldsymbol{x}_0$]} where [$\boldsymbol{x}_0$] is an initial box and Stack is a construct that contains all boxes;
while Stack≠ ∅ **do**
  Select *box* [$\boldsymbol{x}$] from Stack;
  if $f([\boldsymbol{x}]) \neq \emptyset$ *and width (*$[\boldsymbol{x}]$*)* $< \epsilon$*;* **then**
    [$\boldsymbol{x}$] may contain a solution;
  end
  if $f([\boldsymbol{x}]) \neq \emptyset$ *and width (*$[\boldsymbol{x}]$*)* $> \epsilon$*;* **then**
    Bisect([$\boldsymbol{x}$]) into [$\boldsymbol{x}_1$] and [$\boldsymbol{x}_2$] along a single dimension;
    Stack← Stack $\bigcup[\boldsymbol{x}_1] \bigcup[\boldsymbol{x}_2]$;
  end
  if $f([\boldsymbol{x}]) = \emptyset$*;* **then**
    [$\boldsymbol{x}$] does not contain a solution;
    Prune [$\boldsymbol{x}$] from Stack;
  end
end

FIGURE 3.4: Branch and Prune Algorithm

However, in the context of this work, finding all of the interval vectors that satisfy some set of constraints presents a challenging nonlinear inverse problem. Consider two sets, $\mathbb{X}$ and $\mathbb{Y}$, along with a function f that maps $\mathbb{X} \rightarrow \mathbb{Y}$, where $\mathbb{X}$ is the feasible parameter space, f is the governing equation for the system represented by an inclusion function $[f]$, and $\mathbb{Y}$ is the set of modal properties associated with the parameters. Since the measurement data obtained through vibration testing provides the set $\mathbb{Y}$, determination of $\mathbb{X}$ presents a difficult, and possibly ill-posed, set inversion problem, as illustrated in Figure 3.5. Exploration of $\mathbb{X}$ is facilitated by performing interval analysis on subpavings of $\mathbb{X} \in \mathbb{R}^n$ that completely cover the plausible domain of $\mathbb{X}$ with non-overlapping boxes. The formulation of the set inversion problem relies on checking these subsets of the search space via inclusion functions such that $\mathbb{X}$ is bracketed by two subpavings, $\underline{\mathbb{X}}$ and $\overline{\mathbb{X}}$. The inner subpaving, $\underline{\mathbb{X}}$, is a strict subset of $\mathbb{X}$, while the outer subpaving is a superset of $\mathbb{X}$. Through recursive application of inclusion tests that apply the inclusion functions as constraint equations on

interval vectors within the search space, the set inversion develops an enclosure of the set $\mathbb{X} = f^{-1}(\mathbb{Y})$ by checking whether $[f]([\boldsymbol{x}]) \subset \mathbb{Y}$.

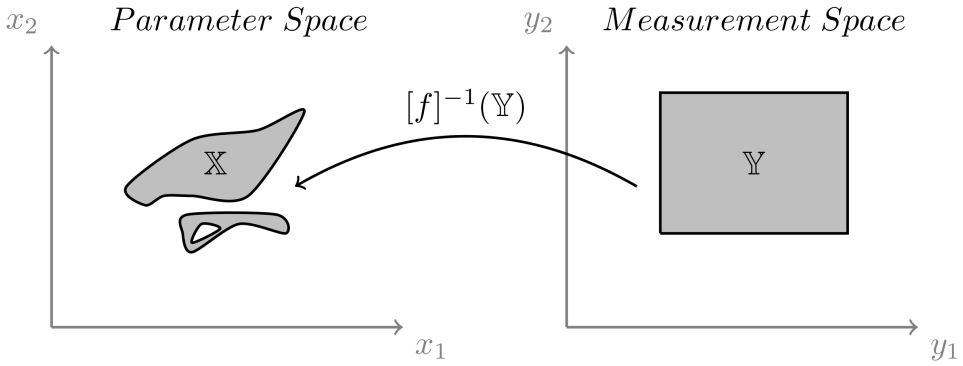


FIGURE 3.5: Set inversion problem mapping modal property measurements, $\mathbb{Y}$, to structural parameters, $\mathbb{X}$

3.4.1 Systematic Search

Systematic search may be viewed as a branch and prune process explored as a tree structure where the root node represents the entire problem and subsequent nodes or leaves of the tree represent subproblems of the root node that differ in variable assignment (Rossi et al., 2006). If it is determined during evaluation of a node that there is constraint violation, backtracking is performed to find a new satisfiable assignment and the subtree below the failed node is pruned from the search space (Golomb and Baumert, 1965). In this way, systematic search improves on the brute force method of trying all possible variable combinations. However, simple backtracking is an "uninformed" and "grotesquely" inefficient approach (Mackworth, 1977) and is not computationally efficient for problems with significant dimensionality. One of the main challenges associated with solving a CSP is improving the performance of the search method such that local inconsistencies are eliminated. *Local inconsistencies* are potential partial solutions that satisfy the constraints, but can not be extended to additional leaves of the search tree by choosing values for some of

the uninstantiated variables. In other words, selecting a value for an uninstantiated variable would cause failure of the node. However, local consistency may be maintained by propagating constraints at each node through the process of constraint propagation (Hyvnen, 1992), which discards values or combinations of values if their assignment violates some set of constraints. One of the simplest examples to understand constraint propagation is to apply the concept to crossword puzzle solving where the abbreviations COS, TAN, COT, and CSC may be eliminated from the set of "three lettered trigonometric functions" given that the first letter must be an "S" while SIN and SEC are retained as potential solutions. Eliminating erroneous assignments reduces the size of the search space to be explored by propagating the implications of a constraint on one variable onto the other variables (Rossi et al., 2006).

3.4.2 Arc Consistency

One method for enforcing local consistency is arc consistency, which provides a swift method for constraint propagation that is faster and detects failure earlier than tedious forward checking (Russell and Norvig, 2002). An arc is simply a directed arrow in the constraint graph that points from one variable to another. A CSP is said to be arc consistent if for every couple of variables, the arc associated with the two variables in the constraint graph satisfies the constraints involving each variable. For example, given two variables x and y and their respective domains, the arc from x to y, denoted (x, y), is said to be consistent if for every assignment of x there is some assignment of y that is consistent (i.e. does not violate the constraint). To more fully understand this concept, consider the simple circle coloring problem (Kumar, 1992) consisting of three variables A, B, and C. For

the sake of brevity, the domains of each variable are given as, $D_A = \{Red, Green, Blue\}$, $D_B = \{Green, Blue\}$, and $D_C = \{Blue\}$, respectively, to represent only a subset of the search tree (Figure 3.6a). The problem consists of coloring the slices of the pie such that no two adjacent edges share the same color (i.e. $A \neq B \neq C$). Note that the domains of the variables represent one node of the root where C has already been assigned, but there are choices left for A and B (even if it is obvious what the answer might be). Although this is a fairly simple problem that would take little reasoning to solve, the same concept applies to problems with much larger dimensionality and more complex constraints. For the first iteration in this example, (A, B) and (B, A) are arc consistent since, for any A chosen, a B may be chosen such that $A \neq B$ and vice versa. However, arc (A, C) is not consistent because selecting $A = blue$ violates the constraint. Therefore *blue* is removed from D_A and the arc checking process continues. The next inconsistency is arc (B, C), which prompts *blue* to be removed from D_B. This process of checking each arc for consistency and removing values that violate the constraint continues until all arcs are consistent (Figure 3.6b). Enforcing arc consistency is a means to efficiently solve constraint satisfaction problems with discrete domains.

3.4.3 Hull Consistency

In dealing with continuous domains, due to the finite precision of floating point numbers, arc consistency cannot be enforced efficiently (Collavizza et al., 1998; Rossi et al., 2006). *Hull consistency*, which may be viewed as a coarse extension of arc consistency, requires that arc consistency only be satisfied at the lower and upper bounds of the interval variable domains (Cruz and Barahona, 2001). A constraint is said to be hull consistent with respect

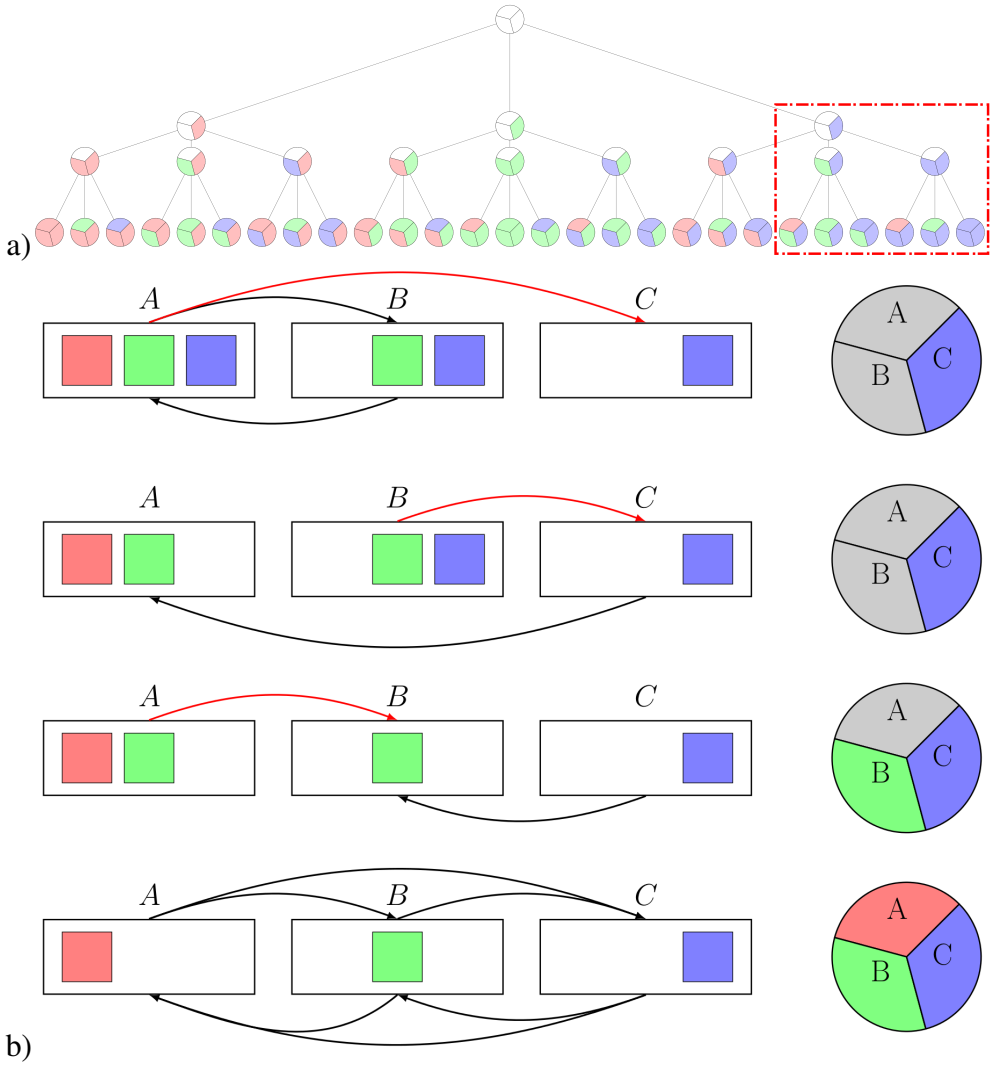


FIGURE 3.6: a) Entire search tree, b) Checking consistency of the arcs in the constraint graph and removing assignments from the variable domains until all arcs are consistent for a subset of the entire problem

to a box if for each bound of the domain of an interval variable there is a real valued combination of variables that satisfy the constraint. The hull consistency algorithm in the interval analysis and constraint programming package utilized to solve the problems within this work employs the HC4Revise (Benhamou et al., 1999), or forward-backward, contraction algorithm just like the method involving subpavings, but without the computational burden of bisections. This algorithm is outlined and its use is demonstrated in Section 3.5.1.

3.5 Contractor Programming

One recent effort toward the integration of interval arithmetic and constraint programming in a formalized solver has been termed Contractor Programming (Chabert and Jaulin, 2009). In this approach, contractors may be viewed as mathematical operators that accept a system (an n-dimensional box) as an input and contract the domain of the system according to a given set of constraints. Contractors yield a reliable set of satisfiable solutions since they must satisfy properties of soundness and completeness. The formal definition of a contractor and its properties are defined as follows:

A contractor (Ctc) is a function from $Ctc : \mathbb{IR}^n \rightarrow \mathbb{IR}^n$ *with the following properties:*

- $\forall [X] \in \mathbb{IR}^n \quad Ctc([X]) \subset [X]$; where $Ctc([X])$ represents box $[X]$ after contraction
- $Ctc([X]) \cap System = [X] \cap System$

The first property ensures that the contraction algorithm or procedure is sound and that the result achieved after contraction is limited to a subset of the original box. The second property elaborates the completeness of the contraction algorithm/procedure, which states that no potential solution is lost after contraction is performed. Adhering to these two properties, contractor programming yields reliable results with a guarantee that feasible solutions within the initial domain are not lost. Following contraction, the interval vector may be bisected into a subset of smaller boxes and contractors can be applied to further refine the interval precision of the solution subpaving. In this respect, solvers employing contractor programming have some parallels to branch and prune algorithms, where subsets of a search space are evaluated and either retained or discarded as potential solutions and then the retained subsets are further divided and evaluated until the desired interval precision is

obtained. However, the process of contraction can result in a significantly faster exploration of the search space than pure branching methods, such as bisection (Jaulin et al., 2001).

3.5.1 HC4 Contractor

The HC4, or forward-backward, contractor is one of the most basic techniques in constraint programming for contracting a domain with respect to a set of constraints. This process is most easily understood visually with a tree-structured decomposition of the equation into individual components, or primitives. Figure 3.7 displays the HC4 algorithm which takes a set of constraints and an interval vector as inputs and reduces the domains of the variables (Benhamou et al., 1999). The HC4Revise portion of the algorithm is illustrated in Figure 3.8, which consists of a forward evaluation from the leaves to the root node followed by a backward propagation from the root to the leaves to narrow the domains of the variables (Goualard and Granvilliers, 2005). If any computation in the backward phase results in the empty set, the variable assignments are inconsistent with respect to the constraint. Otherwise the domain of each variable is intersected with the narrowed domains obtained from the backward propagation of each occurrence of the variable.

*HC*4(**in C** = $\{c_1, ..., c_n\}$; **inout D** = $d_1 \times \cdots \times d_n$)
begin
  Stack ← $\{c_1, ..., c_n\}$;
  while *(Stack* ≠ ∅ *and* ***D*** ≠ ∅*)* **do**
    c ← select one c_i in Stack;
    D′ ← *HC*4*Revise*(*c*, **D**)
    if *(**D′** ≠ **D**)* **then**
      Stack ← Stack ∪ $\{c_j \mid \exists x_k \in Var(c_j) \wedge d'_k \neq d_k\}$
      D ← **D′**
    else
      Stack ←Stack \{*c*}
    end
  end
end

Figure 3.7: HC4 algorithm (Benhamou et al., 1999)

*HC*4*Revise*(**in** *ctc* = $r\{t_1, ..., t_p\}$: real constraint ; **inout D** : *box*;
  in $\mathcal{A}$: approximate domain)
begin
  $\mathbf{D}_{\mathcal{A}}$ ← **D**
  foreach $i \in \{1, \ldots, p\}$ **do**
    ForwardEvaluation(t_i, $\mathbf{D}_{\mathcal{A}}$)
  end
  BackwardPropagation(*c*, $\mathbf{D}_{\mathcal{A}}$)
  D ← $Hull_{\square}(\mathbf{D}_{\mathcal{A}})$
end

Figure 3.8: HC4Revise algorithm (Benhamou et al., 1999)

.

3.5.1.1 HC4 Illustrative Example

Again consider the function,

$$y^2 - 5y + 2x^2 - 3 = [0, 0] \tag{3.11}$$

with the initial box $[x] \times [y] = [-10, 10] \times [-10, 10]$. As previously shown, since this equation is not minimal it produces a pessimistic image of the initial box. The contraction

process is broken down into two steps: a forward evaluation and a backward contraction. The first step is a forward evaluation of the function with the initial box. Starting with the leaves, $[x] = [-10, 10]$ and $[y] = [-10, 10]$, of the tree-structured form of the equation, the first forward evaluation yields $[f] = [-53, 347]$ (Figure 3.9a) which, while satisfying the constraint since $[f] = [0, 0] \in [-53, 347]$, is overly pessimistic. To reduce this pessimism the initial box can be contracted. The backward contraction process begins at the leaf node of a single variable in order to contract the domain of the other variable. Constraining the root node to $[0, 0]$, setting $[y]$ to its initial domain, $[-10, 10]$, and performing backward interval arithmetic yields a contracted domain $[x] = [-5.148, 5.148]$, a subset of its initial domain $[-10, 10]$ (Figure 3.9b). Determining the contracted domain for $[y]$ follows the same process. The root node is again set to $[0, 0]$ to enforce the constraint and $[x]$ is set at its newly contracted domain $[-5.148, 5.148]$. Figure 3.9c illustrates the backward arithmetic for determining the contracted domain for $[y]$. Note that since there are multiple occurrences of the variable y, $5y$ and y^2 need to be evaluated separately and the intersection of each result determines y. Using the contracted domains for each variable, a subsequent forward step is performed to evaluate the root node against the constraint. If the constraint is satisfied, the contraction process is finished, otherwise the forward-backward contraction continues. Figure 3.10 displays the forward function evaluation for the newly contracted domains as well as the backward interval arithmetic steps for determining further reduced domains for $[x]$ and $[y]$. Interestingly, even after a total of 1000 forward-backward contractions, the domain is not contracted to produce the exact image, $[f] = [0, 0]$. In fact, no improvement in the reduced domain is observed after the 12^{th} iteration (Table 3.2). This is due to the functional form of the inclusion function, which has multiple occurrences of the

variable y and is therefore not minimal.

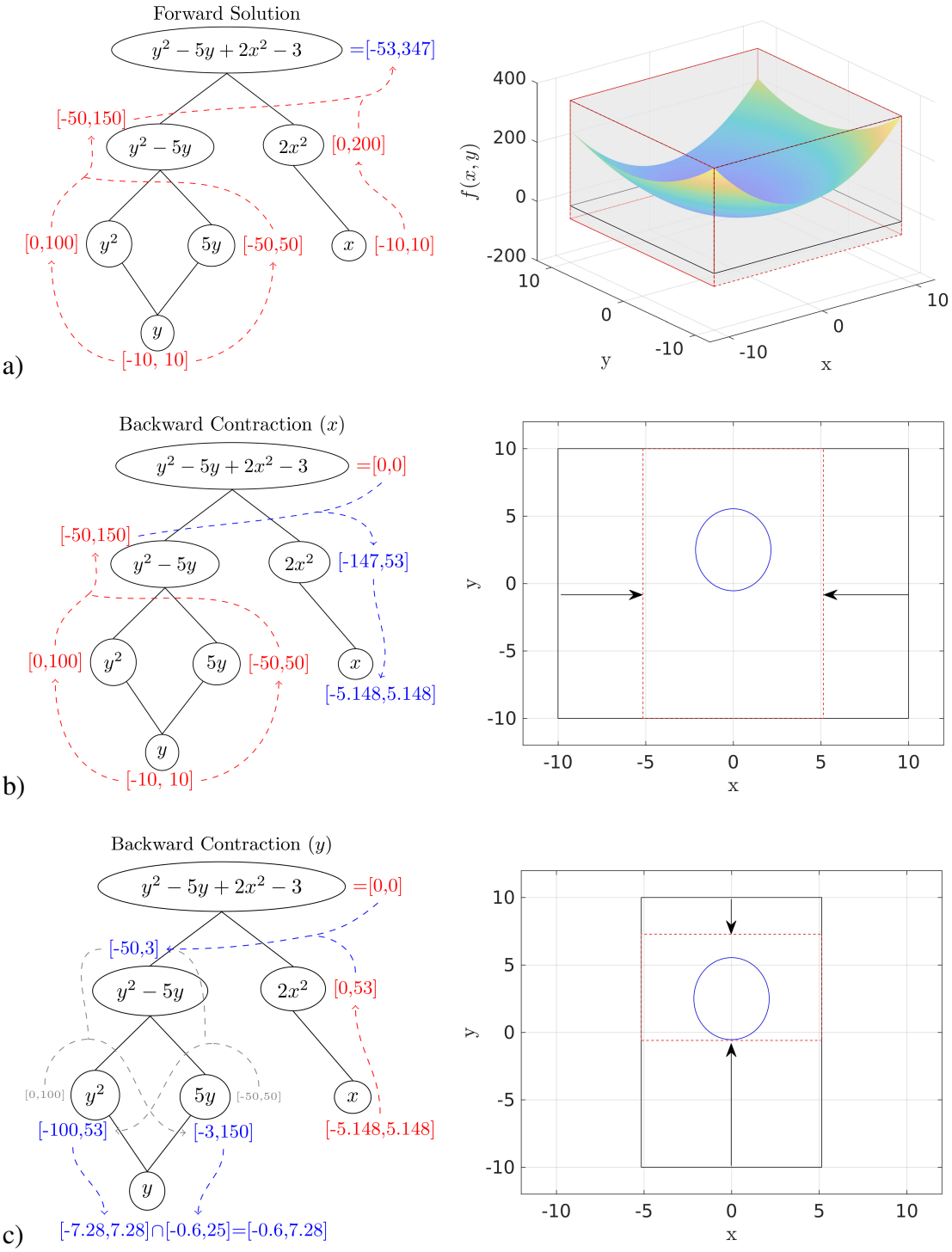


FIGURE 3.9: First forward-backward contraction for $y^2 - 5y + 2x^2 - 3 = [0, 0]$ with $x, y \in [-10, 10]$. a) Forward evaluation, b) Backward contraction w.r.t x, c) Backward contraction w.r.t. y.

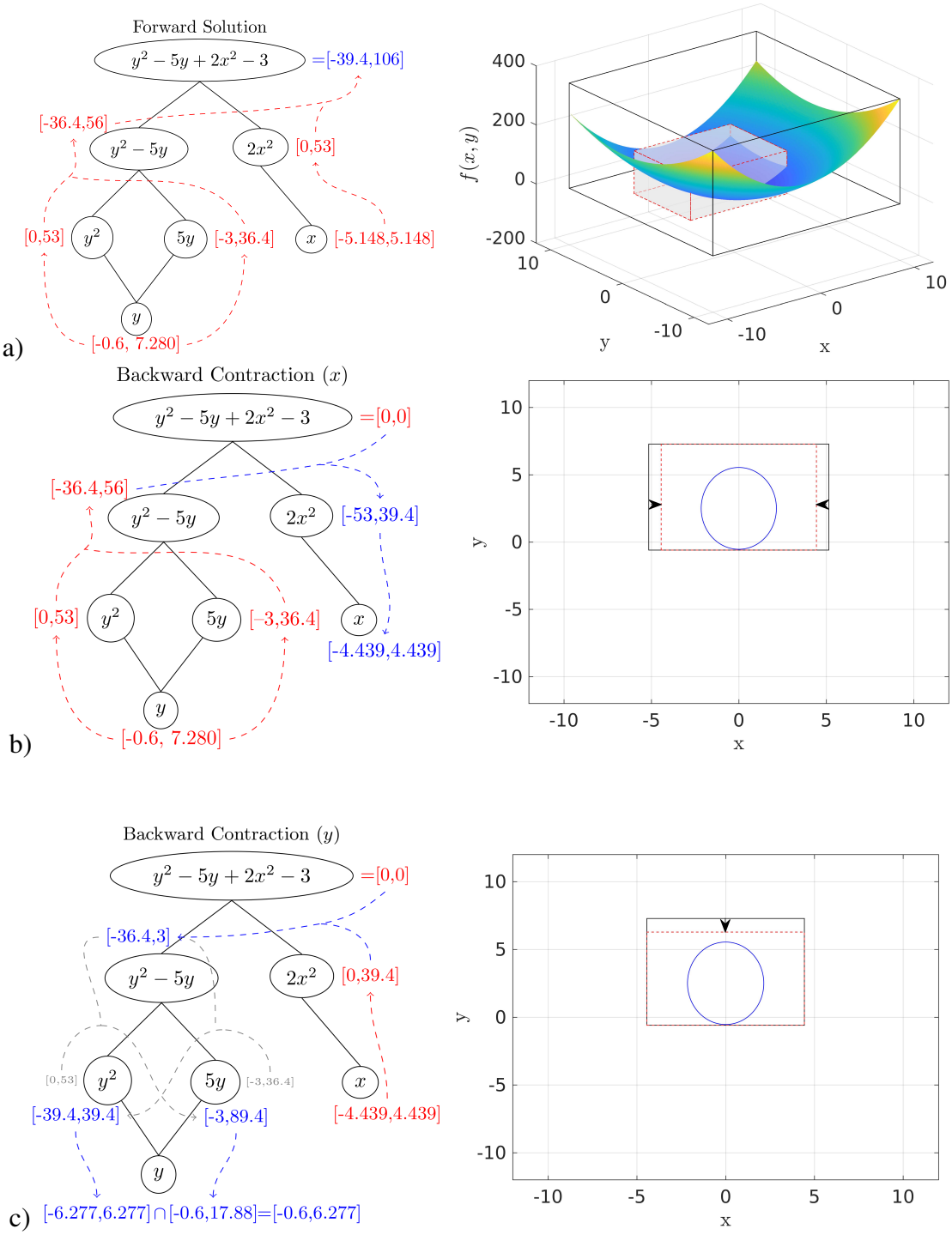


FIGURE 3.10: Second forward-backward contraction for $y^2 - 5y + 2x^2 - 3 = [0, 0]$ with $x, y \in [-10, 10]$. a) Forward evaluation, b) Backward contraction w.r.t x, c) Backward contraction w.r.t. y.

In application, when the contraction process stalls, the contracted interval vector can be bisected and the forward-backward contractor can be applied to the newly generated boxes to improve the precision of the subpaving resolution of the image. However, if the function is expressed in its minimal form such that the number of occurrences of each variable is minimized,

$$(y - 2.5)^2 + 2x^2 - 9.25 = [0, 0] \tag{3.12}$$

then the number of forward-backward contractions may be drastically reduced. Figure 3.11a displays the forward calculation for the same initial box, which exactly bounds the image with $[f] = [-9.25, 347]$. Following the same backward arithmetic process by constraining the root node to $[0, 0]$ and setting $[y] = [-10, 10]$ yields the contracted domain $[x] = [-2.151, 2.151]$, which are the exact domain bounds for the applied constraint $[f] = [0, 0]$ (Figure 3.11b). Figure 3.11c displays the contracted domain $[y] = [-0.541, 5.541]$ which are also the exact bounds given the applied constraint. Therefore, the results indicate that the efficiency of constraint satisfaction by contractors and interval arithmetic may be increased drastically by simplifying the inclusion functions to the minimal form. Of course, stating constraint equations in a form where each and every variable appears no more than once is not always possible and in such cases it is often necessary to explore different functional forms, potentially specific to the application, that result in the most efficient contractions. Note that even if the inclusion function is minimal, the contracted interval is a superset of the image and to fully characterize the nonlinear boundary of the set of solutions that adhere to the constraint $f([x], [y]) = [0, 0]$, bisection of the contracted interval would need to be performed.

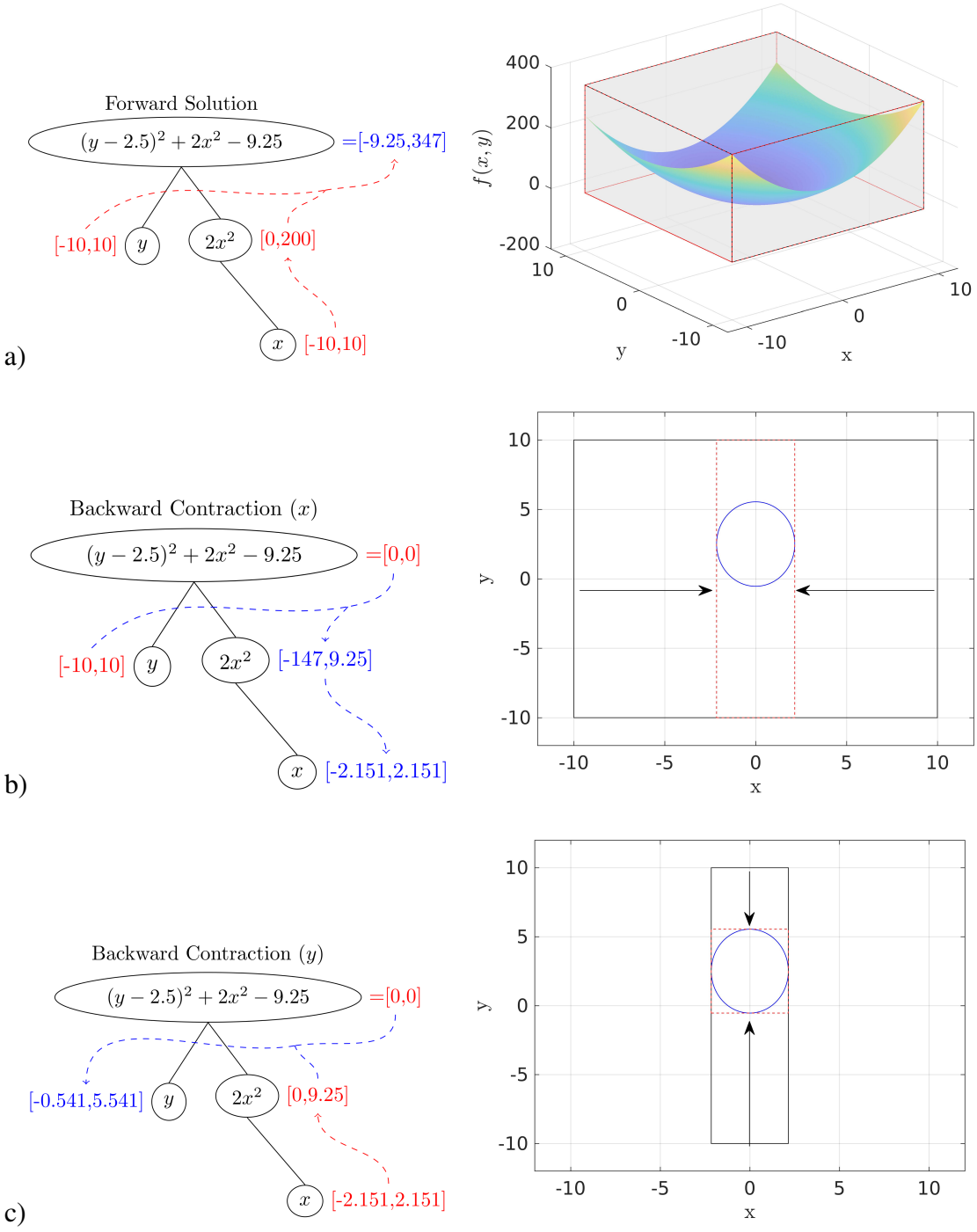


FIGURE 3.11: Forward-backward contraction for $(y-2.5)^2+2x^2-9.25=[0,0]$ with $x,y\in[-10,10]$. a) Forward evaluation, which exactly bounds the image without pessimism, b) Backward contraction w.r.t x, c) Backward contraction w.r.t. y.

TABLE 3.2: Comparison of forward-backward contractor operations on different functional forms of an inclusion function

	$y^2 - 5y + 2x^2 - 3 = [0, 0]$		$(y - 2.5)^2 + 2x^2 - 9.25] = [0, 0]$	
Iteration	[x]	[y]	[x]	[y]
1	[-5.1478, 5.1478]	[-0.6, 7.2801]	[-2.1506, 2.1509]	[-0.54138, 5.5414]
2	[-4.4385, 4.4385]	[-0.6, 6.2769]	⋮	⋮
⋮	⋮	⋮	⋮	⋮
11	[-3.9184, 3.9184]	[-0.6, 5.5415]	⋮	⋮
12	[-3.9184, 3.9184]	[-0.6, 5.5414]	⋮	⋮
⋮	⋮	⋮	⋮	⋮
1000	[-3.9184, 3.9184]	[-0.6, 5.5414]	⋮	⋮
Exact	[-2.1506, 2.1509]	[-0.54138, 5.5414]	⋮	⋮

3.5.2 Interval Hull

When full characterization of a set via subpavings is computationally prohibited, a less precise description of the set may be obtained by contracting to the *interval hull*. The interval hull $[\mathbb{X}]$, which is a pessimistic enclosure that is guaranteed to contain the exact feasible solution, $\mathbb{X}$, is simply the smallest box that contains $\mathbb{X}$ (Jaulin et al., 2001). The open-source IBEX C++ library (Chabert, 1999) provides the ability to contract a box to the interval hull, that is the smallest box enclosing all feasible solutions, with respect to a system of linear inequalities. For problems where the constraint equations are necessarily nonlinear, which is the case for the inverse eigenvalue problem with incomplete mode shape measurement, a means of approximately linearizing the system needs to be provided. In this dissertation, the combined relaxation procedure packaged within the IBEX library that combines a corner-based Taylor relaxation (Araya et al., 2012) and an affine arithmetic-based relaxation (Ninin et al., 2015) is utilized. The contractor employed is a composition of the forward-backward contraction through the HC4 algorithm (Benhamou et al., 1999),

adaptive constructive interval disjunction (ACID) (Neveu et al., 2015), and the interval hull contractor, *CtcPolytopeHull*, which calls the linear solver compiled with IBEX (SoPlex (2017) in this case) and calculates lower and upper bounds for each variable:

$$\min_{Ax \leq b \wedge x \in [x]} \{x_i\} \quad and \quad \max_{Ax \leq b \wedge x \in [x]} \{x_i\} \tag{3.13}$$

The relaxed system is then contracted via the ACID procedure, which handles a single variable at a time, splits the domain of the variable into several sub-intervals, contracts each subproblem with respect to a contractor (HC4 in this case), and returns the interval union of the contracted subproblems (Neveu et al., 2015). This process continues until a prescribed stopping criterion is reached. The criterion chosen in this study is based on the perimeter of the interval vector that defines the interval hull, which is simply the sum of the widths of each interval solution to the uncertain parameters. While not being capable of providing a detailed representation of the set, the interval hull is capable of giving insight into the confidence in the parameter assignments based on the interval components that make up the interval hull.

3.6 Structural Identification Using Nonlinear Constraint Satisfaction

To provide motivation for the use of nonlinear constraint satisfaction with interval analysis and contractor programming for FE model updating, this section presents a simple example of applying nonlinear constraint satisfaction to a small structural system. Greater detail on the challenges of this approach as well as its full implementation are presented in Chapter 5 for multiple degree-of-freedom systems. Recall from Chapter 2 that the finite element model updating problem has traditionally been performed using experimentally

obtained modal parameter estimates that can be numerically predicted using the generalized eigenvalue equation for undamped systems as

$$K\Phi - M\Phi\Omega^2 = 0 \tag{3.14}$$

where M and K are the mass and stiffness matrices, Ω^2 is the diagonal matrix of eigenvalues, and Φ are the corresponding eigenvectors represented as columns of the matrix. The ultimate goal of the finite element model updating problem is to solve for unknown parameters within M and K, which are $n \times n$ square matrices, given a set of eigenvalues and eigenvectors. However, most cases of model updating are partially described where only $m < n$ eigenpairs are measured due to bandwidth limitations of the sensing equipment. In addition, only $s < n$ degrees of freedom are typically measurable, leading to incompletely measured mode shapes and a partitioned matrix of constraint equations:

$$K_{n\times n}\begin{bmatrix}\Phi^M_{s\times m}\\ \Phi^U_{(n-s)\times m}\end{bmatrix} - M_{n\times n}\begin{bmatrix}\Phi^M_{s\times m}\\ \Phi^U_{(n-s)\times m}\end{bmatrix}\Omega^2_{m\times m} = 0_{n\times m} \tag{3.15}$$

where $\Phi^M_{s\times m}$ are the rows of the measured components of the mode shapes and $\Phi^U_{(n-s)\times m}$ are the rows of the unmeasured components of the mode shapes. In this study, the structural matrices are explicitly formed through elemental contributions as:

$$\left[K_o + \sum_{j=1}^{N_K}\alpha_j K_j\right]\begin{bmatrix}\Phi^M_{s\times m}\\ \Phi^U_{(n-s)\times m}\end{bmatrix} - M_{n\times n}\begin{bmatrix}\Phi^M_{s\times m}\\ \Phi^U_{(n-s)\times m}\end{bmatrix}\Omega^2_{m\times m} = 0_{n\times m} \tag{3.16}$$

where α_j is a scalar multiplier applied to the basis matrix, K_j, that provides the stiffness contributions of the j-th member of the model, while K_o represents the contributions of any

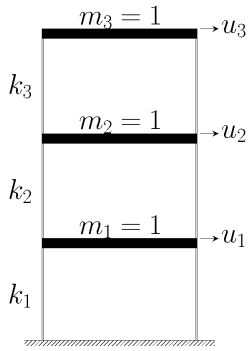
members in the model not subject to updating. Therefore, the unknowns are the N_K α scalar multipliers for the unknown members and the $(n - s) \times m$ unmeasured components of the eigenvectors. Employing interval arithmetic, the constructed stiffness matrix is an interval matrix, K^I, since the uncertain stiffness scalars in the model are encoded as intervals, $\alpha = [\underline{\alpha}, \overline{\alpha}]$, where $\underline{\alpha}$ is the lower bound to the interval for the uncertain parameter and $\overline{\alpha}$ is the upper bound. The unknown eigenvector components are treated as intervals, $\Phi^U_{(n-s)\times m} = [\underline{\Phi}^U_{(n-s)\times m}, \overline{\Phi}^U_{(n-s)\times m}]$ as well.

In Chapter 5, an additional constraint equation termed the eigenvalue inclusion constraint is introduced to accommodate for measurement uncertainty and idealization errors to ensure that the prescribed eigenvalues are contained within the interval eigenvalues of the identified interval stiffness and mass matrices. The constraint checks the prescribed eigenvalues for inclusion by substituting each into the characteristic equation formed from the determinant:

$$\left| K^I - \omega_r^2 M \right| = \left| K_o + \sum_{j=1}^{N_K} [\underline{\alpha}_j, \overline{\alpha}_j] K_j - \omega_r^2 M \right| = 0 \tag{3.17}$$

3.6.1 Illustrative Example on a 3DOF Shear Building Model

As motivation for the methodologies developed and demonstrated in this dissertation, consider the small three degree-of-freedom shear building model with accompanying structural matrices from Chapter 2 and displayed in Figure 3.12. Recall that for the baseline model, the stiffnesses were assigned as $k_1 = k_2 = k_3 = 1$. Elemental contributions to the stiffness matrix from each linear elastic spring are explicitly defined in the structured matrices.



$$M = diag(m_1, m_2, m_3);$$

$$K = 2000 \begin{bmatrix} k_1 + k_2 & -k_2 & 0 \\ -k_2 & k_2 + k_3 & -k_3 \\ 0 & -k_3 & k_3 \end{bmatrix}$$

FIGURE 3.12: Three degree-of-freedom mass-spring system for demonstrating structural identification using nonlinear constraint satisfaction with interval arithmetic and contractor programming

To add uncertainty to the model, 15 sets of synthetic modal parameter estimates with a standard deviation of 0.01 were generated around the natural frequencies and mode shapes corresponding to the baseline model. Constraint equations were developed from the governing eigenvalue equation (3.16) and eigenvalue constraint equation (3.17) with the means and standard deviations of the synthetic measurement data used to prescribe uncertainty in the constraint equations. A case with partially described eigenvalues and incompletely measured mode shapes was explored with the eigeninformation being limited to the first two modes of the structure and mode shape measurement limited to only degrees of freedom u_2 and u_3. The search space for the three unknown stiffness parameters was bounded to $k_i \in [0, 3]$ while the unmeasured mode shape components were bounded to $\phi_{i,j} \in [-10, 10]$. For this example, an interval precision of 0.01 was assigned for the uncertain stiffness assignments and the unmeasured mode shape components. The measurement uncertainty applied to the natural frequencies and measured mode shape components was $\pm\frac{1}{4}\sigma$. Figure 3.13 displays the fully characterized subpaving of the solution space as mapped by the IBEX nonlinear constraint satisfaction solver, which determined 2492 solutions in two

distinct basins in about 5 seconds. It should be noted that all of the solutions found are correct solutions to the inverse eigenvalue subject to the partially described and incompletely measured eigeninformation and specified measurement uncertainty. Since the constraint satisfaction approach uses the governing equation of motion and characteristic equation as constraints, the use of an objective function to perform the model correlation through residuals determination, as well as the assignment of weighting coefficients, is completely avoided. The MATLAB script for this small example is presented in Appendix D.2.

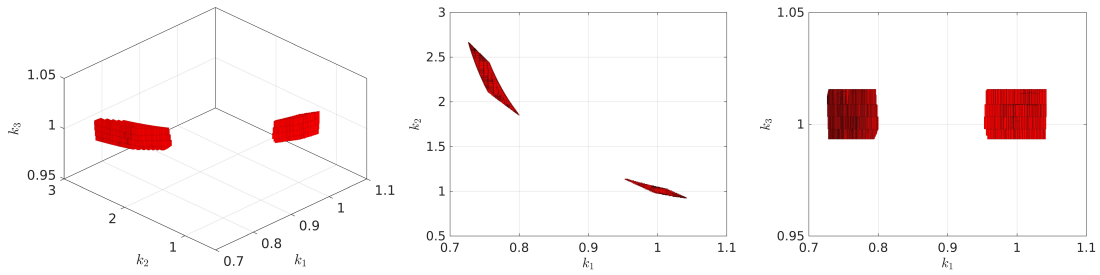


FIGURE 3.13: Subpaving of all feasible solutions to the inverse eigenvalue problem for the three degree-of-freedom system

3.7 Extensions to Different Systems Models and Structural Health Monitoring Applications

This chapter has provided the basic background necessary for understanding the remainder of this work. Preliminaries on intervals and interval arithmetic have been presented as well as the basic principles of constraint satisfaction and contractor programming. Motivation for using nonlinear constraint satisfaction with contractors and interval arithmetic has been provided by revisiting the illustrative three degree-of-freedom example from Chapter 2, which provides a glimpse of the effectiveness of the formulation and the advantages over many traditional approaches to structural identification, which will be further explored in the remaining chapters that will each involve development of methodologies for parameter

identification specific to distinct nonlinear inverse problems in civil engineering applications. Chapter 4 develops, verifies, and validates a methodology suitable for continuous system models. Chapter 5 develops, verifies, and validates a methodology for application to multiple degree-of-freedom (MDOF) system models. Lastly, Chapter 6 addresses challenges in the extension of the methodology to larger MDOF system models as well as successfully demonstrates the application of the methodology for vibration-based damage detection.

For all of the problems presented within, the open-source IBEX C++ numerical library (Chabert, 1999) will be leveraged to perform the interval analysis using C++ scripts written to implement each of the methodologies developed in this dissertation. An interface between the MATLAB interactive environment (MATLAB, 2017) and the IBEX 2.1.17 library has been developed to construct and parameterize the structural matrices, develop mechanics-based constraint equations, pass the formulated CSP to the IBEX solver, and parse any and all interval solutions generated by the contraction algorithm for subsequent analysis and visualization of results.

CHAPTER 4: DYNAMIC IDENTIFICATION OF AXIAL FORCE AND BOUNDARY RESTRAINTS IN TIE RODS AND CABLES WITH UNCERTAINTY QUANTIFICATION USING SET INVERSION VIA INTERVAL ANALYSIS

The following chapter is a direct product of the work of this dissertation and has been submitted for publication in the *Journal of Sound and Vibration* (Kernicky et al., 2018).

Abstract

A methodology is developed for the estimation of internal axial force and boundary restraints within in-service, prismatic axial force members of structural systems using interval arithmetic and contractor programming. The determination of the internal axial force and end restraints in tie rods and cables using vibration-based methods has been a long standing problem in the area of structural health monitoring and performance assessment. However, for structural members with low slenderness where the dynamics are significantly affected by the boundary conditions, few existing approaches allow for simultaneous identification of internal axial force and end restraints and none permit for quantifying the uncertainties in the parameter estimates due to measurement uncertainties. This paper proposes a new technique for approaching this challenging inverse problem that leverages the Set Inversion Via Interval Analysis algorithm to solve for the unknown axial forces and end restraints using natural frequency measurements. The framework developed offers the ability to completely enclose the feasible solutions to the parameter identification problem, given specified measurement uncertainties for the natural frequencies. This ability to propagate measurement

uncertainty into the parameter space is critical towards quantifying the confidence in the individual parameter estimates to inform decision-making within structural health diagnosis and prognostication applications. The methodology is first verified with simulated data for a case with unknown rotational end restraints and then extended to a case with unknown translational and rotational end restraints. A laboratory experiment is then presented to demonstrate the application of the methodology to an axially loaded rod with progressively increased end restraint at one end.

4.1 Introduction

Short cables and hangers in tied arch bridges, struts of truss structures, diagonal bracing in building frames, and tie rods are examples of axial force members in structural systems where knowledge of the actual in-service levels of axial force can significantly aid in performance evaluation and health monitoring of the structure. Estimation of cable tension in bridge suspenders and hangers using measured natural frequencies has been long established as a nondestructive evaluation technique (Zui et al., 1996; Kim and Park, 2007; Fang and Wang, 2012), while the use of dynamic cable force identification as a tool for structural health monitoring of the onset of structural damage in bridges, by evaluating the redistribution of axial forces in bridge cables, has also been investigated (Hua et al., 2009). However, estimation of tension forces in cables and other axial force members with low slenderness, where the bending stiffness of the cable and boundary condition degree of fixity significantly affect the progression of natural frequencies, yields a challenging nonlinear and potentially ill-conditioned inverse problem that remains an active area of research with many practical applications.

In addition to axial force estimation, determination of the end restraint conditions in structural members provides numerous advantages within performance assessment and structural health monitoring. Axial force members are often designed to operate with unrestrained or nominally restrained end rotations. When environmental effects, such as corrosion, introduce unintended end restraint, the structural member may be subject to significant flexural stresses that may lead to fatigue cracking and subsequent failure. There are numerous examples of infrastructure failures driven by seizure of pins, including successive failure of several tied arch hangers in the Sgt. Aubrey Cosens VC Memorial Bridge (Bagnariol et al., 2003) and the collapse of the Mianus River Bridge following failure of pin and hanger assemblies (United States National Transportation Safety Board, 1984). Reliable in-service methods for determining the effective end restraints on axial force members would provide a means for nondestructively testing critical components over the service life to inform corrective actions for mitigating long-term performance issues.

However, while numerous approximation formulas and iterative techniques (Kim and Park, 2007) exist for the determination of axial forces in long slender cables using dynamic measurements, only recently have techniques emerged for the estimation of axial forces in members with significant bending stiffness. Many cable force estimation techniques rely on approximations to the solution of the characteristic equation that are not valid for short cables and beams, where the bending stiffness introduces significant nonlinearity in the progression of natural frequencies (Zui et al., 1996). Furthermore, the dynamic response of members with high relative bending stiffness is significantly affected by the restraint provided by end connections, unlike slender cables where the relative approximation error resulting from idealization of boundary conditions is often negligible. In these cases, the

experimental parameter identification must include the unknown axial force and the boundary condition restraints at the ends of the member. The need to identify these additional coupled parameters make this nonlinear inverse problem significantly more challenging and, to date, only a limited number of techniques based on the use of measured natural frequencies have been proposed for members with significant bending stiffness. Ceballos and Prato (2008) developed a technique for determining the axial force and bending stiffness using least squares minimization. However, this method is limited to cables with identical fixity on each end and, furthermore, the end restraints are not solved for simultaneously with the internal axial force, which may lead to significant errors due to the parameter dependency in this potentially ill-conditioned problem. Within tie-rod applications, analytical models have generally adopted a simply supported beam representation with either elastic rotational end springs or elastic Winkler foundation springs over some length of the beam ends to account for the support condition provided by anchorage. Parameter identification of the axial force and stiffness of the elastic springs has been proposed through model updating (Amabili et al., 2010).

Recently, a technique has been developed to determine the internal axial force and boundary conditions of slender beams using a minimum of five displacement or curvature measurements obtained along the length of the beam under the action of known static loading (Tullini, 2013). The technique was extended to dynamic measurements by leveraging a single flexural mode shape estimate obtained with no less than five sensors and the corresponding natural frequency measurement (Rebecchi et al., 2013). Li et al. (2013) presented a similar approach that uses singular value decomposition to solve for unknowns in the characteristic equation to develop estimates of axial force and boundary restraints

using a distributed array of five accelerometers, strain gages, or displacement transducers. Timoshenko beam theory has been recently introduced to these five transducer approaches to account for the effects of shear deformation and rotary inertia (Maes et al., 2013). These approaches, however, require a fairly large number of sensors for each axial member of interest in a structure and have been shown to be sensitive to the selection of the mode shape used.

The principal shortcoming of all existing methods for the dynamic identification of axial force and boundary restraints in tie-rods and cables is that they are deterministic in nature and do not attempt to account for uncertainties in the natural frequencies estimates derived from the experimental test data (Figure 4.1a). Dynamic identification presents challenges in quantifying the uncertainty in the parameter estimates because the inverse nature of the problem precludes the use of conventional propagation of uncertainty methods. However, since this inverse problem may be ill-posed and ill-conditioned, it is critical that strategies for quantifying uncertainty in the estimates of axial force and boundary restraints are introduced to provide bounds on the reliability of these estimates for practical applications of this nondestructive evaluation technique. In this study, a novel dynamic identification approach is developed for determining the in-service axial force and end restraint conditions in braces, tie-rods, short cables, and other weakly coupled axially loaded prismatic structural elements with significant bending stiffness. By leveraging the Set Inversion Via Interval Analysis algorithm (SIVIA) (Jaulin and Walter, 1993) as an alternative to optimization, the technique is capable of completely enclosing the entire feasible solution space for the unknown axial force and boundary restraints in prismatic axial force elements using a set of natural frequencies with specified measurement uncertainties (Figure 4.1b).

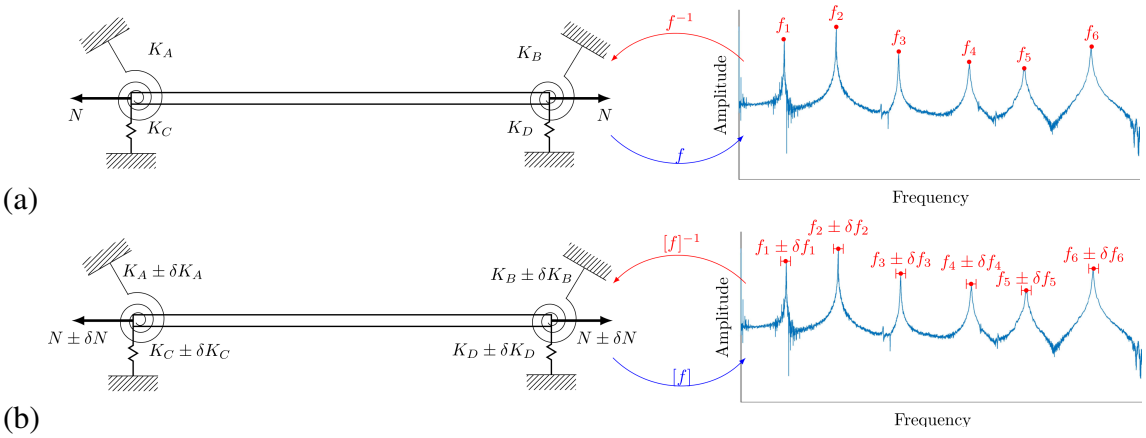


FIGURE 4.1: (a) Conventional deterministic approach to parameter identification of axial force and boundary restraints using inverse methods applied to vibration measurements without uncertainty estimates; (b) Objective of the proposed methodology for inversely propagating measurement uncertainties to the parameter space to quantify confidence in the parameter estimates.

4.2 Theoretical Basis and Formulation

To permit application to structural components where the effects of shear deformations and rotary inertia on the dynamic response are significant, the methodology uses the coupled partial differential equations for the free transverse vibration of a prismatic Timoshenko beam under axial loading (Li, 2013):

$$\kappa GA\left(\frac{\partial^2 u(x,t)}{\partial x^2} - \frac{\partial \theta(x,t)}{\partial x}\right) + N\frac{\partial^2 u(x,t)}{\partial x^2} = \rho A\frac{\partial^2 u(x,t)}{\partial t^2} \tag{4.1a}$$

$$EI\frac{\partial^2 \theta(x,t)}{\partial x^2} + \kappa GA\left(\frac{\partial u(x,t)}{\partial x} - \theta(x,t)\right) = \rho I\frac{\partial^2 \theta(x,t)}{\partial t^2} \tag{4.1b}$$

where $u(x,t)$ and $\theta(x,t)$ are the transverse displacement and rotation of the beam cross section at x varying with time, t, EI is the flexural rigidity of the prismatic cross section, N is the axial force, κ is the Timoshenko shear coefficient, and ρ, G, A, and I are the mass density, shear modulus, cross sectional area, and geometric moment of inertia, which are assumed to be known. By accounting for shear deformation and rotary inertia, the use

of Timoshenko beam theory permits for the application of the developed methodology to both slender and non-slender components and produces more accurate estimates of natural frequencies than Euler-Bernoulli beam theory (Han et al., 1999). With Timoshenko beam theory (Timoshenko, 1921), the bending moment, $M(x,t)$, and shear force, $V(x,t)$, for the beam-column are defined by the constitutive relations (Li, 2013):

$$M(x,t) = -EI\frac{\partial\theta(x,t)}{\partial x} \tag{4.2}$$

$$V(x,t) = \kappa GA\left(\frac{\partial u(x,t)}{\partial x} - \theta(x,t)\right) + N\frac{\partial u}{\partial x} \tag{4.3}$$

By separation of variables, the spatial component of the solution that defines the transverse mode shapes of the beam and the rotation of the cross section can be obtained as:

$$u(x) = C_1 cos\left(\frac{\alpha x}{L}\right) + C_2 sin\left(\frac{\alpha x}{L}\right) + C_3 cosh\left(\frac{\beta x}{L}\right) + C_4 sinh\left(\frac{\beta x}{L}\right) \tag{4.4a}$$

$$\theta(x) = -\frac{1}{d}\left(a\frac{\partial^3 u(x)}{\partial x^3} + e\frac{\partial u(x)}{\partial x}\right) \tag{4.4b}$$

where C_1, C_2, C_3, and C_4 are real-valued constants, L is the length of the beam, and

$$\alpha = L\sqrt{\frac{b + \sqrt{b^2 - 4ac}}{2a}} \tag{4.5a}$$

$$\beta = L\sqrt{\frac{-b + \sqrt{b^2 - 4ac}}{2a}} \tag{4.5b}$$

$$a = EI\left(1 + \frac{N}{\kappa GA}\right) \tag{4.5c}$$

$$b = \frac{EI\rho\omega_i^2}{\kappa G} + \rho I\omega_i^2 - N + \frac{N\rho I\omega_i^2}{\kappa GA} \tag{4.5d}$$

$$c = \frac{\rho^2 I\omega_i^4}{\kappa G} - \rho A\omega_i^2 \tag{4.5e}$$

$$d = \rho I\omega_i^2 - \kappa GA \tag{4.5f}$$

$$e = \frac{EI\rho\omega_i^2}{\kappa G} + \kappa GA \tag{4.5g}$$

where $\omega_i = 2pif_i$ is the corresponding natural frequency of the nth mode shape.

A generalized model for a prismatic beam element under axial loading with uncertain boundary conditions is presented in Figure 4.2. The uncertain boundary conditions are represented by independent rotational springs with stiffness K_A and K_B as well as independent translational springs with stiffness K_C and K_D. Additionally, there may be lumped masses of M_a and M_b and rotational moments of inertia of J_a and J_b at the beam ends, which for this study are assumed to be known. Using the approach suggested by Ceballos and Prato (2008), non-dimensional terms can be introduced to develop normalized parameters quantifying the degree of relative fixity provided by each spring to the respective degree of freedom. By use of these non-dimensional parameters, an assignment of zero degenerates to the idealized free condition, while an assignment of one is equivalent to the idealized fixed condition for the respective degree of freedom. In this paper, we adopt this prior approach for non-dimensionalizing the stiffness of the rotational springs and extend it to the translational springs by defining:

$$k_A = \frac{K_A L}{K_A L + \gamma_R EI} \therefore \frac{K_A}{EI} = \frac{\gamma_R k_A}{L(1-k_A)} \tag{4.6a}$$

$$k_B = \frac{K_B L}{K_B L + \gamma_R EI} \therefore \frac{K_B}{EI} = \frac{\gamma_R k_B}{L(1-k_B)} \tag{4.6b}$$

$$k_C = \frac{K_C L^3}{K_C L^3 + \gamma_T EI} \therefore \frac{K_C}{EI} = \frac{\gamma_T k_C}{L^3(1-k_C)} \tag{4.6c}$$

$$k_D = \frac{K_D L^3}{K_D L^3 + \gamma_T EI} \therefore \frac{K_D}{EI} = \frac{\gamma_T k_D}{L^3(1-k_D)} \tag{4.6d}$$

where γ_R and γ_T are factors introduced to approximately linearize the sensitivities of the

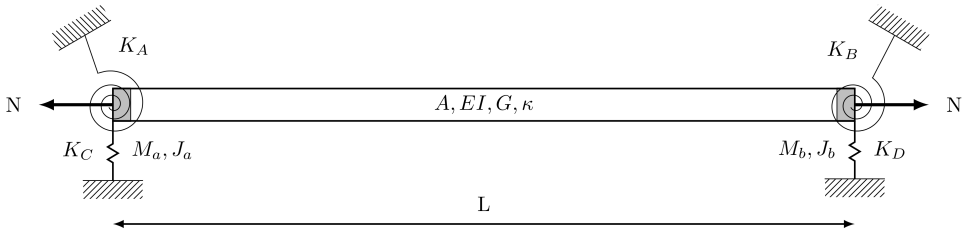


FIGURE 4.2: A prismatic beam element with elastic rotational end restraints under axial loading

natural frequencies to the spring stiffness. These scalar factors need to be developed specific to the element geometry, stiffness, and axial loading. A procedure for establishing these problem-specific scalar factors is presented in Equation 4.6. However, the use of these scalar factors is only necessary if a precise identification of the relative fixity of the boundary conditions is desired.

To solve for the natural frequencies of the generalized beam model, equilibrium conditions can be enforced on the shear force and bending moments at the ends of the beam using the spatial solution expressed in Equation 4.4. Application to the generalized beam model with elastic rotational and translational springs at the beam ends is summarized in Table 4.1 along with the four algebraic equations generated, which are linear and homogeneous with respect to the real constants, C_1 through C_4. These equations can be expressed in matrix form as:

$$\begin{bmatrix} S_{11} & S_{12} & S_{13} & S_{14} \\ S_{21} & S_{22} & S_{23} & S_{24} \\ S_{31} & S_{32} & S_{33} & S_{34} \\ S_{41} & S_{42} & S_{43} & S_{44} \end{bmatrix} \begin{bmatrix} C_1 \\ C_2 \\ C_3 \\ C_4 \end{bmatrix} = \mathbf{S} \begin{bmatrix} C_1 \\ C_2 \\ C_3 \\ C_4 \end{bmatrix} = 0 \tag{4.7}$$

TABLE 4.1: Application of Equilibrium Conditions to Generalized Beam Model

Quantity	Equilibrium Condition	Generalized Equation
$M(0,t)$	$-EI\frac{\partial\theta(0,t)}{\partial x} = -K_A\theta(0,t) - J_a\frac{\partial^2\theta(0,t)}{\partial t^2}$	$S_{11}C_1 + S_{12}C_2 + S_{13}C_3 + S_{14}C_4 = 0$
$M(L,t)$	$-EI\frac{\partial\theta(L)}{\partial x} = K_B\theta(L,t) + J_b\frac{\partial^2\theta(L,t)}{\partial t^2}$	$S_{21}C_1 + S_{22}C_2 + S_{23}C_3 + S_{24}C_4 = 0$
$V(0,t)$	$\kappa GA\left(\frac{\partial u(0,t)}{\partial x} - \theta(0,t)\right) + N\frac{\partial u(0,t)}{\partial x} = K_C u(0,t) + M_a\frac{\partial^2 u(0,t)}{\partial t^2}$	$S_{31}C_1 + S_{32}C_2 + S_{33}C_3 + S_{34}C_4 = 0$
$V(L,t)$	$\kappa GA\left(\frac{\partial u(L,t)}{\partial x} - \theta(L,t)\right) + N\frac{\partial u(L,t)}{\partial x} = -K_D u(L,t) - M_b\frac{\partial^2 u(L,t)}{\partial t^2}$	$S_{41}C_1 + S_{42}C_2 + S_{43}C_3 + S_{44}C_4 = 0$

$S_{11} = (1-k_A)\alpha^2 EI(eL^2 - a\alpha^2)$
$S_{12} = \alpha(eL^2 - a\alpha^2)[EI\gamma_R k_A - (1-k_A)J_a L\omega_i^2]$
$S_{13} = -(1-k_A)\beta^2 EI(eL^2 + a\beta^2)$
$S_{14} = \beta(eL^2 + a\beta^2)[EI\gamma_R k_A - (1-k_A)J_a L\omega_i^2]$
$S_{21} = -\alpha(eL^2 - a\alpha^2)[(1-k_B)EI\alpha cos(\alpha) + EI\gamma_R k_B sin(\alpha) - (1-k_B)J_b L\omega_i^2 sin(\alpha)]$
$S_{22} = -\alpha(eL^2 - a\alpha^2)[(1-k_B)EI\alpha sin(\alpha) - EI\gamma_R k_B cos(\alpha) + (1-k_B)J_b L\omega_i^2 cos(\alpha)]$
$S_{23} = \beta(eL^2 + a\beta^2)[(1-k_B)EI\beta cosh(\beta) + EI\gamma_R k_B sinh(\beta) - (1-k_B)J_b L\omega_i^2 sinh(\beta)]$
$S_{24} = \beta(eL^2 + a\beta^2)[(1-k_B)EI\beta sinh(\beta) + EI\gamma_R k_B cosh(\beta) - (1-k_B)J_b L\omega_i^2 cosh(\beta)]$
$S_{31} = -d(EI\gamma_T k_C - (1-k_C)L^3 M_a\omega_i^2)$
$S_{32} = \alpha(1-k_C)[L^2 Nd + \kappa GA(dL^2 + eL^2 - a\alpha^2)]$
$S_{33} = -d(EI\gamma_T k_C - (1-k_C)L^3 M_a\omega_i^2)$
$S_{34} = \beta(1-k_C)[L^2 Nd + \kappa GA(dL^2 + eL^2 + a\beta^2)]$
$S_{41} = \alpha kGAsin(\alpha)(1-k_D)(dL^2 + eL^2 - a\alpha^2) - EId\gamma_T k_D cos(\alpha) + (1-k_D)L^2 N\alpha d sin(\alpha) + (1-k_D)L^3 M_b d\omega_i^2 cos(\alpha)$
$S_{42} = -\alpha kGAcos(\alpha)(1-k_D)(dL^2 + eL^2 - a\alpha^2) - EId\gamma_T k_D sin(\alpha) - (1-k_D)L^2 N\alpha d cos(\alpha) - (1-k_D)L^3 M_b dk_D\omega_i^2 sin(\alpha)$
$S_{43} = -\beta kGAsinh(\beta)(1-k_D)(dL^2 + eL^2 + a\beta^2) - EId\gamma_T k_D cosh(\beta) - (1-k_D)L^2 N\beta d sinh(\beta) + (1-k_D)L^3 M_b d\omega_i^2 cosh(\beta)$
$S_{44} = -\beta kGAcosh(\beta)(1-k_D)(dL^2 + eL^2 + a\beta^2) - EId\gamma_T k_D sinh(\beta) - (1-k_D)L^2 N\beta d cosh(\beta) + (1-k_D)L^3 M_b d\omega_i^2 sinh(\beta)$

By Cramer's rule, the characteristic equation for the natural frequencies of the system can then be developed by setting the determinant of the matrix **S** to zero. As noted regularly within the literature Li et al. (2013), the nature of this characteristic equation does not permit for the development of closed-form solutions for either the unknown axial force applied to the element or the uncertain boundary restraints. Furthermore, development of any approximate analytical equation for the natural frequencies of the element requires the introduction of simplifying assumptions that are only valid for elements of large slenderness and/or sufficiently high levels of tensioning. Typically, the range for which various approximation formulas are deemed suitable for developing an estimate of the axial force in slender cables and beam members is defined by a non-dimensional parameter, ξ, introduced by (Zui et al., 1996). This non-dimensional parameter is defined as:

$$\xi = L\sqrt{\frac{N}{EI}} \tag{4.8}$$

A survey of recent methodologies for axial force determination with uncertain boundary condition reveals that the current methods employing approximations are only suitable for beams and cables with ξ values greater than 33.3 (Ceballos and Prato, 2008). While alternative methods employing arrays of sensors have been introduced recently for elements of low slenderness and low axial force (Li et al., 2013; Maes et al., 2013), there are significant logistical and economical advantages to performing the internal axial force estimation using natural frequencies measured by a single sensor. The current work develops a technique suitable for determining the internal axial force in weakly coupled prismatic beam and cable elements of any ξ with uncertain boundary conditions using natural frequency estimates obtained from a single sensor. Furthermore, this technique offers the unique capability to incorporate measurement uncertainty into the estimation of the axial force and boundary restraints to inversely map the corresponding confidence in these parameter estimates.

4.3 Set Inversion Via Interval Analysis

In order to understand the approach adopted for the solution of this problem, consider two sets, $\mathbb{X}$ and $\mathbb{Y}$, along with a function f that maps $\mathbb{X} \rightarrow \mathbb{Y}$. In the context of the current problem, $\mathbb{X}$ is the feasible parameter space, f is the characteristic equation for the natural frequencies of the system, and $\mathbb{Y}$ is the set of natural frequencies associated with the parameters. Since the measurement data obtained through vibration testing provides the set $\mathbb{Y}$, determination of $\mathbb{X}$ presents a difficult set inversion problem. However, the Set Inversion Via Interval Analysis (SIVIA) algorithm makes solving this type of problem feasible even when the nature of the problem is ill-conditioned or ill-posed (Jaulin and Walter, 1993). This section provides an overview of the preliminaries of interval analysis and contractor

programming necessary to introduce the reader to this powerful set inversion approach. While interval analysis and set inversion for parameter identification have been previously applied in robotics (Colle and Galerne, 2013), control (Herrero et al., 2004), electrochemistry (Braems et al., 2000), and neural networks (Adam et al., 2015) applications, the approach has not yet been applied to this structural dynamics problem. The authors have recently devised a related approach for structural identification of multiple degree of freedom models (Kernicky et al., 2017), but the extension to continuous system models has yet to be developed. Formal theoretical background of SIVIA can be found in (Jaulin and Walter, 1993), while applied aspects of implementing the algorithm using interval contractor programming can be found in (Jaulin et al., 2001).

Interval arithmetic, or interval-based analysis defines variables as intervals instead of crisp scalar values assuming that the variable may take any value within the interval. For the reader not familiar with interval arithmetic, several pertinent definitions are presented. An *interval* $[x] \in \mathbb{IR}$ is a set of real numbers $[x] = [\underline{x}, \overline{x}] = \{x \in \mathbb{R} | \ \underline{x} \leq x \leq \overline{x}\}$ that is both closed and connected. A *box* $[\boldsymbol{x}] \in \mathbb{IR}^n$ is the Cartesian product of intervals and may be represented as $[\boldsymbol{x}] = [x_1] \times [x_2] ... \times [x_n]$. The *width* of a box, or interval vector, is defined as, $w([\boldsymbol{x}]) = max(\overline{x_i} - \underline{x_i})$. In this paper, intervals are used both for efficient exploration of the feasible parameter space as well as for incorporating measurement uncertainty in $\mathbb{Y}$.

Exploration of $\mathbb{X}$ using the SIVIA algorithm is facilitated by performing interval analysis on subsets of $\mathbb{X} \in \mathbb{IR}^n$ called *subpavings* that completely cover the set $\mathbb{X}$ with non-overlapping boxes. The formulation of the set inversion problem relies on checking these subsets of the search space via *inclusion functions* such that $\mathbb{X}$ is bracketed by two subpavings, $\underline{\mathbb{X}}$ and $\overline{\mathbb{X}}$, which are the inner and outer approximations of $\mathbb{X}$, respectively. The

inner subpaving, $\underline{\mathbb{X}}$, is a strict subset of $\mathbb{X}$, while the outer subpaving is a superset of $\mathbb{X}$. Since the image, $f([\boldsymbol{x}])$, may take any shape, the purpose of an inclusion function is to compute a box, $[f]([\boldsymbol{x}])$, that is guaranteed to contain $f([\boldsymbol{x}])$. Through recursive application of inclusion tests that apply the inclusion functions as constraint equations on interval vectors within the search space, SIVIA develops an enclosure of the set $\mathbb{X} = f^{-1}(\mathbb{Y})$ by checking whether $[f]([\boldsymbol{x}]) \subset \mathbb{Y}$.

In the classic branch and bound SIVIA algorithm (Jaulin and Walter, 1993), the following cases arise from the inclusion test

- If $[f]([\boldsymbol{x}]) \cap \mathbb{Y} = \emptyset$, then $[\boldsymbol{x}] \not\subset \mathbb{X}$ and is discarded as a solution (denoted $[\boldsymbol{x}_o]$ in Figure 4.3)
- If $[f]([\boldsymbol{x}]) \subset \mathbb{Y}$ then $[\boldsymbol{x}]$ is a solution and is stored in $\underline{\mathbb{X}}$ and $\overline{\mathbb{X}}$ (denoted $[\boldsymbol{x}_i]$ in Figure 4.3)
- If $[f]([\boldsymbol{x}]) \cap \mathbb{Y} \neq \emptyset$, but $[f]([\boldsymbol{x}])$ is not entirely in $\mathbb{Y}$ ($[f]([\boldsymbol{x}]) \not\subset \mathbb{Y}$), then $[\boldsymbol{x}]$ may contain a solution (denoted $[\boldsymbol{x}_b]$ in Figure 4.3)

The classic SIVIA algorithm addresses the last case using a branch and bound approach that bisects boxes in the original subpaving until the resolution of the subpaving set approximation to $\mathbb{X}$ satisfies a user defined interval precision, ϵ. When $[\boldsymbol{x}]$ may contain a potential solution and $w([\boldsymbol{x}])$ is greater than ϵ, then $[\boldsymbol{x}]$ is bisected and the inclusion test is applied recursively to the new boxes generated by the bisection. However, if the desired interval precision is satisfied such that $w([\boldsymbol{x}]) < \epsilon$, $[\boldsymbol{x}]$ is stored in $\overline{\mathbb{X}}$. In this way, the outer approximation $\overline{\mathbb{X}}$ is defined as:

$$\overline{\mathbb{X}} = \underline{\mathbb{X}} \cup \delta\mathbb{X}$$

where $\delta\mathbb{X}$ is the set of all boxes with widths less than ϵ that may contain a solution.

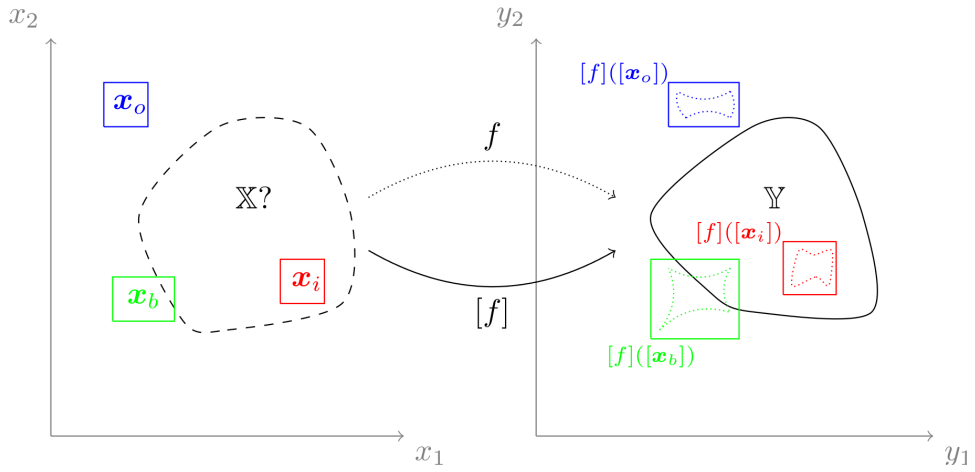


FIGURE 4.3: Inclusion tests applied to determine whether the box being tested lies within the solution set ($\boldsymbol{x_i}$), on the boundary ($\boldsymbol{x_b}$), or outside the solution set ($\boldsymbol{x_o}$)

While the branch and bound technique is guaranteed to completely explore the entire search space, the number of boxes required to be evaluated by this approach to achieve the desired interval precision on the subpavings may be computationally expensive. However, the number of boxes evaluated may be reduced by replacing the pure branch and bound approach for pruning the search space with set contractions. Doing so produces a more compact paving of the solution, $\mathbb{X}$ (Jaulin et al., 2001). The basic idea is to contract or shrink a box, $[\boldsymbol{x}]$, with respect to a set of constraints such that no potential solution within the box is lost. *Contractors* are mathematical operators that accept an n-dimensional box as an input and then contract the domain according to a given set of constraints. Formally, a contractor, *Ctc*, is a function from $\mathbb{IR}^n \rightarrow \mathbb{IR}^n$ with the following properties (Chabert and Jaulin, 2009):

- $\forall [\boldsymbol{x}] \in \mathbb{IR}^n \; Ctc([\boldsymbol{x}]) \subset [\boldsymbol{x}]$, where $Ctc([\boldsymbol{x}])$ is the contracted box.

- $Ctc([\boldsymbol{x}]) \cap System = [\boldsymbol{x}] \cap System$.

The first property ensures that the interval vector returned after the contraction is a subset of the original interval vector on which the contraction is performed. The second property ensures completeness of the subpaving approximation by requiring that no potential solution is lost when the contraction is performed.

To enhance the computational efficiency of SIVIA, the inner and outer inclusion tests are replaced with recursive contractions (Jaulin et al., 2001). In this approach, boxes are evaluated and subsequently reduced with respect to either an inner contractor such that, $f([\boldsymbol{x}]) \subset \mathbb{Y}$, or an outer contractor such that $f([\boldsymbol{x}]) \not\subset \mathbb{Y}$. Replacing the inner and outer tests with set contractions yields the following cases

- If $[\boldsymbol{x}]$ is contracted with respect to the inner contractor such that $[f]([\boldsymbol{x}]) \subset \mathbb{Y}$ then $[\boldsymbol{x}] \subset \mathbb{X}$ and $[\boldsymbol{x}]$ is stored in $\underline{\mathbb{X}}$.

- If $[\boldsymbol{x}]$ is contracted with respect to the outer contractor such that $[f]([x]) \not\subset \mathbb{Y}$ then $[\boldsymbol{x}] \not\subset \mathbb{X}$ and is discarded as a solution.

- If $[\boldsymbol{x}]$ fails to be contracted by either the inner or outer contractor and $w([\boldsymbol{x}]) > \epsilon$ then $[\boldsymbol{x}]$ lies on the boundary and it is bisected and the contractions are applied to the new boxes. If $w([\boldsymbol{x}]) < \epsilon$ then $[\boldsymbol{x}]$ is stored in the outer approximation $\overline{\mathbb{X}}$.

To better understand the effects of replacing the inner and outer inclusion tests from the classic SIVIA algorithm with contractors, consider the function $f(x) = (\frac{x_1}{4})^2 + (\frac{x_2}{2})^2 - 1$ for $[y] \in [-1, 1]$ (Figure 4.4a) with an initial search space of $[\boldsymbol{x}] = [-10, 10] \times [-10, 10]$ (Figure

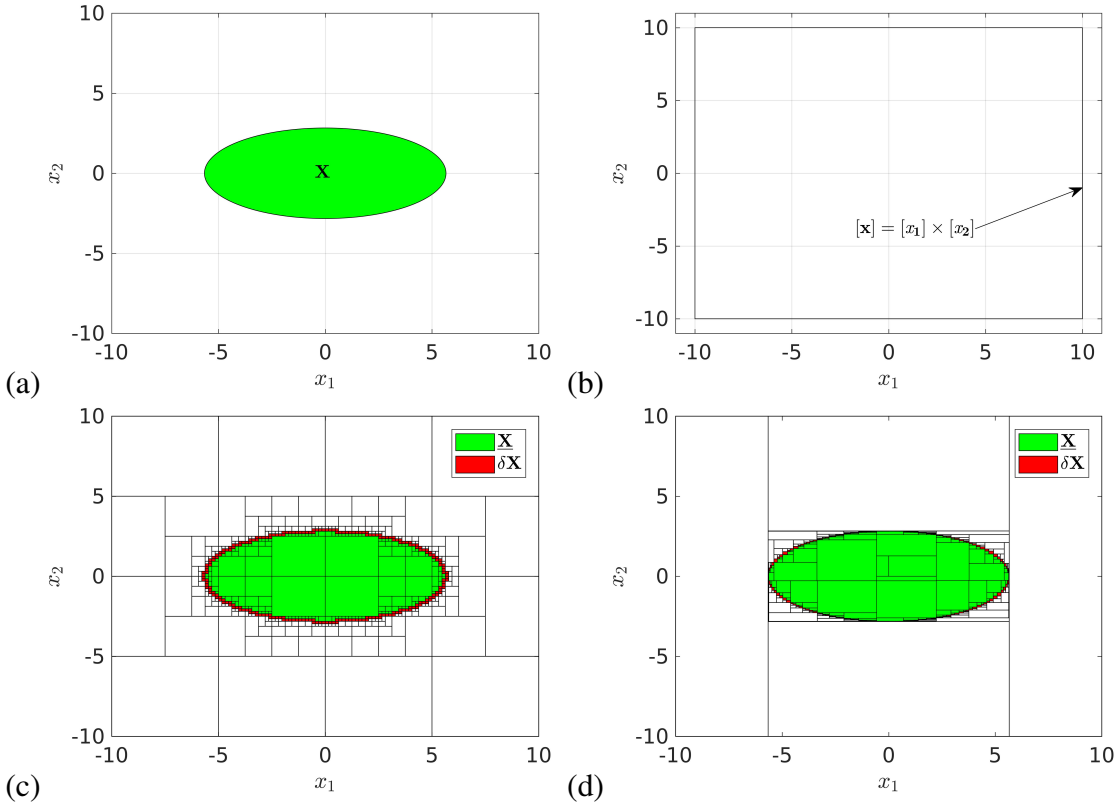


FIGURE 4.4: A set inversion $f(x) \in [y]$ with (a) $f(x) = (\frac{x_1}{4})^2 + (\frac{x_2}{2})^2 - 1$ and $[y] \in [-1, 1]$. (b) The initial box, $[\boldsymbol{x}] = [-10, 10] \times [-10, 10]$. (c) Subpavings from the set inversion using the classic branch and bound SIVIA algorithm. (d) Subpavings from the set inversion using SIVIA with inner and outer contractors.

4.4b). Application of the classic branch and bound SIVIA algorithm requires evaluation of 596 boxes to fully pave the search space to a precision of 0.25 (Figure 4.4c). Replacing the branch and bound approach with contractors, the SIVIA algorithm requires the evaluation of only 460 boxes (Figure 4.4d). The efficiency of the second approach is revealed in the large volumes of the search space discarded in the contraction process that would otherwise be required to be bisected and evaluated within the classic approach. The contractors are particularly efficient at developing a coarse approximation to $\mathbb{X}$ and the majority of the function evaluations are performed simply to refine the nonlinear boundary around the feasible set to achieve the prescribed interval precision.

4.3.1 Accounting for Measurement Uncertainty Using Interval Constraint Equations

In application to the axial force determination problem, measurement uncertainty may be accounted for by expressing the natural frequency measurements as intervals rather than crisp scalar values. For instance, the i^{th} natural frequency could be expressed as $[\underline{f_i}, \overline{f_i}]$, where $\underline{f_i}$ and $\overline{f_i}$ are the expected lower and upper bounds on the natural frequency, respectively. In practical applications, these bounds could be specified using any rational approach and, if desired, specific to each measured natural frequency. A simple means for developing these measurement intervals is to use $[f_i - \chi, f_i + \chi]$, where χ is the specified radius of the interval with respect to the measurement and could be estimated using either a Type A or Type B evaluation of standard uncertainty (Joint Committee for Guides in Metrology (JCGM), 2008). In addition, system identification techniques that provide the means for estimating uncertainty bounds on the modal parameter estimates, including natural frequencies, have been recently developed (Reynders et al., 2008, 2016). Note that a distinct advantage of expressing uncertainty in the form of an interval is that neither the probability distribution functions associated with the uncertainty in the measurement data nor the uncertainty in the parameters need to be defined or assumed.

In order to facilitate use of this approach of introducing the measurement data in the form of an interval rather than a scalar value, the constraint equations for each measured natural frequency are stated as:

$$det(S([\underline{f_i}, \overline{f_i}])) = 0 \tag{4.9}$$

Then, in order to facilitate definition of the inner and outer contractors in the SIVIA algo-

rithm, this constraint equation is split to create two constraint equations for each measured natural frequency. In this way, constraint equations are developed around the limits of the intervals to bound the feasible parameter space, $\mathbb{X}$. Specifically, each lower and upper bound natural frequency estimate is substituted into the characteristic equation to define the boundary of the feasible parameter space using Equations 4.10 and 4.11.

$$det(S(\underline{f_i})) = 0 \tag{4.10}$$

$$det(S(\overline{f_i})) = 0 \tag{4.11}$$

With the boundary of the feasible parameter space defined, the inclusion functions for the inner and outer contractors can be formed through set union and intersection. Figure 4.5 illustrates how the parameter space is divided by the lower and upper bound constraint equations for a single natural frequency prescribed in the characteristic equation. As illustrated within this figure, the feasible solution set $\mathbb{X}$ results from an intersection of two inclusion functions developed by inequality constraint equations, while all infeasible solutions can be excluded through the union of two additional inclusion functions developed by inversions of the inequality constraint equations. To incorporate multiple natural frequencies into the parameter identification, these unions and intersections that are used to define the inclusion functions for the inner and outer contractors, respectively, can be expanded as:

$$\bigcap_{i=1}^{n} \left[(-1)^{i+1} det(S(\underline{f_i})) \leq 0 \cap (-1)^{i+1} det(S(\overline{f_i})) \geq 0 \right] \tag{4.12}$$

$$\bigcup_{i=1}^{n} \left[(-1)^{i+1} det(S(\underline{f_i})) > 0 \cup (-1)^{i+1} det(S(\overline{f_i})) < 0 \right] \tag{4.13}$$

where n is the number of measured natural frequencies included in the parameter identifi-

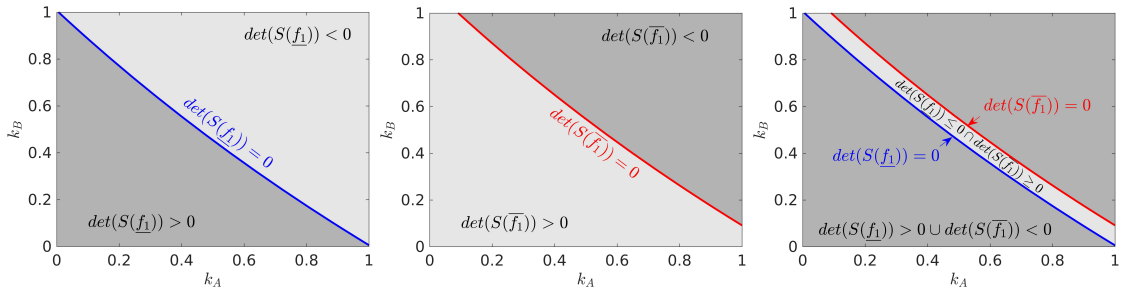


FIGURE 4.5: Illustration of how inequality constraints developed using the characteristic equation with lower and upper bound natural frequency estimates are utilized to form inclusion functions for the inner and outer contractors for the first natural frequency.

cation. It should be noted that a sign inversion is present in these equations, which reflects the directional change in gradient of the characteristic equation as the order of the natural frequency is incremented. It is not necessary to have a continuous set of identified natural frequencies from the vibration testing to employ the proposed method, however, due to this directional change in gradient, it is necessary to know the order of the natural frequencies prescribed.

4.3.2 Simple Illustrative Example of the Application of SIVIA

To illustrate the basic underlying principles behind the methodology using a reduced parameter identification problem having a two-dimensional search space, consider a prismatic beam with fixed translational boundary conditions ($k_C = k_D = 1$) and a known axial force where the objective of the inverse problem is simply to determine the relative rotational end restraints on the beam. For this example, a 5 m long steel (E=200 GPa, ρ=7850 kg/m^3) rod with 6.5 cm diameter is subject to an axial stress of 175 MPa, which corresponds to an axial force of 581 kN. Relative rotational end restraints on the beam were prescribed as 0.70 and 0.30 for k_A and k_B, respectively, and no additional lumped mass or rotational moment of inertia was added to the beam ends. The roots of the characteristic equation were

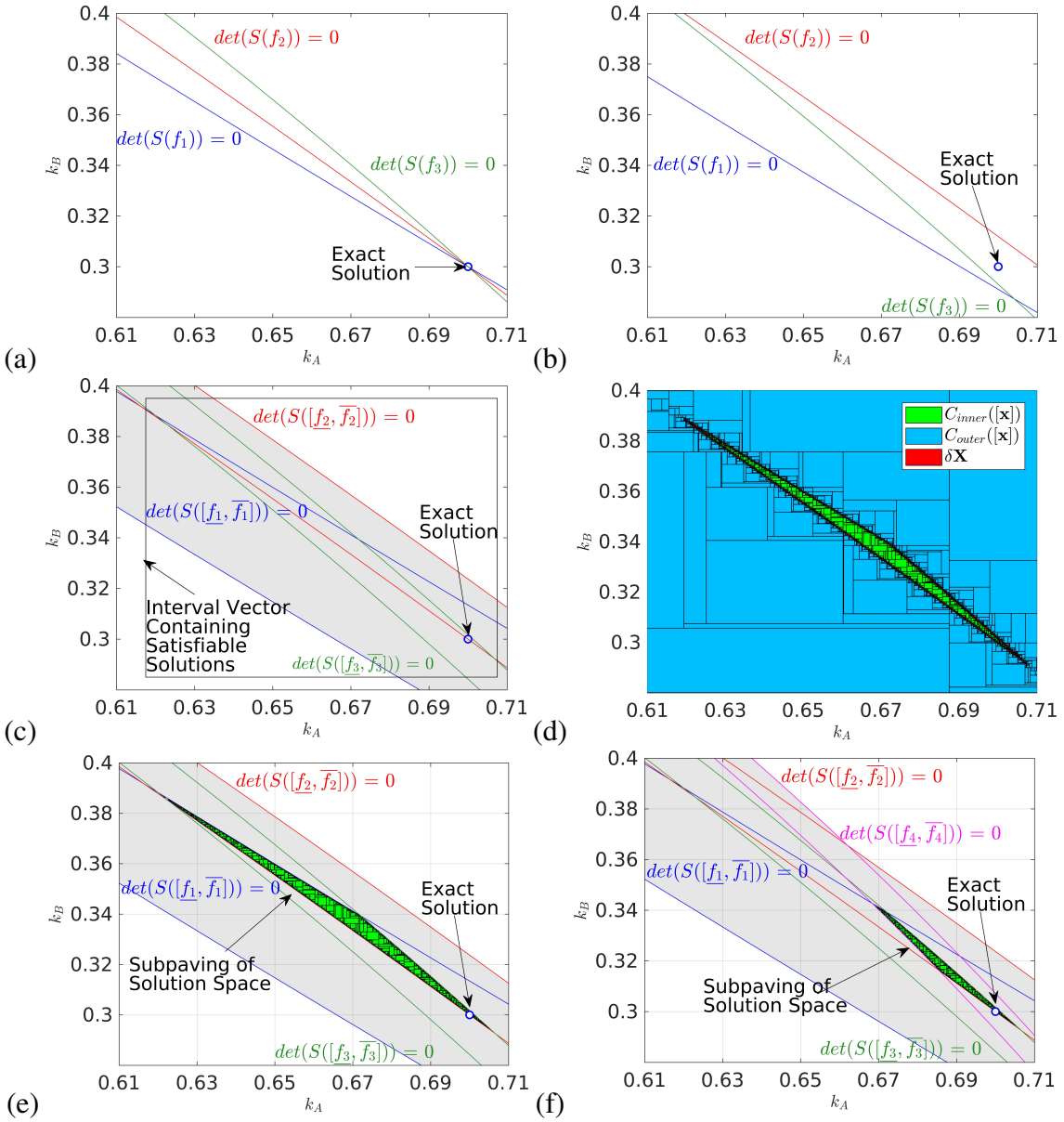


FIGURE 4.6: Illustration of contractor programming for axial force determination in the presence of measurement uncertainty over a two dimensional search space: (a) Noise-free intersection of constraint equations; (b) Constraint equations in the presence of measurement error; (c) Specifying constraint equations with measurement uncertainty of ±0.05 Hz; (d) Subpaving of solutions space displaying inner, outer, and boundary boxes generated with an interval precision of 0.0005; (e) Inner approximation of the feasible parameter set shown with constraint equations; (f) Further pruning of solution space by inclusion of addition constraint equations (additional natural frequency measurement)

determined numerically to generate synthetic measurements of the natural frequencies. In the absence of measurement noise, the constraint equations formed from the characteristic equations with substitution of each of the first three exact natural frequencies will intersect at the exact solution for the spring stiffness parameters (Figure 4.6a). However, since experimentally estimated natural frequencies are always corrupted by measurement and process errors, the constraint equations developed from application of the governing characteristic equation with measurement data will no longer intersect at a single point (Figure 4.6b) and no feasible solutions will be returned by the SIVIA algorithm. If measurement uncertainty is expressed in the prescribed natural frequencies using intervals, the constraint equations are relaxed to bound the regions defined by Equations 4.12 and 4.13 (Figure 4.6c). Through this relaxation of the constraint equations, the set of inclusion functions formed by the application of the characteristic equation with noisy measurements can be satisfied within the region over which they all intersect. The subpavings of boxes generated by the inner and outer contractors of the SIVIA constraint satisfaction algorithm are displayed in Figure 4.6d. The inner subpaving expresses the range of guaranteed feasible combinations of rotational boundary restraints that could yield the measured natural frequencies in the range of the specified uncertainty bounds, while the $\delta\mathbb{X}$ subpaving defines the boundary where additional feasible solutions may exist. Note that, due to sufficient interval relaxation, the exact solution is included in the region of the inner subpaving (Figure 4.6e). Upon further reducing the required interval precision, the widths of the boxes developing the subpaving around the boundary will simply be reduced and the outer approximation, $\overline{\mathbb{X}}$, will approach $\underline{\mathbb{X}}$ to more sharply define the feasible parameter space. Lastly, if an additional natural frequency measurement is introduced to the parameter identification through addi-

tional constraint equations, then the solution space will be further pruned by this additional system information thereby reflecting increased certainty in the identification of the rotational spring stiffnesses (Figure 4.6f). This simplified example illustrates the fundamental techniques and principles proposed for solving the parameter identification problem with uncertainty quantification using SIVIA. In the following sections, the complete methodology will be expanded to the dynamic identification of the internal axial force and boundary restraints.

4.4 Methodology For Parameter Estimation With Uncertainty Quantification

Dynamic identification of the internal axial force and end restraints in prismatic beams with uncertainty quantification can be performed through extension of the simplified illustrative example presented in the prior subsection. In this prior illustration and within the developed methodology, the unknown non-dimensional boundary restraint spring stiffness parameters are treated as continuous variables and SIVIA is used to develop inner and outer approximations to the set of feasible parameter combinations that produce natural frequencies within specified uncertainty from the measured values. While it is possible to establish the constraint equations with the internal axial force also treated as a continuous variable, such a declaration leads to a computationally intractable problem. The reason for this added computational complexity is that the axial force, N, is nested within multiple square roots as well as trigonometric and hyperbolic functions in Equation 4.4. As a result, the parameter space cannot be efficiently reduced by interval contractors for the axial force parameter, thereby leading to a large number of required bisections of the search space to achieve reasonable interval precision. To overcome this computational issue, the

unknown axial force can be restricted to a fixed precision by constraining it to a predefined set of discrete real-valued assignments. In this way, the constraint equations are developed from the characteristic equation using a prescribed value of axial force and the SIVIA algorithm is used to map the corresponding feasible solutions, if any, for the non-dimensional boundary restraint spring stiffness assignments associated with the prescribed value for the axial force. The resulting subpaving is essentially a multi-dimensional slice through the feasible parameter space at a fixed value of internal axial force. By sequentially performing this reduced parameter identification over a set of internal axial force assignments, inner and outer approximations to the feasible parameter space for both the boundary restraints and axial force parameters can be developed. Since the feasible parameter space is a contiguous volume, this approach of subpaving multi-dimensional slices of the feasible parameter space remains accurate to the interval precision used. This methodology for dynamic identification of internal axial force and boundary restraints with uncertainty quantification was implemented in the C++ programming language using the IBEX library for interval arithmetic and contractor programming (Chabert, 1999). In this implementation, forward-backward contractions through the HC4 algorithm (Benhamou et al., 1999) were employed.

4.4.1 Demonstration and Verification for Axial Force and Rotational Boundary Restraints

To demonstrate the application of the proposed algorithm for determination of axial force and boundary restraints, a case limited to unknown rotational boundary restraints and internal axial force is presented first. The analytical model previously described for a 6.5 cm di-

ameter steel rod of 5 m length under an axial load of 581 kN was used to generate synthetic natural frequency measurements through forward solution of the roots of the characteristic equation. The non-dimensional parameter ξ for this rod under the prescribed axial load is 9.1, which is far less than the limit for which existing methods employing approximate analytical formulas are valid. In developing this synthetic data, the translational restraint on both ends of the rod were idealized as fixed ($k_C = k_D = 1$) and the non-dimensional spring assignments for the rotary springs were prescribed as $k_A = 0.70$ and $k_B = 0.30$. Furthermore, the linearization parameters were developed as linear functions of the axial load as $\gamma_R = 6.41 + 0.0092N$ and $\gamma_T = 70 + 0.2N$, respectively, following the procedure described in Appendix A. To add uncertainty to the problem, 15 sets of synthetic natural frequency estimates were generated with Gaussian noise with standard deviations, σ, of 0.1 Hz around the exact natural frequencies. For the development of constraint equations, interval values for each of the synthetic natural frequency measurements were established as:

$$[\underline{f_i}, \overline{f_i}] = [f_i^{avg} - \alpha\sigma, f_i^{avg} + \alpha\sigma] \tag{4.14}$$

where $\underline{f_i}$ and $\overline{f_i}$ are the prescribed lower and upper interval bounds on the measurement for the i-th natural frequency, f_i^{avg} is the average natural frequency computed across the set of 15 noisy synthetic measurements, and $\alpha\sigma$ is a fraction of the standard deviation used to prescribe a confidence interval for the natural frequency measurement.

The search space for the unknown rotational boundary restraints was constrained to $k_A \in [0, 1]$ and $k_B \in [0, 1]$, which encompasses the entire range of physically plausible conditions from fully unrestrained to complete rotational fixity at each boundary. Sequen-

tial applications of the SIVIA algorithm were applied at 2 kN increments of N and, in order to fully encompass the feasible parameter space with subpavings, these increments were initiated and terminated at axial loads that yielded no satisfiable solutions. Figure 4.7 presents the subpavings that define the basins of feasible solutions across the increments of discrete axial force assignments obtained when the first eight synthetic natural frequencies are used in the parameter identification with an interval radius of $\alpha\sigma = \frac{1}{2}\sigma$. In this example, an interval precision of 1e-3 for the uncertain rotational boundary conditions was specified and the total time required for SIVIA to fully characterize the solution set across the entire range of discrete axial forces was 5.6 seconds. The figure presents three perspectives of the three-dimensional parameter space. In the first subplot, each of the individual polygons is a subpaving of the feasible combinations of parameter assignments for a fixed value of internal axial force, analogous to the illustrative example presented in Figure 4.6e. The other subplots present this same set of subpavings from different perspectives, from which the approach of limiting the axial force identification to a set of discrete values is readily apparent. Interpolation between the subpavings generated across the set of discrete axial force assignments can be used to enclose a continuous basin of all possible combinations of k_A, k_B, and N that yield natural frequencies within the specified uncertainty. The incrementation across of the set of discrete axial force assignments is user-prescribed and results in a trade-off between the precision with which the boundary of the continuous basin of the feasible parameter space is developed and the computational time required to develop the subpavings. As evident in Figure 4.7, the solution space is symmetric with respect to k_A and k_B. This non-unique solution results because only natural frequencies are used in the dynamic identification and, consequently, it is not possible to uniquely spatially

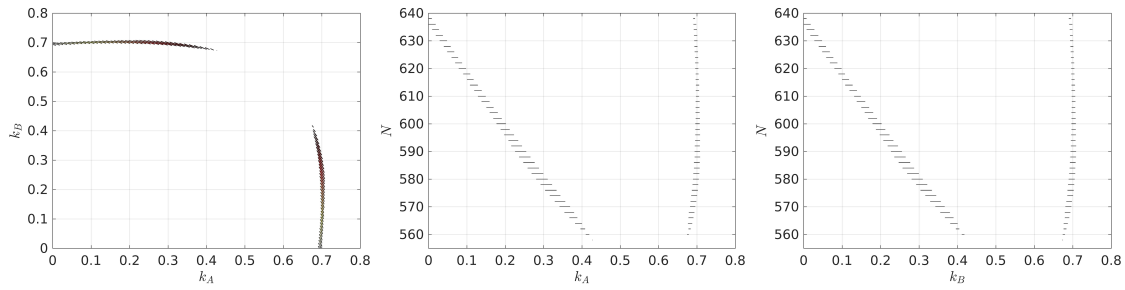


FIGURE 4.7: Sets of subpavings developed across the discrete set of values for N using the first eight natural frequencies in the parameter identification and an interval uncertainty of $\frac{1}{2}\sigma$

identify which end of the beam has greater relative rotational fixity without introducing *a priori* knowledge or engineering judgment. While the developed methodology is capable of mapping the multiple solutions to the symmetric feasible parameter space under this non-uniqueness issue, an additional constraint equation, $k_A \geq k_B$, is introduced in subsequent examples to reduce the feasible parameter space to only half of the symmetric solution.

The development of a continuous basin for the feasible parameter space by interpolating between the subpavings developed at discrete values of axial force assignments is presented in Figure 4.8. In this figure, the sensitivity of the feasible parameter space to the number of natural frequencies, n_f, included in the parameter identification is explored by developing the continuous basins from subpavings obtained using either four, six, or eight natural frequencies. The confidence interval for the synthetic natural frequency measurements was specified as $\pm\frac{1}{2}\sigma$ for all three cases. The results demonstrate that, for the analytical model used, the inclusion of additional natural frequency measurements results in a significant improvement in the certainty of the identification of k_A and a modest improvement in the certainty associated with the identification of k_B. However, the parameter uncertainty for the identified internal axial force is only slightly improved by expanding the measurement

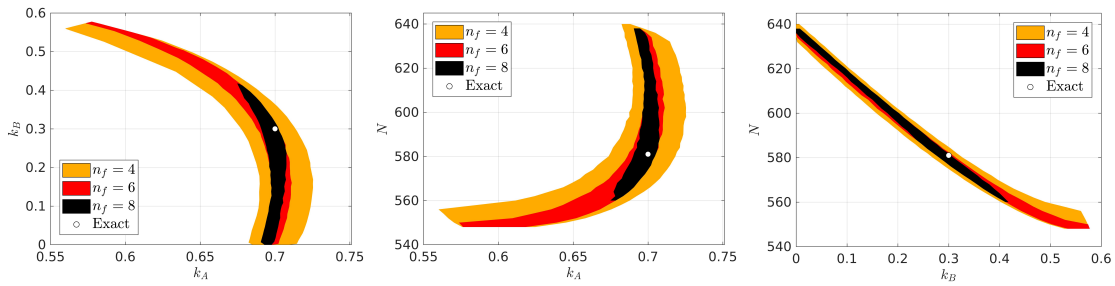


FIGURE 4.8: Interpolation of continuous basins for feasible parameter space for interval uncertainty of $\pm\frac{1}{2}\sigma$ on natural frequencies with four, six, or eight natural frequencies included in parameter identification.

data to eight natural frequencies. The interval hull, which is the smallest box capable of completely enclosing the solution set (Jaulin et al., 2001), is presented in tabular form for each of these solutions in Table 4.2. This table presents the rotational boundary restraint stiffness in the non-dimensional, or relative, form as well as converted to engineering units through Equation 4.6. The hull can be used to illustrate the change in the midpoints and radii of the identified uncertain parameters as the number of natural frequencies used in the parameter identification is varied.

TABLE 4.2: Interval hull of feasible parameters obtained with a confidence interval of $\frac{1}{2}\sigma$ for the natural frequency measurements and interval precision of 1e-3

Parameter	$n_f = 4$	$n_f = 6$	$n_f = 8$
N (kN)	594±46	593±45	599±39
k_A	0.643±0.083	0.642±0.069	0.691±0.016
k_B	0.289±0.289	0.289±0.289	0.209±0.209
K_A (kN· m/Rad)	810.31±296.10	787.30±246.35	926.98±86.11
K_B (kN· m/Rad)	274.33±274.33	274.33±274.33	145.33±145.33

The sensitivity of the feasible parameter space to the specified measurement uncertainty can also be revealed by developing the subpavings of the feasible parameter space with different confidence intervals specified for the uncertain synthetic natural frequency mea-

surements. Figure 4.9 presents such an analysis using eight natural frequencies in the parameter identification with confidence intervals of $\pm\frac{1}{2}\sigma$, $\pm\sigma$, and $\pm 2\sigma$ on the synthetic measurement data. For this case, the results indicate that the relative uncertainty in the parameter identification for the stiffness of the rotational boundary restraints increases faster than the relative uncertainty in the identified internal axial force as the measurement uncertainty increases. The basins formed by these subpavings were further used to verify the methodology by evaluating the forward solution of the roots of the characteristic equation developed using discrete parameter combinations sampled from the volumes defined by each basin. A total of 1000 points were randomly sampled from each volume, as presented in Figure 4.10a. The natural frequencies for the rod with internal axial force and spring stiffness assignments associated with each sampled point were then computed and the residuals between these natural frequencies for the model and the prescribed synthetic natural frequency measurements were calculated. Figure 4.10b presents the maximum natural frequency residual, normalized to the standard deviation, for all of the sampled points. The results successfully verify the methodology, as the maximum residual for all of the sampled points was found to be correctly bounded within the prescribed interval radii used to express the confidence intervals for the synthetic measurements.

4.4.2 Demonstration and Verification for Axial Force and Translational and Rotational Boundary Restraints

The developed methodology can be further extended for the dynamic identification of both rotational and translational boundary restraints as well as the internal axial force. However, the introduction of two additional unknowns increases the dimensionality of the

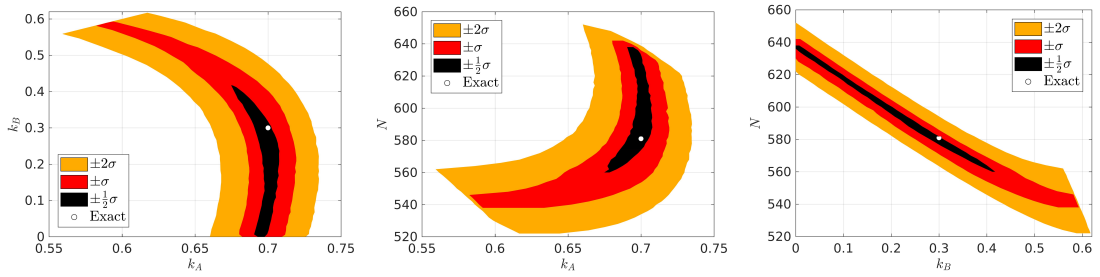


FIGURE 4.9: Sensitivity of the identified parameter uncertainty with measurement uncertainty; shown for interval uncertainties of $\pm\frac{1}{2}\sigma$, $\pm\sigma$, and $\pm 2\sigma$ using the first eight natural frequencies in the parameter identification

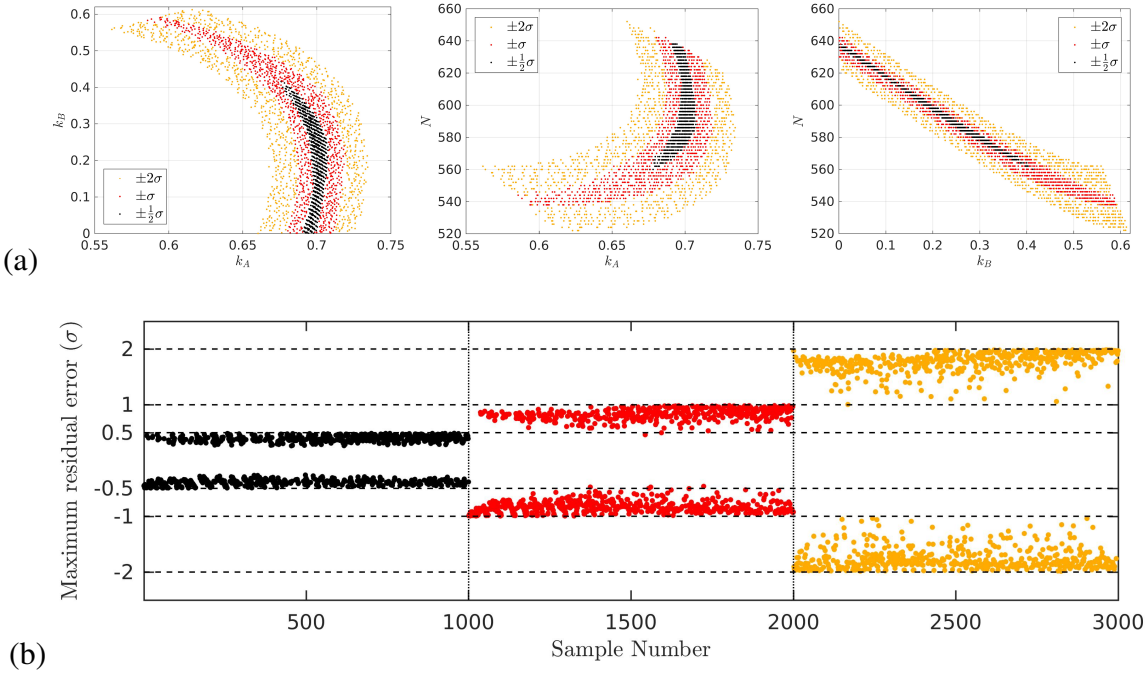


FIGURE 4.10: Verification of extended methodology: (a) sampling of real-valued parameter assignments for verification; (b) maximum residual errors computed for the sampled verification points

problem such that the SIVIA algorithm, which has complexity exponential in the number of unknown parameters, no longer provides subpavings with sufficiently high precision within reasonable computational time. The reason for computational inefficiency with increased dimensionality is that the subpavings tend to accumulate on the boundary of the solution space, $\delta\mathbb{X}$, when the number of variables is large or the feasible solution space is nonlinear

(Jaulin et al., 2001). For the dynamic identification problem involving both rotational and translational boundary restraint parameters, the dimensionality of the problem is increased to four dimensions and the feasible parameter space is significantly nonlinear across these dimensions. To overcome this computational challenge, the developed methodology was modified to yield subpavings of the feasible solution space using only inner contractors. This approach leverages the rationale that a box may be discarded from the solution if it does not belong to the set defined by the inner contractors, instead of discarding it only if it is able to be contracted by the outer contractors (Chabert and Jaulin, 2009). Therefore, the equations developed for the outer contractor (Equation 4.13) may be discarded and only the equations defining the inner contractor (Equation 4.12) are utilized to obtain the subpavings of the four-dimensional feasible solution space across a discrete set of internal axial force values. Note that boxes that meet the prescribed interval precision, but do not lie wholly within the inner approximation are still included in the solution set. Consequently, the subpaving returned by this modified approach is limited to the outer approximation, $\overline{\mathbb{X}}$.

To demonstrate, and subsequently verify, the use of this methodology for the identification of both rotational and translational boundary restraints as well as internal axial force, the prior analytical model of a 6.5 cm diameter steel rod of 5 m length under an axial load of 581 kN was modified to replace the fixed translational restraints on the rod ends with linear springs. The relative fixity of these linear springs, k_C and k_D, were arbitrarily assigned as 0.75 and 0.45, respectively, while the relative fixity of the rotational springs remained unchanged. Synthetic natural frequency measurements were generated by applying Gaussian noise with standard deviations of 0.1 Hz to the exact analytical solutions for the natural frequencies. The average natural frequencies computed across a set of 15

noisy synthetic measurements were then used to establish the midpoint of interval bounds for the measured natural frequencies with confidence intervals defined by the standard deviations, as in Equation 4.14. The search space for all four of the boundary restraints was bounded to [0, 1], which makes no assumptions on any of the restraint conditions and fully encompasses the range of physically plausible conditions from fully unrestrained to complete fixity in each degree of freedom. Sequential applications of set inversion using only the inner interval contractors with an interval precision of 1e-3 were applied at fixed 2 kN incrementation of axial load.

Figure 4.11 presents the interpolated continuous basins of feasible solutions developed by the set of subpavings returned using a confidence interval of $\frac{1}{2}\sigma$ on the synthetic natural frequency measurements. Basins developed using either 6, 8, 10, or 12 natural frequencies in the parameter identification are presented in this figure. The ability to reflect the effect of the measurement uncertainty in the parameter space allows for significant differences in the confidence of the identified parameters to be readily identified and quantified. For this example, the natural frequencies of the rod are significantly more sensitive to the relative stiffness of the translational boundary restraints and, consequently, the parameter identification is able to obtain estimates for k_C and k_D with significantly greater certainty than the relative stiffness of the rotational boundary restraints. Table 4.3 summarizes the interval hull for each parameter using the midpoint and radius of the identified parameter space. For this example, the midpoints of the identified feasible parameter space were generally consistent as the number of natural frequencies included within the parameter identification was increased, while the confidence in the identified parameter assignments was significantly improved. It should be noted that the exact solution for the internal axial

force and boundary restraints is close to, but not contained within, the interval hull or the mapped continuous basin of the feasible parameter space for translational spring k_D. This example was intentionally provided to emphasize the need to prescribe sufficiently accurate uncertainty to the natural frequencies in order to ensure enclosure of the exact solution within the set of all feasible solutions. For instance if the uncertainty was increased from $\frac{1}{2}\sigma$ to σ, the exact solution for k_D would lie within the feasible solutions space.

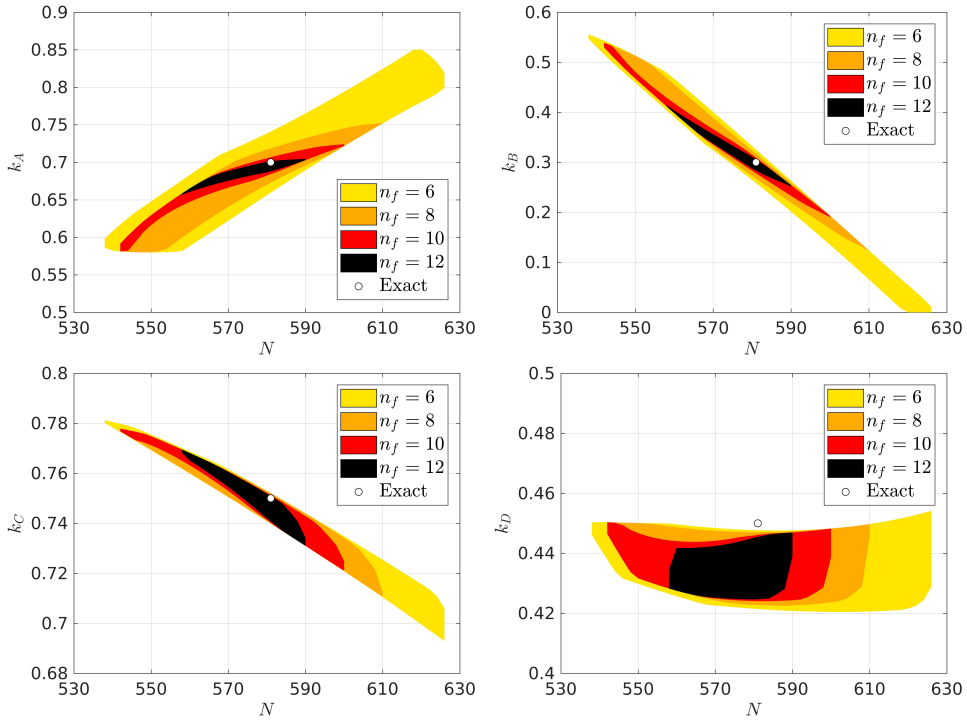


FIGURE 4.11: Extension of methodology to the identification of rotational boundary restraints, translational boundary restraints, and internal axial force with uncertainty quantification; confidence intervals of $\pm\frac{1}{2}\sigma$ using either 6, 8, 10, or 12 natural frequencies in the parameter identification

Verification of the extended methodology for parameter identification of rotational boundary restraints, translational boundary restraints, and internal axial force was performed similarly to the prior example by evaluating 1000 randomly sampled real-valued parameter combinations from the volumes defined by each feasible solution basin (Figure 4.12a).

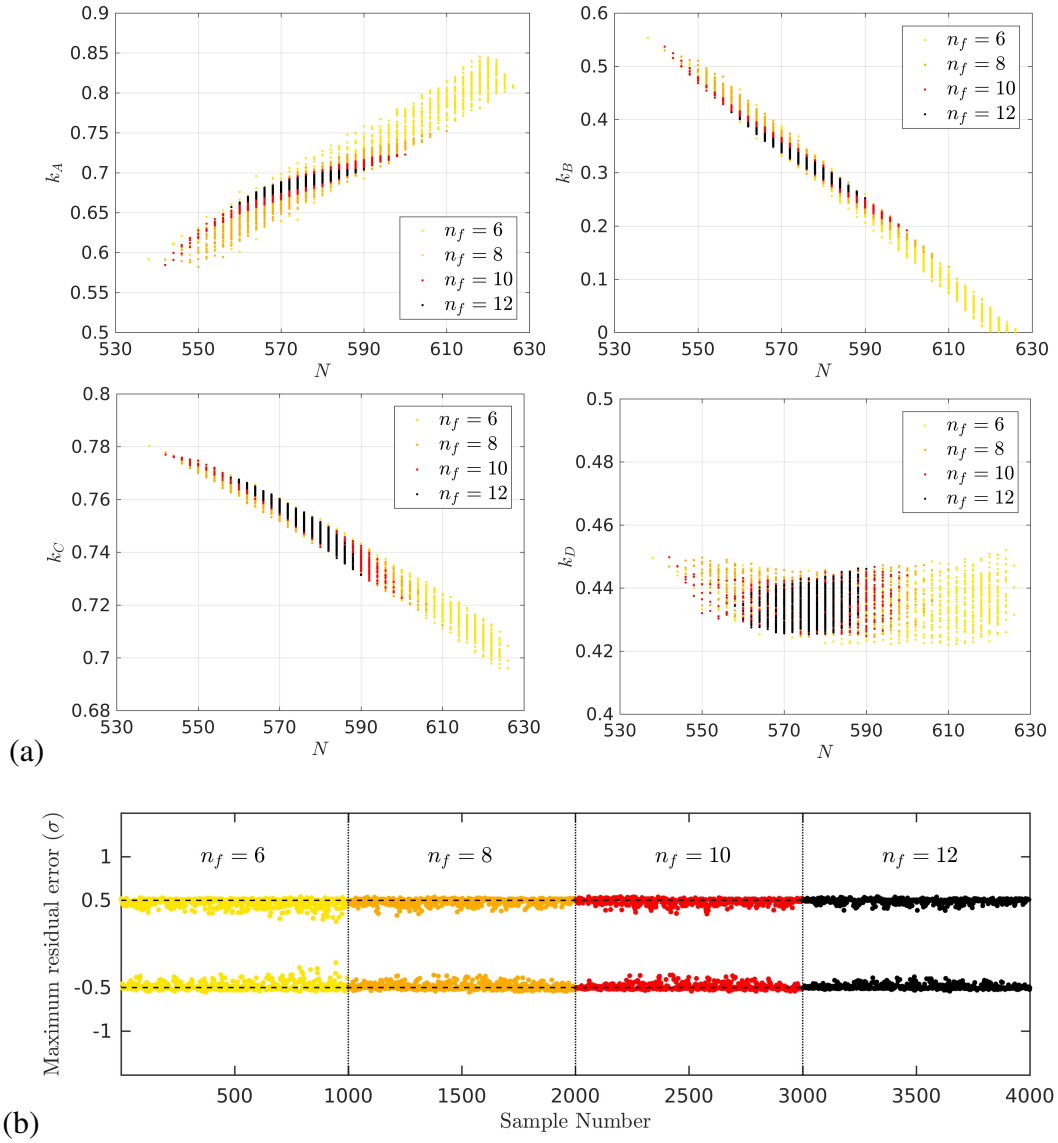


FIGURE 4.12: Verification of methodology: (a) sampling of discrete parameter set from the subpavings; (b) maximum residual relative to standard deviation of measurements computed by the forward solution with sampled points.

TABLE 4.3: Interval hull of feasible parameters obtained with a confidence interval of $\pm\frac{1}{2}\sigma$ for the natural frequency measurements and interval precision of 1e-3

Parameter	$n_f = 6$	$n_f = 8$	$n_f = 10$	$n_f = 12$
N (kN)	582±44	576±34	571±29	574±16
k_A	0.715±0.135	0.666±0.086	0.653±0.071	0.681±0.024
k_B	0.278±0.278	0.331±0.208	0.365±0.174	0.333±0.081
k_C	0.737±0.044	0.744±0.034	0.749±0.028	0.750±0.019
k_D	0.437±0.017	0.436±0.014	0.437±0.013	0.436±0.011
K_A (kN· m/Rad)	1487±933.4	917.1±363.5	826.3±271.7	881.9±107.4
K_B (kN· m/Rad)	249.4±249.4	263.2±204.1	282.8±184.5	212.8±73.2
K_C (kN/m)	1192±229.4	768.6±107.4	782.3±93.7	783.2±66.9
K_D (kN/m)	326.8±28.04	205.1±15.0	203.4±13.0	201.7±11.3

Forward solution of the roots of the characteristic equation was used to determine the natural frequencies associated with each set of sampled parameter assignments and the residual errors relative to the mean of the synthetic natural frequency measurements were computed. Figure 4.12b presents the maximum residual error, normalized to the standard deviation, for all of the sampled points. The results successfully verify the methodology, as the maximum residual for all of the sampled points was found to be within, or close to, the prescribed interval radius used to express the confidence intervals for the synthetic measurements. It is acknowledged that, for some of the sampled parameter assignments, the maximum residual error was found to slightly exceed the prescribed interval radius. The reason for this apparent violation of the strict constraint enforcement is that the subpaving produced by the extended methodology is the outer approximation, $\overline{\mathbb{X}}$. Consequently, some of the verification points are sampled from the boundary of the solution space, $\delta\mathbb{X}$, rather than the guaranteed enclosure, $\underline{\mathbb{X}}$. However, since the interval precision prescribed for the set inversion was sufficiently small, the maximum residual errors computed for points sampled from the boundary of the solution space only exceed the prescribed confidence interval by

at most 5% of the width or approximately 0.005 Hz. At the expense of increased computational time, the boundary of the outer approximation could be further refined by reducing the interval precision specified as the stopping criteria, which would more strictly enforce the prescribed confidence interval within the subpavings.

The computational time required for generating subpavings using the developed methodology is highly dependent on the complexity of the problem. When the parameter identification is restricted to the internal axial force and rotational boundary restraints, individual subpavings for the example problem could be obtained within fractions of a second with the entire parameter identification problem being completed on the order of seconds. However, the computational time required to generate subpavings when translational boundary restraints were included as additional uncertain parameters was significantly increased. Figure 4.13 presents the solution time required to generate the subpaving at each prescribed axial force value. The average solution time per subpaving was 81.1, 21.1, 6.36, and 2.38 seconds when 6, 8, 10, or 12 natural frequencies were included in the parameter identification, respectively. These averages correspond to cumulative solution times of 4135, 1077, 324, and 121 seconds to produce the interpolated feasible solution space across axial forces ranging from 530–630 kN. However, by adjusting the resolution of the basins through modifying the incrementation of the axial force values used to develop individual subpavings, the cumulative solution time can be reduced with a corresponding trade-off in the resolution of the basin definition in the dimension of the internal force parameter. As illustrated by the figure, the solution time is directly linked to the number of natural frequencies included in the identification since adding more constraint equations narrows the feasible solution space. However, when the feasible solution space is over-constrained leading to no feasi-

ble solutions, the interval contractors are capable of very efficiently determining within a fraction of a second that the set approximation is empty.

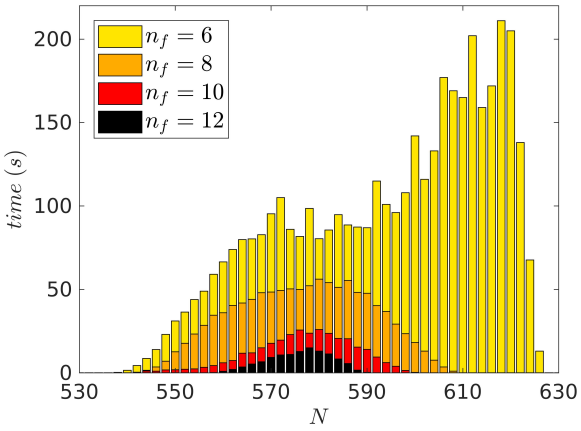


FIGURE 4.13: Illustration of the solution time for the entire discrete range of axial forces for 6, 8, 10, and 12 frequencies included in the parameter identification with confidence intervals of $\pm\frac{1}{2}\sigma$

4.5 Experimental Application of the Methodology

To demonstrate the experimental application of the proposed methodology to an axial force element with varying end restraint, a 0.945 cm diameter steel rod was threaded at its ends and connected to internally threaded ball joint rod ends. Each rod end was connected to pairs of aluminum gusset plates with a steel clevis pin and the gusset plates were bolted to an MTS 810 universal load testing machine (Figure 4.14a). Due to the stiffness provided by the aluminum gusset plates, translational motion at the rod ends was assumed to be fully restrained, while only partial rotational fixity would develop due to friction in the ball joint connections. The length between the clevis pins was measured to be 1304 mm and the mass density of the rod was measured to be 7800 kg/m^3. The elastic modulus of the steel was assumed to be 200GPa, the shear modulus was assumed to be 77.5 GPa, and the Timoshenko shear coefficient was calculated as 0.8856 assuming a Poisson ratio of 0.29.

The rotational moment of inertia associated with the rod end connections was approximated as 3.82×10^{-5} kg$\cdot$ m^2.

Several cases developing progressively increased partial fixity at only one of the rod ends were examined to validate the methodology and demonstrate its application for nondestructively assessing changes in end restraint conditions. For all cases, the rod was subjected to a constant axial tension force of 2.5 kN by the load frame, which resulted in a nondimensional bending stiffness, ξ, of 7.4. For the first case, vibration testing was performed with the nominally identical rod ends at each connection (Figure 4.14b). For the second and third cases, short lengths of taut steel wire were used to increase the rotational end restraint in the connection by tensioning the wire between the rod end and the gusset plate (Figure 4.14c). In both cases, this additional end restraint was introduced at only one of the two rod ends. A 24 gage wire was used for the second case, while the wire diameter was increased to 18 gage for the third case. Finally, vibration testing was performed on a fourth case where seizure of one of the rod ends was simulated using an industrial epoxy.

For each of the four cases, experimental modal analysis was performed using a single axis PCB Piezotronics accelerometer bonded to the rod. A PCB Piezotronics 086C03 modally tuned impact hammer with hard metal tip was used to provide the impulse excitation. A National Instruments PXIe-4497 24-bit dynamic signal analyzer was employed for acquisition of the accelerometer and impulse signals with a sampling rate of 5 kHz over 2 second test durations. Frequency response functions (FRFs) were developed using the classical H_1 estimator (Brandt, 2011) for subsequent system identification of the undamped natural frequencies. A representative FRF for each of the four cases is presented in Figure 4.15, which illustrates the progressive increases in natural frequencies with the

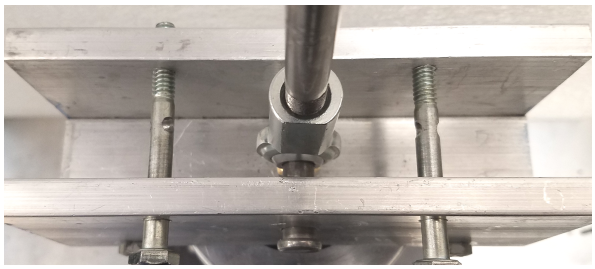
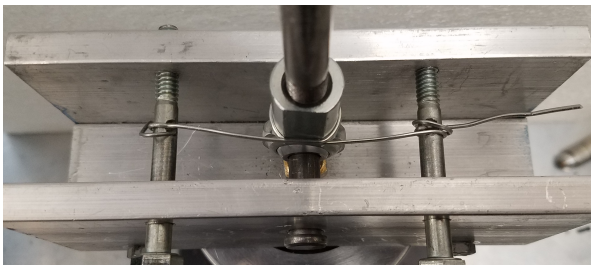
(a)  (b)  (c) 

FIGURE 4.14: (a) Photograph of experimental rod subjected to constant tension using a MTS load frame; (b) photograph of ball joint rod end connection to end gusset plates; (c) photograph of introduced rotational restraint through taut wires at rod end

increased end restraint. Experimental estimates of the natural frequencies were obtained using the least squares complex frequency-domain estimator (Cauberghe, 2004). In this system identification, a stabilization diagram was used to select stable pole estimates for the first eight natural frequencies across a range of model orders. A total of 15 data sets were analyzed for each end restraint case and a minimum of 45 stable pole estimates were averaged to determine each natural frequency.

Given the details of the experimental test fixture, translations at the ends of the rod were assumed to be fixed and parameter identification was performed using set inversion to obtain subpavings for the rotational boundary restraints, k_A and k_B, across a discrete set of axial force values. For this set inversion, the average experimental natural frequency estimates were used to establish the midpoint of the interval bounds on the natural frequencies of the system. Consistent with the analytical demonstrations, the search space for the unknown rotational restraints k_A and k_B was [0, 1], which covers the full range of fixity, and

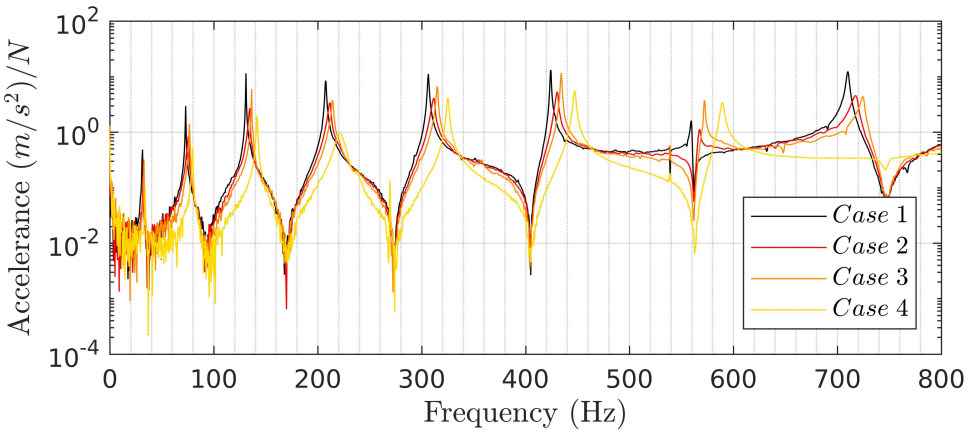


FIGURE 4.15: Representative frequency response functions obtained through impulse testing of the experimental specimen for each of the four cases

the constraint $k_A \geq k_B$ was enforced to reduce the feasible parameter space to only one half of the symmetric solution. Successive applications of the set inversion were applied over fixed axial load increments of 0.005 kN with an interval precision of 1e-3 on the subpavings for the rotational spring stiffness identification. For this experimental case, the linearization parameters were established as $\gamma_R = 6.7 + 1.1257N$ and $\gamma_T = 16.2 + 45.84N$ using the methodology detailed in Section 4.6.

Figure 4.16 presents interpolated continuous basins of feasible solutions developed for each of the four experimental cases of end fixity. In developing these basins, the confidence intervals around the average natural frequency measurements ranged from ±1.1 to 1.6 Hz across the four cases. The continuous basins of feasible solutions indicate a small degree of rotational fixity in the rod ends for the first case, which is partially attributed to friction in the rod end under load. In addition, any error in the assumed rotational moment of inertia of the rod end, as well as other assumed properties of the experimental specimen, may have influenced the results. Regardless, the identified rotational fixity for this case is small and the methodology correctly identifies a progressive increase in the rotational stiffness at

only one end of the rod, k_A. For the other rotational spring stiffness, k_B, the uncertainty in the parameter identification increases with each case, but the hull for this parameter in the initial case is contained within the hull of the subsequent cases. Consequently, no definitive change in the rotational spring stiffness at this end is identified across the four cases. With respect to the axial force identification, the continuous basins for all four cases contain the experimentally prescribed force of 2.5 kN. The uncertainty in the axial force identification notably increases for Case 4, however the largest uncertainty on the natural frequency measurements needed to be prescribed in this case in order to admit feasible solutions. If the subpavings of the feasible parameter space are generated for the experimentally prescribed axial force of 2.5 kN, the identification of a significant progressive increase in the rotational restraint at the "A" side of the rod without any definitive change in the rotational restraint at the "B" side of the rod across all cases is readily apparent (Figure 4.17).

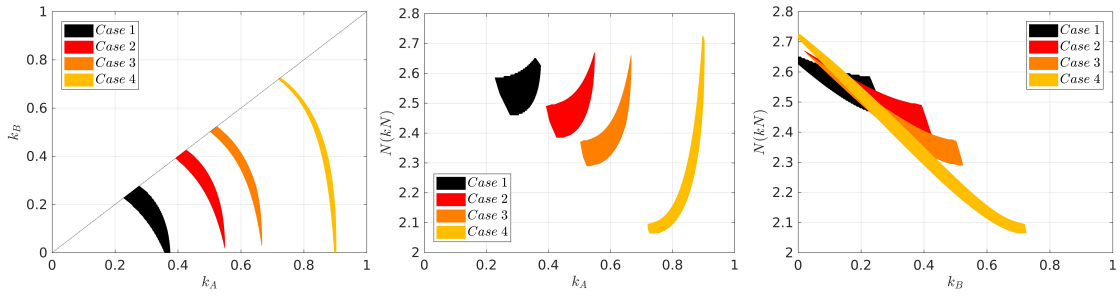


FIGURE 4.16: Interpolation of continuous basins for the feasible parameter space for all four experimental cases using the first eight natural frequencies

In addition to interpolating the continuous basins for the feasible parameter space, the boxes forming the subpavings can be statistically analyzed in order to quantify the posterior probability distributions for the unknown parameters identified through the set inversion using the experimental data. Histograms for the midpoints of the interval vector solutions

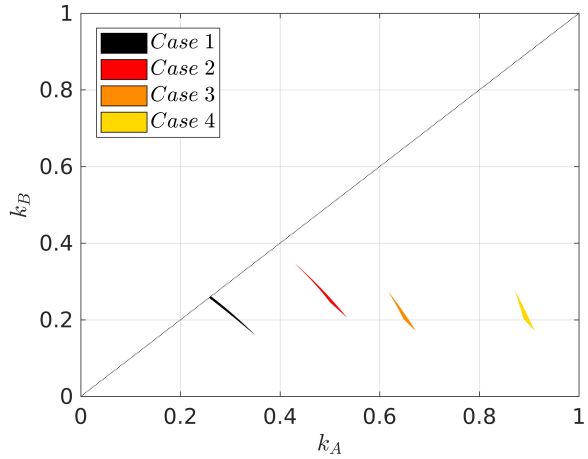


FIGURE 4.17: Feasible parameter space for all four experimental cases with fixed axial force of 2.5kN using the first eight natural frequencies

of the subpavings of the basins originally presented in Figure 4.16 are presented in Figure 4.18. In addition to supporting the prior discussion of the experimental results, this figure illustrates that the posterior probability distributions are generally not Gaussian.

4.6 Determination of Scale Factors, γ_T and γ_R

In the formulation of the non-dimensional parameters that quantify the relative stiffness of translational and rotational springs (Equation 4.6), the terms γ_T and γ_R were introduced to provide a means of approximately linearizing the relationships between the non-dimensional parameters and the natural frequencies. By linearizing these relationships, the sensitivity of the natural frequencies to changes in the non-dimensional parameters becomes more uniform over the range of the non-dimensional parameter assignments. In the absence of the γ terms, the natural frequencies of the analytical model may be largely insensitive to the non-dimensional spring stiffness over a large portion of the feasible range and highly sensitive over a very narrow range. Typical unconditioned relationships between the non-dimensional spring stiffness and fundamental natural frequency are presented in

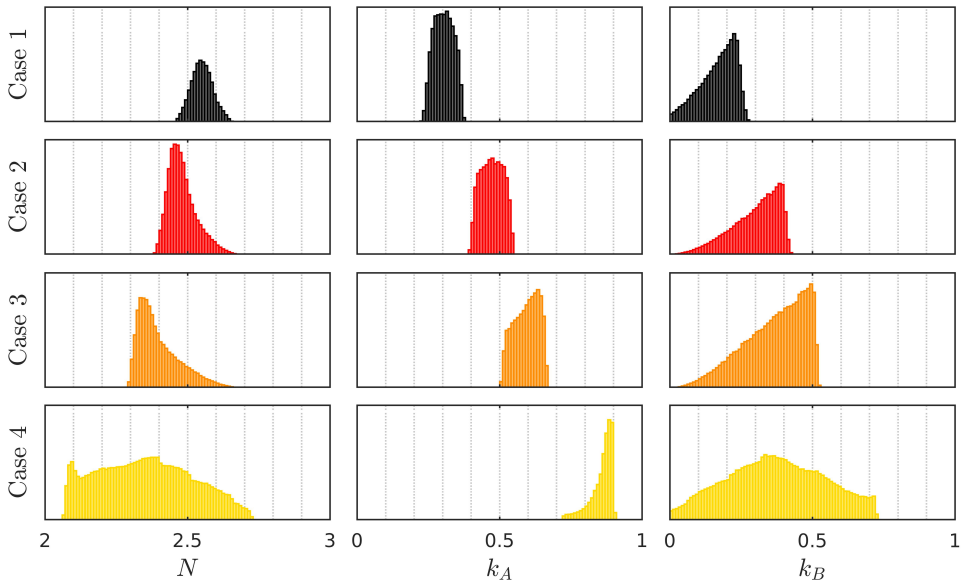


FIGURE 4.18: Histograms for the posterior probability distributions of the identified parameters generated from the subpavings

Figure 4.19, denoted with the data series for $\gamma_R = 1$ and $\gamma_T = 1$. Optimal conditioning terms are specific to the element geometry and magnitude of axial loading. A simple iterative routine was developed to determine suitable values for each term. The rotational conditioning term γ_R is first determined by setting an estimated axial force, N, and a static fixity for k_B and calculating the fundamental natural frequency of the member at a number of stiffness assignments across the range of relative fixity for k_A. The conditioning term, γ_R is then perturbed iteratively until the normalized change in the fundamental frequency is approximately linear for various of combinations of k_A, k_B, and N. Determination of the translational conditioning term, γ_T follows the same process using the translational springs k_C and k_D. Figure 4.19 displays the results of this process with k_B=0.50 and k_D=0.50. The results indicate that by setting the γ terms appropriately, the relationship between the non-dimensional parameters and natural frequencies can be linearized for the model around the

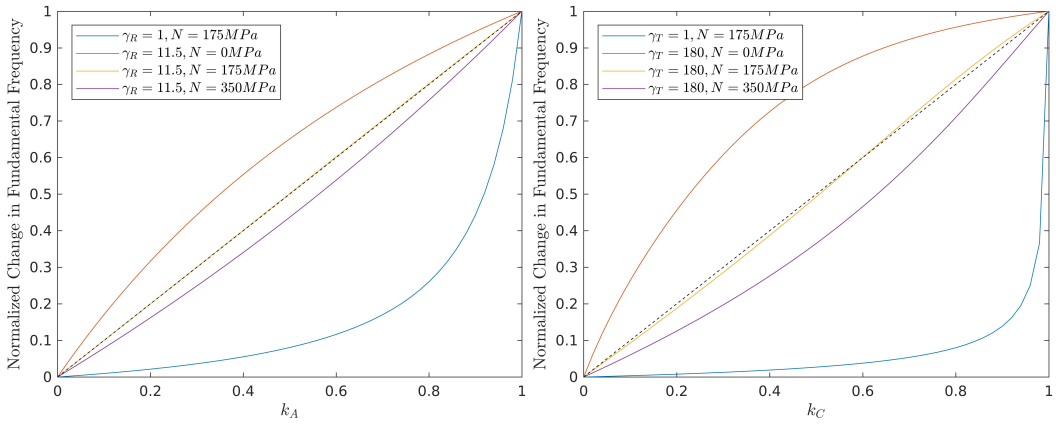


FIGURE 4.19: Determining suitable values for γ_R and γ_T to ensure that the generalized equation is uniform across the entire range of fixity.

estimated axial force. Even with large changes in the axial force, the analytical model exhibits significantly more uniform sensitivity to the conditioned non-dimensional parameters than without the use of γ_R and γ_T. In addition, γ_R and γ_T may themselves be formulated as functions of the axial force, N, by simply performing the conditioning for a range of axial forces and fitting the data to a linear model. Stating the γ terms as a function of the axial force provides a better representation of the solution space than simply using fixed terms for an estimated axial force.

4.7 Conclusion

A novel technique for determining the axial force and boundary restraints in axially loaded, prismatic structural members, such as tie rods and cables, has been presented by casting the parameter identification as a constraint satisfaction problem and using interval analysis and contractor programming to solve the set inversion problem. In the formulation, measurement uncertainties are accounted for within constraint equations developed from the governing differential equation to define the feasible and infeasible solution space

within a bounded region. This capability allows for propagating the effects of measurement uncertainty into the parameter space to quantify the confidence in the identified parameters. Through verified numerical simulations, the developed methodology has been shown to be capable of mapping the complete set of feasible solutions for dynamic identification of internal axial force and boundary restraints in prismatic beam elements. Since the methodology does not adopt any assumptions or approximations within the approach for set inversion of the characteristic equation, it is suitable for application to structural members with any degree of nondimensional bending stiffness, ξ. In addition to the analytical verifications, the methodology was applied to experimental data sets to validate the ability of the approach to identify the applied axial load as well as changes in boundary restraints, while quantifying the uncertainties and posterior probability distributions for the identified parameters.

Acknowledgement

This material is based upon work supported by the National Science Foundation under Grant No. 1331825. Any opinions, findings, conclusions, or recommendations expressed in the material are those of the authors and do not necessarily reflect the views of the sponsor.

CHAPTER 5: STRUCTURAL IDENTIFICATION USING A NONLINEAR CONSTRAINT SATISFACTION PROCESSOR WITH INTERVAL ARITHMETIC AND CONTRACTOR PROGRAMMING

The following chapter is a direct product of the work of this dissertation and has been accepted for publication in *Computers and Structures* (Kernicky et al., 2017).

Abstract

Structural identification through finite element model updating has gained increased importance as an applied experimental technique for performance-based structural assessment and health monitoring. However, practical challenges associated with computability, feasibility, and uniqueness present in the structured nonlinear inverse eigenvalue problem develop as a result of the necessary use of partially described and incompletely measured mode shapes. As an alternative to direct methods and optimization-based approaches, this paper proposes a new paradigm for model updating that is based on formulating the structured inverse eigenvalue problem as a Constraint Satisfaction Problem. Interval arithmetic and contractor programming are introduced as a means for generating feasible solutions to a structured inverse eigenvalue problem within a bounded parameter search space. This frame work offers the ability to solve under-determined and non-unique inverse problems as well as accommodate measurement uncertainty through relaxation of constraint equations. These abilities address key challenges in quantifying uncertainty in parameter estimates obtained through structural identification and enable the exploration of alternative

solutions to the global minimum that may better reflect the true physical properties of the structure. These capabilities are first demonstrated using synthetic data from a numerical mass-spring model and then extended to experimental data from a laboratory shear building model. Lastly, the methodology is contrasted with probabilistic model updating to highlight the advantages and unique capabilities offered by the methodology in addressing the effects of measurement uncertainty on the parameter estimation.

5.1 Introduction

Over the past several decades, numerous techniques have been devised to develop updated structural stiffness and mass matrices from modal parameter estimates obtained from either experimental or operational modal analysis. Within structural identification, the properties of the updated model are used to infer the behavior and performance of the structure to inform decision-making (Aktan and Brownjohn, 2013). Consequently, instilling confidence that parameter assignments in the updated model closely reflect physical reality is critical to the use of structural identification for applications in performance-based civil engineering and structural health monitoring. Likewise, understanding the uncertainty in the parameter estimates in the presence of measurement noise and potential ill-conditioning of the inverse problem is necessary to provide reliable and actionable information.

Traditionally, the finite element model updating problem has been cast using the generalized eigenvalue problem for undamped linear systems:

$$M\Phi\Omega^2 - K\Phi = 0 \tag{5.1}$$

where M and K are the mass and stiffness matrices, Ω^2 is a diagonal matrix of the eigen-

values, and Φ is the matrix of the corresponding eigenvectors as columns of the matrix. This generalized eigenvalue problem has been adopted for the majority of structural identification applications since the finite element method can be used to readily construct the mass and stiffness matrices, while experimentally measured relative damping factors can be used to construct the corresponding damping matrix for the system. The general objective of model updating is to modify the stiffness and mass matrices of an analytical model of the structure such that the eigenproperties of the model obtain the best possible match to experimentally measured values, while preserving physical meaning and structural constraints in the matrices. Although this objective is easily described, there are many practical challenges that arise from the nature of vibration testing and analytical modeling that are ubiquitous to all methods employed for model updating. Namely:

- The practical measurement bandwidth of vibration transducers is limited, which effectively limits the measurement of the eigenvalues and eigenvectors of the system under test to typically a small subset of all of those that would exist in the corresponding analytical model. This case is commonly referred to as having partially described eigeninformation pairs (Chu and Golub, 2005).

- It is impractical to completely measure all corresponding degrees of freedom in the analytical model, so the experimental mode shapes are incomplete measurements of the eigenvector. For models of even modest size structures, the number of sensors required to measure every degree of freedom in a sufficiently discretized finite element model is generally prohibitive. Furthermore, the direct measurement of some rows of the eigenvector, such as those associated with the rotational degrees of freedom, is

not even possible with conventional transducers (Avitabile and O'Callahan, 2003).

- Noise and uncertainty in the measurements, as well as assumptions inherent to system identification algorithms, yield mode shapes that no longer satisfy orthogonality relationships and are unlikely to satisfy equality constraints. Likewise, discretization errors and idealizations inherent to the model, such as element type and mesh connectivity, are not explicitly corrected in conventional finite element model updating schemes (Mottershead et al., 2011).

Currently, the two most prevalent techniques applied for structural identification are deterministic and probabilistic methods of finite element model updating. Deterministic methods seek to identify optimal assignments for a set of uncertain parameters in the model by minimizing the residuals between measured and estimated modal parameters by application of various optimization techniques (Bakir et al., 2008; Deng and Cai, 2009; Marwala, 2010). While these techniques have been applied for structural identification of several full-scale structures (Morassi and Tonon, 2008; Catbas et al., 2013) their application is generally plagued by issues associated with computational speed, solution uniqueness, ill-conditioning, and parameter selection and sensitivity (Friswell et al., 2001). Furthermore, finite element model updating problems suffer from the underlying issue that the global minimum may not necessarily reflect the best match to the physical reality due to uncorrected errors arising from idealization and discretization in the model and uncertainties in the measurements (Mottershead et al., 2011). These challenges have given rise to probabilistic finite element model updating approaches (Beck and Katafygiotis, 1998), which incorporate uncertainties in the model and the measurements to identify the most proba-

ble solutions using statistical methods. However, these probabilistic methods require an assumed probability density function for uncertain variables and often require computationally expensive simulations to arrive at the solution (Marwala, 2010). Lastly, it should be noted that direct methods for solving inverse eigenvalue problems with incompletely measured mode shapes through solution of a descriptor Sylvester equation have recently emerged (Carvalho et al., 2007; Kuo and Datta, 2012), however their application has yet to demonstrate the capability to preserve the connectivity structure of the matrices.

Although probabilistic approaches have been the most prevalently used to address uncertainties in structural models, interval methods provide an alternative approach that may offer computational advantages over probabilistic techniques (Köylüoğlu et al., 1995; Moens and Vandepitte, 2005). Recently, interval-based model updating strategies have been proposed for handling inherent uncertainties in the experimental modal parameter estimates and the finite element model (Madarshahian et al., 2013). The most closely related work to the current study leverages interval global optimization to arrive at solutions to the model updating problem (Gabriele and Valente, 2009). However, the technique proposed in this prior work is formulated on an inclusion set for the eigenvalues of an interval stiffness matrix and employs a simple branch and bound algorithm to minimize an objective function rather than solve a constraint satisfaction problem. An extension of this work incorporated interval eigenvectors in the optimization through an acceptance criteria based on the modal assurance criterion (Gabriele, 2011). It should also be noted that the term interval model updating has also been recently used to described the application of interval arithmetic techniques in the estimation of parameter variability (Khodaparast et al., 2011; Fang et al., 2015). However, these approaches address the field of stochastic model updating (Mares

et al., 2006) wherein the objective is to characterize the variabilities across a number of experimental tests performed on nominally identical structures. While the constraint satisfaction formulation proposed in the current work may have extensions to stochastic model updating, the subject of this current paper is on the class of model updating applications where measurements obtained from a single structure are used to calibrate a numerical model. This paper presents a novel formulation of the finite element model updating problem as a constraint satisfaction problem and explores the use of a nonlinear constraint satisfaction processor with interval arithmetic and contractor programming to yield estimates of uncertain model parameters and unmeasured components of the eigenvectors. The method is shown to be capable of delivering a complete set of feasible solutions to the structured inverse eigenvalue problem with partially described and incompletely measured eigeninformation pairs from either synthetic or experimental data. Furthermore, the approach is successfully demonstrated on ill-posed problems with multiple solutions to illustrate its capability for addressing this challenge as well as providing a foundation to introduce practitioner heuristics into the identification of physically plausible solution sets.

5.2 Nonlinear Constraint Satisfaction With Contractor Programming and Interval Analysis

In the domain of engineering sciences, many applications require finding all possible and potentially isolated solutions satisfiable to a set of constraints over real numbers. The system of equations may be non-polynomial and the computational complexity to solve such systems in NP-hard. This set of problems are called Constraint Satisfaction Problems (CSPs) (Dechter, 2003; Rossi et al., 2006; Hentenryck, 1999). The approach explored in this paper for the solution of partially described and incompletely measured inverse eigen-

value problems relies on framing the structured inverse eigenvalue problem as a nonlinear CSP. By developing the model updating problem in this framework, unique capabilities for addressing challenges related to ill-posedness and ill-conditioning are revealed, as detailed in later sections. The following discussion provides some details on the fundamentals of CSPs, interval analysis, and contractor programming that are essential for the understanding of the rest of the paper.

Fundamentally, a CSP can be defined as a *4-tuple* $< V, D, C, L >$ where:

- $V = \{v_1, v_2, ..., v_n\}$ is a set of variables
- $D = \{d_1, d_2, ..., d_n\}$ is a set of domains for the prospective variables
- $C = \{c_1, c_2, ..., c_n\}$ is a set of constraints over the variables
- L is a set of labels that map constraints to the variables and corresponding domains, formally: $L : C_i \rightarrow (v_i, d_i)$

Each variable, v_i, can assume any real value in the corresponding non-empty domain d_i. The constraint $c_i \in C$ is defined over a pair (v_i, d_i) through a label function $l \subset L$. In the process of finding a satisfiable solution to a CSP, different values are assigned to the variables (in set V) from the domain set (D) through constraint propagation algorithms (also called filtering/contraction algorithms). The evaluation of label (true/false) determines whether the corresponding assignments to variables for a given constraint lead to a satisfiable solution or not. While assigning values to different variables (through a "systematic search process"), consistency algorithms (Hyvnen, 1992) take into account whether any violation of constraints has occurred during any assignment. This whole process is called constraint

propagation. Likewise, the paradigm for solving CSPs through integration of Systematic Search and Arc Consistency techniques is called Constraint Programming (CP).

A sub-domain of constraint programming that integrates interval arithmetic, called Interval Constraint Programming, offers unique advantages for developing solutions to the inverse eigenvalue problem with experimental data. In interval arithmetic, variables as well as constraint relationships among variables can be defined using intervals and mathematical operations can be applied using principles of interval arithmetic (Alefeld and Claudio, 1998). Consequently, interval-based computation offers a means of placing bounds on round off errors in numerical calculations, measurement uncertainties, and uncertain model parameters. Therefore, rather than defining the exact value of a variable or constraint, it can be defined over an interval, which implies that it may take any value within that interval. The Cartesian product of intervals, or interval vector, generates a multi-dimensional volume, or box. Formally, a variable "X" defined over an interval and the realization of interval vectors can be explained as follows:

$$X : [a, b] \rightarrow \{X \in \mathbb{R} | a \leq X \leq b\} \tag{5.2a}$$

$$[X] = [x_1] \times [x_2] ... \times [x_n] \tag{5.2b}$$

and is illustrated graphically in Figure 5.1a for the product of two intervals. In an interval constraint programming problem, the objective is to completely and correctly identify all interval vectors, to a specified interval precision, that satisfy the set of constraint equations within the bounded domains for each set of interval variables.

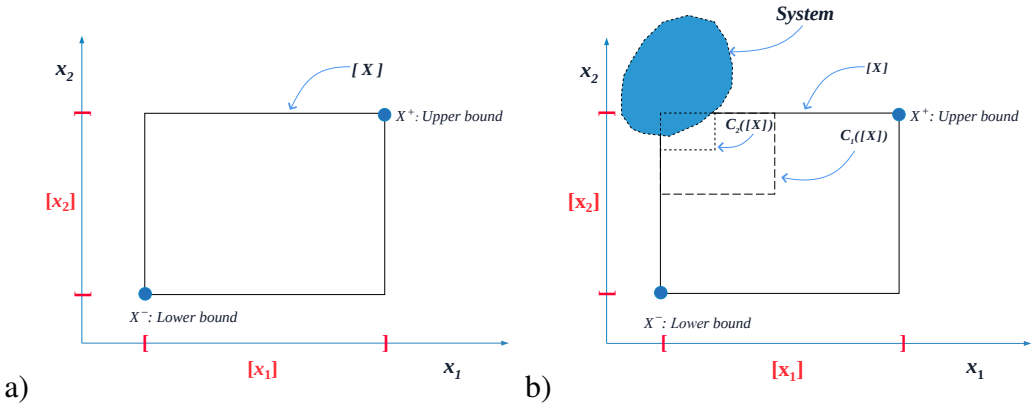


FIGURE 5.1: a) An interval vector, or box, generated from the product of two intervals. b) contraction of an interval vector on a system of constraints

5.2.1 Contractor Programming

One recent effort toward the integration of interval arithmetic and constraint programming in a formalized solver has been termed Contractor Programming (Chabert and Jaulin, 2009). In this approach, contractors can be viewed as mathematical operators that accept a system (an n-dimensional box) as an input and contract the domain of the system according to a given set of constraints. Contractors yield a reliable set of satisfiable solutions since they must satisfy properties of soundness and completeness. The formal definition of a contractor and its properties are defined as follows:

A contractor (Ctc) is a function from $Ctc : \mathbb{IR}^n \rightarrow \mathbb{IR}^n$ *with the following properties:*

- $\forall [X] \in \mathbb{IR}^n \quad Ctc([X]) \subset [X]$; where $Ctc([X])$ represents box $[X]$ after contraction
- $Ctc([X]) \cap System = [X] \cap System$

The first property ensures that the contraction algorithm or procedure is sound and that the result achieved after contraction contains a subset of the original box (Figure 5.1b). The

second property elaborates the completeness of the contraction algorithm/procedure, which states that no potential solution is lost after contraction is performed. Adhering to these two properties, contractor programming yields reliable results with a guarantee that feasible solutions are not lost within the search space. Following contraction, the interval vector can be bisected into a subset of smaller boxes where contractors can be applied to further refine the interval precision of the solution. In this respect, solvers employing contractor programming have some parallels to branch and bound algorithms, where subsets of a search space are evaluated and either retained or discarded as potential solutions and then the retained subsets are further divided and evaluated until the desired interval precision is obtained. However, the process of contraction can result in a significantly faster exploration of the search space than pure branching methods, such as bisection (Jaulin et al., 2001).

Although many domain experts in structural engineering will be unfamiliar with the concept of constraint programming and contractors, the general application to a variety of challenging nonlinear engineering problems has been made possible through the open-source IBEX C++ numerical library (Chabert, 1999). For the current study, the authors have developed a interface between the MATLAB interactive environment (MATLAB, 2017) and the IBEX 2.1.17 library to construct and parameterize the structural stiffness and mass matrices, develop mechanics-based constraint equations, pass the formulated CSP to the IBEX solver, and parse any and all interval solutions generated by the contraction algorithm for subsequent analysis. In this study, the generic default solver in this release of IBEX, which employs forward-backward contraction through the HC4 algorithm (Benhamou et al., 1999) and adaptive constructive interval disjunction (Neveu et al., 2015), has been used for all of the examples presented to promote accessibility of the developed model

updating formulation to a broader audience. Details on the implementation for finite element model updating are presented following a short illustrative example demonstrating the key benefits sought from this alternative to optimization-based strategies for inverse problems.

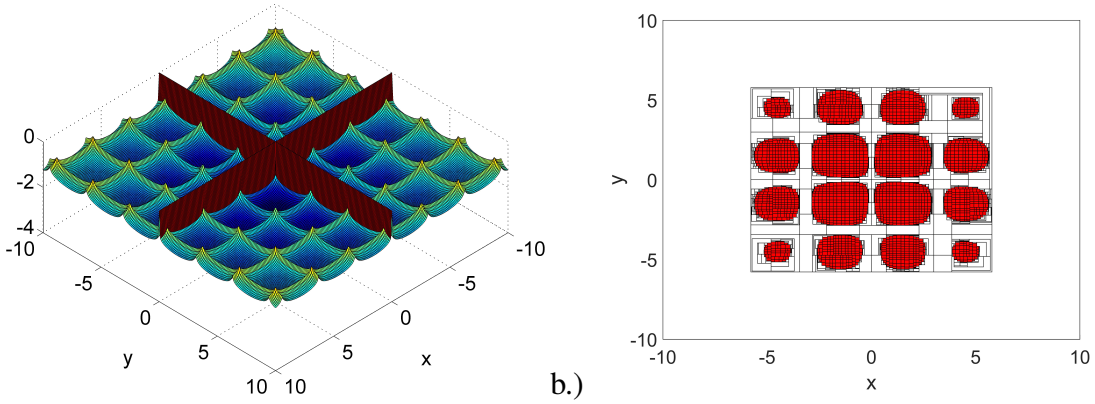
5.2.2 Illustrative Example Using Cross-in-Tray Function

A brief example illustrating the computational advantages offered by contractor programming techniques is presented to provide motivation for its use in finite element model updating. Specifically, the finite element model updating challenges related to ill-posedness and the desire to obtain alternative solutions in the presence of experimental noise and uncertainty are highlighted by use of a nonlinear function with a large number of local extrema, multiple global minima, and discontinuities. For this illustration, we consider the Cross-in-Tray function:

$$f(x,y) = -0.0001\left(\left|sin(x)sin(y)\exp\left(\left|100 - \frac{\sqrt{x^2+y^2}}{\pi}\right|\right)\right| + 1\right)^{0.1} \tag{5.3}$$

which has been adopted as a benchmark for performance testing of optimization algorithms and features four global minima at $\{x, y\} = (\pm 1.34941, \pm 1.34941)$ corresponding to a function value of -2.06261. The domain of the search space was bounded to $x \in [-10, 10]$ and $y \in [-10, 10]$, which corresponds to the region shown in Figure 5.2a. This function was first encoded in an equality constraint equation where satisfiable solutions were required to adhere to the exact function minimum and the IBEX constraint processor successfully identified all four global minima in approximately 0.02 seconds. This ability to identify multiple solutions by contractor programming will be leveraged to overcome uniqueness

challenges in the inverse eigenvalue problem. In addition, by relaxing the equality constraint to an inequality constraint, $f(x, y) \leq -1.75$, the solver demonstrates the ability to identify all feasible alternative solutions to the unknown parameters x and y that yield results similar to the global minima of this challenging nonlinear and discontinuous function within half of a second (Figure 5.2b). This ability to completely identify all feasible solutions to a set of relaxed constraint equations will be leveraged to address challenges associated with measurement uncertainties and the effects of potential ill-conditioning in the finite element model updating problem. Note that the boxes shown in this plot reflect the bisection and contraction processes performed to arrive at the interval solutions, which illustrates the computational efficiency over pure branch and bound algorithms.



a.) b.)

FIGURE 5.2: a.) Cross-in-Tray Function, b.) Set of satisfiable solutions produced with relaxed inequality constraint using contractor programming (all boxes shown represent interval vectors after subsequent contractions and shaded boxes indicate satisfiable solutions)

5.3 Formulation of Interval Constraint Equations for the Structured Inverse Eigenvalue Problem

The real-valued inverse eigenvalue problem aims to solve for the symmetric matrices M and K, which are positive-definite and positive-semidefinite, respectively, given specified eigeninformation matrices (Ω^2, Φ). Within the application to finite element model updat-

ing, additional conditions are generally applied to the inverse eigenvalue problem, such as conditions to maintain the sparsity structure of the matrices to ensure proper connectivity of elements in the model and to ensure physically meaningful solutions. In our proposed approach to model updating, we formulate the generalized eigenvalue problem as a matrix-based constraint equation and apply additional mechanics-based constraint equations to enforce desired qualities on the structural matrices associated with the updated model. In the generalized eigenvalue problem for undamped multiple degree-of-freedom (MDOF) discrete systems, the structural matrices are $n \times n$ square, where n is the number of unrestrained degrees of freedom in the model. Numerically, eigendecomposition of these matrices will produce n eigenpairs. However, in practical applications of model updating it is generally prohibitive to obtain corresponding measurements of all of these eigenpairs due to a variety of experimental limitations, including the measurement bandwidth of conventional vibration transducers, insufficient excitation of all modes, and restrictions on the number of sensors available. Therefore, the majority of model updating problems are classified as partially described, where only $m < n$ eigenpairs are measured. Under these conditions, the constraint equations developed for the inverse eigenvalue problem must necessarily be formulated using only m modes, as:

$$K_{n\times n}\Phi_{n\times m} - M_{n\times n}\Phi_{n\times m}\Omega^2_{m\times m} = 0_{n\times m} \tag{5.4}$$

Consequently, the partially described eigenvalue problem yields a total of $n \times m$ unique constraint equations. However, since it is generally impractical or impossible to measure all n degrees of freedom associated with the analytical model being updated, the eigenvec-

tors included in these constraint equations will be incompletely measured. As a result, the number of unknowns in the eigenvector matrix will be of size $(n - s) \times m$, where s corresponds to the number of measured degrees of freedom or sensors, and the matrix constraint equation can be partitioned as:

$$K_{n\times n}\begin{bmatrix}\Phi^{M}_{s\times m}\\ \\ \Phi^{U}_{(n-s)\times m}\end{bmatrix} - M_{n\times n}\begin{bmatrix}\Phi^{M}_{s\times m}\\ \\ \Phi^{U}_{(n-s)\times m}\end{bmatrix}\Omega^{2}_{m\times m} = 0_{n\times m} \tag{5.5}$$

where $\Phi^{M}_{s\times m}$ are the rows of the measured components of the mode shapes and $\Phi^{U}_{(n-s)\times m}$ are the rows of the unmeasured components of the mode shapes. Conventional approaches for linear parameterization of the structural matrices can also be introduced to the governing constraint equations to enforce additional mechanics-based constraints on the updated model. In the formulation of generalized eigenvalue problem employed for all numerical and experimental examples in this paper, the structural matrices are explicitly formed through elemental contributions, or basis matrices. Consequently, the constraints on the sparsity pattern of the structural matrices are explicitly encoded in Equation 5.5 to produce:

$$\left[K_o + \sum_{j=1}^{N_K}\alpha_j K_j\right]\begin{bmatrix}\Phi^{M}_{s\times m}\\ \\ \Phi^{U}_{(n-s)\times m}\end{bmatrix} - M_{n\times n}\begin{bmatrix}\Phi^{M}_{s\times m}\\ \\ \Phi^{U}_{(n-s)\times m}\end{bmatrix}\Omega^{2}_{m\times m} = 0_{n\times m} \tag{5.6}$$

where α_j is a scalar multiplier applied to the basis matrix, K_j, that provides the stiffness contributions of the j-th element of the model, while K_o represent the contributions of any elements in the model not subject to updating. In this formulation, the unknowns in the inverse eigenvalue problem are the N_K scalar multipliers and the $(n - s) \times m$ unmeasured

components of the eigenvector matrix. Using interval arithmetic and contractor programing, the solutions for these unknown quantities that satisfy the constraint equation in Equation 6 within a bounded search space will be determined to a prescribed interval precision, or width. Consequently, the methodology develops an interval stiffness matrix, K^I, since the uncertain parameters in the model are treated as the intervals:

$$\alpha = [\underline{\alpha}, \overline{\alpha}] \tag{5.7}$$

where $\underline{\alpha}$ is the lower bound to the interval for the uncertain parameter and $\overline{\alpha}$ is the upper bound. Likewise, the unknown components of eigenvector matrix are treated as intervals that are subsequently bisected and contracted until the desired precision of the solution is achieved:

$$\Phi^U_{(n-s)\times m} = [\underline{\Phi}^U_{(n-s)\times m}, \overline{\Phi}^U_{(n-s)\times m}] \tag{5.8}$$

It should be noted that, in addition to the stiffness matrix, the mass matrix can also be parameterized. The authors have successfully implemented such cases, however the current paper focuses only on parameterization of the stiffness matrix to yield results with a physical basis that is more readily interpreted for cases with multiple solutions.

In the presence of measurement uncertainty and idealization errors in the model, an additional set of constraint equations must also be introduced to ensure that the prescribed eigenvalues are consistent with the stiffness and mass matrices assembled with the interval uncertain parameter assignments. In other words, while feasible solutions to the equality constraints in Equation 5.6 with noise-free eigeninformation pairs guarantee that the prescribed values in $\Omega^2_{n\times m}$ are contained within the interval eigenvalues of the mass and

stiffness matrix, this is not guaranteed if $\Phi^M_{s\times m}$ are not exact eigenvectors of the structural matrices. Consequently, an additional set of constraints, which we refer to herein as the eigenvalue inclusion constraints, must be introduced to ensure that the specified eigenvalues are contained within the interval eigenvalues of the structural matrices. However, solving for the eigenvalues of systems described by interval mass and stiffness matrices requires iterative methods to perform the eigenvalue decomposition that are not compatible with the direct arithmetic operations used within contractor programming to contract the interval vectors. In order to overcome this limitation, the specified eigenvalues are checked for inclusion by substituting each into the characteristic equation formed from the determinate:

$$\left|K^I - \omega_r^2 M\right| = \left|K_o + \sum_{j=1}^{N_K} [\underline{\alpha_j}, \overline{\alpha_j}] K_j - \omega_r^2 M\right| = 0 \tag{5.9}$$

Finally, in addition to these eigenvalue inclusion constraints, orthogonality constraints are introduced to aid with the identification of the unmeasured components of each mode shape. For each of the eigenvectors included in the prescribed eigeninformation matrix, ϕ, the following constraint equations can be enforced:

$$\phi_r^T M \phi_q = 0, r \neq q \tag{5.10a}$$

$$\phi_r^T K^I \phi_q = 0, r \neq q \tag{5.10b}$$

$$\frac{\phi_r^T K^I \phi_r}{\phi_r^T M \phi_r} = \omega_r^2 \tag{5.10c}$$

For synthetic data absent of measurement noise and fully consistent with the underlying analytical model, the matrix equality constraints in Equations 5.6, 5.9, and 5.10 can

be applied in the constraint satisfaction problem to yield satisfiable solutions to the inverse problem. However, in practical applications, the matrix constraint equations need to be relaxed to account for measurement errors and the idealizations inherent within the discrete representation of the physical structure. In our treatment of this problem, we treat the measured natural frequencies as exact and account for measurement uncertainties by relaxing the measured mode shape components from real numbers to intervals centered around the experimental estimates. In this relaxation, each partially described eigenvector, ϕ_r^M, in the matrix containing the measured components of the mode shapes, $\Phi_{s\times m}^M$, is first scaled to unity maximum amplitude and then an interval is constructed around all but the maximum amplitude component of the measured mode shape as:

$$\phi_{i,r}^{I,M} = [\underline{\phi}_{i,r}, \overline{\phi}_{i,r}] = \begin{cases} [\phi_{i,r}^M - \chi, \phi_{i,r}^M + \chi] & \text{if } \phi_{i,r}^M \neq 1 \\ [1,1] & \text{if } \phi_{i,r}^M = 1 \end{cases} \tag{5.11}$$

where χ is a specified radius for the intervals. This relaxation applies to the constraint equations in Equations 5.6 and 5.10. The motivation behind not relaxing the maximum amplitude component of the mode shape is to establish this component as a fixed reference for the eigenvector, since the amplitude of an eigenvector is not unique.

The radius of the intervals can either be established based on a measure of uncertainty in the experimentally estimated mode shapes, if available, or can be iteratively assigned based on the solvability of the constraint satisfaction problem. If the radius is prescribed too low in the presence of measurement and idealization errors, the nonlinear constraint satisfaction processor will return no solutions indicating that there are no satisfiable solutions to the inverse eigenvalue problem. This would be analogous to establishing a constraint equa-

tion for the Cross-in-Tray function described in Section 5.3.2 with the function equated to a value below the global minimum. Fortunately, the IBEX nonlinear constraint satisfaction solver can very efficiently identify non-satisfiable cases, which allows for progressive widening of the radius, χ, until satisfiable solutions are first yielded. In addition, one can continue to increase this radius to further relax the constraint equation, which can be used to provide a measure of how well conditioned the inverse problem is for the given uncertain parameters in the model as well as identify alternative solutions similar to those identified around the global minimum. This extension would be analogous to application of the relaxed inequality constraint for the Cross-in-Tray function described in Section 5.3.2, where the relative steepness of the basins around the global minimum and the presence of local minima were exposed. These unique features of the developed methodology are demonstrated for the model updating problem using both numerical and experimental data in the following sections of this paper.

5.4 Numerical Verification of Methodology

To demonstrate the capabilities of the formulated constraint satisfaction-based approach for the model updating problem, this study first numerically considers a 1st-order statically indeterminate spring-mass system with six degrees of freedom, shown in Figure 5.3. The structural configuration of this model was intentionally selected in order to generate ill-posed cases to the inverse eigenvalue problem admitting multiple solutions as well as spurious modes. Through linear parameterization of the model, elemental contributions to the stiffness matrix from each linear elastic spring are explicitly defined in the structured matrices. The mass and stiffness properties of the system were assigned to closely parallel

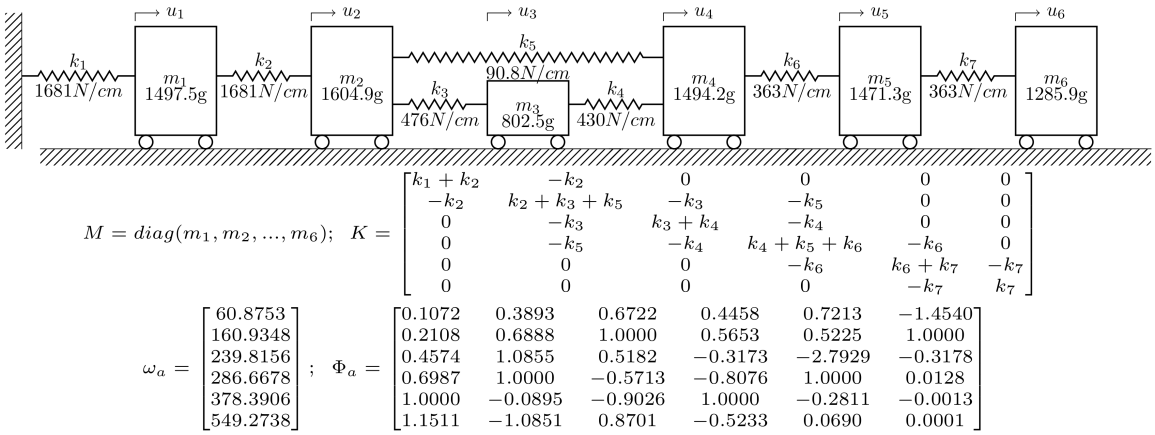


FIGURE 5.3: Six degree-of-freedom mass-spring system considered in numerical verification

an experimental analog to this numerical model that is subsequently presented in this paper for experimental validation. The eigenpairs of this undamped system were generated through eigendecomposition and are presented below the schematic representation of the MDOF model in Figure 5.3. The eigenvectors are normalized with respect to the measured sensors such that the magnitude of the largest entry in each eigenvector is one, rather than mass normalized. This is done to minimize any bias in the interval precision applied to the solution of the unmeasured components of each eigenvector when applying contractor programming to solve the constraint equations. Furthermore, the normalization serves to demonstrate that the generalized approach is applicable both to cases of model updating applied with results from experimental modal analysis (EMA), where mass normalization of the modes is possible, and operational modal analysis (OMA), where mass normalization of the modes is prohibited due to the lack of measurement of the input excitation forces.

5.4.1 Application to a Well-Posed Problem

To verify the framework on a well-posed problem, the seven spring stiffness assignments, $\{k_1, k_2, ..., k_7\}$ were treated as uncertain parameters in the model. In order to produce a par-

tially described inverse eigenvalue problem with incompletely measured modes, synthetic measurements of the mode shapes were limited to those from degrees of freedom u_2, u_4, and u_5 and the eigeninformation was limited to the first three modes. Consequently, the eigenpairs provided to the finite element model updating problem were:

$$\Omega = \begin{bmatrix} 60.8753 & 0 & 0 \\ 0 & 160.9348 & 0 \\ 0 & 0 & 239.8156 \end{bmatrix} \quad \Phi = \begin{bmatrix} \phi_{1,1} & \phi_{1,2} & \phi_{1,3} \\ 0.2108 & 0.6888 & 1.0000 \\ \phi_{3,1} & \phi_{3,2} & \phi_{3,3} \\ 0.6987 & 1.0000 & -0.5713 \\ 1.0000 & -0.0895 & -0.9026 \\ \phi_{6,1} & \phi_{6,2} & \phi_{6,3} \end{bmatrix}$$

where the measured eigenvector components are actually prescribed as intervals, $[\underline{\phi}_{i,r}, \overline{\phi}_{i,r}]$, centered around these values, as in Equation 5.11. Since the unmeasured components of the mode shapes appear in the constraint equations formed from the generalized eigenvalue problem, the incomplete eigenvector matrix introduces nine additional unknowns to the seven unknown stiffness parameters. The search space for these 16 unknowns was constrained by introducing bounds on the uncertain parameters in the model, $k_j \in [0.1\ N/cm,\ 2500\ N/cm]$, and on the unmeasured components of the mode shapes, $\phi_{i,r} \in [-10, 10]$. For this example, an interval precision of 25 for the uncertain stiffness assignments and 0.025 for the unmeasured components of the mode shapes were specified for the stopping criteria of the CSP. The difference in the specified required interval precisions was chosen to reflect the differences in the relative amplitude of the stiffness assignments compared to the components of the normalized mode shapes.

Despite the significant number of unknown variables in the coupled nonlinear constraint equations and the large search space associated with these unknowns, the nonlinear con-

straint solver was found to be capable of mapping the feasible solution space in only a few seconds of CPU time. Figure 5.4 presents the sets of interval vector solutions developed with three different radii of measurement uncertainty, χ, introduced around the synthetic measurements of the three mode shapes. For the smallest radius, $\chi = 0.0001$, the solution consists of three interval vectors, one of which contains the exact solution for the stiffness values and unmeasured components of the mode shapes. By increasing the radius associated with the measurement uncertainty, a set of interval vector solutions is developed that produce a basin around the exact solution. This ability to map the feasible solutions under a set of relaxed constraints provides a means of quantifying the uncertainty in the identified parameters of the model, while retaining the relationships between the parameters contained in the solution set. In this example, these basins reveal that the relative uncertainty associated with the inverse solution to parameters k_6 and k_7 with $\chi = 0.001$ is very low (less than $\pm 0.4\%$), while the conditioning of the inverse problem leads to larger uncertainty for parameters k_1, k_2, k_3, and k_4 (approximately $\pm 5\%$) and the parameter with the greatest uncertainty is k_5 (approximately $\pm 10\%$). It should also be noted here that refining the interval precision of the solutions was found to not significantly alter the basins of solutions yielded by the solver. However, by reducing the required interval precision, the boundary of each basin is refined to a smoother approximation as boxes with smaller width can more accurately map the curvature along this perimeter.

5.4.2 Application to an Ill-Posed Problem

Model updating has conventionally not been applied to problems that are ill-posed as a result of limited experimental data relative to the uncertain parameters in the model,

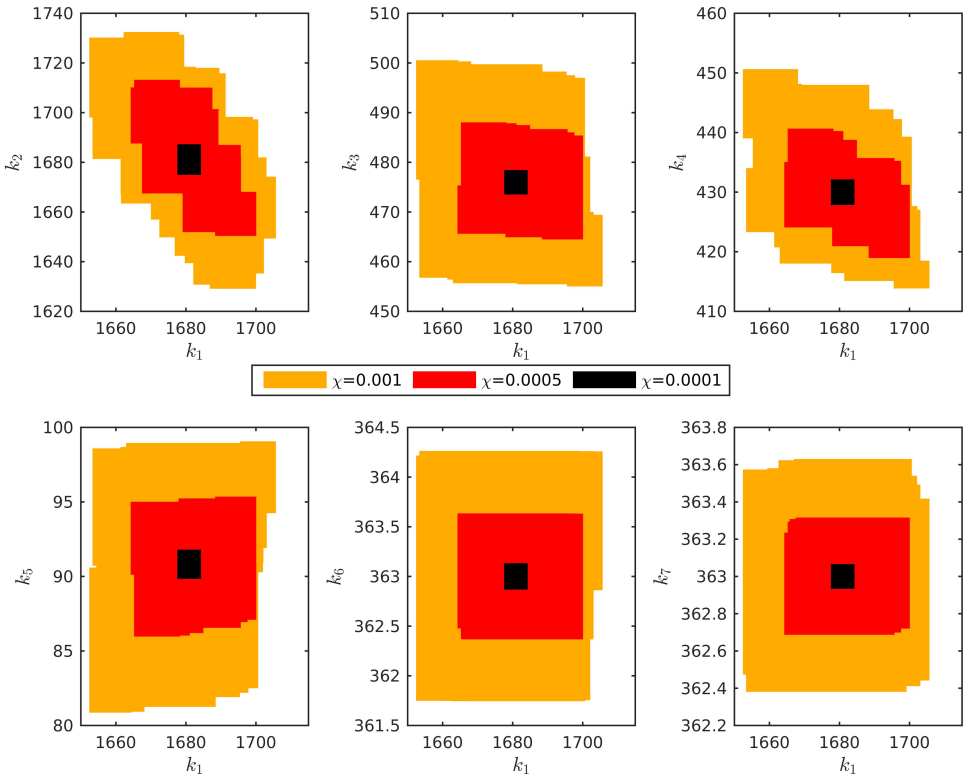


FIGURE 5.4: Feasible solutions for a well-posed analytical case of model updating with increasing uncertainty on the measured components of the mode shapes

since optimization schemes are not suitable for cases with non-unique solutions. However, framing the model updating problem as a CSP allows for solution of such problems and, as demonstrated in the following example, may introduce novel capabilities for parameter identification in structural health monitoring applications. Extension of this problem to an ill-posed case can be demonstrated by limiting the prescribed eigeninformation to the first two eigenvalues and the corresponding incomplete eigenvectors. In this case, the synthetic measurement data for the model updating problem is provided as:

$$\Omega = \begin{bmatrix} 60.8753 & 0 \\ 0 & 160.9348 \end{bmatrix} \quad \Phi = \begin{bmatrix} \phi_{1,1} & \phi_{1,2} \\ 0.2108 & 0.6888 \\ \phi_{3,1} & \phi_{3,2} \\ 0.6987 & 1.0000 \\ 1.0000 & -0.0895 \\ \phi_{6,1} & \phi_{6,2} \end{bmatrix}$$

Since the problem is ill-posed due to the non-uniqueness of the inverse solution, there are a large number of solutions to this inverse eigenvalue problem without having to introduce the interval relaxation on the measured components of the mode shapes. In developing the CSP for this problem, the same bounds previously enforced on the uncertain parameters and unmeasured components of the eigenvector matrix were specified. An interval precision of 2 for the uncertain stiffness parameters and 0.002 for the unmeasured components of the mode shapes were specified for the stopping criteria. Application of the IBEX nonlinear constraint solver for solution of the CSP using contractor programming produced 4,386 feasible interval vector solutions. Across all feasible solutions to the inverse eigenvalue problem, three distinct basins of interval solutions were discovered within the bounded search space. These basins of feasible solutions are presented for each of the seven stiffness assignments in Figure 5.5a, where the stiffness assignments in the model used to generate the synthetic data are presented as a marker in each subplot. It should be emphasized that, due to the intentionally ill-posed nature of the problem, all of the solutions obtained are correct solutions to the inverse eigenvalue subject to the partially described and incompletely measured eigeninformation matrices. Forward solution of the eigenvalue problem with the identified parameter sets was used to confirm that each of the feasible solutions correctly exhibits the two prescribed eigenvalues and corresponding

measured components of the eigenvectors.

There are several important features of the set of feasible solutions developed that provide motivation for further exploration of this constraint satisfaction approach to model updating. First, a closer examination of the complete modal parameters produced by eigenvalue decomposition of the reconstructed models generated with each set of feasible parameter sets reveals that the solutions in two of the basins exhibit spurious modes. As indicated by Figure 5.5b, only the parameter sets contained within the first basin exhibit natural frequencies for the first two modes that match the prescribed eigenvalues. Parameter sets within the other two basins produce models where the natural frequencies of higher-order modes match the prescribed eigenvalues. Assuming that either vibration testing or engineering judgment is able to discredit the presence of any additional modes within the bandwidth of prescribed data, these basins of solutions could be discarded as physically implausible to reduce the feasible solution space.

Second, in addition to identifying the uncertain parameters in the model, the approach also identifies feasible values for the unmeasured components of the mode shapes in the prescribed eigenvector matrix. This permits the identification of spurious solutions, or feasible solutions that do not exhibit reconstructed mode shapes consistent with expectations, without requiring eigenvalue decomposition of the each feasible model, which can be computationally intensive for large analytical models. Figure 5.5c presents a comparison between the complete mode shapes from the original model and reconstructed mode shapes typical of each basin produced through constraint satisfaction. These comparisons reveal that the parameter sets admitting spurious modes can be readily identified by their reconstructed mode shapes, which differ significantly from the complete solution since they are

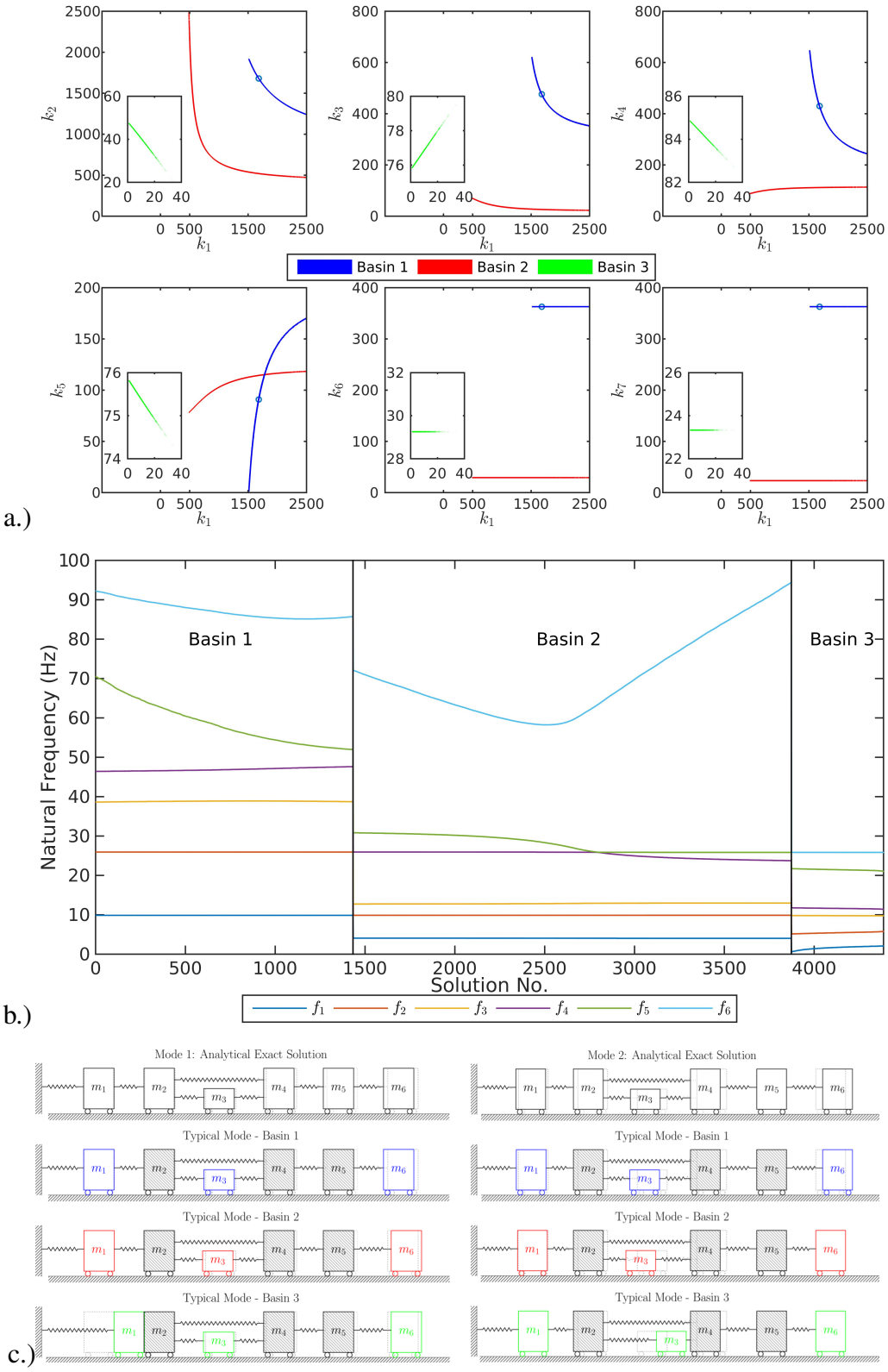


FIGURE 5.5: Complete set of feasible solutions for non-unique model updating problem with numerical data: a.) Basins of feasible stiffness assignments; b.) Natural frequencies associated with the feasible solutions; c.) Comparison of reconstructed mode shapes to the complete analytical modes from the reference structure

higher-order modes. Therefore, with practitioner judgment is it possible to discard spurious solutions by simply evaluating the reconstructed mode shapes, which are included in the solution set and therefore can be evaluated with no additional computational expense in this methodology. This concept of integrating "human-in-the-loop" strategies for assessing alternative solutions within finite element model updating has been recently proposed by Caicedo and Yun (2011) and is a possible extension of the current study that will be explored in future work. Additionally, techniques such as finding the natural, or minimum-length, solution with respect to the expected parameter values can be used to select updated parameter sets within under-determined problems (Hu and Li, 2008).

Third, in addition to being able to describe the nonlinear interrelationships among spring stiffness assignments yielding feasible solutions, the basins establish the permissible range, or uncertainty, associated with each identified stiffness parameter. While the ill-posed nature of the problem explored produces a wide range of uncertainty across five of the spring stiffnesses, two spring stiffness assignments (k_6 and k_7) were identified as constants within each basin. Consequently, the approach exactly identified uncertain parameters in a substructure of the model despite the severely limited data provided. It is particularly interesting to note that the nonlinear constraint solver exactly identifies the spring stiffness k_7 despite the absence of a measurement on the attached mass, m_6. The development of sensor placement strategies to produce parameter identification within targeted substructures may be an interesting future extension of this work.

5.5 Experimental Application on a Shear Building Model

To validate the application of the proposed methodology on an experimental dataset, a laboratory-scale six-story shear building structure was developed as an analog to the mass-spring model used in the numerical verification (Figure 5.6a). This structure was constructed of 15.2 cm deep and 1.3 cm thick aluminum plate masses serving as rigid diaphragm floors at each story elevation. The plate mass at the third floor elevation was 10.2 cm wide, while the other plate masses were 20.3 cm wide. These plates were supported by 15.2 cm wide aluminum sheets with different thicknesses, as indicated in Figure 5.6b, to vary their stiffness. An aluminum plate washer and row of four flange-head cap screws were used on each side of the plate masses to secure the sheets to each floor. Prior to experimental modal analysis, each cap screw was torqued to 1084 N·cm to ensure uniform connectivity. If the behavior of the test structure is idealized with the typical assumptions adopted for a shear building model, a six degree of freedom simplified analytical representation of the system can be constructed that corresponds to the model used for the numerical verification in the prior section, shown in Figure 5.3. A lumped mass matrix formulation was adopted for this study and the lumped masses used in the model were measured by weighing individual components of the structure. Likewise, estimations of the stiffness contributions for each of the aluminum sheets serving as columns were obtained by approximating each as a fixed-fixed beam subject to relative end deflection. Both the measured masses and approximated stiffness contributions in the model are presented in Figure 5.3 and were used in the prior numerical verification.

5.5.1 Vibration Testing and System Identification

Experimental modal analysis of the structure was conducted using six Measurement Specialties 4000A-002 single-axis accelerometers featuring a full-scale range of ± 2g, 0-200 Hz measurement bandwidth, and 35 $\mu g/\sqrt{Hz}$ spectral noise. These vibration transducers were mounted to each plate mass of the test structure with a thin layer of wax to measure the in-plane lateral response in the weak direction of the building frame. A PCB Piezotronics 086C03 modally tuned impact hammer with super-soft tip was used to provide impulse excitation to the structure. A National Instruments PXIe-4497 24-bit simultaneously sampling dynamic signal analyzer was used for signal conditioning and acquisition of the accelerometer signals as well as the impact force with a sampling rate of 10 kHz. Frequency response functions developed using the classical H_1 estimator (Brandt, 2011) are presented in Figure 5.6c for the bandwidth encompassing the six modes associated with the response of shear building model in the weak-axis of bending.

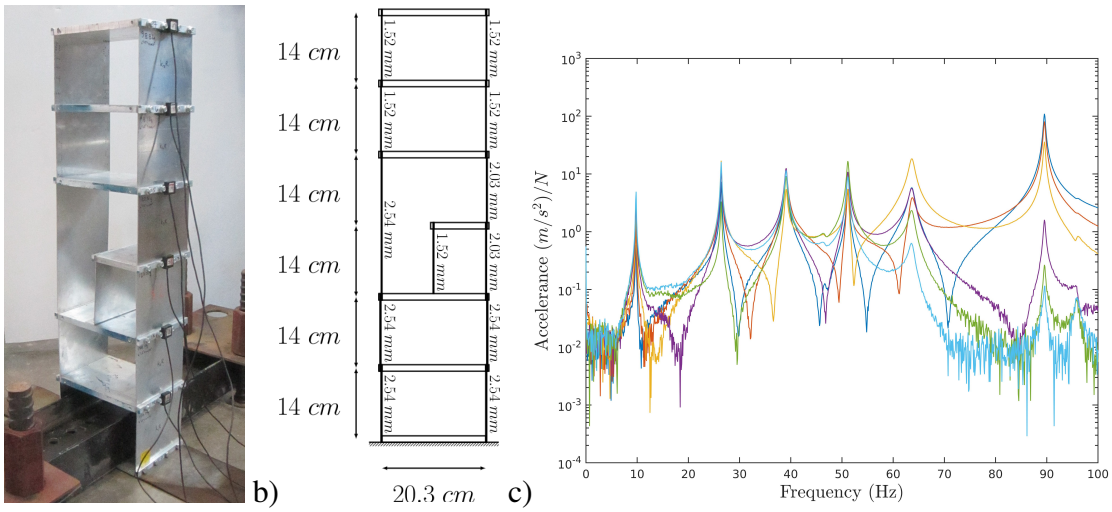


FIGURE 5.6: Laboratory six-story shear building model: a.) photograph of instrumented test structure, b.) structural geometry and thickness of aluminum sheet columns, c.) frequency response functions obtained from impact excitation at elevation of first story mass

Experimental estimates of the modal parameters were obtained through system identification using the combined deterministic stochastic subspace state-space system identification algorithm (VanOverschee and DeMoor, 1996). In application of this algorithm, experimental modal parameter estimates for the structure were calculated through eigendecomposition of the state matrix across a range of model orders and stabilization plots were utilized to select consistent pole estimates. In order to obtain improved estimates of modal parameters to attenuate effects of measurement and process noise, five stable poles and their corresponding eigenvectors were averaged for each experimental mode. The identified undamped natural frequencies are presented in Figure 5.7 along with the identified real-valued mode shapes.

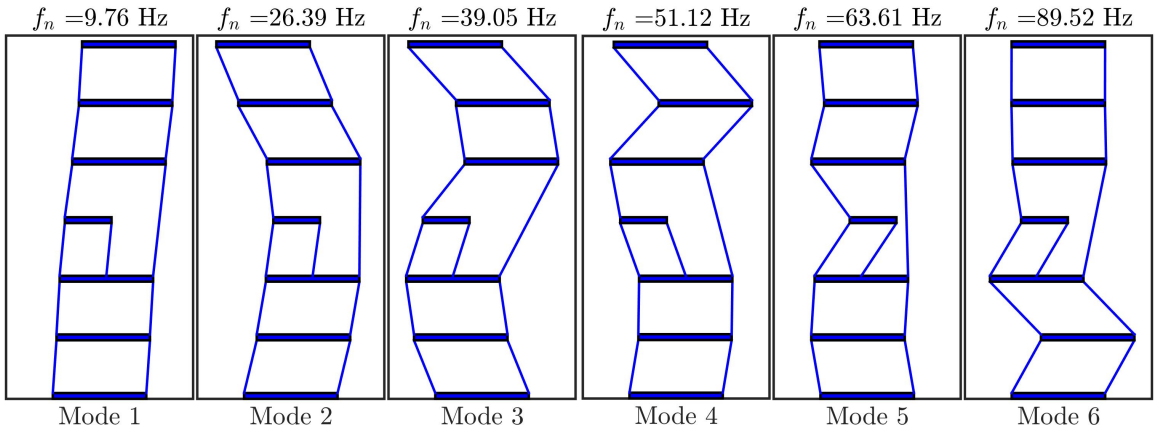


FIGURE 5.7: Undamped natural frequency and mode shape estimates of the test structure obtained through system identification

5.5.2 Experimental Application to a Well-Posed Problem

Consistent with the numerical verification, the seven stiffness assignments were treated as uncertain parameters in the analytical model of the shear building structure and the experimental data was limited to measurements from degrees of freedom u_2, u_4, and u_5. To parallel the construction of the problem in Section 4.1, the partially-described and incom-

plete experimental eigeninformation was first provided to the nonlinear constraint solver as:

$$\Omega = \begin{bmatrix} 61.2953 & 0 & 0 \\ 0 & 165.8179 & 0 \\ 0 & 0 & 245.3396 \end{bmatrix}; \quad \Phi = \begin{bmatrix} \phi_{1,1} & \phi_{1,2} & \phi_{1,3} \\ 0.2606 & 0.9582 & -0.9963 \\ \phi_{3,1} & \phi_{3,2} & \phi_{3,3} \\ 0.7436 & 1.0000 & 1.0000 \\ 1.0000 & -0.2527 & 0.7103 \\ \phi_{6,1} & \phi_{6,2} & \phi_{6,3} \end{bmatrix}$$

with the measured eigenvector components are prescribed as intervals, $[\underline{\phi}_{i,r}, \overline{\phi}_{i,r}]$, centered around the values shown with the radius χ. Likewise, the search space for unknowns in the constraint equations was established by bounding the uncertain parameters in the model to $k_i \in [0\ N/cm, 2500\ N/cm]$ and bounding the unmeasured components of the mode shapes to $\phi_{j,k} \in [-10, 10]$. As in the numerical verification, an interval precision of 25 for the uncertain stiffness assignments and 0.025 for the unmeasured components of the mode shapes were specified for the stopping criteria of the CSP.

The nonlinear constraint solver was applied iteratively to the set of constraint equations by incrementing the size of the radius, χ, around the measured eigenvector components until feasible solutions were generated. When the radius was increased to 0.0027, the nonlinear constraint solver generated 3 solutions within the parameter search space in less than 10 seconds of computational time. To quantify the uncertainty in the parameter estimates and reflect the relative conditioning of the inverse problem for each uncertain parameter, the radius on the uncertain eigenvector measurements was further increased over two increments and the basins of solutions are presented in Figure 5.8. As in the numerical verification, these basins provide a means of assessing the relative uncertainties in individual parameters

and indicate that relatively small changes in the measured components of the mode shapes result in admitting a large number of solutions for this problem. This is a reflection of the conditioning of this inverse problem, however the formulated approach allows for quantifying the sensitivity of the individual parameters to the measurement uncertainties. As in the numerical example, certain parameter estimates (k_6 and k_7) are found to be less sensitive to measurement uncertainties and can be reliably identified in the presence of conditioning issues.

A representative interval solution for the uncertain parameters obtained from the original solution basin is presented in Table 5.1. Despite the large search space, the nonlinear constraint solver identified assignments for the stiffness parameters that are generally consistent with the idealized approximations. Discrepancies between the identified stiffness assignments and approximations can be partially attributed to the assumptions used to develop the theoretical estimates, material and fabrication tolerances in the construction of the experimental model, and idealization errors introduced by modeling this continuous system as a discrete MDOF system. Additionally, as demonstrated in Figure 5.8, the problem is not particularly well-conditioned and, consequently, select parameter estimates are sensitive to measurement errors and could be improved by inclusion of additional eigeninformation in the inverse problem. To verify the interval solution, interval modal analysis was performed using the assumed mass matrix and the interval stiffness matrix constructed with the interval vector for the identified stiffness parameters. The interval eigenvalues for this system were then derived using the interval modal analysis technique presented in Sim et al. (2007). Table 5.2 provides a comparison between the experimentally estimated natural frequencies and the interval natural frequencies produced by the updated model. The

solution is found to contain each of the three prescribed natural frequencies with a tight enclosure around the experimental estimates.

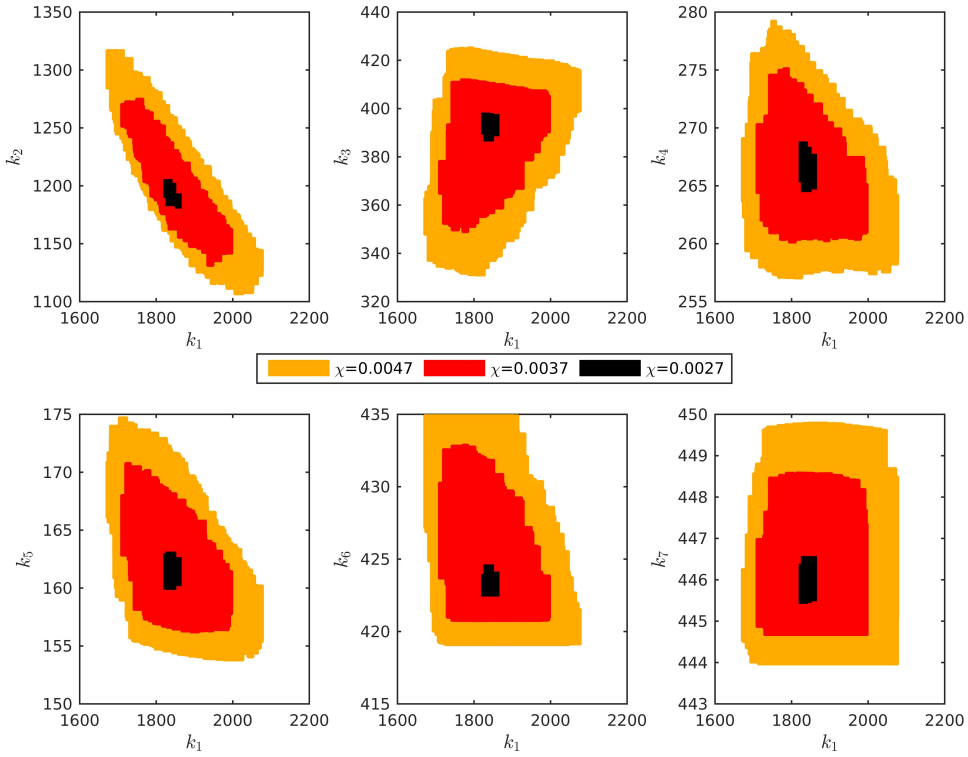


FIGURE 5.8: Feasible solutions for a well-posed experimental case of model updating with increasing uncertainty on the measured components of the mode shapes

5.5.3 Experimental Application to an Ill-Posed Problem

Similar to the numerical verification, an ill-posed case with uniqueness challenges was also investigated using incomplete measurement data from the first two modes. In this example, the following partially-described and incompletely measured experimental eigeninformation matrices were provided as prescribed data for the model updating problem:

$$\Omega = \begin{bmatrix} 61.2953 & 0 \\ 0 & 165.8179 \end{bmatrix}; \quad \Phi = \begin{bmatrix} \phi_{1,1} & \phi_{1,2} \\ 0.2606 & 0.9582 \\ \phi_{3,1} & \phi_{3,2} \\ 0.7436 & 1.0000 \\ 1.0000 & -0.2527 \\ \phi_{6,1} & \phi_{6,2} \end{bmatrix}$$

TABLE 5.1: Comparison of stiffness estimates to experimental results obtained using three incompletely measured eigenpairs

Parameter	Interval Solution, $[\underline{k}_i, \overline{k}_i]$
k_1	[1850.4 , 1864.6]
k_2	[1180.99 , 1192.8]
k_3	[388.85 , 397.41]
k_4	[264.74 , 267.70]
k_5	[160.23 , 162.60]
k_6	[422.47 , 424.09]
k_7	[445.50 , 446.55]

TABLE 5.2: Comparison between experimental modal estimates and updated model

Mode	f_{exp}	$[\underline{f}, \overline{f}]$	$[\Delta\underline{f}(\%), \Delta\overline{f}(\%)]$
1	9.7555	[9.7251, 9.7786]	[-0.3110, 0.2377]
2	26.3907	[26.3343, 26.4080]	[-0.2137, 0.0653]
3	39.0470	[39.0123, 39.0550]	[-0.0888, 0.0204]

The CSP for this problem was established with the same bounds on the unknown variables as the prior examples and, due to the ill-posed nature of the problem, the measured components of the mode shapes were not relaxed to interval estimates. An interval precision of 2 for the uncertain stiffness parameters and 0.002 for the unmeasured components of the mode shapes were specified for the stopping criteria. Application of the IBEX nonlinear constraint solver to the formulated constraint satisfaction problem yielded 5,890 feasible interval vector solutions with three distinct basins similar to those developed in the numerical verification discovered within the bounded search space (Figure 5.9a). Forward solution of the eigenvalue problem with the identified stiffness parameter sets was used to confirm that each of the feasible solutions correctly exhibit the two prescribed eigenvalues and corresponding measured components of the eigenvectors within the pre-

scribed relaxation tolerance. As in the numerical example, two of the basins of feasible solutions were found to exhibit spurious mode development. For these combinations of stiffness parameter assignments, the updated model gives rise to additional eigenvalues within the frequency bandwidth of the two prescribed eigenvalues (Figure 5.9b). Typical reconstructed mode shapes for each basin using the identified missing components of the prescribed mode shapes are provided in Figure 5.5c, which parallel the solutions obtained with the numerical example to further validate the extension of the proposed methodology to experimental data. In addition, two of the uncertain parameters in the model (k_6 and k_7) were exactly identified in all three of the solution basins, despite the ill-posed nature of the problem. Furthermore, the identified assignments for these parameters in the first basin agree with those identified in the previous solution to the well-posed problem.

5.6 Comparison to Bayesian Model Updating Approaches

As noted in the introduction, the developed methodology offers an alternative to probabilistic methods of finite element model updating. Beyond simply accounting for the challenges of measurement uncertainty in model updating, nonlinear constraint satisfaction provides unique advantages and capabilities that are not offered by current probabilistic techniques. To highlight these differences, particularly with respect to addressing the effects of measurement uncertainty on the parameter estimation, the challenges and limitations of probabilistic model updating are briefly reviewed and a comparison between probabilistic model updating and the nonlinear constraint satisfaction approach is presented using a simple benchmark example problem.

In contrast to the constraint satisfaction methodology presented in this paper, Bayesian

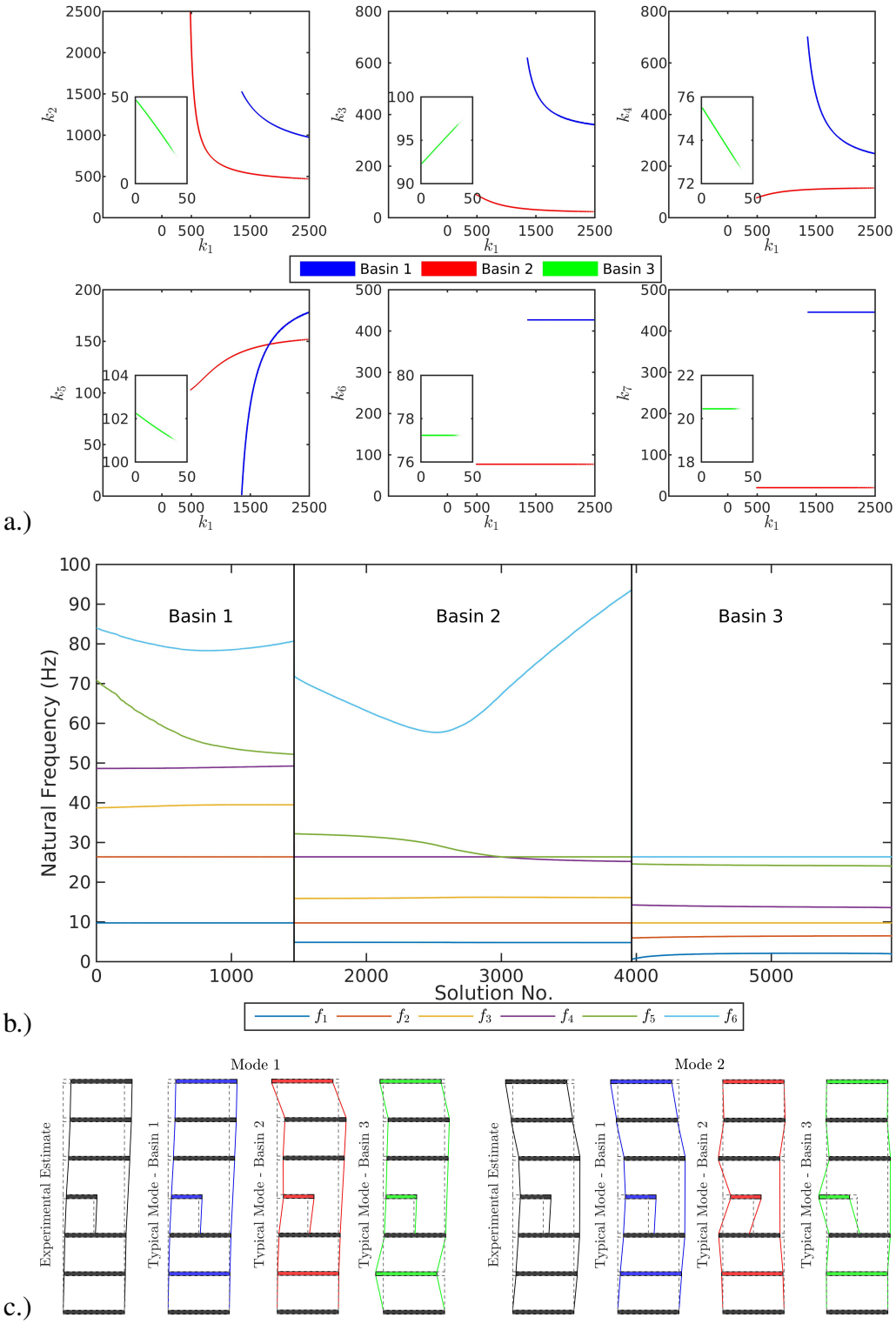


FIGURE 5.9: Complete set of feasible solutions for non-unique model updating problem with experimental data: a.) Basins of feasible stiffness assignments; b.) Natural frequencies associated with the feasible solutions; c.) Comparison of reconstructed mode shapes to the complete experimental measurements

model updating approaches rely on an likelihood function to quantify the model correlation. When modal data is used, the likelihood function includes a modal measure of fit function that incorporates an objective function for the natural frequencies and an objective function for the partially described mode shapes. For illustration, a commonly used modal measure of fit, provided by Vanik et al. (2000), is:

$$J(\theta) = \sum_{r=1}^{N_m} \sum_{j=1}^{N_s} \left[\left(\frac{(1 - \hat{\omega}_{r,j}^2/\omega_r^2)^2}{\varepsilon^2} \right) + \left(\frac{\phi_r^T (I - \hat{\phi}_{r,j} \hat{\phi}_{r,j}^T) \phi_r}{\delta^2 \|\phi_r\|^2} \right) \right] \tag{5.12}$$

where N_m is the number of modes included in the identification, N_s is the number of sets of modal data, $\hat{\omega}_{r,j}$ and $\hat{\phi}_{r,j}$ are the experimental natural frequency and incomplete mode shape, respectively, for the r-th mode of the j-th data set, ω_r and ϕ_r are the corresponding natural frequency and incomplete mode shape for the model with parameter assignments θ, and ε and δ are parameters that reflect the uncertainty in the experimentally measured natural frequencies and mode shapes, respectively. There are several noteworthy issues associated with the use of the modal measure of fit in Bayesian model updating. First, the updating results can be very sensitive to the weighting coefficients, ε^2 and δ^2, that express the relative importance of the modal frequency and partially described mode shape correlations to the objective function (Goller et al., 2012). Second, direct matching of modes is required, which can be challenging with incompletely measured mode shapes (Sun and Büyüköztürk, 2016). Lastly, the measure of fit aggregates the model correlations and therefore does not ensure that each of the individual modal parameters of the identified modal are consistent with the experimental measurements within prescribed uncertainty bounds.

Additional challenges associated with Bayesian model updating stem from the need to

evaluate multidimensional integrals that can not be solved analytically. A favored approach, particularly for models with many parameters, has been to leverage stochastic simulation methods, such as Metropolis-Hastings or Gibbs sampling, to develop the posterior probability density functions for the uncertain parameters. However, such approaches introduce several additional challenges. First, since the parameter space is evaluated by discrete sampling, the development of posterior joint probability distribution functions can be computationally intensive, particularly if either the size of the model or the uncertainty in the prior distributions is large. Second, the specification of the prior distributions influences the development and accuracy of the posterior probability distribution functions (Beck and Au, 2002). Transitional, or adaptive, methods have been introduced to address this later challenge by converging on the posterior distribution through intermediate probability distribution functions (Ching and Chen, 2007). However, these methods introduce additional complexity and computational cost. Lastly, stochastic simulation methods are sensitive to user specified settings, such as the number of iterations before adaptation of the intermediate probability distribution functions, and can not guarantee complete exploration of the parameter search space and complete mapping of feasible solutions.

A two degree of freedom mass spring model sourced from Goller et al. (2012) is used to illustrate these limitations within Bayesian model updating approaches and further demonstrate advantages of the proposed methodology. Consistent with the case presented in the literature, the structural matrices for this model are taken as:

$$M = \begin{bmatrix} 1 & 0 \\ 0 & 1 \end{bmatrix} \quad , \quad K = 2000 \begin{bmatrix} \theta_1 + \theta_2 & -\theta_2 \\ -\theta_2 & \theta_2 \end{bmatrix} \tag{5.13}$$

where θ_1 and θ_2 are uncertain stiffness parameters. Synthetic measurement data was generated for 15 sets of modal parameter estimates by generating Gaussian distributions with coefficient of variation of 0.01 around the two natural frequencies and mode shapes for the model specified with $\theta_1 = \theta_2 = 1$. For Bayesian model updating, an adaptive Metropolis-Hastings Markov Chain Monte Carlo method was used to sample posterior probability distribution functions with a likelihood function incorporating the modal measure of fit function in Equation 5.12. For all cases described, a uniform prior distribution was assigned to the two uncertain parameters in the model over the range [0,3]. Relative weighting of the natural frequency and mode shape terms in the modal measure of fit function was adjusted to yield three representative cases. The first two cases serve to illustrate the sensitivity of the Bayesian model updating results to the assignment of the relative weighting coefficients prescribed to the mode shape and natural frequency correlations in the modal measure of fit function. When the relative weighting is prescribed in a way that over-expresses the mode shape correlations relative to the natural frequency correlations, an under-determined problem is developed and the posterior distribution of the Markov Chain samples suggest non-uniqueness of the uncertain parameters (Figure 5.10a). When the relative weighting is prescribed in a way that over-expresses the natural frequency correlations relative to the mode shape correlations, the posterior distribution of the Markov Chain samples suggest two alternative solutions (Figure 5.10b). Only when the relative weighting is prescribed such that the natural frequency and mode shape correlations are balanced to express an appropriate degree of importance of each to the modal measure of fit is a posterior distribution uniquely generated around the two stiffness parameters used to develop the measurement data (Figure 5.10c). It should be noted that strategies for determining balanced

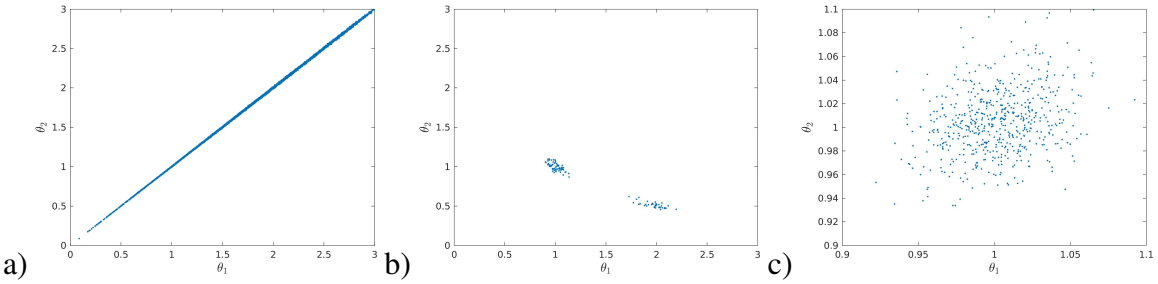


FIGURE 5.10: Samples of the posterior distribution obtained from Bayesian model updating of two degree of freedom model with uncertain stiffness parameters: a) mode shapes over-expressed in the measure of fit; b) natural frequencies over-expressed in the measure of fit; c) balanced model class

weighting factors for Bayesian model updating have been developed (Goller et al., 2012), however these strategies require an additional layer of heuristic model updating on the relative weighting assignments to assess and select the appropriate model class. Consequently, these approaches further increase the computational burden associated with probabilistic model updating.

Constraint equations for the same two degree of freedom mass spring model were developed using the new methodology proposed by the authors. The standard deviations, σ, of the synthetic measurements of the natural frequencies and mode shapes were used to establish interval assignments about the mean of these modal parameters within the constraint equations. Nonlinear constraint satisfaction using interval arithmetic and contractor programming was then used to map all feasible solutions within a search space developed by bounding the parameters in the model using $\theta_j \in [0, 3]$. In order to generate solutions for non-unique cases analogous to those presented for Bayesian model updating, the synthetic measurement data provided in the constraint equations was first restricted to either the mode shapes (Figure 5.11a) or the natural frequencies (Figure 5.11b). In both cases, subpavings were generated for interval uncertainties on the prescribed measurement components using

confidence intervals of $\pm 2\sigma$, $\pm\sigma$, and $\pm\frac{1}{2}\sigma$. In both cases, the nonlinear constraint satisfaction approach correctly identifies and maps the non-unique solutions in basins consistent with the Bayesian posterior distributions. However, unlike the samples of the posterior distributions produced by Bayesian model updating that require further statistical inference to estimate the probabilities associated with the parameter assignments, the nonlinear constraint satisfaction approach successfully propagates the measurement uncertainty through the inverse problem to completely and crisply map the associated confidence in the identified feasible parameter assignments. Furthermore, it should be emphasized that these non-unique cases need to be intentionally generated by omitting measurement data in the constraint equations, whereas they can arise unintentionally within the Bayesian method if relative weighting coefficients are prescribed in an unbalanced manner. When the synthetic data prescribed in the constraint equations includes both the natural frequencies and mode shapes, the nonlinear constraint solver correctly identifies the stiffness parameters used to generate the modal parameter data and encloses the confidence in the parameter estimates through the subpavings of the search space (Figure 5.11c). Comparison with current probabilistic model updating approaches, illustrates the advantages of both being able to directly specify the measurement uncertainty and completely enclose the feasible parameter space associated with the uncertain measurements using the nonlinear constraint satisfaction approach. In the Bayesian approach, the modal measure of fit aggregates all of the model correlations, which can not guarantee that modal parameters of the identified models strictly adhere to prescribed uncertainty bounds for individual parameters. Furthermore, statistical inference of the posterior samples is required to estimate parameter confidence, as opposed to the new methodology that crisply encloses the confidence intervals.

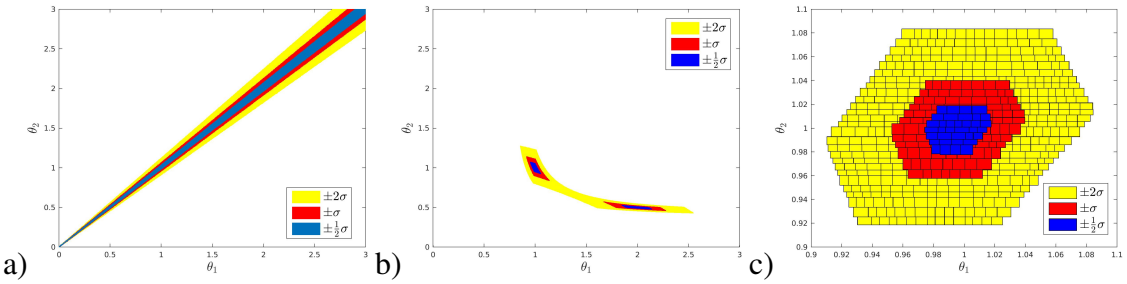


FIGURE 5.11: Subpavings of feasible solution space for parameters in two degree of freedom model: a) using only the mode shape measurements in the constraint equations; b) using only the natural frequency measurements in the constraint equations; c) using both the mode shape and natural frequency measurements

In terms of computational efficiency, the nonlinear constraint solver was able to map the feasible solution space to the nonlinear constraint satisfaction problem in a fraction of a second, while the Metropolis-Hastings Markov Chain Monte Carlo method used to perform Bayesian Model updating required several seconds to converge on the posterior distribution presented. It should be noted again that the computational time associated with the Bayesian method does not account for additional time required to select appropriate relative weighting factors. Since the nonlinear constraint satisfaction approach operates directly on the governing mechanics equations rather than objective functions that aggregate model correlations, potentially time consuming selection of model class is not required within the proposed methodology.

5.7 Conclusion

A novel technique for structural identification through model updating has been presented by formulating the inverse problem as a constraint satisfaction problem. The formulation structures a set of coupled, nonlinear constraint equations over a bounded search space and efficiently obtains a complete of feasible solutions to the constraint equations using interval arithmetic and contractor programming. The use of interval arithmetic in

the approach has been further leveraged to introduce relaxation of the constraint equations to accommodate uncertainties in the model and measurements. Through numerical verification as well as application to an experimental dataset, unique capabilities of this methodology for the model updating problem have been demonstrated.

Foremost, the approach is capable of completely mapping all feasible solutions to the structured inverse eigenvalue problem, which offers significant advantages over optimization-based techniques. An efficient process of progressive relaxation of the constraints equations to accommodate measurement uncertainties is used to identify the global optimal solution. Through further relaxation, the sensitivity of the parameter estimates to the measurement data can be revealed to quantify uncertainty in the parameter estimates associated with the conditioning of the problem as well as expose alternative solutions residing in local minima. Consequently, the approach provides a means of projecting uncertainty in the measurements to the parameter space and can permit future research to explore the incorporation of "human-in-the-loop" practitioner heuristics for the evaluation of alternative solutions to the global minimum. Furthermore, an additional unique capability of the approach is the demonstrated ability of the solver to completely enumerate the feasible solutions to ill-posed formulations of the model updating problem. Despite the uniqueness issues resulting from the limited measurement data used in the ill-posed form, results from the examples presented in this paper reveal the capability of this approach to exactly identify select uncertain parameters in substructures of the model. This capability may provide the foundation for developing novel vibration-based structural health monitoring strategies for condition assessment of local substructures with limited sensor deployments.

Future work will be directed toward leveraging the capabilities offered by this approach

to challenges in vibration-based damage detection. In addition, the exploration of specific contractors and design of contraction strategies beyond the default solver of the IBEX library offer the potential to enhance the performance of the methodology. Furthermore, the incorporation of model reduction strategies into the constraint equations may provide a means of improving the efficiency of the algorithm by eliminating the need to solve for unmeasured components of the eigenvectors. Lastly, the scalability of the proposed technique to larger structural models with more degrees of freedom will need to be investigated to extend the application to structures of greater complexity.

Acknowledgment

This material is based upon work supported by the National Science Foundation under Grant No. 1331825. Any opinions, findings, conclusions, or recommendations expressed in the material are those of the authors and do not necessarily reflect the views of the sponsor.

CHAPTER 6: VIBRATION-BASED DAMAGE DETECTION WITH UNCERTAINTY QUANTIFICATION BY STRUCTURAL IDENTIFICATION USING NONLINEAR CONSTRAINT SATISFACTION WITH INTERVAL ARITHMETIC

Abstract

Structural identification has received increased attention over recent years for performance-based structural assessment and health monitoring. Recently, an approach for formulating the finite element model updating problem as a Constraint Satisfaction Problem has been developed. In contrast to widely used probabilistic model updating through Bayesian inference methods, the technique naturally accounts for measurement and modeling errors through the use of interval arithmetic to determine the set of all feasible solutions to the partially described and incompletely measured inverse eigenvalue problem. This paper presents extensions of the constraint satisfaction approach permitting the application to larger multiple degree-of-freedom system models. To accommodate for the drastic increase in the dimensionality of the inverse problem, the extended methodology replaces computation of the complete set of solutions with an approach that contracts the initial search space to the interval hull, which encompasses the complete set of feasible solutions with a single interval vector solution. The capabilities are demonstrated using vibration data acquired through hybrid simulation of a forty-five degree-of-freedom planar truss, where a two-bar specimen with bolted connections representing a single member of the truss serves as the experimental substructure. Structural identification is performed using data acquired

with the undamaged experimental member as well as over a number of damage scenarios with progressively increased severity developed by exceeding a limit state capacity of the member. Interval hull solutions obtained through application of the nonlinear constraint satisfaction methodology demonstrate the capability to correctly identify and quantify the extent of the damage in the truss while incorporating measurement uncertainties in the parameter identification.

6.1 Introduction

In recent years, numerous methods have emerged for the updating of structural matrices using vibration data obtained from experimental and operational modal analyses. These updated stiffness and mass matrices have in turn been proposed for inferring properties of in-service structures and predicting behavior and performance to aid in decision making. Despite successful demonstrations of finite element model updating on full-scale structures, there are several persistent challenges. The primary challenge is that model updating is an inverse problem that is greatly affected by numerous sources of uncertainty including: the selection of uncertain parameters, modeling assumptions, and measurement uncertainties (Simoen et al., 2015). In addition to being an inverse problem, the finite element updating problem is typically partially described, wherein only a subset of the natural frequencies of the model are measurable given the bandwidth limitations of transducers (Chu and Golub, 2005). Similarly, from a practical standpoint, it is impossible to measure every degree of freedom represented in the analytical model, so the experimentally derived mode shapes are also inherently incomplete. Understanding how the effect of the limited measurements and measurement uncertainties propagate into the identified parameter space to quantify

the confidence in the results is paramount for decision making purposes, especially when the application relates to vibration-based damage detection.

In the past decade, the predominant approach for model updating in the presence of uncertainties is a class of methods referred to as probabilistic model updating(Beck and Katafygiotis, 1998). Probabilistic model updating employs statistical methods to provide a family of potential structural models (Beck and Au, 2002), instead of determining a single best deterministic solution, that incorporate measurement uncertainties in the posterior distributions of the model parameters. However, these methods require assumed probability density functions, a likelihood function with associated weighting coefficients to express relative importance of the natural frequency and mode shapes residuals, and rely heavily on the stochastic simulation method chosen (Marwala, 2010; Zhang et al., 2013). In addition, probabilistic methods can be computationally expensive, often requiring tens of thousands of simulations (Marwala, 2010), even when the number of uncertain parameters is relatively small (Behmanesh et al., 2015). In general, probabilistic model updating presents several challenges including: the results remaining highly dependent on the initial finite element model and the selection of uncertain parameters included in the updating (Behmanesh et al., 2015), direct matching of modes is required (Sun and Büyüköztürk, 2016), and the weights assigned to residuals in the objective function greatly affect the solution space (Goller et al., 2012; Behmanesh et al., 2015).

There have been numerous applications of probabilistic model updating for vibration-based damage detection (Sohn and Law, 1997; Vanik et al., 2000; Yuen et al., 2004, 2005; Ching et al., 2006; Huang et al., 2012; Behmanesh et al., 2015; Mustafa and Matsumoto, 2017; Biswal and Ramaswamy, 2017), which have underlined the importance of addressing

remaining challenges for practical application. An early study on probabilistic model updating determined that some identified parameter sets, while providing strong correlations with the experimental modal parameter estimates, may erroneously locate and quantify damage in the presence of measurement and modeling errors(Sohn and Law, 1997). The identifiability of damage is dictated by several factors including: the number and location of measurement sensors deployed during the vibration test and the quality of the measurement data. The first factor determines whether the problem is identifiable or unidentifiable, which is dependent on there being more unique modal measurements than the number of uncertain parameters in the model (Ching et al., 2006). However, it has also been shown that employing more modes in the identification does not guarantee better damage identification results (Behmanesh et al., 2017). Mustafa and Matsumoto (2017) explored practical application of Bayesian model updating for detection of simulated damage of a single diagonal member of a truss bridge and indicated that identification of local damage was not possible using only global modes. In addition, the authors indicated that detection of local damage may only be possible if the modal properties utilized in the finite element model updating scheme are significantly affected by the damage. Huang et al. (2012) outlined several uncertainties associated with vibration-based Bayesian model updating and how those uncertainties affect the ability to successfully identify damage. The authors stated that quality of the measured data has the largest effect on the ability to identify damage and demonstrated that successful identification of low level damage may not be possible even if the measurement noise is low. Utilization of damage identification results in such cases may lead to incorrect conclusions regarding the early onset or absence of damage. Likewise, high levels of measurement noise preclude successful damage detection. Con-

sequently, it was stated that an appropriate threshold must be chosen to distinguish damaged elements from undamaged elements, which itself is a practical challenge. Setting the threshold low, which increases the detection of damaged elements, may falsely identify undamaged elements as damaged. Conversely, if the damage threshold is set too high, there is a high probability of missing actual damage. In addition, since the sensitivity of the modal parameters estimates to the individual uncertain parameters in the model to be updated may vary significantly, the threshold for damage detection may also need to vary for individual structural members.

Recently, alternatives to probabilistic model updating that also offer the capability to account for measurement uncertainties are based on interval methods (Köylüoğlu et al., 1995). Interval analysis techniques have an advantage over probabilistic methods in that they do not require assumptions regarding the probability density functions of uncertain parameters and are capable of completely exploring the feasible parameter space without using discrete sampling techniques or a modal measure of fit function. Gabriele et al. (2007) presented one of the first studies employing interval analysis to place bounds on uncertain parameters, measurements, and modeling errors. The authors of that study utilized the inclusion property of interval analysis to place bounds on uncertain model parameters for damage identification. Wang et al. (2013b) employed interval analysis for damage detection using a membership-set identification method. The two-step sensitivity-based interval model updating technique employed in that study used static displacement measurements across different load cases to identify uncertain stiffness parameters. The intersection of the updated interval stiffness parameter vectors for each load cases resulted in tight bounds on the stiffness parameter estimates. In a subsequent study (Wang et al.,

2013a), measured natural frequencies as well as uncertain acceleration responses were employed for damage detection using the same two-step interval finite element model updating approach with membership-set identification. It was concluded that utilizing more than a single type of measured data (i.e. just static displacements) resulted in higher accuracy of damage identification. Khodaparast et al. (2011) explored the use of a meta-model using the Kriging predictor for model updating, which was implemented successfully for interval model updating of a three degree-of-freedom mass-spring system. However, although the approach presented utilized interval model updating, the approach addresses the field of stochastic model updating, where multiple sets of data from nominally identical structures are employed for identification of parameter variability, instead of identifying uncertain parameters for a single structure. Fang et al. (2015) also presented a stochastic model updating method, which adopted the use of measured eigenvalues as well as eigenvectors. The authors of that study indicated that the proposed interval response surface method (IRSM) provided higher precision than the Kriging predictor and that it was more computationally efficient given that interval arithmetic operations are easily performed on the response surface model. Gabriele and Valente (2009) prescribed modal properties as intervals and model updating was performed using branch and bound processes until the prescribed modal intervals were encompassed by the modal properties of the interval FE model. In an extension of that work, the authors introduced mode shapes within the model correlation through the use of the Modal Assurance Criterion (MAC) (Gabriele, 2011). The exploration of the parameter space was again based on branch and bound techniques, although the authors concluded that the convergence was slow compared to sensitivity-based optimization techniques and the application was limited to a small numerical beam model.

A recent effort has been made to combine both probabilistic and interval methods for damage detection using a modified Metropolis-Hastings algorithm with interval measurements (Biswal and Ramaswamy, 2017). In that study, intervals are created around the parameters sampled by the MH algorithm and then two separate finite element analyses are performed using the lower and upper bounds for the parameters to obtain the lower and upper bounds for the dynamic response of the model. In the process, the Markov chain only moves to a new position if the intersection of the response bounds calculated from the finite element models with the interval measurements is non-empty. Although the method was shown to reduce the computational burden of both the probabilistic and interval-based methods, it still required over 10,000 finite element analysis runs.

The updating procedure in the majority of the existing probabilistic and interval-based model updating techniques relies on global optimization of an objective function that is an amalgamation of natural frequency and mode shape residuals across a number of measured modes and does not guarantee that the modal properties of the updated model are contained within the uncertainty bounds of the experimental measurements. To address this shortcoming, model updating has recently been cast as a constraint satisfaction problem with interval arithmetic and contractor programming to provide the ability to efficiently characterize the set of all feasible solutions to a structured inverse eigenvalue problem capable of solving under-determined and non-unique problems in the presence of measurement uncertainties (Kernicky et al., 2017). In addition to full exploration of the parameter space, the method does not require weighting of correlation residuals, which can have drastic effects on the identification. To date, the method has been numerically verified and experimentally validated using a six degree-of-freedom laboratory shear building model.

This paper introduces adaptations to the aforementioned approach to finite element model updating with interval arithmetic and contractor programming that are necessary to permit the application of the methodology to larger multiple degree-of-freedom (MDOF) system models with larger sets of uncertain parameters. The extension of the methodology produces interval estimates for the uncertain parameters in the form of an interval hull that is guaranteed to enclose the set of all feasible solutions to the structured inverse eigenvalue problem with partially described and incompletely measured eigeninformation pairs corrupted by measurement noise and uncertainty. The methodology is demonstrated for structural identification of a truss using experimental data obtained through hybrid testing. The experiments are then extended to several cases of progressive damage severity at bolt connections to demonstrate the capability of the method to correctly identify the onset, location, and severity of damage in the presence of measurement uncertainties.

6.2 Finite Element Model Updating Using Nonlinear Constraint Satisfaction

In this section, the methodology developed by the authors for structural identification using nonlinear constraint satisfaction in Kernicky et al. (2017) is briefly reviewed and then extensions of the methodology are introduced to facilitate the application to larger multiple degree of freedom system models.

The finite element model updating problem is most commonly applied to multiple degree of freedom system models using the undamped natural frequencies and mode shapes. The generalized eigenvalue problem for undamped linear systems is

$$K\Phi - M\Phi\Omega^2 = 0 \tag{6.1}$$

where M and K are the mass and stiffness matrices, Ω^2 is the diagonal matrix of eigenvalues (ω_n^2, where ω_n are the undamped natural frequencies), and Φ are the corresponding eigenvectors, or mode shapes, represented as columns of the matrix. The ultimate goal of the finite element model updating problem is to solve for a set of parameters within M and K, which are $n \times n$ square matrices, given a set of estimated eigenvalues and eigenvectors obtained through physical testing of the structure. However, most cases of model updating are partially described where only $m < n$ eigenpairs are measured due to bandwidth limitations of the sensing equipment and practical limitations within the system identification of the modal parameters from the vibration test data. In addition, only $s < n$ degrees of freedom of the corresponding numerical model are typically measured in the physical testing, leading to incompletely measured mode shapes. In the context of this partially described eigenvalue problem with incompletely measured modes, the matrix equation can be partitioned as:

$$K_{n\times n}\begin{bmatrix}\Phi^M_{s\times m}\\ \Phi^U_{(n-s)\times m}\end{bmatrix} - M_{n\times n}\begin{bmatrix}\Phi^M_{s\times m}\\ \Phi^U_{(n-s)\times m}\end{bmatrix}\Omega^2_{m\times m} = 0_{n\times m} \tag{6.2}$$

where $\Phi^M_{s\times m}$ are the rows of the measured components of the m measured mode shapes and $\Phi^U_{(n-s)\times m}$ are the rows of the unmeasured components of the same m measured mode shapes. In this study, the structural matrices are explicitly formed through elemental contributions as:

$$\left[K_o + \sum_{j=1}^{N_K}\alpha_j K_j\right]\begin{bmatrix}\Phi^M_{s\times m}\\ \Phi^U_{(n-s)\times m}\end{bmatrix} - M_{n\times n}\begin{bmatrix}\Phi^M_{s\times m}\\ \Phi^U_{(n-s)\times m}\end{bmatrix}\Omega^2_{m\times m} = 0_{n\times m} \tag{6.3}$$

where α_j is a scalar multiplier applied to a basis matrix, K_j, that provides the stiffness

contributions of the j-th member of the model, while K_o represents the contributions of any members in the model not subject to updating. In such a formulation, the unknowns in the inverse eigenvalue problem are the N_K scalar multipliers for the member stiffness contributions subject to updating and the $(n-s)\times m$ unmeasured components of the eigenvectors. Employing interval arithmetic, the constructed stiffness matrix can be developed as an interval matrix, K^I, where the uncertain stiffness scalars in the model are encoded as intervals

$$\alpha = [\underline{\alpha}, \overline{\alpha}] \tag{6.4}$$

where $\underline{\alpha}$ is the lower bound to the interval for the uncertain parameter and $\overline{\alpha}$ is the upper bound. Likewise, the unknown eigenvector components are treated as intervals

$$\Phi^U_{(n-s)\times m} = [\underline{\Phi}^U_{(n-s)\times m}, \overline{\Phi}^U_{(n-s)\times m}] \tag{6.5}$$

In this formulation, intervals are also employed to account for measurement uncertainties by relaxing the measured modal parameters from crisp scalars to intervals centered around the experimental measurements. To do this, each partially described eigenvector, ϕ^M_r, is first scaled to unity maximum amplitude and then an interval is developed around all components except the one with maximum amplitude as:

$$\phi^{I,M}_{i,r} = [\underline{\phi}_{i,r}, \overline{\phi}_{i,r}] = \begin{cases} [\phi^M_{i,r} - \chi_{i,r}, \phi^M_{i,r} + \chi_{i,r}] & \text{if } \phi^M_{i,r} \neq 1 \\ [1, 1] & \text{if } \phi^M_{i,r} = 1 \end{cases} \tag{6.6}$$

where $\chi_{i,r}$ is a specified radius for the intervals. The reason why the component with the maximum amplitude is not relaxed is to establish that component as a reference since the amplitude of an eigenvector is not unique. In a similar manner, the experimentally mea-

sured eigenvalues can be prescribed as intervals:

$$\omega_r^I = [\underline{\omega}_r, \overline{\omega}_r] \tag{6.7}$$

to reflect uncertainty in the experimental estimates of the natural frequencies. Relaxation of the experimental estimates to account for measurement and modeling uncertainties allows for Equation 6.3 to create a set of $n \times m$ constraint equations.

The extent of the relaxation dictates the satisfiability of the constraint equations. If the radius of the intervals is too narrowly prescribed in the presence of measurement and modeling uncertainties, then satisfiability of the constraints will not be met and no solution will be present. Conversely, if the radius is too wide, then the solution space may simply encompass the initial ranges of the uncertain variables. Choosing the extent of relaxation may either be performed iteratively based on the solvability of the constraints or may be determined by a measure of uncertainty in the modal parameter estimates. For the latter case, when multiple sets of modal parameter estimates are available, the radius of relaxation, χ, may be represented by the standard deviation from the mean of each modal parameter estimate, σ.

In the original formulation of this methodology (Kernicky et al., 2017), an additional constraint termed the eigenvalue inclusion constraint was introduced to ensure that the prescribed eigenvalues are contained within the interval eigenvalues of the identified interval stiffness and mass matrices, which can not be ensured solely by the constraint equations in Equation 6.3. For small system models, the inclusion test can be implemented by substituting each of the measured eigenvalues into the characteristic equation formed from the determinant:

$$\left|K^I - (\omega_r^I)^2 M\right| = \left|K_o + \sum_{j=1}^{N_K} [\underline{\alpha}_j, \overline{\alpha}_j] K_j - (\omega_r^I)^2 M\right| = 0 \tag{6.8}$$

6.2.1 Constraint Satisfaction with Interval Arithmetic

A fundamental difference between the developed methodology and most existing approaches for model updating is that, instead of casting the problem as an optimization problem using an objective function or modal measure of fit function, the approach solves for the complete feasible parameter space that satisfies the constraints formed through Equations 6.3 and 6.8. Formally, a constraint satisfaction problem aims to determine all possible solutions for a set of variables, V, in a prescribed domain, D, over a set of constraints, C, through systematic search and constraint propagation (Rossi et al., 2006). Systematic search may be viewed as a branch and bound approach explored as a tree structure, where the root node represents the entire problem. Subsequent nodes of the tree represent subproblems of the root node, which differ in variable assignment. If during evaluation of a node it is determined that there is constraint violation, backtracking is performed to find a new satisfiable assignment and the subtree below the failed node is pruned from the search space. In this way, systematic search improves on the brute force method of trying all possible variable combinations. However, simple backtracking is an "uninformed" approach and is not effective for problems with significant dimensionality. One of the main challenges associated with solving a CSP is improving the performance of the search methods such that local inconsistencies are eliminated. Local inconsistencies are potential partial solutions that satisfy the constraints, but cannot be extended by choosing values for some of the uninstantiated variables. In other words, selecting a value for a uninstanti-

ated variable would cause failure of the node. One method to enforce local consistency is arc consistency, which provides a swift method for constraint propagation (Hyvnen, 1992) that discards values, or combinations of values, if their assignment violates some set of constraints. Eliminating erroneous assignments reduces the size of the search space to be explored by propagating the implications of a constraint on one variable onto the other variables. Combining the processes of systematic search and arc consistency is called Constraint Programming (Dechter, 2003; Rossi et al., 2006; Hentenryck, 1999).

Interval arithmetic may be incorporated into constraint programming so that variables and the relationships among them in the constraint equations are defined as intervals (Alefeld and Claudio, 1998), which provides a natural way to place bounds on numerical rounding errors and measurement uncertainties. Parameters defined as intervals instead of crisp scalars are able to assume any value within the interval. An interval $[x]$ is a subset of the real numbers, $\mathbb{R}$, that can be represented using a pair of real numbers $[\underline{x}, \overline{x}]$ to denote the interval $\underline{x} \leq x \leq \overline{x}$. If the endpoints, $\underline{x}$ and $\overline{x}$, of an interval are equal, the interval is known as *degenerate* and may be represented as a single real number. The Cartesian product of intervals creates an n-dimensional box, or interval vector, that belongs to the set $\mathbb{IR}^n$. This product is defined as

$$[\boldsymbol{x}] = [x_1] \times [x_2] \times \cdots \times [x_n] \tag{6.9}$$

and is illustrated graphically in Figure 6.1 for the product of three intervals.

The objective of the interval constraint programming problem is now to identify all interval vector solutions that satisfy the set of constraint equations within the bounded domains for each set of interval variables. Note that in dealing with continuous domains,

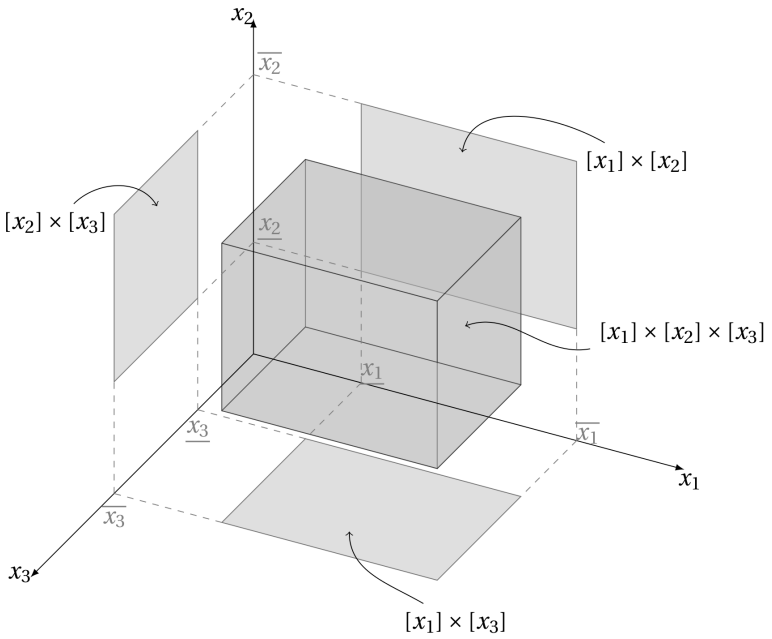


FIGURE 6.1: An interval vector, or box, generated from the product of three intervals

arc consistency cannot be held due to limitations on machine precision so hull consistency (Benhamou et al., 1999) is introduced. Hull consistency may be viewed as a coarse extension of arc consistency that requires arc consistency to only be satisfied at the lower and upper bounds of the interval variable domains. A constraint is hull consistent with respect to a box if, for each bound of the domain of an interval variable, there is a real valued combination of variables satisfying the constraint.

6.2.2 Contractor Programming

A programming method that integrates interval analysis and constraint programming, termed Contractor Programming (Chabert and Jaulin, 2009), has recently been developed to address interval constraint programming problems. Contractors are powerful mathematical operators that take an n-dimensional box as an input and contract the domain according to a set of constraints. The formal definition of a contractor and its properties are defined as

follows (Benhamou and Granvilliers, 1997): *A contractor (Ctc) is a function from Ctc* : $\mathbb{IR}^n \rightarrow \mathbb{IR}^n$*, where* $\mathbb{IR}$ *is interval over reals, with the following properties:*

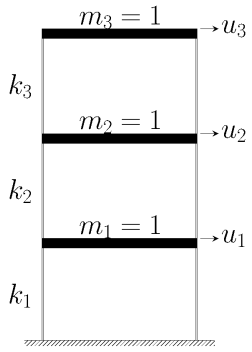
- $\forall[\boldsymbol{x}] \in \mathbb{IR}^n \quad Ctc([\boldsymbol{x}]) \subset [\boldsymbol{x}]$; where $Ctc([\boldsymbol{x}])$ represents box $[\boldsymbol{x}]$ after contraction
- $Ctc([\boldsymbol{x}]) \cap System = [\boldsymbol{x}] \cap System$

The first property guarantees that the algorithm is sound in that the contracted box is a subset of the original, while the second property states that no potential solution is lost after the contraction is performed. Following contraction, the interval vector can be bisected into a subset of smaller boxes and the contractors can be applied to further characterize the solution space.

For the current study, the authors have developed an interface between the MATLAB interactive environment (MATLAB, 2017) and the IBEX C++ 2.1.17 library (Chabert, 1999) to construct and parameterize the structural stiffness and mass matrices, develop mechanics-based constraint equations, pass the formulated CSP to the IBEX solver, and parse the interval vector solutions generated by the contraction algorithm for subsequent analysis. In the following subsection, motivation for casting the updating problem as one of constraint satisfaction is developed though a simple illustrative example. Then, issues with the scalability of the original formulation are addressed through a novel extension of the methodology suitable for application to larger MDOF system models. Finally, application of the methodology to a 45 degree-of-freedom truss model with experimental hybrid testing data is presented to demonstrate its capabilities for vibration-based damage detection.

6.2.3 Illustrative Example on a 3DOF Shear Building Model

As motivation for the methodology presented in this paper, consider the small three degree-of-freedom shear building model with accompanying structural matrices presented in Figure 6.2. For the baseline model, the stiffnesses were assigned as $k_1 = k_2 = k_3 = 1$. The sparsity structure of the elemental contributions to the stiffness matrix from each linear elastic spring are explicitly defined in the structured matrices and constraint equations for the dynamic properties of the structure can be developed using Equations 6.3 and 6.8.



$$M = diag(m_1, m_2, m_3);$$

$$K = 2000 \begin{bmatrix} k_1 + k_2 & -k_2 & 0 \\ -k_2 & k_2 + k_3 & -k_3 \\ 0 & -k_3 & k_3 \end{bmatrix}$$

FIGURE 6.2: Three degree-of-freedom mass-spring model used to demonstrate structural identification using nonlinear constraint satisfaction with interval arithmetic and contractor programming

To add uncertainty to the measurements, 15 sets of synthetic modal parameter estimates with a standard deviation of 0.01 were generated around the natural frequencies and mode shapes derived from the baseline model. Constraint equations were developed with the means and standard deviations of the synthetic measurement data used to prescribe uncertainty in the constraint equations. Similar to the six degree-of-freedom illustration presented in Kernicky et al. (2017), a case with partially described eigenvalues and incompletely measured mode shapes was explored by limiting the eigeninformation to the first two modes of the structure and mode shape measurement to only degrees of free-

dom u_2 and u_3. The search space for the three unknown stiffness parameters was bounded to $k_i \in [0, 3]$, while the search space for the unmeasured mode shape components was bounded to $\phi_{i,j} \in [-10, 10]$. For this example, an interval precision of 0.01 for the uncertain stiffness assignments and the unmeasured mode shape components was assigned as stopping criteria for the solver. The measurement uncertainty applied to the natural frequencies and measured mode shape components was prescribed as $\pm\frac{1}{4}\sigma$. Figure 6.3 displays the fully characterized subpaving of the space as mapped by the IBEX nonlinear constraint satisfaction solver, which identified 2492 feasible interval solutions in two distinct basins in about 5 seconds. It should be noted that all of the solutions found are correct solutions to the inverse eigenvalue problem subject to the partially described, incompletely measured, and noisy eigeninformation. This is illustrated in Figure 6.3, which presents the natural frequencies and mode shapes associated with a representative feasible solution taken from each basin. Both representative feasible solutions correctly reproduce the limited measurements, consisting of the first two natural frequencies and the corresponding mode shapes measured at only the second and third elevations of the structure. Naturally, there are significant differences in the unmeasured modal parameters and it would be difficult to determine which solution is more appropriate and, correspondingly, whether damage is present in the structure. For example, while it can be confidently stated that no significant damage is present in k_3, the same confidence can not be placed on k_1 and k_2 given the uncertainty associated with each parameter. As a consequence of the effect of the limited and uncertain measurement data on the identified parameters, methods for vibration-based damage detection need to not only be capable of providing parameter estimates for damage identification, but also provide information on the confidence that may be placed on the

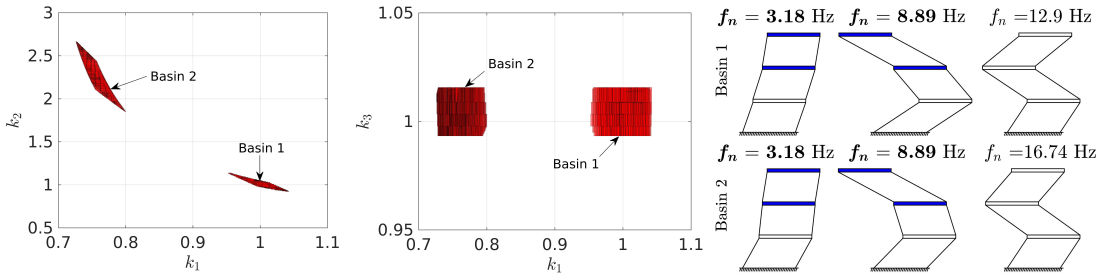


FIGURE 6.3: Subpavings of the feasible parameter space for the inverse eigenvalue problem subject to partially described, incomplete, and uncertain modal parameters of the three degree-of-freedom system (synthetic measurements of natural frequencies and mode shape coordinates highlighted in bold)

identification given the partially described, incomplete, and uncertain measurement data provided.

6.2.4 Issues with Scalability

This approach for fully characterizing the feasible solution space becomes computationally intractable when the dimensionality of the parameter space is significantly increased. Specifically, the boxes of the subpaving tend to accumulate on the boundary due to the amount of bisections required to reach the requested interval precision (Jaulin et al., 2001). Furthermore, the use of the characteristic equation formed through the determinant for the eigenvalue inclusion constraint (Equation 6.8) does not scale to matrices of higher order. This paper contributes two modifications to the original methodology, described in the following subsections, that permit the approach to be extended to larger multiple degree-of-freedom system models.

6.2.4.1 Subpavings vs. Interval Hull

To overcome the issue associated with the computational intractability of subpaving nonlinear problems of large dimensionality, an alternative to subpaving the feasible solution

space through bisection and contraction is introduced. Instead of subpaving, a single interval vector solution, $[\mathbb{X}]$, called the *interval hull* can be computed, which is a pessimistic enclosure that is guaranteed to contain the exact feasible solution, $\mathbb{X}$ (Jaulin et al., 2001). The open-source IBEX C++ library (Chabert, 1999) provides the ability to contract a box to the interval hull, that is the smallest box enclosing all feasible solutions, with respect to a system of linear inequalities. For problems where the constraint equations are necessarily nonlinear, which is the case for the inverse eigenvalue problem with incomplete mode shape measurement, a means of approximately linearizing the system needs to be provided. In this study, the combined relaxation procedure packaged within the IBEX library that combines a corner-based Taylor relaxation (Araya et al., 2012) and an affine arithmetic-based relaxation (Ninin et al., 2015) is utilized. The contractor employed is a composition of the forward-backward contraction through the HC4 algorithm (Benhamou et al., 1999), adaptive constructive interval disjunction (Neveu et al., 2015), and the interval hull contractor, *CtcPolytopeHull*, which calls the linear solver compiled with IBEX (SoPlex (2017) in this case) and calculates lower and upper bounds for each variable:

$$\min_{Ax \leq b \wedge x \in [x]} \{x_i\} \quad and \quad \max_{Ax \leq b \wedge x \in [x]} \{x_i\} \tag{6.10}$$

The relaxed system is then re-evaluated over the reduced domain and further contracted recursively until a prescribed stopping criterion is reached. The criterion chosen in this study is based on the perimeter of the interval vector that defines the interval hull, which is simply the sum of the widths of each interval solution to the uncertain parameters.

Figure 6.4 presents the application of the interval hull to enclose the feasible parame-

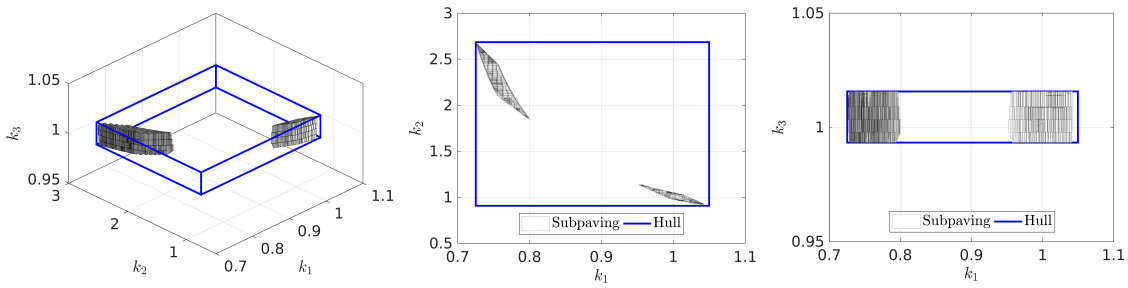


FIGURE 6.4: Illustration of the use of the interval hull to enclose the feasible parameter space as an alternative to subpavings

ter space for the previously described three degree-of-freedom system model with partially described, incompletely measured, and uncertain modal parameter estimates. Comparisons of the interval hull to the subpavings that fully characterize the feasible parameter space reveals that the interval hull provides a complete, although slightly pessimistic, enclosure of the solution basins. In this case, which produced multiple solutions due to the limited data provided, the knowledge of two distinct basins is lost in the interval hull solution. However, the widths of the interval solutions to the uncertain parameters developed through the interval hull still reflect the relative confidence in the estimates of the uncertain parameters, which is sufficient for informing reliable damage detection. For instance, in this case the interval hull contains the expected solution $k_1 = k_2 = k_3 = 1$ so the solution correctly does not suggest damage in any of the stiffnesses. In terms of computational performance, the interval hull was returned in less than a second of computational time for this problem, which is significantly more efficient than the approach of subpaving.

6.2.4.2 Eigenvalue Inclusion Constraint

Since the use of the determinant does not scale to structural systems with larger matrices, an alternative eigenvalue inclusion constraint is developed by leveraging the response

surface methodology (RSM) to create a surrogate model for estimating the interval natural frequencies associated with the interval stiffness and mass matrices of the system model. The RSM has been frequently utilized in prior deterministic and probabilistic model updating studies to replace finite element models with approximations that are generally more computationally efficient for estimating the modal properties of parameterized models than eigenvalue decomposition (Ren and Chen, 2010; Marwala, 2010). Response surface methodology is a mathematical technique used to establish a relationship between responses, y, and associated inputs, x. This relation can be approximated using a polynomial model:

$$y_i = g(x_1, x_2, ..., x_k)\beta + \epsilon \tag{6.11}$$

where $g(\vec{x})$ is a vector consisting of powers and cross-products of unknown input variables, β is a vector of regression coefficients obtained through the response surface mapping, and ϵ is the residual error in the estimate. Typically, either linear or quadratic polynomials are chosen to approximate the relationship between inputs and outputs and interaction terms may be additionally included in these models. For the interested reader, further information about the foundations of response surface methodology can be found in Box and Draper (1987).

In the context of this paper, a response surface is generated from a large set of structural parameters (inputs) and their corresponding responses in the finite element model (output), usually calculated for model updating as the difference between analytical and measured natural frequencies (Ren and Chen, 2010), from which an approximation model is generated by regression. The application of the RSM in this study is used to develop a

relationship between the uncertain member stiffnesses, α, and the corresponding residual error in the natural frequencies of the parameterized model. This equation is represented as,

$$\omega_r - \omega_r^{exp} = g(\alpha_1, \alpha_2, ..., \alpha_k)\beta \in [-\epsilon, \epsilon] \tag{6.12}$$

In this study, a set of 1000 unique scalar combinations of member stiffnesses are generated via Latin Hypercube Sampling to ensure an evenly sampled search space and subsequently mapped to a set of outputs in the form of the difference between the natural frequency of the system model and the average measured natural frequency. Multilinear regression is then performed on the set of stiffness scalar combinations and frequency differences to fit a response surface using a quadratic model with interaction terms using the MATLAB Statistics and Machine Learning Toolbox. The regression coefficients and the root-mean-squared-error (RMSE) are extracted to reformulate the eigenvalue inclusion constraint equations from Equation 6.8 as:

$$\omega_r - \omega_r^{exp} = g(\alpha_1, \alpha_2, ..., \alpha_k)\beta \in [-\sigma_r, \sigma_r] + [-1.96\text{RMSE}_r, 1.96\text{RMSE}_r] \tag{6.13}$$

where $[-1.96\text{RMSE}_r, 1.96\text{RMSE}_r]$ and $[-\sigma_r, \sigma_r]$ are the 95% confidence interval for the response surface estimate and the standard deviation from the mean for the r-th natural frequency, respectively. The 95% confidence interval for the response surface estimate is introduced as a relaxation of the constraint equation to account for the potential error introduced by using the response surface as a surrogate for the exact eigenvalue decomposition of the system model.

6.3 Details of Experimental Program for Validation of the Methodology

Recently, hybrid simulation has been explored as an alternative to full-scale vibration testing for structural health monitoring and damage detection (Kernicky et al., 2016). Hybrid testing provides the benefit of limiting the physical testing to only a portion of the structure, while the remainder is strictly numerical and interacts with the experimental member through a substructured form of the dynamic equation of motion. The interaction between the experimental and analytical substructures is illustrated schematically in Figure 6.5a. This type of testing alleviates the costs associated with full-scale vibration-based damage detection experimentation and, unlike field experimentation where damage is often necessarily simulated through saw cuts or bolt removal, provides a means for faithfully replicating the influence of limit state damage on the dynamic response of the structure. Modeling uncertainties and discretization errors are also alleviated when using hybrid simulation. Consequently, the experiments performed in this paper do not specifically address challenges associated with model and discretization errors in the model updating problem, but rather seek to validate that the methodology is capable of being successfully applied for structural identification and damage detection of well characterized MDOF system models. It should be noted, however, that noise, uncertainties, and nonlinearities are introduced in the hybrid simulation through the experimental measurements obtained from the experimental substructure.

In this paper, hybrid simulation is used to perform vibration testing of a truss model for acquisition of experimental modal analysis data. Between hybrid simulations, realistic damage is progressively introduced in the member of the truss by exceeding a limit

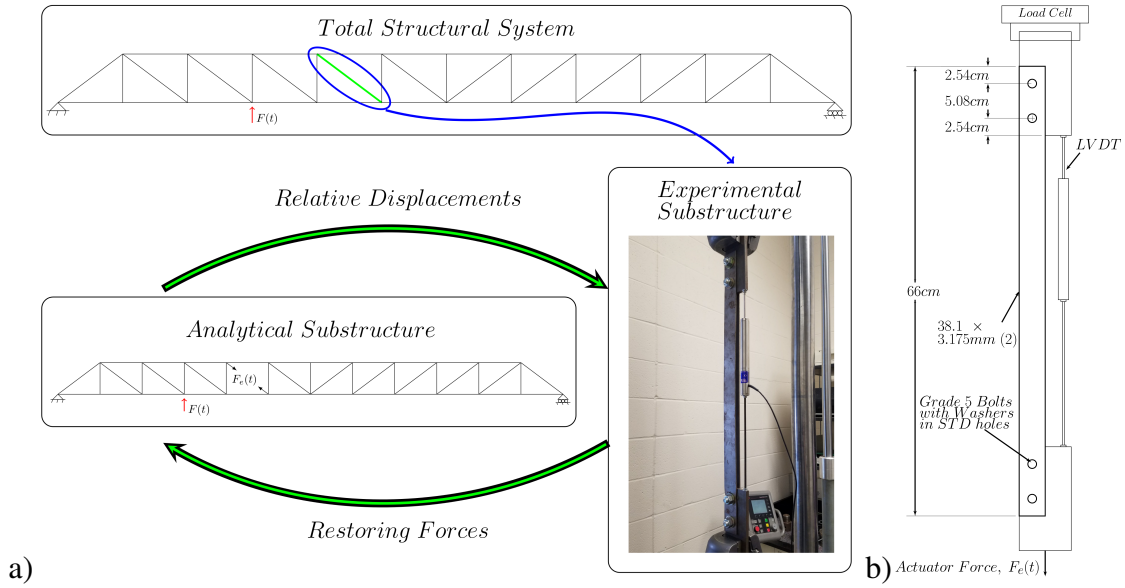


FIGURE 6.5: a) Schematic of the hybrid simulation applied in the current study, b) details of the experimental substructure and instrumentation

state capacity of the experimental substructure. The damage developed in the experimental substructure is the development and progression of fracture cracks at a bolted connection through net section rupture of the experimental member.

6.3.1 Details on the Experimental Substructure and Hybrid Simulation

To demonstrate the application of the extended constraint satisfaction-based approach for structural identification using the interval hull, this study employs data from hybrid testing of a simply supported, 45 member 2D Pratt truss with 45 degrees of freedom, shown in Figure 6.6. All members were modeled as nominally identical A36 steel bars with a gross cross sectional area of 2.42cm^2.

The experimental substructure represented a diagonal member of the truss in each experiment and consisted of two 66cm long steel bars with the same gross cross sectional area. The pair of bars was bolted at each end to a 9.5mm thick steel gusset plate using 1.27cm

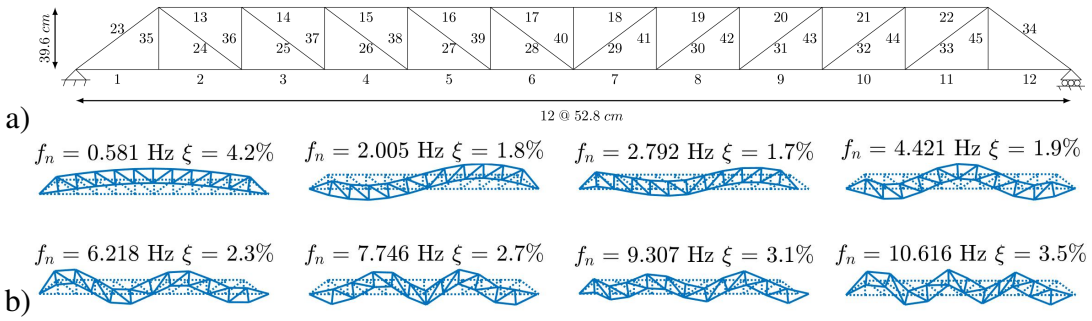


FIGURE 6.6: a) Forty-five degree-of-freedom Pratt truss used in hybrid testing program for structural identification and damage detection, b) First eight natural frequencies and mode shapes of the truss

diameter grade 5 bolts and flat washers (Figure 6.5b). The gusset plates were secured in an MTS 810 universal load testing frame using mechanical wedge grips. Since the mechanical grips displace under changes in load to increase the grip strength, the internal LVDT signal from the load frame could not be utilized for accurate measurement of the specimen elongation. Instead, an RDP Electrosense ACT1000C LVDT was installed between the gusset plates to directly measure the elongation in the experimental substructure. A control loop was established using the LVDT as a feedback signal for strain controlled loading of the experimental substructure that was tuned using the MTS actuator as the control signal. Measurement of the restoring force provided by the experimental member was obtained from the MTS 661.23S-01 load cell on the load frame. Measurements of force and member elongation were acquired with a MTS FlexTest GT controller with Series 493 electronics and were passed to the computer running the hybrid simulation software over a National Instruments X-Series USB data acquisition unit that additionally sent displacement commands to the controller using a 16-bit analog output signal. Within the analytical portion of the structure, all members were idealized with pinned connections and linear-elastic ma-

terial properties, although the hybrid simulation routine accounts for nonlinear geometric effects. The joint masses were scaled and Rayleigh damping was prescribed to generate natural frequencies and damping ratios for the first eight modes of the full structure that are typical for bridges (Figure 6.6b).

The hybrid simulations were conducted using a MATLAB-based pseudo-dynamic implementation developed in-house and verified in Tedeschi (2015). The hybrid simulation framework incorporates nonlinear geometric effects and implements the incremental-iterative implicit integration scheme developed by Mosqueda and Ahmadizadeh (2011). In the framework, the acceleration is initially assumed to be zero and then iteratively corrected to remove unbalanced forces in the system to converge on a state of dynamic equilibrium. The iterative scheme is used to account for nonlinearities and is performed virtually to avoid unintentional plastic deformations of the experimental substructure. The iterations fit the most recent force-displacement measurements using second-order polynomials to simulate the virtual response of the experimental substructure while the displacements are iteratively adjusted. Greater details on the hybrid simulation framework may be found in Mosqueda and Ahmadizadeh (2011).

A total of six experimental vibration tests were conducted for the healthy condition and all subsequent damage conditions of the structure through hybrid simulation. Single shaker excitation was applied in the gravity direction at node 4 for three tests and applied in gravity direction at node 9 for the remaining three tests per condition. A constant force amplitude swept-sine signal was applied over a bandwidth from 0 to 20Hz for a duration of 20 seconds followed by three additional seconds to allow for the free decay response at the end of each test. The amplitude of the applied excitation was scaled such that the stresses in

the experimental substructure remained in the linear elastic range. In addition, the experimental member was preloaded prior to each vibration test to simulate the self-weight of the truss and remained in tension throughout the duration of each test. For all vibration tests conducted, a time step of 0.002 seconds was used for the hybrid simulation, resulting in an effective sampling rate of 500Hz for the measured accelerations.

6.3.2 Damage Prescription and Progression

Following initial vibration testing of the truss with the experimental substructure in the healthy state, the specimen was progressively subjected to static overloading exceeding the limit state capacity to develop cases with increasing extents of damage severity. This overloading was provided through displacement-control loading of the experimental substructure. The force versus elongation response during this overloading is provided in Figure 6.7a to document the relative reduction in load capacity of the experimental substructure for the first two levels of damage. The first stage of loading developed damage in the form of a single crack on one side of a bolt hole (Figure 6.7b), while the second stage loading resulted in development and propagation of the crack on both sides of the hole (Figure 6.7c). For the third damage case, the pair of bars in the experimental substructure consisted of one bar that had completely failed through net section rupture (Figure 6.7d), while the second bar had not yet developed a crack. Consequently, the reductions in stiffness and strength relative to the healthy condition are expected to be 50% for this case.

An additional benefit of the use of hybrid simulation for experimental vibration-based damage detection research is that the measurement of the force-elongation response of the experimental substructure provides a direct, ground truth measurement of the condition

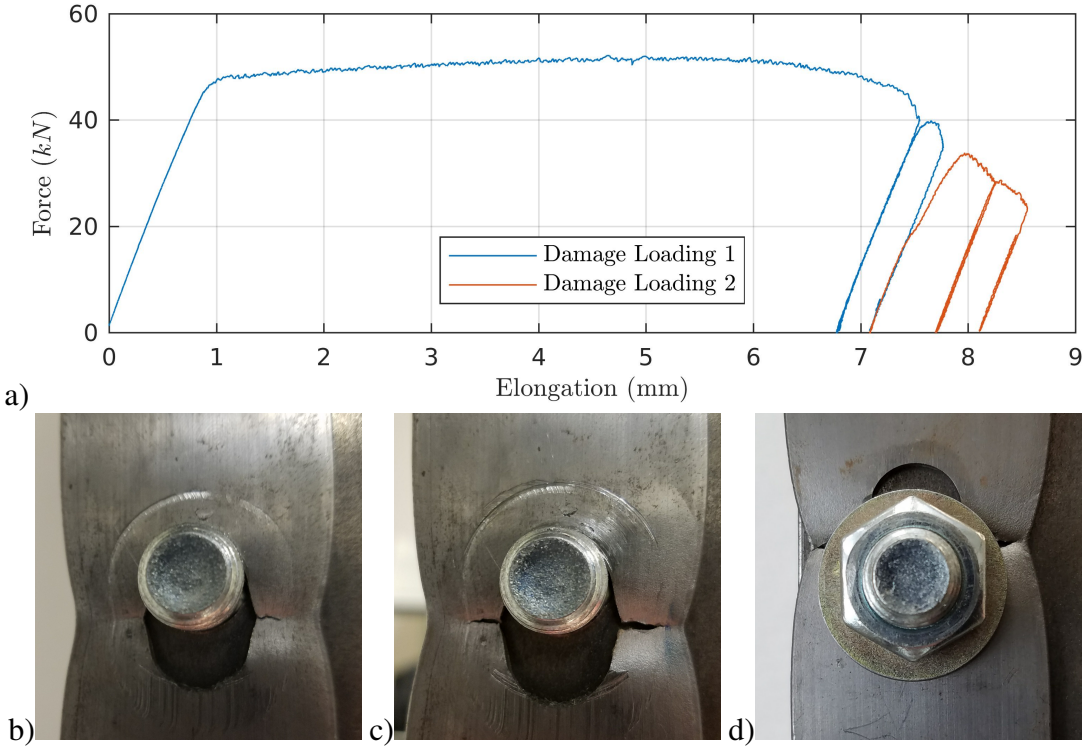


FIGURE 6.7: a) Force-elongation curve for the first two damage scenarios of specimen one, b) crack initiation on one side of a bolt hole (specimen one) , c) cracking on both sides of bolt hole (specimen one), and d) net section rupture of one bar (specimen two)

of the damaged member. Figure 6.8 displays the measured force-elongation response of the experimental substructure acquired during the vibration tests, from which the actual stiffness loss in the experimental member may be estimated. From the change in slope of these responses, it is estimated that the initial damage case resulted in a 7% reduction in the axial stiffness, while the second and third cases produced approximately 12% and 50% reductions, respectively. The hysteresis in the force-elongation response for damage case 3 indicated moderate nonlinearity that is likely a result of slip at the bolted connection for the one bar with complete net section rupture through the cross section.

Since the experimental substructure represented a diagonal member of the truss, it could be used to replace any of the diagonals of the truss in the corresponding analytical model of

the hybrid simulation. This ability of hybrid simulation to place the experimental substructure at different locations within the structure was leveraged to validate the methodology over a larger set of cases. For each state of damage, vibration tests were performed where the experimental substructure represented either member 27 or member 31. For each of these tests, the remaining members of the truss were treated as undamaged, but to include cases with damage to multiple members of the truss, two additional sets of vibration tests were performed. In the first, simulated damage was prescribed in member 5 through a 25% reduction in the member stiffness in the analytical model, while real damage remained in the experimental substructure representing member 27. In the second set, simulated damage was prescribed in both members 8 and 9 through a 25% reduction in the member stiffnesses in the analytical model, while real damage remained in the experimental structure representing member 31. A summary of the damage cases investigated is provided in Table 6.1.

TABLE 6.1: Summary of damage cases investigated (*represents reduction in analytical portion of hybrid test)

Case	Damage Scenario	Experimental Substructure	Relative Stiffness
1	D0 (no damage)	Member 27	$\alpha_{27} \approx 1.00$
2	D1 (small damage)	Member 27	$\alpha_{27} \approx 0.93$
3	D2 (moderate damage)	Member 27	$\alpha_{27} \approx 0.89$
4	D3 (severe damage)	Member 27	$\alpha_{27} \approx 0.51$
5	D4 (severe + simulated* damage)	Member 27	$\alpha_{27} \approx 0.51,\ \alpha_5^* = 0.75$
6	D0 (no damage)	Member 31	$\alpha_{31} \approx 1.00$
7	D1 (small damage)	Member 31	$\alpha_{31} \approx 0.94$
8	D2 (moderate damage)	Member 31	$\alpha_{31} \approx 0.89$
9	D3 (severe damage)	Member 31	$\alpha_{31} \approx 0.48$
10	D4 (severe + simulated* damage)	Member 31	$\alpha_{31} \approx 0.48,\ \alpha_8^* = \alpha_9^* = 0.75$

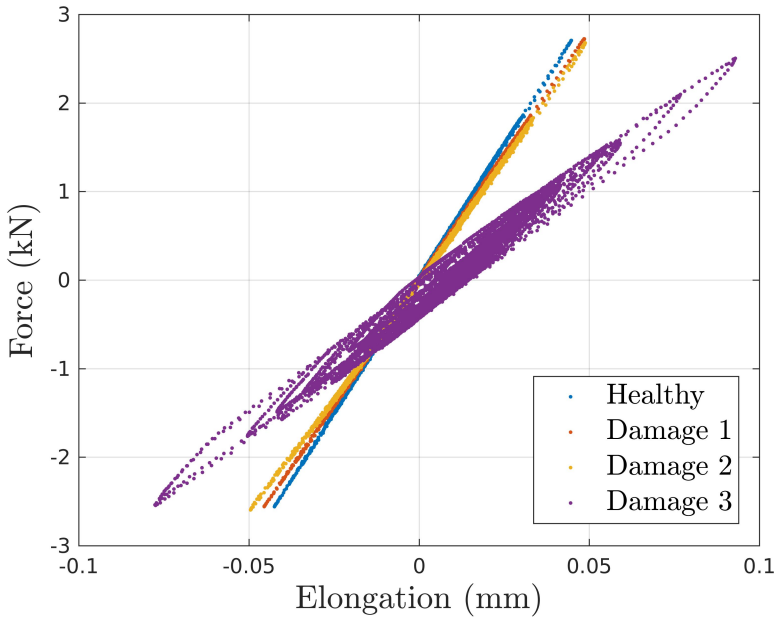


FIGURE 6.8: Force-elongation histories for healthy and damage cases for the experimental substructure

6.3.3 System Identification

Experimental modal parameter estimates were obtained from the time series data acquired in each test using the combined deterministic stochastic subspace state-space system identification algorithm (VanOverschee and DeMoor, 1996). Although the hybrid simulation produces acceleration time histories for all of the degrees of freedom in the truss, only those corresponding to a limited sensor array, described in a subsequent section, were used for the system identification. Experimental modal parameter estimates were calculated across a range of model orders and stabilization plots were developed to identify stable estimates according to frequency, damping, and mode shape criteria. If available, five stable poles per mode were selected from each of the six data sets providing a maximum of 30 poles per mode. The standard deviations, σ, of the collected natural frequencies and mode shape components were used to establish interval assignments around the means of

TABLE 6.2: Comparison between modal parameter estimates of the healthy structure to each damage case where member 27 was the experimental substructure

	Damage 1		Damage 2		Damage 3		Damage 4	
Mode	$\Delta f(\%)$	MAC	$\Delta f(\%)$	MAC	$\Delta f(\%)$	MAC	$\Delta f(\%)$	MAC
1	0.003	1.000	0.005	1.000	-0.064	1.000	-1.024	1.000
2	-0.056	1.000	-0.115	1.000	-0.793	1.000	-1.865	0.999
3	0.000	1.000	-0.002	1.000	-0.029	1.000	-0.150	1.000
4	-0.176	1.000	-0.316	1.000	-2.307	0.996	-2.412	0.996
5	-0.006	1.000	-0.015	1.000	-0.040	1.000	-1.102	0.999
6	-0.138	1.000	-0.291	1.000	-1.829	0.986	-2.403	0.983
7	-0.013	1.000	-0.026	1.000	-0.092	0.998	-0.145	0.996
8	-0.344	0.999	-0.629	0.998	-4.122	0.929	-4.135	0.932

the modal property estimates when formulating the constraint equations.

The changes in modal parameter estimates from the healthy state through each damage scenario are summarized in Tables C.1 and C.4 using the percentage change in natural frequency and modal assurance criterion (MAC). These statistics indicate that the change in global modal properties of the truss with damage is very small, even for the case where one bar has completely failed through net section rupture. Specifically, for the most severe damage scenario, where the stiffness of the experimental substructure is reduced by half in addition to members 8 and 9 being prescribed 25% stiffness reductions in the analytical model, the largest change in natural frequency across the first eight modes is only 3.4% and the lowest MAC is 0.901. The magnitude of changes in modal parameters observed in this experiment are typical of those that have been observed in field tests of structures (Farrar et al., 1994; Alampalli et al., 1997; Brincker et al., 2001a).

6.4 Structural Identification

The application of the proposed approach of using constraint satisfaction with interval arithmetic and the interval hull for structural identification will be presented first for the

TABLE 6.3: Comparison between modal parameter estimates of the healthy structure to each damage case where member 31 was the experimental substructure

	Damage 1		Damage 2		Damage 3		Damage 4	
Mode	$\Delta f(\%)$	MAC	$\Delta f(\%)$	MAC	$\Delta f(\%)$	MAC	$\Delta f(\%)$	MAC
1	-0.004	1.000	-0.025	1.000	-0.145	1.000	-1.732	1.000
2	-0.005	1.000	-0.007	1.000	-0.044	1.000	-1.272	0.998
3	-0.014	1.000	-0.023	1.000	-0.274	0.999	-1.611	0.998
4	-0.182	1.000	-0.331	1.000	-2.541	0.993	-2.844	0.991
5	-0.133	1.000	-0.274	1.000	-1.399	0.992	-1.601	0.989
6	-0.050	1.000	-0.089	1.000	-0.305	0.998	-2.220	0.990
7	-0.076	1.000	-0.122	1.000	-0.564	0.993	-1.187	0.978
8	-0.089	1.000	-0.226	0.998	-1.874	0.888	-3.405	0.901

cases where the experimental substructure is in the healthy, undamaged state. Subsequently, application of the methodology for damage detection of the truss across the damage cases in Table 6.1 will be presented.

6.4.1 Parameter Selection and Sensor Layout

The selection of parameters to include in the model updating routine is of the utmost importance for structural identification as parameters that greatly affect the modal properties should be included, while parameters that have negligible effect should be excluded for the sake of computational efficiency. The selection of parameters is also dependent on the sensor layout, as the uniqueness of the inverse problem depends on the availability of the partially described and incompletely measured modal parameter estimates. Existing methods for parameter selection have often relied on sensitivity analyses and/or sub-structuring to significantly narrow down the set of uncertain parameters to a mere handful of structural properties (Moaveni et al., 2013). In the current study, a sensitivity analysis revealed that the vertical members of the truss had little impact on the first eight natural frequencies and mode shapes. Consequently, the stiffnesses of these members were excluded from

the structural identification, while the remaining horizontal and diagonal members were considered as potential candidates for parameter identification. The final set of uncertain parameters included in the subsequent structural identifications was determined through a parameter identifiability study informed by the sensor layout.

As previously stated, it is impractical/impossible to physically measure all degrees of freedom of a model. In this study, a total of 23 sensor axes were used over the 45 unrestrained degrees of freedom of the truss (Figure 6.9a) to provide incomplete measurement of the mode shapes. Parameter identifiability was assessed using purely analytical modal parameters for the first eight modes, although small uncertainty of ±0.0001 was introduced on the normalized "measured" mode shape components. The extended methodology for structural identification using nonlinear constraint satisfaction with interval arithmetic was applied using the analytical data with an initial search space for each stiffness parameter covering the range of 0.5 to 1.5. Figure 6.9b presents the interval hull solution for the horizontal and diagonal members obtained from the structural identification, which indicates that the available partially described and incompletely measured modal parameter estimates acquired from the sensor configuration are capable of identifying the stiffness of all diagonal members and all but six of the horizontal members. The unidentifiable nature of these parameters, as indicated by the inability of the constraint solver to shrink the domains of these variables, can logically be attributed to the sparsity of the sensor layout around these members. As a result of the parameter identifiability, all verticals and these six horizontal members were excluded from all subsequent identification, and the scalar stiffness multiplier for each of these members, α, was set to one leaving a total of 28 remaining member scalar stiffness assignments as unknown parameters.

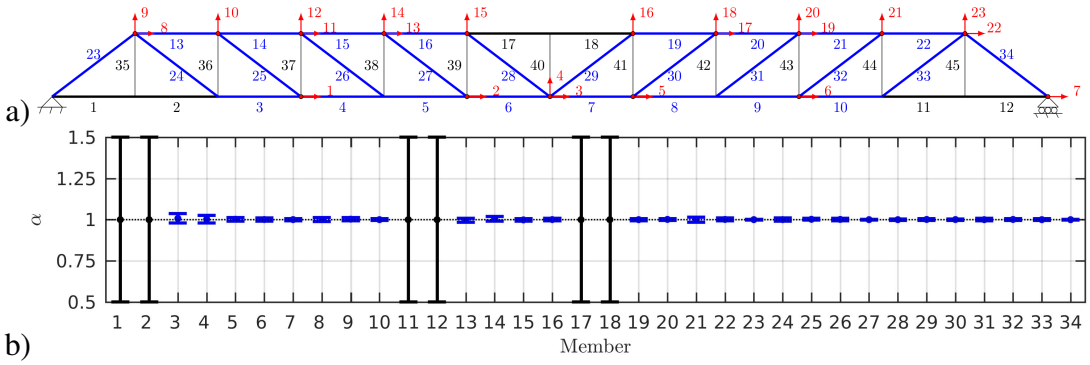


FIGURE 6.9: a) Sensor layout chosen to identify all of the diagonal members of the truss b)Determination of identifiable diagonal and horizontal members based on the interval hull

6.4.2 Identification of the Undamaged Case Using the Interval Hull

The extended methodology of structural identification through nonlinear constraint satisfaction with interval arithmetic was first applied to the experimental modal parameter estimates acquired from the two cases obtained from the healthy structure to validate the approach. For both cases, the eigeninformation was limited to the first eight modes and the 28 aforementioned stiffness scalars were treated as unknowns. However, given the incomplete mode shape measurement, an additional 176 unmeasured components of the mode shapes arise as additional unknowns, creating a 204-dimensional search space. To incorporate measurement uncertainty into the problem, the measured eigenvector components were prescribed as intervals, $[\phi_{i,r}^{avg} - \sigma_{\phi_{i,r}}, \phi_{i,r}^{avg} + \sigma_{\phi_{i,r}}]$ where $\phi_{i,r}^{avg}$ and $\sigma_{\phi_{i,r}}$ are the average and standard deviation of the normalized experimental estimate of the i-th degree of freedom of the r-th mode shape, respectively. However, consistent with Equation 6.6, the component with the maximum amplitude for each mode was prescribed the degenerate interval [1,1] to anchor the eigenvector, since the amplitude of an eigenvector is not unique. In this implementation, the eigenvalues were prescribed exactly as the confidence intervals

for the response surface models for the eigenvalue inclusion constraint exceeded the standard deviation of the individual natural frequency estimates by an order of magnitude. The search space for the unknown stiffness parameters was bounded to $\alpha_k \in [0.25, 1.5]$, where a value of 1 represents no change from the baseline assumption, while the unmeasured components of the mode shape were bounded to $\phi_{j,r} \in [-10, 10]$.

The constraint equations generated by Equations 6.3 and 6.13 using the first 8 natural frequencies and corresponding incomplete mode shapes of the healthy structure were passed to the developed interval hull solver and the domain of the unknown parameters was contracted until the perimeter of the search space, that is the sum of the widths of each interval, changed less that 0.0001 between two consecutive interval hull contractions. Figure 6.10 displays the calculated interval hull obtained for the healthy case where member 27 was represented by the experimental substructure. Although the set of 204 unknown parameters was significantly large, especially with respect to traditional FE model updating techniques, the proposed approach was able to successfully contract the interval hull in approximately 20 minutes of computational time to identify the uncertain stiffness parameters. As illustrated in the figure, each interval solution for the stiffness parameters correctly contains the nominal stiffness of the healthy members associated with α=1. The width of each interval in the hull reflects the confidence in each parameter estimate and is guaranteed to be a complete enclosure, or superset, of the feasible parameter range under the prescribed constraints and measurement uncertainty. The propagation of measurement uncertainties to the parameter domain is reflected in uncertainties in the identified parameters on the order of a few percent. In addition to the uncertain stiffness parameters, the 176 additional unknown eigenvector components were also returned with similarly narrow

intervals.

To verify the solution, the upper and lower bounds of the identified stiffness parameters were used to construct an interval stiffness matrix for the structure and the approach in Modares et al. (2006) was utilized to determine the interval natural frequencies of the identified model. Table 6.4 presents these interval natural frequencies, which confirms that the identified model constructed by the interval hull correctly encompasses the eight prescribed natural frequencies associated with the healthy model. Most of the interval natural frequencies are centered about the experimental estimates and the width of all the intervals are within 1% of the experimental values. Similar results were obtained when the undamaged experimental substructure was used to represent member 31 of the truss (Figure 6.11).

TABLE 6.4: Comparison between experimental natural frequencies and interval natural frequencies of the identified model for case 1

Mode	f_{exp}	$[\underline{f}, \overline{f}]$	$[\Delta\underline{f}(\%), \Delta\overline{f}(\%)]$
1	0.581	[0.577, 0.584]	[-0.803, 0.531]
2	2.005	[1.991, 2.017]	[-0.685, 0.622]
3	2.792	[2.777, 2.805]	[-0.519, 0.485]
4	4.421	[4.393, 4.448]	[-0.634, 0.599]
5	6.218	[6.180, 6.255]	[-0.614, 0.595]
6	7.746	[7.716, 7.777]	[-0.391, 0.399]
7	9.307	[9.262, 9.357]	[-0.482, 0.529]
8	10.616	[10.553, 10.687]	[-0.587, 0.671]

6.4.3 Identification of the Damaged Cases Using the Interval Hull

To demonstrate the capabilities of the proposed method for damage detection applications, the same methodology applied in the identification of the undamaged cases was applied to the data sets acquired for the remaining eight damaged cases in Table 6.1. The

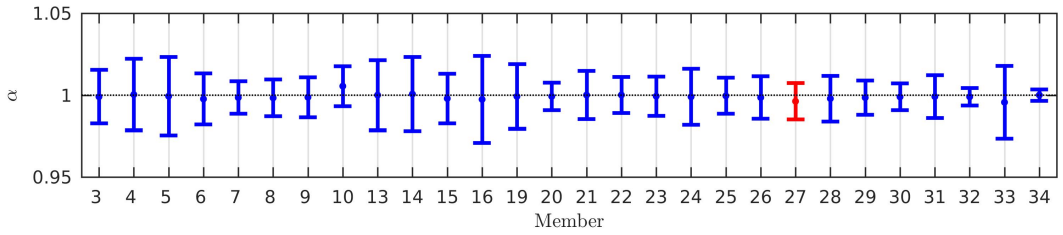


FIGURE 6.10: Interval hull solution for the stiffness scalars with member 27 as the experimental substructure and tested in the healthy condition

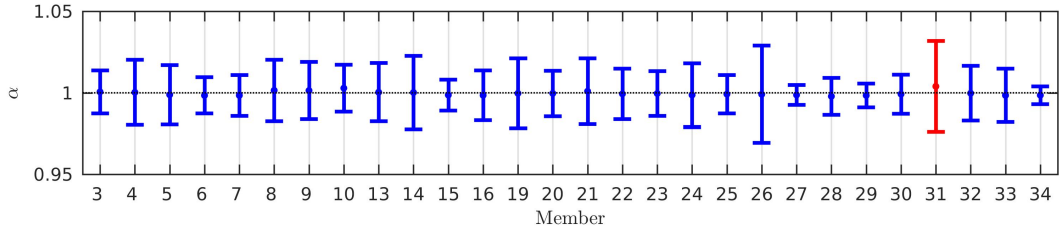


FIGURE 6.11: Interval hull solutions for the stiffness scalars with member 31 as the experimental substructure and in the healthy condition

constraint equations generated by Equations 6.3 and 6.13 were generated with the experimental modal parameter estimates for each case and passed to the developed interval hull solver. As in the prior analysis, the domain of the resulting 207 unknown parameters was contracted until the perimeter of the search space changed less that 0.0001 between two consecutive interval hull contractions. Figure 6.12 displays the solutions for the interval hulls for the damaged cases where the experimental substructure represented member 27 of the truss. In all cases of damage, the proposed method clearly and correctly identifies member 27 as the damaged element. In addition, Table 6.5 presents the interval solutions for the scalar stiffness parameter of member 27, which shows that the identified extent of damage agrees well with the expected stiffness loss calculated by the change in slope of the force-elongation responses of the experimental substructure. It should also be noted that it can be stated with certainty that there is a loss of stiffness in the experimental sub-

TABLE 6.5: Comparison between expected stiffness parameter estimates to those identified by the interval hull for both experimental substructures and all damage cases (* represents the cases with significant nonlinearity in the force-elongation response)

Member 27	Expected α	Identified α	Member 31	Expected α	Identified α
Healthy	1.000	[0.985, 1.007]	Healthy	1.000	[0.976, 1.032]
Damage 1	0.935	[0.925, 0.948]	Damage 1	0.937	[0.921, 0.966]
Damage 2	0.887	[0.877, 0.905]	Damage 2	0.886	[0.848, 0.937]
Damage 3	0.509*	[0.496, 0.568]	Damage 3	0.483*	[0.556, 0.587]
Damage 4	0.509*	[0.530, 0.570]	Damage 4	0.483*	[0.481, 0.600]

structure since $\alpha = 1$ is not an element of the identified intervals. Additionally, Figure 6.12 illustrates that, even when the uncertainty in the identified stiffness parameters for the undamaged members increases to the damage 3 severity due to the significant nonlinearity in the damaged experimental substructure (Figure 6.12c), it cannot be stated with certainty that the stiffness of the undamaged elements has changed since $\alpha = 1$ is a member of the identified intervals for those parameters. Furthermore, the means of the identified intervals for the stiffness of the undamaged parameters are nearly centered around one. For case 5, where the stiffness of element 5 was decreased by 25% in the analytical portion of the structure, the proposed approach correctly identified the severity of damage for both elements 5 and 27 of the truss (Figure 6.12d).

Results for the cases where the experimental substructure represented member 31 of the truss are presented in Figure 6.13 and Table 6.5. As in the prior cases, the interval hull solutions in all four damage cases clearly and correctly identify the damaged element. However, for damage case 9, where only member 31 is damaged, it cannot be stated with certainty that no other members are damaged. As illustrated in Figure 6.13c, the identified interval solutions for the stiffness of members 8 and 9 do not contain $\alpha = 1$, which lies just outside of the intervals. In this case, since members 8 and 9 are connected to the dam-

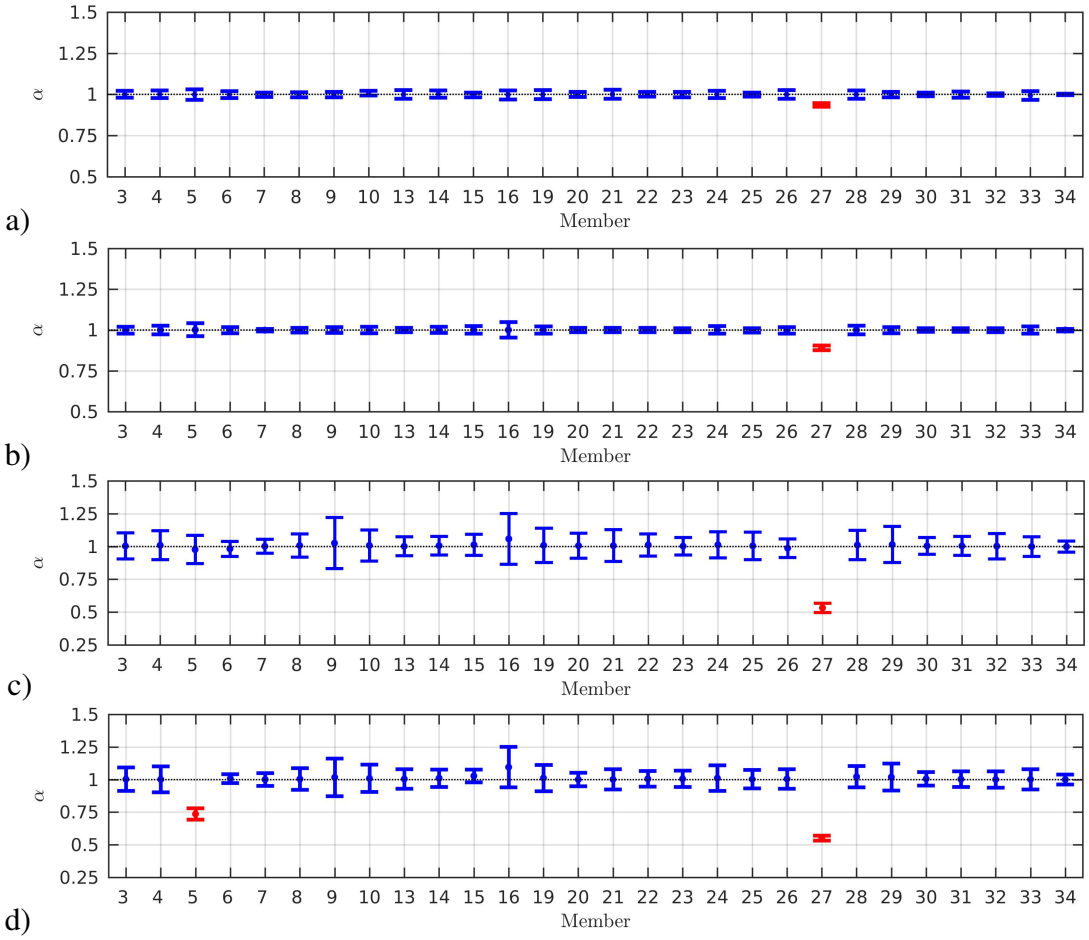


FIGURE 6.12: Interval hull solutions for the stiffness scalars with the experimental substructure representing member 27 a) damage case D1, b) damage case D2, c) damage case D3, and d) damage case D4, where member 5 was subjected to a 25% stiffness reduction in the analytical model

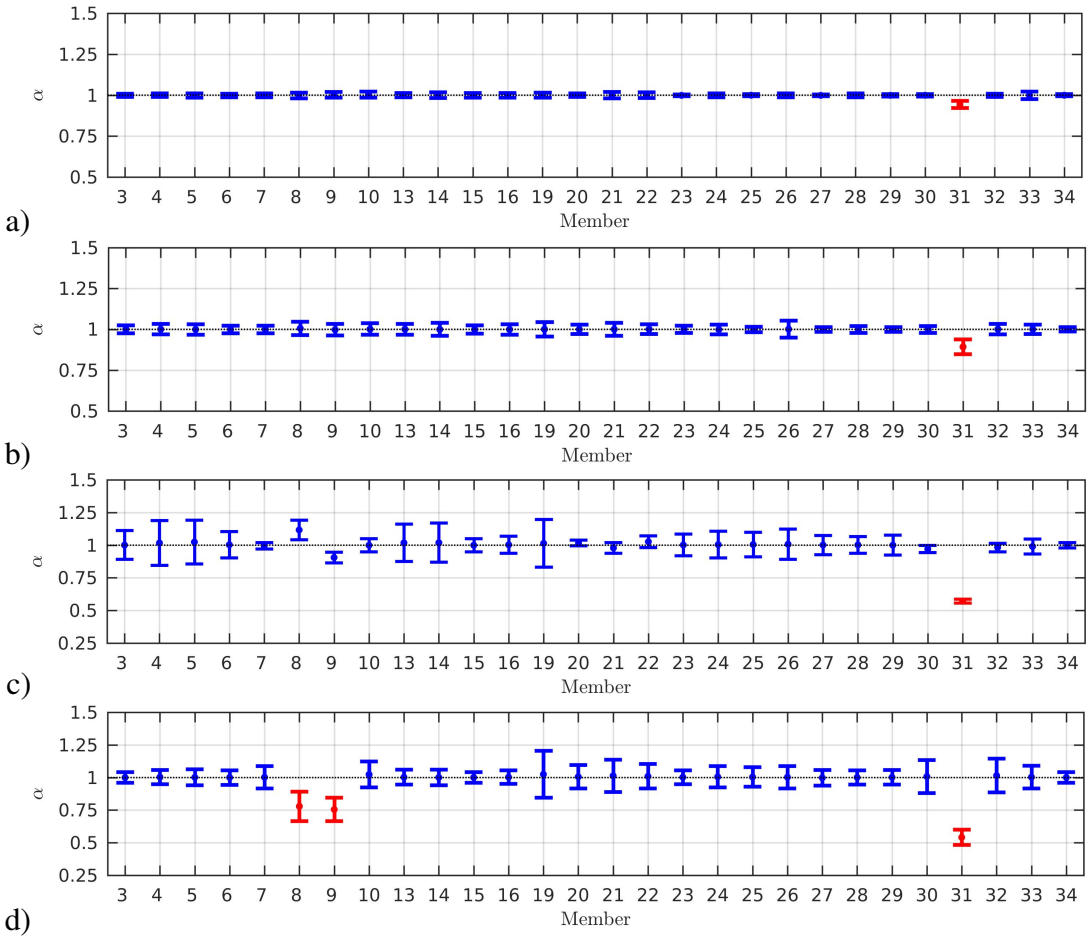


FIGURE 6.13: Interval hull solutions for the stiffness scalars with the experimental substructure representing member31 a) damage case D1, b) damage case D2, c) damage case D3, and d) damage case D4, where members 8 and 9 were subjected to 25% stiffness reductions in the analytical model

aged experimental substructure and no measurement sensor is located at the node where members 8, 9, and 31 connect, the severity of the damage leads to a false positive identification of very minor damage in these connected elements. For case 10, where elements 8 and 9 were artificially subjected to 25% losses in stiffness in addition to the experimentally damaged member 31, the proposed approach clearly and correctly identified the location and severity of damage, while providing no misidentification of undamaged elements as damaged.

6.5 Conclusion

Extensions of a newly developed method for structural identification using nonlinear constraint satisfaction with interval arithmetic has been presented to permit the approach to be applied to larger MDOF system models. The basis of the extended formulation relies on foregoing computation of a complete set of feasible solutions and instead contracts the search domain to the interval hull, which encompasses the complete set of feasible solutions with a single interval vector solution. The use of interval analysis in the methodology has been leveraged to account for measurement and model uncertainties. In addition, a response surface model was introduced to allow for enforcement of an eigenvalue inclusion constraint equation while still enabling interval contraction over the constraint equations.

Hybrid simulation was utilized for acquisition of vibration data from both healthy and damaged states of a planar truss structure subjected to realistic structural damage. In this paper, a two-bar specimen with bolted connection representing a single member of the truss served as the experimental substructure. Multiple sets of vibration data were acquired for each damage state from which the standard deviations about the means of the modal parameter estimates were used to establish interval assignments in the constraint equations. Application of the methodology to data from the undamaged structure demonstrated the ability of the constraint satisfaction approach to identify the subset of identifiable parameters in the model subject to the measurement data and validated that the response surface methodology introduced into the eigenvalue inclusion constraint correctly constrained the interval hull solutions to enclose the measured natural frequencies. In addition to correctly identifying the uncertain stiffness parameters in the undamaged case, the proposed methodology

provided accurate damage identification for all cases of severity without misidentifying undamaged members as damaged, except in a single case where the two members directly connected to the severely damaged member were identified as having minor changes in stiffness.

Acknowledgement

This material is based upon work supported by the National Science Foundation under Grant No. 1331825. Any opinions, findings, conclusions, or recommendations expressed in the material are those of the authors and do not necessarily reflect the views of the sponsor.

CHAPTER 7: CONCLUSION

7.1 Summary and Concluding Remarks

The methodologies presented within this dissertation provide novel techniques for structural identification that are an attractive alternative to traditional forms of model updating that address many of the challenges and limitations of those techniques by leveraging interval arithmetic and contractor programming by casting the structural identification problem as one of constraint satisfaction. A concise overview of some of the most widely used techniques for finite element model updating was presented with illustrative application to a small three degree-of-freedom system model to highlight the advantages and limitations of each method. While each of the successive techniques presented were shown to partially address challenges remaining in the prior methods, none were able to completely account for modeling and measurement uncertainties or were capable of determining the set of all feasible solutions to the partially described and incompletely measured inverse eigenvalue problem. In order to cast the structural identification problem as one of constraint satisfaction, a brief introduction to interval arithmetic and interval-based methods for set inversion was presented followed by the foundations of constraint and contractor programming necessary for understanding the methodologies developed within this dissertation.

The first methodology developed in this dissertation provides a framework for determining the set of all feasible solutions to the inverse problem of identifying the internal

axial force and boundary restraints within in-service prismatic beam elements such as short cables, struts, bracing, and tie-rods using vibration measurements. In the developed approach, a continuous system model based on Timoshenko beam theory was used as the analytical model to allow for application to weakly coupled axial force members with any non-dimensional bending stiffness. As an alternative to conventional optimization techniques, this challenging inverse problem was solved using application of the Set Inversion Via Interval Analysis (SIVIA) algorithm. The framework uniquely allows for propagation of measurement uncertainties to the parameter space and offers the ability to completely enclose the feasible solution space for the unknown axial force and boundary restraints using a set of natural frequencies obtained from measurements of a single transducer. This unique ability to propagate the measurement uncertainty into the parameter space is necessary for quantifying the confidence in the parameter estimates, which better informs decision making for structural health diagnosis and prognostication applications. In addition to possessing the capability of completely mapping the solution space, the framework presented does not make assumptions or approximations in the formulation of the constraint equations and is therefore applicable to structural members with any degree of non-dimensional bending stiffness. The methodology was first demonstrated and verified with numerical models and subsequently validated using datasets obtained from an experimental steel rod with a prescribed axial load and progressively increased fixity at one end of the rod. The results successfully identified the progression of rotational restraint in one end of the rod without misidentifying changes in the end restraint in the other end.

A second methodology was developed using contractor programming with interval arithmetic to completely map all feasible solutions to both well- and ill-posed constructions of

the structured inverse eigenvalue problem for multiple degree-of-freedom models. The methodology was demonstrated to provide unique capabilities that offer significant advantages over optimization-based techniques and probabilistic methods for model updating. The formulation develops coupled nonlinear constraint equations over a bounded search space that lend to the natural inclusion of measurement uncertainty through the use of intervals, which is necessary for the quantification of uncertainty in the parameter assignments and allows for exploration of alternative solutions other than the global optimal solution. Through relaxation of the constraints, the sensitivity of the parameter estimates to the measurement data is reflected in the subpaved feasible solution space to provide confidence measurements for the parameter estimates and can offer the ability to expose alternative solutions residing in local minima. The methodology was first demonstrated and verified on a numerical six degree-of-freedom mass-spring system model followed by an experimental application to a laboratory six story aluminum shear building designed such that it permits for multiple solutions to be generated. Experimental modal analysis through vibration-based testing and subsequent system identification was employed to identify the modal properties of the structure. Interval representations of the acquired natural frequencies and mode shapes were then utilized to develop a set of relaxed constraint equations. Instead of the traditional approach of solving the forward eigenvalue problem and then calculating the correlation between the analytical and experimental modal properties to drive an optimization, the problem was formulated using matrix-based constraints coupled with additional mechanics-based constraints over a bounded search space. The approach demonstrated the capability to map the entire feasible solution space for the stiffness parameters in the model, which is not possible through existing techniques for model updating. In

addition, propagating measurement uncertainty into the parameter space allowed for the involvement of "human-in-the-loop" practitioner heuristics for evaluation of alternative solutions other than the global minimum, which may better represent the actual behavior of in-service structures. Furthermore, despite the limited measurement data provided in the ill-posed construction of the inverse eigenvalue problem, the results indicated that certain parameters were identified exactly, which may lay the foundation for future work on selective sensor placement strategies to target certain substructures for structural identification and damage detection using space sensor configurations.

Extensions of this methodology were then introduced to permit scaling the constraint satisfaction approach to structural identification of larger multiple degree-of-freedom system models. Due to the dramatic increase in dimensionality of the problem due to significantly more uncertain parameters and unmeasured components of the mode shapes, the basis of the formulation relied on foregoing computation of the complete set of feasible solutions and instead contracting the search domain to the interval hull that encompasses the complete set with a single interval vector solution. In addition, response surface methodology was utilized to generate eigenvalue inclusion constraint equations capable of ensuring that the resulting interval hull yields natural frequencies that are a product of the forward problem. Despite the modification of the original formulation, the use of interval arithmetic can still be leveraged to account for measurement and model uncertainties and the effect of these uncertainties is reflected in the confidence of the resulting parameter estimates. To demonstrate and experimentally validate the methodology, hybrid testing was utilized to acquire vibration data from both healthy and damaged states of a 45 degree-of-freedom planar truss structure subjected to realistic structural damage. In this study, a two-bar spec-

imen with bolted connections representing a single diagonal member of the truss served as the experimental substructure and real limit state damage was introduced in the form of onset and propagation of net section rupture through overloading of the member. Multiple sets of vibration data were acquired for each damage state from which the standard deviations about the means of the modal parameters were used to establish interval assignments in the constraint equations. The extended methodology was shown to be capable of providing correct solutions to the structural identification in each case and was proven capable of detecting, locating, and quantifying various degrees of structural damage, including in cases with multiple damaged members.

7.2 Recommendations for Future Work

Recommendations for future work that would further advance the methodologies developed and studies performed in this dissertation are itemized below.

- *Application to more case studies* - As with any new method for structural identification, more case studies are needed to strengthen the library of successful applications of the method. Specifically, application to larger multiple degree-of-freedom system models and a greater diversity of structural configurations would provide more insight into the practical limitations and application opportunities suitable for real-world deployment of the developed methodologies. Additionally, the methodology in Chapter 4 was experimentally validated with only identification of rotational end restraints due to practical challenges in the controlled laboratory experimentation. The development and application of laboratory experiments to apply the methodology for damage detection with identification of both rotational and translational end

restraints would enhance the validation of the complete formulation.

- *Examining alternative sensor placement strategies* - As noted in Chapter 2, the number of sensors deployed for vibration-based testing is often limited. In addition, the performance of structural identification is affected by not only the number of degrees of freedom measured, but also by sensor placement. In Chapter 6, the sensor placement utilized was chosen such that the number of sensors was minimized while still being able to identify the members of interest in the parameter identification. While the sensor layout was informed through analysis of a large number of potential configurations, brute force evaluation of all potential combinations was prohibited by the associated computational time required for the analysis. The development of prescriptive methodologies to inform sensor placement for constraint satisfaction-based approaches is recommended to support the adoption and use of the techniques in future studies.

- *Exploration of targeted damage detection of limited substructures* - The results for the formulations of the inverse eigenvalue problem developed in Chapter 4 demonstrate the ability of the methodology to solve ill-posed formulations of the model updating problem. In the solutions to the ill-posed formulations, some of the uncertain parameters were shown to be unidentifiable due to the limited eigeninformation provided, but other parameters remained identifiable despite the ill-posed nature of the formulation. This unique capability of the developed methodology to solve ill-posed formations of the partially described and incompletely measured inverse eigenvalue problem could be exploited to perform structural health monitoring and damage de-

tection on targeted substructures of more complex structural systems using sparse sensor arrays. Further research is needed to understand how the sensor placement can be used to target specific substructures and to investigate if such capabilities can be scaled to larger and more complex system models.

- *Parallelizing contraction process* - The version of the IBEX C++ library utilized in this work was limited to single core computations. Parallelization of the solver, while technically possible by running the solver on different sub-boxes of the initial, does not guarantee improved computational efficiency. As such, techniques to improve computational efficiency need to be explored so that problems with high dimensionality may be efficiently addressed.

REFERENCES

Adam, S., Karras, D., Magoulas, G., and Vrahatis, M. (2015). Reliable estimation of a neural networks domain of validity through interval analysis based inversion. In *International Joint Conference on Neural Networks*.

Ahmadian, H., Gladwell, G. M. L., and Ismail, F. (1997). Parameter selection strategies in finite element model updating. *Journal of Vibration and Acoustics*, 119:37–45.

Aktan, A. and Brownjohn, J. (2013). Structural identification: opportunities and challenges. *Journal of Structural Engineering*, 139:1639–1647.

Aktan, A., Catbas, N., Trer, A., and Zhang, Z. (1998a). Structural identification: Analytical aspects. *Journal of Structural Engineering*, 124:817–829.

Aktan, A. E., Farhey, D. N., Helmicki, A. J., Brown, D. L., Hunt, V. J., Lee, K.-L., and Levi, A. (1997). Structural identification for condition assessment: Experimental arts. *Journal of Structural Engineering*, 123:1674–1684.

Aktan, A. E., Helmicki, A. J., and Hunt, V. J. (1998b). Issues in health monitoring for intelligent infrastructure. *Smart Materials and Structures*, 7(5):674.

Alampalli, S., Fu, G., and Dillon, E. W. (1997). Signal versus noise in damage detection by experimental modal analysis. *Journal of Structural Engineering*, 123(2):237–245.

Alefeld, G. and Claudio, D. (1998). The basic properties of interval arithmetic, its software realizations and some applications. *Computers & Structures*, 67(1):3–8.

Allemang, A. J. (2003). The modal assurance criterion (mac): Twenty years of use and abuse. *Sound Vib*, pages 14–21.

Amabili, M., Carra, S., Collini, L., Garziera, R., and Panno, A. (2010). Estimation of tensile force in tie-rods using a frequency-based identification method. *Journal of Sound and Vibration*, 329:2057.

Araya, I., Trombettoni, G., and Neveu, B. (2012). *A Contractor Based on Convex Interval Taylor*, pages 1–16. Springer Berlin Heidelberg, Berlin, Heidelberg.

ASCE (2017). *2013 Report Card for America's Infrastructure*. American Society of Civil Engineers.

ASCE-SEI (2011). *Structural Identification (St-Id) of Constructed Facilities*. ASCE-SEI.

Avitabile, P. and O'Callahan, J. (2003). Frequency response function expansion for unmeasured translation and rotation dofs for impedance modelling applications. *Mechanical systems and signal processing*, 17(4):723–745.

Bagnariol, D., Tharmabala, B., and Peltier, B. (2003). Sgt. Aubrey Cosens V.C. Memorial Bridge over the Montreal River at Latchford: investigation of failure: final report. Technical report, Ontario Ministry of Transportation.

Bakir, P., Reynders, E., and Roeck, G. D. (2008). An improved finite element model updating method by the global optimization technique coupled local minimizers. *Computers and Structures*, 86:1339–1352.

Bansal, S. (2015). A new gibbs sampling based bayesian model updating approach using modal data from multiple setups. *International Journal for Uncertainty Quantification*, 5(4):361–374.

Baruch, M. (1978). Optimization procedure to correct stiffness and flexibility matrices using vibration tests. *AIAA Journal*, 16:1208–1210.

Beck, J. L. and Au, S.-K. (2002). Bayesian updating of structural models and reliability using markov chain monte carlo simulation. *Journal of Engineering Mechanics*, 128:380–391.

Beck, J. L. and Katafygiotis, L. S. (1998). Updating models and their uncertainties. I: Bayesian statistical framework. *Journal of Engineering Mechanics*, 124(4):455–461.

Behmanesh, I., Moaveni, B., Lombaert, G., and Papadimitriou, C. (2015). Hierarchical bayesian model updating for structural identification. *Mechanical Systems and Signal Processing*, 64-65(Supplement C):360 – 376.

Behmanesh, I., Moaveni, B., and Papadimitriou, C. (2017). Probabilistic damage identification of a designed 9-story building using modal data in the presence of modeling errors. *Engineering Structures*, 131:542 – 552.

Benhamou, F., Goualard, F., Granvilliers, L., and Puget, J.-F. (1999). Revising hull and box consistency. In *Logic Programming: Proceedings of the 1999 International Conference on Logic Programming*, page 230. MIT press.

Benhamou, F. and Granvilliers, L. (1997). Automatic generation of numerical redundancies for non-linear constraint solving. *Reliable Computing*, 3(3):335–344.

Biswal, S. and Ramaswamy, A. (2017). Damage identification in concrete structures with uncertain but bounded measurements. *Structural Health Monitoring*, 16(6):649–662.

Boscato, G., Russo, S., Ceravolo, R., and Fragonara, L. Z. (2015). Global sensitivity-based model updating for heritage structures. *Computer-Aided Civil and Infrastructure Engineering*, 30(8):620–635.

Boulkabeit, I., Mthembu, L., Marwala, T., and de Lima Neto, F. B. (2013). Finite element model updating using fish school search optimization method. *CoRR*, abs/1308.2307.

Box, G. and Draper, N. (1987). *Empirical Model-Building and Response Surfaces*. Wiley.

Braems, I., Berthier, F., Jaulin, L., Kieffer, M., and Walter, E. (2000). Guaranteed estimation of electrochemical parameters by set inversion using interval analysis. *Journal of Electroanalytical Chemistry*, 495:1–9.

Brandt, A. (2011). *Noise and Vibration Analysis: Signal Analysis and Experimental Procedures*. John Wiley & Sons, Ltd.

Brincker, R., Andersen, P., and Cantieni, R. (2001a). Identification and level i damage detection of the Z24 highway bridge. *Experimental Techniques*, 25(6):51–57.

Brincker, R., Zhang, L., and Andersen, P. (2001b). Modal identification of output-only systems using frequency domain decomposition. *Smart Materials and Structures*, 10(3):441.

Brownjohn, J., Xia, P.-Q., Hao, H., and Xia, Y. (2001). Civil structure condition assessment by fe model updating methodology and case studies. *Finite Elements in Analysis and Design*, 37:761–775.

Brownjohn, J. M. W., De Stefano, A., Xu, Y.-L., Wenzel, H., and Aktan, A. E. (2011). Vibration-based monitoring of civil infrastructure: challenges and successes. *Journal of Civil Structural Health Monitoring*, 1(3):79–95.

Brownjohn, J. M. W., Moyo, P., Omenzetter, P., and Lu, Y. (2003). Assessment of highway bridge upgrading by dynamic testing and finite-element model updating. *Journal of Bridge Engineering*, 8:162–172.

Brownjohn, J. M. W. and Xia, P.-Q. (2000). Dynamic assessment of curved cable-stayed bridge by model updating. *Journal of Structural Engineering*, 126:252–260.

Caicedo, J. M. and Yun, G. (2011). A novel evolutionary algorithm for identifying multiple alternative solutions. *Structural Health Monitoring*, 10:491–501.

Carvalho, J., Datta, B. N., Gupta, A., and Lagadapati, M. (2007). A direct method for model updating with incomplete measured data and without spurious modes. *Mechanical Systems and Signal Processing*, 21(7):2715–2731.

Catbas, F., Kijewski-Correa, T., and Aktan, A. (2013). *Structural identification of constructed systems*. Reston(VI): American Society of Civil Engineers.

Catbas, F. N. and Aktan, A. E. (2002). Condition and damage assessment: Issues and some promising indices. *Journal of Structural Engineering*, pages 1026–1036.

Catbas, F. N., Ciloglu, S. K., Hasancebi, O., Grimmelsman, K., and Aktan, A. E. (2007). Limitations in structural identification of large constructed structures. *Journal of Structural Engineering*, 133:1051–1066.

Cauberghe, B. (2004). *Applied Frequency-Domain System Identification in the Field of Experimental and Operational Modal Analysis*. PhD thesis, Vrije Universiteit Brussel.

Cawley, P. and Adams, R. D. (1979). The location of defects in structures from measurements of natural frequency. *Journal of Strain Analysis*, pages 49–57.

Ceballos, M. and Prato, C. (2008). Determination of the axial force on stay cables accounting for their bending stiffness and rotational end restraints by free vibration tests. *Journal of Sound and Vibration*, 317:127–141.

Chabert, G. (1999). IBEX C++ library for constraint processing over real numbers.

Chabert, G. and Jaulin, L. (2009). Contractor programming. *Artificial Intelligence*, 173(11):1079–1100.

Cheung, S. H. and Bansal, S. (2017). A new gibbs sampling based algorithm for bayesian model updating with incomplete complex modal data. *Mechanical Systems and Signal Processing*, 92(Supplement C):156 – 172.

Ching, J. and Chen, Y.-C. (2007). Transitional markov chain monte carlo method for bayesian model updating, model class selection, and model averaging. *Journal of Engineering Mechanics*, 133(7):816–832.

Ching, J., Muto, M., and Beck, J. L. (2006). Structural model updating and health monitoring with incomplete modal data using gibbs sampler. *Computer-Aided Civil and Infrastructure Engineering*, 21(4):242–257.

Chou, J.-H. and Ghaboussi, J. (2001). Genetic algorithm in structural damage detection. *Computers and Structures*, pages 1335–1353.

Chu, M. and Golub, G. (2005). *Inverse Eigenvalue Problems: Theory, Algorithms, and Applications*.

Collavizza, H., Delobel, F., and Rueher, M. (1998). A note on partial consistencies over continuous domains. In Maher, M. and Puget, J.-F., editors, *Principles and Practice of Constraint Programming — CP98*, pages 147–161, Berlin, Heidelberg. Springer Berlin Heidelberg.

Colle, E. and Galerne, S. (2013). Mobile robot localization by multiangulation using set inversion. *Robotics and Autonomous Systems*, 61:39–48.

Coppolino, R. N. and Rubin, S. (1980). Detectability of structural failures in offshore platforms by ambient vibration monitoring. In *Proceeding of the Offshore Conference Society of Petroleum Engineering*, pages 101–110, Richardson, TX.

Cruz, J. and Barahona, P. (2001). Global hull consistency with local search for continuous constraint solving. In Brazdil, P. and Jorge, A., editors, *Progress in Artificial Intelligence*, pages 349–362, Berlin, Heidelberg. Springer Berlin Heidelberg.

Darwin, C. (1909). *The Origin of Species*. P. F. Collier & Son.

Dascotte, E. (2003). The use of fe model updating and probabilistic analysis for dealing with uncertainty in structural dynamics simulation. In *JMAC Conference*, pages 1095–1101, Tokyo, Japan.

Dechter, R. (2003). *Constraint Processing*. Morgan Kaufmann, 1 edition.

Deng, L. and Cai, C. (2009). Bridge model updating using response surface method and genetic algorithm. *Journal of Bridge Engineering*, 15:553–564.

Ding, Z., Huang, M., and Lu, Z. (2016). Structural damage detection using artificial bee colony algorithm with hybrid search strategy. *Swarm and Evolutionary Computation*, 28:1 – 13.

Dougill, J. W., Wright, J. R., Parkhouse, J. G., and Harrison, R. E. (2006). Human structure interaction during rhythmic bobbing. *The Structural Engineer*, 84(22):32–39.

Fang, S.-E., Zhang, Q.-H., and Ren, W.-X. (2015). An interval model updating strategy using interval response surface models. *Mechanical Systems and Signal Processing*, 60-61:909–927.

Fang, Z. and Wang, J.-Q. (2012). Practical formulas for cable tension estimation by vibration method. *Journal of Bridge Engineering*, 17(1):161.

Farrar, C., Baker, W., Bell, T., Cone, K., Darling, T., Duffey, T., Eklund, A., and Migliori, A. (1994). Dynamic characterization and damage detection in the I-40 bridge over the rio grande. Technical report, Los Alamos National Laboratory.

Franco, G., Betti, R., and Lus, H. (2004). Identification of structural systems using evolutionary strategy. *Journal of Engineering Mechanics*, 130:1125–1139.

Friswell, M. I., Inman, D. J., and Pilkey, D. F. (1998a). The direct updating of damping and stiffness matrices. *AIAA Journal*.

Friswell, M. I. and Mottershead, J. E. (1995). *Finite Element Model Updating in Structural Dynamics*. Kluwer Academic Publishers.

Friswell, M. I., Mottershead, J. E., and Ahmadian, H. (2001). Finite-element model updating using experimental test data: parametrization and regularization. *Philosophical Transactions of the Royal Society of London A: Mathematical, Physical and Engineering Sciences*, 359(1778):169–186.

Friswell, M. I., Penny, J. E. T., and Garvey, S. D. (1998b). A combined genetic and eigensensitivity algorithm for the location of damage in structures. *Computers and Structures*, pages 547–556.

Gabriele, S. (2011). The interval intersection method for fe model updating. *Journal of Physics: Conference Series*, 305.

Gabriele, S. and Valente, C. (2009). An interval-based technique for fe model updating. *International Journal of Reliability and Safety*, 3:79–103.

Gabriele, S., Valente, C., and Brancaleoni, F. (2007). An interval uncertainty based method for damage identification. In *Damage Assessment of Structures VII*, volume 347 of *Key Engineering Materials*, pages 551–556. Trans Tech Publications.

García, O., Vehí, J., e Matos, J. C., Henriques, A. A., and Casas, J. R. (2008). Structural assessment under uncertain parameters via interval analysis. *Journal of Computational and Applied Mechanics*, 218:43–52.

Ghedira, K. and Dubuisson, B. (2013). *Foundations of CSP*, pages 1–28. John Wiley and Sons, Inc.

Goller, B., Beck, J. L., and Schuëller, G. I. (2012). Evidence-based identification of weighting factors in bayesian model updating using modal data. *Journal of Engineering Mechanics*, 138(5):430–440.

Golomb, S. W. and Baumert, L. D. (1965). Backtrack programming. *Journal of the ACM*, 12(4):516–524.

Goualard, F. and Granvilliers, L. (2005). Controlled propagation in continuous numerical constraint networks. In *Proceedings of the 2005 ACM Symposium on Applied Computing*, SAC '05, pages 377–382, New York, NY, USA. ACM.

Granvilliers, L. (2012). Adaptive bisection of numerical csps. In Milano, M., editor, *Principles and Practice of Constraint Programming*, pages 290–298, Berlin, Heidelberg. Springer Berlin Heidelberg.

Han, S., Benaroya, H., and Wei, T. (1999). Dynamics of transversely vibrating beams using four engineering theories. *Journal of Sound and Vibration*, 225(5):935–988.

Hentenryck, P. V. (1999). *The OPL Optimization Programming Language*. MIT PRESS.

Hentenryck, P. V., McAllester, D., and Kapur, D. (1997). Solving polynomial systems using a branch and prune approach. *SIAM Journal on Numerical Analysis*, 34(2):797–827.

Herrero, P., Sainz, M. A., Vehí, J., and Jaulin, L. (2004). Quantified set inversion with applications to control. In *International Symposium on Computer Aided Control Systems Design*.

Holland, J. H. (1975). *Adaptation in Natural and Artificial Systems*. The University of Michigan Press, Ann Arbor, MI.

Hu, S. J. and Li, H. (2008). A systematic linear space approach to solving partially described inverse eigenvalue problems. *Inverse Problems*, 24(3):1–12.

Hua, X., Ni, Y., Chen, Z., and Ko, J. (2009). Structural damage detection in cable-stayed bridges using changes in cable forces and model updating. *Journal of Structural Engineering*, 135(9):1093–1106.

Huang, Q., Gardoni, P., and Hurlebaus, S. (2012). A probabilistic damage detection approach using vibration-based nondestructive testing. *Structural Safety*, 38:11 – 21.

Hyvnen, E. (1992). Constraint reasoning based on interval arithmetic: the tolerance propagation approach. *Artificial Intelligence*, 58:71–112.

Jaulin, L., Kieffer, M., Didrit, O., and Walter, E. (2001). *Applied Interval Analysis*. Springer.

Jaulin, L. and Walter, E. (1993). Set inversion via interval analysis for nonlinear bounded-error estimation. *Automatica*, 29(4):1053–1064.

Jin, S.-S., Cho, S., Jung, H.-J., Lee, J.-J., and Yun, C.-B. (2014). A new multi-objective approach to finite element model updating. *Journal of Sound and Vibration*, 333(11):2323 – 2338.

Joint Committee for Guides in Metrology (JCGM) (2008). Evaluation of measurement data - guide to the expression of uncertainty in measurement. Technical report, JCGM.

Juang, J. N. and Pappa, R. S. (1985). An eigensystem realization algorithm for modal parameter identi"cation and model reduction. *International Journal of Guidance, Control, and Dynamics*, pages 620–627.

Jung, D.-S. and Kim, C.-Y. (2013). Finite element model updating on small-scale bridge model using the hybrid genetic algorithm. *Structure and Infrastructure Engineering*, 9(5):481–495.

Kennedy, M. and O'Hagan, A. (2001). Bayesian calibration of computer models. *Journal of the Royal Statistical Society*, 63:425–464.

Kernicky, T., Whelan, M., and Al-Shaer, E. (2018). Dynamic identification of axial force and boundary restraints in tie rods and cables with uncertainty quantification using set inversion via interval analysis. *Journal of Sound and Vibration*, 426:401–420.

Kernicky, T., Whelan, M., Rauf, U., and Al-Shaer, E. (2017). Structural identification using a nonlinear constraint satisfaction processor with interval arithmetic and contractor programming. *Computers and Structures*, 188:1–16.

Kernicky, T. P., Tedeschi, M., and Whelan, M. J. (2016). *Leveraging Hybrid Simulation for Vibration-Based Damage Detection Studies*, pages 333–341. Springer International Publishing.

Kernicky, T. P., Whelan, M. J., Weggel, D. C., and Rice, C. D. (2014). Structural identification and damage characterization of a masonry infill wall in a full-scale building subjected to internal blast load. *Journal of Structural Engineering*, 141.

Khodaparast, H. H., Mottershead, J. E., and Badcock, K. J. (2011). Interval model updating with irreducible uncertainty using the kriging predictor. *Mechanical Systems and Signal Processing*, 25:1204–1226.

Kieffer, M., Braems, I., Walter, É., and Jaulin, L. (2001). *Guaranteed Set Computation with Subpavings*, pages 167–178. Springer US, Boston, MA.

Kim, B. and Park, T. (2007). Estimation of cable tension force using the frequency-based system identification method. *Journal of Sound and Vibration*, 304:660.

Kim, G.-H. and sik Park, Y. (2008). An automated parameter selection procedure for finite-element model updating and its applications. *Journal of Sound and Vibration*, 309(3):778 – 793.

Köylüoğlu, H. U., Çakmak, A. Ş., and Nielsen, S. R. K. (1995). Interval algebra to deal with pattern loading and structural uncertainties. *Journal of Engineering Mechanics*, 121:1149–1157.

Kumar, V. (1992). Algorithms for constraint-satisfaction problems: A survey. *AAAI*, 13(1):32–44.

Kuo, Y.-C. and Datta, B. N. (2012). Quadratic model updating with no spill-over and incomplete measured data: Existence and computation of solution. *Linear Algebra and its Applications*, 436(7):2480–2493.

Larson, C. B. and Zimmerman, D. C. (1993). Structural model refinement using a genetic algorithm approach. In *IMAC XI- 11th International Modal Analysis Conference*, pages 1095–1101, Kissimmee.

Li, J., shui Huang, M., and ping Zhu, H. (2009). Study on different residual and weight coefficient in model updating of bridge structure. In *ICCTP 2009: Critical Issues In Transportation Systems Planning, Development, and Management*, pages 100–107. ASCE.

Li, S., Reynders, E., Maes, K., and De Roeck, G. (2013). Vibration-based estimation of axial force for a beam member with uncertain boundary conditions. *Journal of Sound and Vibration*, 332(4):795–806.

Li, X. (2013). Free vibration of axially loaded shear beams carrying elastically restrainted lumpted-tip masses via asymptotic Timoshenko beam theory. *Journal of Engineering Mechanics*, 139:418–428.

Lipschutz, S. (1965). *Schaum's Outline of General Topology*. Schaum's Outline Series in Mathematics. McGraw-Hill Companies,Incorporated.

Liu, S.-C. and Yao, J. T. (1978). Structural identification concept. *Journal of the Structural Division*, 104(12):1845–1858.

Lo, W., Shih, C., and Hinote, G. (2001). Ground vibration test of a commercial aircraft.

Lu, Y. and Tu, Z. (2005). Dynamic model updating using a combined genetic-eigensensitivity algorithm and application in seismic response prediction. *Earthquake Engineering and Structural Dynamics*, 34:1149–1170.

Mackworth, A. K. (1977). Consistency in networks of relations. *Artificial Intelligence*, 8(1):99 – 118.

Madarshahian, R., Caicedo, J. M., and Zárate, B. A. (2013). Using P-Box and PiFE to Express Uncertainty in Model Updating. In *Topics in Model Validation and Uncertainty Quantification, Volume 5*, pages 81–88. Springer.

Maes, K., Peeters, J., Reynders, E., Lombaert, G., and De Roeck, G. (2013). Identification of axial forces in beam members by local vibration measurements. *Journal of Sound and Vibration*, 332(21):5417–5432.

Mares, C., Mottershead, J., and Friswell, M. (2006). Stochastic model updating: Part 1-theory and simulated example. *Mechanical Systems and Signal Processing*, 20(7):1674–1695.

Mares, C. and Surace, C. (1996). An application of genetic algorithms to identify damage in elastic structures. *Journal of Sound and Vibration*, pages 195–215.

Martí, R. (2003). *Multi-Start Methods*, pages 355–368. Springer US, Boston, MA.

Marwala, T. (2010). *Finite-element-model updating using computional intelligence techniques*. Springer.

Marwala, T., Mdlazi, L., and Sibisi, S. (2007). Finite element model updating using bayesian approach.

MATLAB (2017). *version 9.2.0 (R2017a)*. The MathWorks Inc., Natick, Massachusetts.

Mitchell, M. (1995). *An Introduction to Genetic Algorithms*. MIT Press.

Moaveni, B., Stavridis, A., Lombaert, G., and Conte, J. P. (2013). Finite-element model updating for assessment of progressive damage in a 3-story infilled rc frame. *Journal of Structural Engineering*, 139:1664–1674.

Modares, M., Mullen, R. L., and Muhanna, R. L. (2006). Natural frequencies of a structure with bounded uncertainty. *Journal of Engineering Mechanics*, 132(12):1363–1371.

Moens, D. and Vandepitte, D. (2005). A survey of non-probabilistic uncertainty treatment in finite element analysis. *Computer methods in applied mechanics and engineering*, 194:1527–1555.

Moore, R. (1966). *Interval Analysis*. Prentice Hall.

Moore, R., Kearfott, R., and Cloud, M. (2009). *Introduction to Interval Analysis*. Society for Industrial and Applied Mathematics, Philadelphia, PA.

Moore, R. E. (1962). *Interval Arithmetic and Automatic Error Analysis in Digital Computing*. PhD thesis, Standford University.

Morassi, A. and Tonon, S. (2008). Dynamic testing for structural identification of a bridge. *Journal of Bridge Engineering*, 13:573–585.

Mosqueda, G. and Ahmadizadeh, M. (2011). Iterative implicit integration procedure for hybrid simulation of large nonlinear structures. *Earthquake Engineering and Structural Dynamics*, 40(9):945–960.

Mottershead, J. E., Link, M., and Friswell, M. I. (2011). The sensitivity method in finite element model updating: A tutorial. *Mechanical Systems and Signal Processing*, 25:2275–2296.

Mustafa, S. and Matsumoto, Y. (2017). Bayesian model updating and its limitations for detecting local damage of an existing truss bridge. *Journal of Bridge Engineering*, 22(7):04017019.

Neveu, B., Trombettoni, G., and Araya, I. (2015). Adaptive constructive interval disjunction: algorithms and experiments. *Constraints*, 20:452–467.

Ninin, J., Messine, F., and Hansen, P. (2015). A reliable affine relaxation method for global optimization. *4OR*, 13(3):247–277.

NYSDOT (2012). The lake champlain bridge emergency replacement project. Technical report.

Pandey, A. K., Biswas, M., and Samman, M. M. (1991). Damage detection from changes in curvature mode shapes. *Journal of Sound and Vibration*, pages 321–332.

Papadimitriou, C. (2004). Optimal sensor placement methodology for parametric identification of structural systems. *Journal of Sound and Vibration*, 278(4):923 – 947.

Peeters, B. (2000). *System Identification and Damage Detection in Civil Engineering*. Heverlee - Katholieke Universiteit Leuven.

Perera, R. and Ruiz, A. (2008). A multistage fe updating procedure for damage identification in large-scale structures based on multiobjective evolutionary optimization. *Mechanical Systems and Signal Processing*, 22:970–991.

Perry, M. J., Koh, C. G., and Choo, Y. S. (2006). Modified genetic algorithm strategy for structural identification. *Computers and Structures*, pages 529–540.

Ratz, D. (1996). *On extended interval arithmetic and inclusion isotonicity*. Institut fur Angewandte Mathematik, Universitat Karlsruhe.

Rebecchi, G., Tullini, N., and Laudiero, F. (2013). Estimate of the axial force in slender beams with unknown boundary conditions using one flexural mode shape. *Journal of Sound and Vibration*, 332(18):4122–4135.

Ren, W.-X. and Chen, H.-B. (2010). Finite element model updating in structural dynamics by using the response surface method. *Engineering Structures*, 32(8):2455 – 2465.

Reynders, E., Maes, K., Lombaert, G., and Roeck, G. D. (2016). Uncertainty quantification in operational modal analysis with stochastic subspace identification: Validation and applications. *Mechanical Systems and Signal Processing*, 66-67:13–30.

Reynders, E., Pintelon, R., and Roeck, G. D. (2008). Uncertainty bounds on modal parameters obtained from stochastic subspace identification. *Mechanical Systems and Signal Processing*, 22:948–969.

Reynolds, P. and Pavic, A. (2000). Impulse hammer versus shaker excitation for the modal testing of building floors. *Experimental Techniques*, 24(3):39–44.

Ribeiro, D., Calada, R., Delgado, R., Brehm, M., and Zabel, V. (2012). Finite element model updating of a bowstring-arch railway bridge based on experimental modal parameters. *Engineering Structures*, 40:413–435.

Ribeiro, D., Calada, R., Delgado, R., Brehm, M., and Zabel, V. (2013). Finite-element model calibration of a railway vehicle based on experimental modal parameters. *Vehicle System Dynamics*, 51:821–856.

Rossi, F., van Beek, P., and Walsh, T. (2006). *Handbook of Constraint Programming (Foundations of Artificial Intelligence)*. Elsevier Science.

Roy, K. (2017). Structural damage identification using mode shape slope and curvature. *Journal of Engineering Mechanics*, 143(9):04017110.

Russell, S. and Norvig, P. (2002). *Artificial Intelligence: A Modern Approach*. Prentice Hall Press, Upper Saddle River, NJ, USA, 2rd edition.

Salawu, O. S. (1997). Detection of structural damage through changes in frequency: a review. *Engineering Structures*, pages 718–723.

Schlune, H., Plos, M., and Gylltoft, K. (2009). Improved bridge evaluation through finite element model updating using static and dynamic measurements. *Engineering Structures*, 31(7):1477 – 1485.

Sim, J., Zhiping, Q., and Xiaojun, W. (2007). Modal analysis of structures with uncertain-but- bounded parameters via interval analysis. *J of Sound and Vibration*, 303:29–45.

Simoen, E., Roeck, G. D., and Lombaert, G. (2015). Dealing with uncertainty in model updating for damage assessment: A review. *Mechanical Systems and Signal Processing*, 56-57:123–49.

Sohn, H. and Law, K. H. (1997). A bayesian probabilistic approach for structure damage detection. *Earthquake Engineering and Structural Dynamics*, 26(12):1259–1281.

SoPlex (2017). Sequential object-oriented simplex.

Sun, H. and Betti, R. (2015). A hybrid optimization algorithm with bayesian inference for probabilistic model updating. *Computer-Aided Civil and Infrastrucure Engineering*, 30:602–619.

Sun, H. and Büyüköztürk, O. (2016). Probabilistic updating of building models using incomplete modal data. *Mechanical Systems and Signal Processing*, 75(Supplement C):27 – 40.

Sun, H., LuÅ, H., and Betti, R. (2013). Identification of structural models using a modified artificial bee colony algorithm. *Computers and Structures*, 116(Supplement C):59 – 74.

Tedeschi, M. (2015). Development, verification, and validation of a hybrid testing framework for latticed structures with nonlinear geometric effects. Master's thesis, University of North Carolina at Charlotte.

Teughels, A. and DeRoeck, G. (2004). Structural damage identification of the highway bridge z24 by fe model updating. *Journal of Sound and Vibration*, 278:589–610.

Timoshenko, S. P. (1921). On the correction for shear of the differential equation for transverse vibrations of prismatic bars. *The London, Edinburgh, and Dublin Philosophical Magazine and Journal of Science*, 41(245):744–746.

Tullini, N. (2013). Bending tests to estimate the axial force in slender beams with unknown boundary conditions. *Mechanics Research Communications*, 53:15–23.

United States National Transportation Safety Board (1984). Collapse of a suspended span of interstate route 95 highway bridge over the mianus river, greenwich, connecticut june 28, 1983. Technical report, National Transportation Safety Board, Washington, DC.

Vandiver, J. K. (1975). Detection of the structural failure of fixed platforms by measurement of dynamic response. In *Proceeding of the Offshore Conference Society of Petroleum Engineering*, pages 243–252, Richardson, TX.

Vanik, M. W., Beck, J. L., and Au, S. K. (2000). Bayesian probabilistic approach to structural health monitoring. *Journal of Engineering Mechanics*, 126(7):738–745.

VanOverschee, P. and DeMoor, B. (1996). *Subspace Identifcation for Linear Systems, Theory–implementation–applications*. Dordrect: Kluwer Academic Publishers.

Wahab, M. A. and Roeck, G. D. (1999). Damage detection in bridges using modal curvatures: Application to a real damage scenario. *Journal of Sound and Vibration*, 226(2):217 – 235.

Wan, H.-P. and Ren, W.-X. (2015). Parameter selection in finite-element-model updating by global sensitivity analysis using gaussian process metamodel. *Journal of Structural Engineering*, 141(6):04014164.

Wang, H., qun Li, A., and Li, J. (2010). Progressive finite element model calibration of a long-span suspension bridge based on ambient vibration and static measurements. *Engineering Structures*, 32(9):2546 – 2556.

Wang, X., Yang, C., and Qiu, Z.-P. (2013a). Non-probabilistic information fusion technique for structural damage identification based on measured dynamic data with uncertainty. *Acta Mechanica Sinica*, 29:202–210.

Wang, X., Yang, C., Wang, L., Yang, H., and Qiu, Z. (2013b). Membership-set identification method for structural damage based on measured natural frequencies and static displacements. *Structural Health Monitoring*, 12:23–34.

Wang, X., Yang, H., Wang, L., and Qiu, Z. (2012). Interval analysis method for structural damage identification based on multiple load cases. *Journal of Applied Mechanics*, 79.

Wenzel, H. and Pichler, D. (2005). John Wiley and Sons, Ltd.

Whelan, M., Salas Zamudio, N., and Kernicky, T. (2018). Structural identification of a tied arch bridge using parallel genetic algorithms and ambient vibration monitoring with a wireless sensor network. *Journal of Civil Structural Health Monitoring*.

Whelan, M. J., Gangone, M. V., Janoyan, K. D., and Jha, R. (2009). Real-time wireless vibration monitoring for operational modal analysis of an integral abutment highway bridge. *Engineering Structures*, 31(10):2224 – 2235.

Woeginger, G. J. (2003). *Exact Algorithms for NP-Hard Problems: A Survey*, pages 185–207. Springer Berlin Heidelberg, Berlin, Heidelberg.

Xie, F. and Levinson, D. (2011). Evaluating the effects of the I35W bridge collapse on road-users in the twin cities metropolitan region. *Transportation Planning and Technology*, 34(7):691–703.

Yang, Y. and Chen, Y. (2009). A new direct method for updating structural models based on measured modal data. *Engineering Structures*, 31(1):32 – 42.

Yuen, K.-V., Beck, J. L., and Au, S. K. (2004). Structural damage detection and assessment by adaptive markov chain monte carlo simulation. *Structural Control and Health Monitoring*, 11(4):327–347.

Yuen, K.-V., Beck, J. L., and Katafygiotis, L. S. (2005). Unified probabilistic approach for model updating and damage detection. *Journal of Applied Mechanics*, 73.

Zapico, J. L., Gonzlez-Buelga, A., Gonzlez, M. P., and Alonso, R. (2008). Finite element model updating of a small steel frame using neural networks. *Smart Materials and Structures*, 17(4).

Zárate, B. A. and Caicedo, J. M. (2008). Finite element model updating: Multiple alternatives. *Engineering Structures*, 30(12):3724 – 3730.

Zhang, J., Maes, K., Roeck, G. D., Reynders, E., Papadimitriou, C., and Lombaert, G. (2017). Optimal sensor placement for multi-setup modal analysis of structures. *Journal of Sound and Vibration*, 401:214 – 232.

Zhang, J., Wan, C., and Sato, T. (2013). Advanced markov chain monte carlo approach for finite element calibration under uncertainty. *Computer-Aided Civil and Infrastructure Engineering*, 28:522–530.

Zhang, Q. W., Chang, C. C., and Chang, T. Y. (2000). Finite element model updating for structures with parametric constraints. *Earthquake Engineering and Structural Dynamics*, 29:927–944.

Zhong, H. and Yang, M. (2016). Damage detection for plate-like structures using generalized curvature mode shape method. *Journal of Civil Structural Health Monitoring*, 6(1):141–152.

Zhu, Y. and Zhang, L. (2009). *Finite Element Model Updating Based on Least Squares Support Vector Machines*, pages 296–303. Springer Berlin Heidelberg, Berlin, Heidelberg.

Zimmerman, D. C. (2000). Model validation and verification of large and complex space structures. *Inverse Problems in Engineering*, 8(2):93–118.

Zimmerman, D. C. and Kaouk, M. (1992). Eigenstructure assignment approach for structural damage detection. *AIAA Journal*, 30:1848–1855.

Zui, H., Shinke, T., and Namita, Y. (1996). Practical formulas for estimation of cable tension by vibration method. *Journal of Structural Engineering*, 122(6):651.

APPENDIX A: CABLE FORCE NATURAL FREQUENCIES

A.1 Generation of Synthetic Frequencies For the Two Spring Analytical Example

The analytical model previously described in Chapter 4 for a 6.5 cm diameter, 5 m long steel rod under an axial load of 581 kN was used to generate synthetic natural frequency measurements through forward solution of the roots of the characteristic equation. In developing this synthetic data, the translational restraint on both ends of the rod was idealized as fixed ($k_C = k_D = 1$) and the non-dimensional spring assignments for the rotary springs were prescribed as $k_A = 0.70$ and $k_B = 0.30$. To add uncertainty to the problem, 15 sets of synthetic natural frequency estimates were generated with Gaussian noise with standard deviations, σ, of 0.1 Hz around the exact natural frequencies. The means and standard deviations across the 15 sets of synthetic data for the first eight frequencies are displayed in Table A.1.

TABLE A.1: Average natural frequencies and standard deviations for the first eight natural frequencies of the two spring problem where k_A=0.70, k_B=0.30, and $k_C = k_D$=0.70 and the applied force was $581kN$.

No.	f^{avg} (Hz)	σ (Hz)
1	17.855	0.10603
2	40.213	0.08221
3	70.025	0.12397
4	108.58	0.10375
5	156.38	0.05817
6	213.65	0.08825
7	280.52	0.09402
8	356.83	0.10113

A.2 Generation of Synthetic Frequencies For the Four Spring Analytical Example

The analytical model previously described in Chapter 4 for a 6.5 cm diameter steel rod of 5 m length under an axial load of 581 kN was used to generate synthetic natural frequency measurements through forward solution of the roots of the characteristic equation. In developing this synthetic data, the non-dimensional spring assignments for the rotary springs were prescribed as $k_A = 0.70$ and $k_B = 0.30$ and the translational springs as $k_C = 0.75$ and $k_D = 0.45$. To add uncertainty to the problem, 15 sets of synthetic natural frequency estimates were generated with Gaussian noise with standard deviations, σ, of 0.1 Hz around the exact natural frequencies. The means and standard deviations across the 15 sets of synthetic data for the first twelve frequencies are displayed in Table A.2.

TABLE A.2: Average natural frequencies and standard deviations for the first twelve natural frequencies of the four spring problem where k_A=0.70, k_B=0.30, k_C=0.75, and k_D=0.45

Mode	f^{avg} (Hz)	σ (Hz)
1	10.208	0.09567
2	23.528	0.07617
3	40.939	0.12981
4	65.305	0.07821
5	98.385	0.12789
6	141.11	0.08487
7	193.41	0.08684
8	255.43	0.11472
9	327.11	0.09547
10	408.22	0.07437
11	498.74	0.11503
12	598.33	0.07339

A.3 Two Spring Experimental Validation

The mean natural frequencies extracted through system identification of the experimental modal analysis data are presented in Table A.3 for all four cases of rotational end fixity. Note that the means were calculated using 45 pole estimates across 15 sets of experimental data.

TABLE A.3: Average natural frequencies for the first eight natural frequencies of the two spring problem with $k_C = k_D = 1$ and $N = 2.5kN$

Mode	Case 1 f^{avg} (Hz)	Case 2 f^{avg} (Hz)	Case 3 f^{avg} (Hz)	Case 4 f^{avg} (Hz)
1	31.313	32.496	32.910	34.463
2	72.988	75.156	76.438	79.503
3	131.01	134.35	136.40	141.53
4	207.69	211.51	214.11	221.20
5	306.41	311.22	314.70	325.04
6	424.15	430.03	434.28	447.08
7	559.56	566.27	571.79	589.01
8	709.83	717.40	723.58	746.64

APPENDIX B: EXPERIMENTAL MODAL ANALYSIS DATA FOR SIX DOF SYSTEM MODEL

Experimental modal parameter estimates for the six degree-of-freedom experimental structure in Chapter 5 were obtained through system identification using the combined deterministic stochastic subspace state-space system identification algorithm (VanOverschee and DeMoor, 1996). These estimates were calculated through eigendecomposition of the state matrix across a range of model orders and stabilization plots were utilized to select consistent pole estimates. In order to obtain improved estimates of modal parameters to attenuate effects of measurement and process noise, five stable poles and their corresponding eigenvectors were averaged for each experimental mode. The identified undamped natural frequencies along with the corresponding real-valued mode shapes are presented in Table B.1.

TABLE B.1: Average natural frequencies and corresponding mode shapes for the six degree-of-freedom experimental shear structure in Chapter 5

Mode	1	2	3	4	5	6
f_n^{avg}	9.7555	26.3907	39.0470	51.1219	63.6133	89.5157
$\phi_{1,n}^{avg}$	0.1251	0.4340	-0.7286	0.3036	-0.3146	1
$\phi_{2,n}^{avg}$	0.2323	0.7467	-0.9963	0.3287	-0.2005	-0.7437
$\phi_{3,n}^{avg}$	0.4106	1	-0.4288	-0.3187	1	0.3219
$\phi_{4,n}^{avg}$	0.6630	0.7793	1	-0.6550	-0.3075	0.0305
$\phi_{5,n}^{avg}$	0.8917	-0.1969	0.7103	1	0.1262	-0.0073
$\phi_{6,n}^{avg}$	1	-0.9484	-0.9185	-0.5386	-0.0337	-0.0029

APPENDIX C: EXPERIMENTAL MODAL PROPERTIES ESTIMATES OF THE TRUSS

This appendix provides the modal properties utilized in the structural identification of the forty-five degree-of-freedom 2D Pratt truss in Chapter 6. Table C.1 provides the average undamped natural frequencies across 60 estimates for all cases of damage where the experimental structure represented member 27. The corresponding average mode shape estimates and standard deviations are displayed in Tables C.2 and C.3, respectively. Table C.4 provides the average undamped natural frequencies across 60 estimates for all cases of damage where the experimental structure represented member 31. The corresponding average mode shape estimates and standard deviations are displayed in Tables C.5 and C.6, respectively.

TABLE C.1: Average natural frequencies and standard deviations for the first eight natural frequencies for all states of damage where the experimental substructure represented member 27

	Undamaged		Damage 1		Damage 2		Damage 3		Damage 4	
Mode	f_n^{avg}	σ_n	f_n^{avg}	σ_n	f_n^{avg}	σ_n	f_n^{avg}	σ_n	f_n^{avg}	σ_n
1	0.581	0	0.581	0	0.581	0	0.581	0	0.575	0
2	2.005	0	2.004	0	2.003	0	1.989	0.001	1.968	0.001
3	2.792	0	2.792	0	2.791	0	2.791	0	2.787	0
4	4.421	0	4.414	0	4.407	0	4.319	0.002	4.315	0.002
5	6.218	0	6.218	0	6.217	0	6.216	0.001	6.15	0
6	7.746	0	7.735	0.001	7.723	0.002	7.604	0.013	7.56	0.014
7	9.307	0	9.306	0.001	9.305	0.001	9.299	0.001	9.294	0.002
8	10.616	0.003	10.579	0.003	10.549	0.003	10.178	0.006	10.177	0.006

TABLE C.2: Average of the measured mode shape components for all cases of damage where the experimental substructure represented member 27

Component	Undamaged	Damage 1	Damage 2	Damage 3	Damage 4
$\phi_{5,1}^{avg}$	-0.1832	-0.1831	-0.1830	-0.1821	-0.1842
$\phi_{9,1}^{avg}$	0.2597	0.2595	0.2596	0.2582	0.2606
$\phi_{11,1}^{avg}$	0.5024	0.5021	0.5021	0.4994	0.5043
$\phi_{12,1}^{avg}$	-0.1550	-0.1548	-0.1548	-0.1540	-0.1564
$\phi_{13,1}^{avg}$	0.7099	0.7096	0.7095	0.7057	0.7134
$\phi_{17,1}^{avg}$	-0.1347	-0.1345	-0.1345	-0.1339	-0.1364
$\phi_{23,1}^{avg}$	0.8685	0.8680	0.8678	0.8633	0.8742
$\phi_{24,1}^{avg}$	0.9674	0.9675	0.9676	0.9680	0.9718
$\phi_{25,1}^{avg}$	0.9658	0.9656	0.9657	0.9655	0.9629
$\phi_{27,1}^{avg}$	-0.0424	-0.0422	-0.0423	-0.0417	-0.0461
$\phi_{28,1}^{avg}$	0.8655	0.8653	0.8653	0.8651	0.8611
$\phi_{29,1}^{avg}$	-0.0220	-0.0219	-0.0219	-0.0214	-0.0262
$\phi_{30,1}^{avg}$	0.7060	0.7058	0.7057	0.7055	0.7013
$\phi_{31,1}^{avg}$	0.4981	0.4980	0.4979	0.4978	0.4944
$\phi_{33,1}^{avg}$	0.0062	0.0064	0.0063	0.0068	0.0014
$\phi_{37,1}^{avg}$	0.2562	0.2562	0.2561	0.2560	0.2542
$\phi_{38,1}^{avg}$	-0.0891	-0.0890	-0.0890	-0.0887	-0.0945
$\phi_{39,1}^{avg}$	1.0000	1.0000	1.0000	1.0000	1.0000
$\phi_{40,1}^{avg}$	-0.1741	-0.1739	-0.1741	-0.1734	-0.1777
$\phi_{41,1}^{avg}$	-0.0270	-0.0269	-0.0270	-0.0269	-0.0266
$\phi_{43,1}^{avg}$	-0.1499	-0.1498	-0.1499	-0.1493	-0.1541
$\phi_{44,1}^{avg}$	-0.1123	-0.1121	-0.1122	-0.1118	-0.1172
$\phi_{45,1}^{avg}$	-0.0657	-0.0656	-0.0657	-0.0653	-0.0716
$\phi_{5,2}^{avg}$	0.3718	0.3724	0.3729	-0.3700	-0.3699
$\phi_{9,2}^{avg}$	-0.5746	-0.5755	-0.5763	0.5710	0.5678
$\phi_{11,2}^{avg}$	-0.9150	-0.9167	-0.9183	0.9136	0.9089
$\phi_{12,2}^{avg}$	0.2581	0.2586	0.2591	-0.2580	-0.2628
$\phi_{13,2}^{avg}$	-0.9942	-0.9965	-0.9987	1.0000	1.0000
$\phi_{17,2}^{avg}$	0.2119	0.2124	0.2128	-0.2125	-0.2201
$\phi_{23,2}^{avg}$	-0.7986	-0.8014	-0.8041	0.8162	0.8282
$\phi_{24,2}^{avg}$	-0.3828	-0.3807	-0.3788	0.3445	0.3410
$\phi_{25,2}^{avg}$	0.5708	0.5718	0.5728	-0.5696	-0.5875
$\phi_{27,2}^{avg}$	0.2860	0.2865	0.2869	-0.2848	-0.3017
$\phi_{28,2}^{avg}$	0.8996	0.9001	0.9005	-0.8818	-0.8988

Continued on next page

Table C.2 – continued from previous page

Component	Undamaged	Damage 1	Damage 2	Damage 3	Damage 4
$\phi^{avg}_{29,2}$	0.3615	0.3620	0.3623	-0.3577	-0.3759
$\phi^{avg}_{30,2}$	1.0000	1.0000	1.0000	-0.9737	-0.9870
$\phi^{avg}_{31,2}$	0.8442	0.8440	0.8438	-0.8194	-0.8281
$\phi^{avg}_{33,2}$	0.5082	0.5085	0.5088	-0.4987	-0.5180
$\phi^{avg}_{37,2}$	0.4716	0.4714	0.4713	-0.4571	-0.4612
$\phi^{avg}_{38,2}$	0.4995	0.4996	0.4997	-0.4877	-0.5064
$\phi^{avg}_{39,2}$	0.1226	0.1242	0.1257	-0.1410	-0.1552
$\phi^{avg}_{40,2}$	0.2229	0.2233	0.2236	-0.2216	-0.2379
$\phi^{avg}_{41,2}$	0.2628	0.2629	0.2629	-0.2565	-0.2540
$\phi^{avg}_{43,2}$	0.3481	0.3484	0.3485	-0.3417	-0.3580
$\phi^{avg}_{44,2}$	0.4713	0.4715	0.4715	-0.4603	-0.4778
$\phi^{avg}_{45,2}$	0.4492	0.4493	0.4494	-0.4389	-0.4595
$\phi^{avg}_{5,3}$	0.2347	0.2347	0.2346	0.2340	0.2269
$\phi^{avg}_{9,3}$	-0.2360	-0.2360	-0.2359	-0.2349	-0.2226
$\phi^{avg}_{11,3}$	-0.0053	-0.0055	-0.0054	-0.0050	0.0125
$\phi^{avg}_{12,3}$	0.3948	0.3946	0.3945	0.3941	0.3907
$\phi^{avg}_{13,3}$	0.2965	0.2960	0.2962	0.2950	0.3095
$\phi^{avg}_{17,3}$	0.5132	0.5130	0.5129	0.5126	0.5107
$\phi^{avg}_{23,3}$	0.5312	0.5309	0.5308	0.5274	0.5314
$\phi^{avg}_{24,3}$	0.5991	0.6000	0.6002	0.6126	0.6137
$\phi^{avg}_{25,3}$	0.0773	0.0774	0.0772	0.0776	0.0741
$\phi^{avg}_{27,3}$	0.8629	0.8628	0.8627	0.8627	0.8622
$\phi^{avg}_{28,3}$	-0.3363	-0.3366	-0.3369	-0.3427	-0.3490
$\phi^{avg}_{29,3}$	0.8620	0.8619	0.8618	0.8609	0.8599
$\phi^{avg}_{30,3}$	-0.5978	-0.5985	-0.5987	-0.6083	-0.6157
$\phi^{avg}_{31,3}$	-0.6147	-0.6155	-0.6156	-0.6251	-0.6316
$\phi^{avg}_{33,3}$	0.7811	0.7808	0.7807	0.7776	0.7754
$\phi^{avg}_{37,3}$	-0.3833	-0.3838	-0.3838	-0.3895	-0.3932
$\phi^{avg}_{38,3}$	0.5743	0.5740	0.5739	0.5702	0.5689
$\phi^{avg}_{39,3}$	0.4849	0.4855	0.4855	0.4923	0.4914
$\phi^{avg}_{40,3}$	1.0000	1.0000	1.0000	1.0000	1.0000
$\phi^{avg}_{41,3}$	0.4370	0.4369	0.4367	0.4350	0.4276
$\phi^{avg}_{43,3}$	0.8191	0.8188	0.8187	0.8168	0.8158
$\phi^{avg}_{44,3}$	0.6346	0.6343	0.6341	0.6306	0.6290
$\phi^{avg}_{45,3}$	0.5500	0.5498	0.5497	0.5469	0.5470
$\phi^{avg}_{5,4}$	-0.0948	-0.0943	-0.0939	-0.0876	-0.0950

Continued on next page

Table C.2 – continued from previous page

Component	Undamaged	Damage 1	Damage 2	Damage 3	Damage 4
$\phi^{avg}_{9,4}$	0.4373	0.4354	0.4336	0.4097	0.4241
$\phi^{avg}_{11,4}$	0.9482	0.9466	0.9449	0.9231	0.9408
$\phi^{avg}_{12,4}$	0.3118	0.3111	0.3105	0.3020	0.2994
$\phi^{avg}_{13,4}$	0.8653	0.8670	0.8684	0.8882	0.8968
$\phi^{avg}_{17,4}$	0.4174	0.4167	0.4161	0.4067	0.4049
$\phi^{avg}_{23,4}$	0.2293	0.2355	0.2414	0.3207	0.3123
$\phi^{avg}_{24,4}$	-0.5398	-0.5478	-0.5546	-0.6499	-0.6574
$\phi^{avg}_{25,4}$	-0.8148	-0.8128	-0.8113	-0.7883	-0.7877
$\phi^{avg}_{27,4}$	0.1352	0.1357	0.1364	0.1427	0.1433
$\phi^{avg}_{28,4}$	-0.1507	-0.1471	-0.1443	-0.1042	-0.1024
$\phi^{avg}_{29,4}$	0.1496	0.1508	0.1521	0.1664	0.1675
$\phi^{avg}_{30,4}$	0.6317	0.6338	0.6354	0.6591	0.6602
$\phi^{avg}_{31,4}$	1.0000	1.0000	1.0000	1.0000	1.0000
$\phi^{avg}_{33,4}$	0.4277	0.4290	0.4302	0.4457	0.4470
$\phi^{avg}_{37,4}$	0.7034	0.7027	0.7021	0.6942	0.6938
$\phi^{avg}_{38,4}$	0.2389	0.2411	0.2433	0.2721	0.2743
$\phi^{avg}_{39,4}$	-0.9119	-0.9144	-0.9165	-0.9460	-0.9488
$\phi^{avg}_{40,4}$	0.0957	0.0972	0.0987	0.1157	0.1172
$\phi^{avg}_{41,4}$	0.0732	0.0749	0.0765	0.0983	0.0884
$\phi^{avg}_{43,4}$	0.4146	0.4153	0.4163	0.4263	0.4275
$\phi^{avg}_{44,4}$	0.4148	0.4164	0.4180	0.4382	0.4400
$\phi^{avg}_{45,4}$	0.0866	0.0887	0.0908	0.1184	0.1211
$\phi^{avg}_{5,5}$	-0.3090	-0.3091	-0.3096	-0.3104	-0.3299
$\phi^{avg}_{9,5}$	0.8644	0.8645	0.8647	0.8646	0.8840
$\phi^{avg}_{11,5}$	1.0000	1.0000	1.0000	1.0000	1.0000
$\phi^{avg}_{12,5}$	0.0038	0.0034	0.0024	-0.0001	-0.0248
$\phi^{avg}_{13,5}$	0.1012	0.1014	0.1018	0.1033	0.0883
$\phi^{avg}_{17,5}$	-0.0925	-0.0932	-0.0946	-0.0984	-0.1179
$\phi^{avg}_{23,5}$	-0.8874	-0.8867	-0.8856	-0.8816	-0.9120
$\phi^{avg}_{24,5}$	-0.9187	-0.9224	-0.9298	-0.9514	-0.9031
$\phi^{avg}_{25,5}$	0.7346	0.7374	0.7436	0.7603	0.7509
$\phi^{avg}_{27,5}$	0.1189	0.1187	0.1185	0.1180	0.1244
$\phi^{avg}_{28,5}$	0.8360	0.8390	0.8455	0.8635	0.8157
$\phi^{avg}_{29,5}$	0.3429	0.3433	0.3445	0.3478	0.3418
$\phi^{avg}_{30,5}$	0.0757	0.0758	0.0756	0.0756	0.0494
$\phi^{avg}_{31,5}$	-0.7515	-0.7544	-0.7612	-0.7795	-0.7575

Continued on next page

Table C.2 – continued from previous page

Component	Undamaged	Damage 1	Damage 2	Damage 3	Damage 4
$\phi^{avg}_{33,5}$	0.3058	0.3058	0.3059	0.3064	0.2971
$\phi^{avg}_{37,5}$	-0.7755	-0.7784	-0.7849	-0.8026	-0.7679
$\phi^{avg}_{38,5}$	0.1735	0.1741	0.1754	0.1791	0.1772
$\phi^{avg}_{39,5}$	-0.0274	-0.0278	-0.0282	-0.0299	0.0106
$\phi^{avg}_{40,5}$	0.6423	0.6434	0.6462	0.6544	0.6319
$\phi^{avg}_{41,5}$	-0.3846	-0.3846	-0.3846	-0.3845	-0.4234
$\phi^{avg}_{43,5}$	0.1237	0.1232	0.1222	0.1197	0.1223
$\phi^{avg}_{44,5}$	0.1293	0.1293	0.1294	0.1296	0.1256
$\phi^{avg}_{45,5}$	-0.0999	-0.0996	-0.0990	-0.0975	-0.0792
$\phi^{avg}_{5,6}$	-0.4700	-0.4698	-0.4696	0.4616	0.4368
$\phi^{avg}_{9,6}$	0.8965	0.9033	0.9110	-0.9756	-0.8968
$\phi^{avg}_{11,6}$	0.2708	0.2825	0.2956	-0.4239	-0.3643
$\phi^{avg}_{12,6}$	-0.5725	-0.5657	-0.5582	0.4757	0.4619
$\phi^{avg}_{13,6}$	-0.7487	-0.7490	-0.7492	0.7387	0.7006
$\phi^{avg}_{17,6}$	-0.6587	-0.6526	-0.6458	0.5683	0.5392
$\phi^{avg}_{23,6}$	-0.6969	-0.7133	-0.7316	0.9041	0.8439
$\phi^{avg}_{24,6}$	0.3736	0.3864	0.4005	-0.5349	-0.5683
$\phi^{avg}_{25,6}$	-0.0152	-0.0213	-0.0280	0.0966	0.1227
$\phi^{avg}_{27,6}$	0.3149	0.3156	0.3163	-0.3191	-0.3028
$\phi^{avg}_{28,6}$	-0.9787	-0.9813	-0.9844	1.0000	1.0000
$\phi^{avg}_{29,6}$	0.2410	0.2402	0.2394	-0.2284	-0.1984
$\phi^{avg}_{30,6}$	-0.5207	-0.5182	-0.5154	0.4788	0.4697
$\phi^{avg}_{31,6}$	0.6971	0.7001	0.7036	-0.7282	-0.7254
$\phi^{avg}_{33,6}$	0.4769	0.4759	0.4750	-0.4598	-0.4096
$\phi^{avg}_{37,6}$	0.9430	0.9442	0.9457	-0.9464	-0.9407
$\phi^{avg}_{38,6}$	-0.2062	-0.2066	-0.2071	0.2094	0.1952
$\phi^{avg}_{39,6}$	1.0000	1.0000	1.0000	-0.9830	-0.9501
$\phi^{avg}_{40,6}$	0.1712	0.1692	0.1670	-0.1445	-0.0909
$\phi^{avg}_{41,6}$	-0.7331	-0.7342	-0.7354	0.7382	0.7094
$\phi^{avg}_{43,6}$	0.6134	0.6126	0.6119	-0.5970	-0.5552
$\phi^{avg}_{44,6}$	0.0039	0.0045	0.0053	-0.0130	-0.0096
$\phi^{avg}_{45,6}$	-0.2974	-0.2973	-0.2972	0.2932	0.2450
$\phi^{avg}_{5,7}$	-0.3474	-0.3489	-0.3502	-0.3571	-0.3590
$\phi^{avg}_{9,7}$	0.1233	0.1186	0.1217	0.1168	0.1226
$\phi^{avg}_{11,7}$	-0.5831	-0.5880	-0.5888	-0.6042	-0.5997
$\phi^{avg}_{12,7}$	-0.7005	-0.7044	-0.7076	-0.7258	-0.7293

Continued on next page

Table C.2 – continued from previous page

Component	Undamaged	Damage 1	Damage 2	Damage 3	Damage 4
$\phi^{avg}_{13,7}$	-0.2326	-0.2294	-0.2316	-0.2285	-0.2323
$\phi^{avg}_{17,7}$	-0.5323	-0.5357	-0.5393	-0.5570	-0.5645
$\phi^{avg}_{23,7}$	0.5518	0.5573	0.5593	0.5786	0.5783
$\phi^{avg}_{24,7}$	0.3530	0.3419	0.3390	0.3030	0.2807
$\phi^{avg}_{25,7}$	-0.7859	-0.7783	-0.7757	-0.7486	-0.7287
$\phi^{avg}_{27,7}$	-0.2183	-0.2172	-0.2160	-0.2097	-0.2044
$\phi^{avg}_{28,7}$	0.1992	0.1970	0.1951	0.1844	0.1767
$\phi^{avg}_{29,7}$	0.0839	0.0857	0.0869	0.0945	0.1005
$\phi^{avg}_{30,7}$	0.8514	0.8427	0.8403	0.8114	0.7908
$\phi^{avg}_{31,7}$	-0.0394	-0.0382	-0.0364	-0.0289	-0.0233
$\phi^{avg}_{33,7}$	0.6471	0.6496	0.6503	0.6587	0.6648
$\phi^{avg}_{37,7}$	-0.8261	-0.8177	-0.8146	-0.7845	-0.7624
$\phi^{avg}_{38,7}$	-0.4385	-0.4380	-0.4383	-0.4383	-0.4393
$\phi^{avg}_{39,7}$	-0.3449	-0.3432	-0.3393	-0.3244	-0.3116
$\phi^{avg}_{40,7}$	1.0000	1.0000	1.0000	1.0000	1.0000
$\phi^{avg}_{41,7}$	-0.4910	-0.4913	-0.4936	-0.5000	-0.4999
$\phi^{avg}_{43,7}$	0.2643	0.2678	0.2698	0.2842	0.2947
$\phi^{avg}_{44,7}$	0.0139	0.0134	0.0130	0.0104	0.0081
$\phi^{avg}_{45,7}$	-0.5148	-0.5171	-0.5173	-0.5249	-0.5342
$\phi^{avg}_{5,8}$	0.1704	0.1685	0.1671	0.1448	0.1465
$\phi^{avg}_{9,8}$	0.8234	0.7853	0.7557	0.4607	0.4674
$\phi^{avg}_{11,8}$	0.6283	0.6183	0.6102	0.5213	0.5019
$\phi^{avg}_{12,8}$	0.4403	0.4383	0.4365	0.3975	0.4070
$\phi^{avg}_{13,8}$	-0.9388	-0.8951	-0.8609	-0.5472	-0.5237
$\phi^{avg}_{17,8}$	0.3719	0.3690	0.3669	0.3308	0.3516
$\phi^{avg}_{23,8}$	-0.4153	-0.4303	-0.4416	-0.5369	-0.5117
$\phi^{avg}_{24,8}$	1.0000	1.0000	1.0000	1.0000	1.0000
$\phi^{avg}_{25,8}$	-0.7363	-0.7318	-0.7284	-0.7399	-0.7113
$\phi^{avg}_{27,8}$	0.0561	0.0463	0.0386	-0.0434	-0.0411
$\phi^{avg}_{28,8}$	-0.1508	-0.1361	-0.1241	0.0203	0.0084
$\phi^{avg}_{29,8}$	-0.2397	-0.2361	-0.2333	-0.1990	-0.2070
$\phi^{avg}_{30,8}$	0.7589	0.7511	0.7453	0.7075	0.7102
$\phi^{avg}_{31,8}$	-0.0422	-0.0454	-0.0481	-0.0881	-0.0834
$\phi^{avg}_{33,8}$	-0.4650	-0.4483	-0.4352	-0.3013	-0.3095
$\phi^{avg}_{37,8}$	-0.7817	-0.7720	-0.7648	-0.7212	-0.7182
$\phi^{avg}_{38,8}$	0.2686	0.2516	0.2384	0.1058	0.1127

Continued on next page

Table C.2 – continued from previous page

Component	Undamaged	Damage 1	Damage 2	Damage 3	Damage 4
$\phi^{avg}_{39,8}$	0.2023	0.1825	0.1665	-0.0101	-0.0172
$\phi^{avg}_{40,8}$	-0.3336	-0.3150	-0.3002	-0.1429	-0.1518
$\phi^{avg}_{41,8}$	0.1260	0.1244	0.1231	0.1129	0.1006
$\phi^{avg}_{43,8}$	-0.4963	-0.4849	-0.4761	-0.3864	-0.3964
$\phi^{avg}_{44,8}$	0.2115	0.2022	0.1950	0.1389	0.1306
$\phi^{avg}_{45,8}$	0.6308	0.6060	0.5864	0.3929	0.4013

TABLE C.3: Standard deviations of the measured mode shape components for all cases of damage where the experimental substructure represented member 27

Component	Undamaged	Damage 1	Damage 2	Damage 3	Damage 4
$\sigma_{5,1}$	0.0002	0.0001	0.0001	0.0002	0.0005
$\sigma_{9,1}$	0.0001	0.0002	0.0002	0.0003	0.0008
$\sigma_{11,1}$	0.0001	0.0002	0.0002	0.0007	0.0014
$\sigma_{12,1}$	0.0001	0.0001	0.0001	0.0002	0.0004
$\sigma_{13,1}$	0.0003	0.0002	0.0003	0.0009	0.0015
$\sigma_{17,1}$	0.0001	0.0002	0.0002	0.0001	0.0002
$\sigma_{23,1}$	0.0002	0.0003	0.0006	0.0008	0.0017
$\sigma_{24,1}$	0.0001	0.0004	0.0006	0.0005	0.0010
$\sigma_{25,1}$	0.0002	0.0001	0.0002	0.0004	0.0008
$\sigma_{27,1}$	0.0001	0.0001	0.0002	0.0001	0.0003
$\sigma_{28,1}$	0.0001	0.0001	0.0003	0.0004	0.0007
$\sigma_{29,1}$	0.0001	0.0001	0.0002	0.0001	0.0003
$\sigma_{30,1}$	0.0001	0.0001	0.0003	0.0003	0.0007
$\sigma_{31,1}$	0.0002	0.0002	0.0003	0.0003	0.0005
$\sigma_{33,1}$	0.0001	0.0002	0.0003	0.0001	0.0005
$\sigma_{37,1}$	0.0001	0.0002	0.0002	0.0001	0.0003
$\sigma_{38,1}$	0.0002	0.0001	0.0003	0.0001	0.0003
$\sigma_{39,1}$	0.0002	0.0003	0.0003	0.0004	0.0008
$\sigma_{40,1}$	0.0001	0.0001	0.0003	0.0002	0.0003
$\sigma_{41,1}$	0.0001	0.0002	0.0002	0.0001	0.0002
$\sigma_{43,1}$	0.0001	0.0001	0.0003	0.0002	0.0004
$\sigma_{44,1}$	0.0001	0.0001	0.0002	0.0001	0.0003
$\sigma_{45,1}$	0.0003	0.0001	0.0004	0.0002	0.0004

Continued on next page

Table C.3 – continued from previous page

Component	Undamaged	Damage 1	Damage 2	Damage 3	Damage 4
$\sigma_{5,2}$	0.0001	0.0001	0.0001	0.0002	0.0002
$\sigma_{9,2}$	0.0001	0.0001	0.0000	0.0003	0.0003
$\sigma_{11,2}$	0.0001	0.0001	0.0001	0.0007	0.0008
$\sigma_{12,2}$	0.0001	0.0001	0.0001	0.0003	0.0002
$\sigma_{13,2}$	0.0002	0.0002	0.0002	0.0014	0.0014
$\sigma_{17,2}$	0.0001	0.0000	0.0001	0.0003	0.0003
$\sigma_{23,2}$	0.0001	0.0002	0.0003	0.0021	0.0021
$\sigma_{24,2}$	0.0001	0.0003	0.0002	0.0027	0.0027
$\sigma_{25,2}$	0.0001	0.0001	0.0001	0.0004	0.0004
$\sigma_{27,2}$	0.0001	0.0002	0.0001	0.0002	0.0002
$\sigma_{28,2}$	0.0001	0.0001	0.0001	0.0006	0.0007
$\sigma_{29,2}$	0.0001	0.0001	0.0001	0.0001	0.0001
$\sigma_{30,2}$	0.0001	0.0002	0.0001	0.0012	0.0012
$\sigma_{31,2}$	0.0001	0.0002	0.0001	0.0012	0.0012
$\sigma_{33,2}$	0.0001	0.0001	0.0001	0.0002	0.0003
$\sigma_{37,2}$	0.0001	0.0001	0.0001	0.0007	0.0007
$\sigma_{38,2}$	0.0001	0.0001	0.0001	0.0005	0.0005
$\sigma_{39,2}$	0.0001	0.0002	0.0001	0.0016	0.0016
$\sigma_{40,2}$	0.0001	0.0001	0.0001	0.0002	0.0001
$\sigma_{41,2}$	0.0001	0.0000	0.0001	0.0003	0.0003
$\sigma_{43,2}$	0.0001	0.0001	0.0001	0.0001	0.0002
$\sigma_{44,2}$	0.0001	0.0001	0.0001	0.0004	0.0004
$\sigma_{45,2}$	0.0001	0.0002	0.0001	0.0004	0.0004
$\sigma_{5,3}$	0.0001	0.0001	0.0002	0.0004	0.0003
$\sigma_{9,3}$	0.0002	0.0001	0.0002	0.0005	0.0004
$\sigma_{11,3}$	0.0002	0.0001	0.0005	0.0002	0.0002
$\sigma_{12,3}$	0.0001	0.0001	0.0002	0.0003	0.0003
$\sigma_{13,3}$	0.0004	0.0001	0.0009	0.0005	0.0004
$\sigma_{17,3}$	0.0002	0.0001	0.0003	0.0004	0.0003
$\sigma_{23,3}$	0.0003	0.0002	0.0007	0.0014	0.0011
$\sigma_{24,3}$	0.0002	0.0002	0.0013	0.0036	0.0031
$\sigma_{25,3}$	0.0003	0.0001	0.0005	0.0001	0.0001
$\sigma_{27,3}$	0.0000	0.0001	0.0002	0.0004	0.0004
$\sigma_{28,3}$	0.0001	0.0002	0.0005	0.0016	0.0013
$\sigma_{29,3}$	0.0001	0.0001	0.0002	0.0007	0.0006
$\sigma_{30,3}$	0.0001	0.0002	0.0008	0.0026	0.0022

Continued on next page

Table C.3 – continued from previous page

Component	Undamaged	Damage 1	Damage 2	Damage 3	Damage 4
$\sigma_{31,3}$	0.0003	0.0002	0.0008	0.0025	0.0022
$\sigma_{33,3}$	0.0001	0.0001	0.0004	0.0014	0.0012
$\sigma_{37,3}$	0.0002	0.0001	0.0005	0.0015	0.0013
$\sigma_{38,3}$	0.0001	0.0001	0.0005	0.0014	0.0013
$\sigma_{39,3}$	0.0002	0.0001	0.0009	0.0019	0.0016
$\sigma_{40,3}$	0.0001	0.0001	0.0002	0.0005	0.0004
$\sigma_{41,3}$	0.0001	0.0001	0.0003	0.0007	0.0006
$\sigma_{43,3}$	0.0001	0.0001	0.0003	0.0010	0.0009
$\sigma_{44,3}$	0.0001	0.0001	0.0004	0.0014	0.0012
$\sigma_{45,3}$	0.0001	0.0001	0.0005	0.0012	0.0010
$\sigma_{5,4}$	0.0003	0.0001	0.0001	0.0002	0.0002
$\sigma_{9,4}$	0.0003	0.0004	0.0001	0.0005	0.0006
$\sigma_{11,4}$	0.0001	0.0005	0.0001	0.0007	0.0008
$\sigma_{12,4}$	0.0003	0.0001	0.0001	0.0003	0.0004
$\sigma_{13,4}$	0.0002	0.0001	0.0001	0.0001	0.0003
$\sigma_{17,4}$	0.0003	0.0002	0.0002	0.0003	0.0004
$\sigma_{23,4}$	0.0004	0.0007	0.0004	0.0013	0.0016
$\sigma_{24,4}$	0.0006	0.0005	0.0004	0.0015	0.0018
$\sigma_{25,4}$	0.0002	0.0002	0.0001	0.0007	0.0007
$\sigma_{27,4}$	0.0005	0.0006	0.0001	0.0001	0.0001
$\sigma_{28,4}$	0.0004	0.0002	0.0002	0.0008	0.0008
$\sigma_{29,4}$	0.0004	0.0005	0.0001	0.0002	0.0002
$\sigma_{30,4}$	0.0002	0.0002	0.0000	0.0002	0.0002
$\sigma_{31,4}$	0.0001	0.0001	0.0001	0.0003	0.0003
$\sigma_{33,4}$	0.0003	0.0002	0.0001	0.0001	0.0002
$\sigma_{37,4}$	0.0001	0.0001	0.0001	0.0003	0.0003
$\sigma_{38,4}$	0.0002	0.0003	0.0001	0.0004	0.0005
$\sigma_{39,4}$	0.0003	0.0002	0.0001	0.0002	0.0003
$\sigma_{40,4}$	0.0005	0.0005	0.0001	0.0003	0.0004
$\sigma_{41,4}$	0.0002	0.0002	0.0001	0.0003	0.0004
$\sigma_{43,4}$	0.0004	0.0005	0.0001	0.0001	0.0000
$\sigma_{44,4}$	0.0002	0.0003	0.0001	0.0002	0.0002
$\sigma_{45,4}$	0.0003	0.0005	0.0002	0.0005	0.0005
$\sigma_{5,5}$	0.0002	0.0004	0.0005	0.0017	0.0009
$\sigma_{9,5}$	0.0005	0.0013	0.0023	0.0065	0.0030
$\sigma_{11,5}$	0.0004	0.0014	0.0030	0.0080	0.0036

Continued on next page

Table C.3 – continued from previous page

Component	Undamaged	Damage 1	Damage 2	Damage 3	Damage 4
$\sigma_{12,5}$	0.0001	0.0004	0.0008	0.0019	0.0008
$\sigma_{13,5}$	0.0001	0.0001	0.0003	0.0003	0.0006
$\sigma_{17,5}$	0.0003	0.0004	0.0007	0.0020	0.0009
$\sigma_{23,5}$	0.0008	0.0019	0.0032	0.0090	0.0041
$\sigma_{24,5}$	0.0006	0.0015	0.0025	0.0070	0.0033
$\sigma_{25,5}$	0.0004	0.0011	0.0022	0.0057	0.0026
$\sigma_{27,5}$	0.0001	0.0003	0.0006	0.0014	0.0006
$\sigma_{28,5}$	0.0004	0.0010	0.0021	0.0056	0.0026
$\sigma_{29,5}$	0.0001	0.0002	0.0004	0.0006	0.0002
$\sigma_{30,5}$	0.0001	0.0003	0.0003	0.0007	0.0003
$\sigma_{31,5}$	0.0004	0.0013	0.0025	0.0065	0.0030
$\sigma_{33,5}$	0.0002	0.0006	0.0010	0.0023	0.0010
$\sigma_{37,5}$	0.0003	0.0011	0.0022	0.0059	0.0027
$\sigma_{38,5}$	0.0001	0.0004	0.0005	0.0012	0.0006
$\sigma_{39,5}$	0.0001	0.0003	0.0002	0.0007	0.0003
$\sigma_{40,5}$	0.0002	0.0004	0.0003	0.0001	0.0003
$\sigma_{41,5}$	0.0002	0.0006	0.0012	0.0029	0.0014
$\sigma_{43,5}$	0.0002	0.0006	0.0012	0.0029	0.0013
$\sigma_{44,5}$	0.0001	0.0002	0.0003	0.0009	0.0004
$\sigma_{45,5}$	0.0002	0.0004	0.0007	0.0019	0.0008
$\sigma_{5,6}$	0.0001	0.0001	0.0003	0.0020	0.0022
$\sigma_{9,6}$	0.0001	0.0002	0.0008	0.0041	0.0035
$\sigma_{11,6}$	0.0004	0.0006	0.0019	0.0123	0.0118
$\sigma_{12,6}$	0.0004	0.0005	0.0015	0.0098	0.0099
$\sigma_{13,6}$	0.0001	0.0001	0.0003	0.0035	0.0037
$\sigma_{17,6}$	0.0003	0.0004	0.0015	0.0097	0.0096
$\sigma_{23,6}$	0.0005	0.0007	0.0025	0.0149	0.0147
$\sigma_{24,6}$	0.0005	0.0006	0.0019	0.0115	0.0125
$\sigma_{25,6}$	0.0002	0.0003	0.0010	0.0068	0.0074
$\sigma_{27,6}$	0.0000	0.0000	0.0000	0.0007	0.0008
$\sigma_{28,6}$	0.0001	0.0001	0.0001	0.0016	0.0012
$\sigma_{29,6}$	0.0000	0.0001	0.0002	0.0017	0.0019
$\sigma_{30,6}$	0.0001	0.0002	0.0007	0.0054	0.0053
$\sigma_{31,6}$	0.0001	0.0001	0.0002	0.0006	0.0009
$\sigma_{33,6}$	0.0001	0.0001	0.0003	0.0029	0.0031
$\sigma_{37,6}$	0.0001	0.0001	0.0003	0.0030	0.0026

Continued on next page

Table C.3 – continued from previous page

Component	Undamaged	Damage 1	Damage 2	Damage 3	Damage 4
$\sigma_{38,6}$	0.0001	0.0001	0.0001	0.0007	0.0005
$\sigma_{39,6}$	0.0001	0.0001	0.0005	0.0049	0.0051
$\sigma_{40,6}$	0.0002	0.0001	0.0004	0.0025	0.0028
$\sigma_{41,6}$	0.0001	0.0001	0.0002	0.0019	0.0021
$\sigma_{43,6}$	0.0001	0.0001	0.0004	0.0031	0.0033
$\sigma_{44,6}$	0.0001	0.0000	0.0002	0.0009	0.0007
$\sigma_{45,6}$	0.0002	0.0002	0.0002	0.0019	0.0020
$\sigma_{5,7}$	0.0007	0.0023	0.0015	0.0020	0.0029
$\sigma_{9,7}$	0.0003	0.0201	0.0010	0.0008	0.0013
$\sigma_{11,7}$	0.0016	0.0125	0.0036	0.0035	0.0059
$\sigma_{12,7}$	0.0020	0.0051	0.0042	0.0048	0.0076
$\sigma_{13,7}$	0.0001	0.0124	0.0004	0.0006	0.0006
$\sigma_{17,7}$	0.0019	0.0026	0.0039	0.0049	0.0075
$\sigma_{23,7}$	0.0020	0.0104	0.0044	0.0050	0.0075
$\sigma_{24,7}$	0.0031	0.0198	0.0063	0.0078	0.0125
$\sigma_{25,7}$	0.0020	0.0106	0.0043	0.0050	0.0087
$\sigma_{27,7}$	0.0004	0.0017	0.0009	0.0013	0.0021
$\sigma_{28,7}$	0.0009	0.0018	0.0019	0.0025	0.0040
$\sigma_{29,7}$	0.0007	0.0019	0.0014	0.0018	0.0029
$\sigma_{30,7}$	0.0021	0.0136	0.0047	0.0058	0.0096
$\sigma_{31,7}$	0.0006	0.0024	0.0013	0.0018	0.0028
$\sigma_{33,7}$	0.0011	0.0063	0.0020	0.0023	0.0038
$\sigma_{37,7}$	0.0022	0.0104	0.0049	0.0063	0.0101
$\sigma_{38,7}$	0.0002	0.0010	0.0003	0.0003	0.0003
$\sigma_{39,7}$	0.0011	0.0076	0.0024	0.0031	0.0051
$\sigma_{40,7}$	0.0005	0.0033	0.0009	0.0007	0.0011
$\sigma_{41,7}$	0.0008	0.0039	0.0017	0.0019	0.0029
$\sigma_{43,7}$	0.0013	0.0043	0.0029	0.0035	0.0055
$\sigma_{44,7}$	0.0002	0.0004	0.0004	0.0005	0.0007
$\sigma_{45,7}$	0.0008	0.0072	0.0018	0.0018	0.0031
$\sigma_{5,8}$	0.0002	0.0002	0.0002	0.0045	0.0011
$\sigma_{9,8}$	0.0015	0.0015	0.0014	0.0152	0.0068
$\sigma_{11,8}$	0.0004	0.0002	0.0002	0.0044	0.0031
$\sigma_{12,8}$	0.0007	0.0005	0.0005	0.0145	0.0027
$\sigma_{13,8}$	0.0017	0.0016	0.0015	0.0098	0.0033
$\sigma_{17,8}$	0.0005	0.0004	0.0004	0.0188	0.0045

Continued on next page

Table C.3 – continued from previous page

Component	Undamaged	Damage 1	Damage 2	Damage 3	Damage 4
$\sigma_{23,8}$	0.0018	0.0016	0.0015	0.0108	0.0049
$\sigma_{24,8}$	0.0016	0.0015	0.0014	0.0062	0.0057
$\sigma_{25,8}$	0.0008	0.0008	0.0007	0.0223	0.0030
$\sigma_{27,8}$	0.0006	0.0006	0.0006	0.0022	0.0025
$\sigma_{28,8}$	0.0009	0.0008	0.0009	0.0089	0.0050
$\sigma_{29,8}$	0.0001	0.0001	0.0001	0.0054	0.0006
$\sigma_{30,8}$	0.0006	0.0006	0.0006	0.0050	0.0019
$\sigma_{31,8}$	0.0003	0.0003	0.0003	0.0052	0.0004
$\sigma_{33,8}$	0.0004	0.0004	0.0005	0.0028	0.0034
$\sigma_{37,8}$	0.0004	0.0005	0.0005	0.0024	0.0027
$\sigma_{38,8}$	0.0007	0.0008	0.0008	0.0025	0.0032
$\sigma_{39,8}$	0.0012	0.0011	0.0011	0.0052	0.0018
$\sigma_{40,8}$	0.0008	0.0008	0.0008	0.0030	0.0040
$\sigma_{41,8}$	0.0002	0.0001	0.0001	0.0050	0.0007
$\sigma_{43,8}$	0.0001	0.0000	0.0002	0.0055	0.0018
$\sigma_{44,8}$	0.0003	0.0003	0.0003	0.0088	0.0011
$\sigma_{45,8}$	0.0007	0.0008	0.0009	0.0036	0.0017

TABLE C.4: Average natural frequencies and standard deviations for the first eight natural frequencies for all states of damage where the experimental substructure represented member 31

	Undamaged		Damage 1		Damage 2		Damage 3		Damage 4	
Mode	f_n^{avg}	σ_n	f_n^{avg}	σ_n	f_n^{avg}	σ_n	f_n^{avg}	σ_n	f_n^{avg}	σ_n
1	0.581	0	0.581	0	0.581	0	0.580	0.001	0.571	0.001
2	2.005	0	2.005	0	2.005	0	2.004	0.001	1.980	0
3	2.792	0	2.791	0	2.791	0	2.784	0	2.747	0
4	4.422	0.001	4.414	0.001	4.407	0.001	4.310	0.007	4.296	0.002
5	6.219	0.003	6.211	0	6.202	0.004	6.132	0.012	6.120	0.009
6	7.747	0	7.743	0	7.740	0	7.723	0.003	7.575	0.003
7	9.308	0.001	9.301	0.001	9.297	0.004	9.256	0.003	9.198	0.015
8	10.616	0.001	10.607	0.001	10.592	0.003	10.417	0.006	10.255	0.002

TABLE C.5: Average of the measured mode shape components for all cases of damage where the experimental substructure represented member 31

Component	Undamaged	Damage 1	Damage 2	Damage 3	Damage 4
$\phi_{5,1}^{avg}$	-0.1832	-0.1832	-0.1832	-0.1828	-0.1809
$\phi_{9,1}^{avg}$	0.2598	0.2597	0.2597	0.2592	0.2560
$\phi_{11,1}^{avg}$	0.5025	0.5024	0.5023	0.5014	0.4958
$\phi_{12,1}^{avg}$	-0.1550	-0.1550	-0.1550	-0.1548	-0.1538
$\phi_{13,1}^{avg}$	0.7101	0.7100	0.7098	0.7088	0.7018
$\phi_{17,1}^{avg}$	-0.1347	-0.1347	-0.1348	-0.1345	-0.1343
$\phi_{23,1}^{avg}$	0.8686	0.8685	0.8683	0.8674	0.8608
$\phi_{24,1}^{avg}$	0.9675	0.9673	0.9673	0.9666	0.9623
$\phi_{25,1}^{avg}$	0.9658	0.9659	0.9660	0.9671	0.9731
$\phi_{27,1}^{avg}$	-0.0423	-0.0423	-0.0424	-0.0427	-0.0450
$\phi_{28,1}^{avg}$	0.8654	0.8657	0.8658	0.8682	0.8821
$\phi_{29,1}^{avg}$	-0.0220	-0.0219	-0.0220	-0.0224	-0.0252
$\phi_{30,1}^{avg}$	0.7058	0.7056	0.7051	0.6977	0.7156
$\phi_{31,1}^{avg}$	0.4981	0.4979	0.4975	0.4924	0.5038
$\phi_{33,1}^{avg}$	0.0063	0.0063	0.0062	0.0055	0.0023
$\phi_{37,1}^{avg}$	0.2562	0.2561	0.2559	0.2533	0.2589
$\phi_{38,1}^{avg}$	-0.0890	-0.0890	-0.0890	-0.0883	-0.0857
$\phi_{39,1}^{avg}$	1.0000	1.0000	1.0000	1.0000	1.0000
$\phi_{40,1}^{avg}$	-0.1740	-0.1740	-0.1739	-0.1727	-0.1804
$\phi_{41,1}^{avg}$	-0.0270	-0.0270	-0.0270	-0.0267	-0.0259
$\phi_{43,1}^{avg}$	-0.1498	-0.1498	-0.1499	-0.1486	-0.1569
$\phi_{44,1}^{avg}$	-0.1122	-0.1122	-0.1122	-0.1113	-0.1081
$\phi_{45,1}^{avg}$	-0.0657	-0.0656	-0.0656	-0.0651	-0.0631
$\phi_{5,2}^{avg}$	0.3718	0.3714	0.3710	0.3673	0.3536
$\phi_{9,2}^{avg}$	-0.5746	-0.5741	-0.5735	-0.5678	-0.5486
$\phi_{11,2}^{avg}$	-0.9150	-0.9141	-0.9132	-0.9044	-0.8842
$\phi_{12,2}^{avg}$	0.2581	0.2578	0.2575	0.2550	0.2409
$\phi_{13,2}^{avg}$	-0.9942	-0.9932	-0.9922	-0.9831	-0.9722
$\phi_{17,2}^{avg}$	0.2119	0.2117	0.2114	0.2093	0.1931
$\phi_{23,2}^{avg}$	-0.7986	-0.7979	-0.7971	-0.7904	-0.7962
$\phi_{24,2}^{avg}$	-0.3830	-0.3828	-0.3825	-0.3803	-0.4042
$\phi_{25,2}^{avg}$	0.5708	0.5700	0.5691	0.5612	0.5303
$\phi_{27,2}^{avg}$	0.2859	0.2857	0.2854	0.2825	0.2454
$\phi_{28,2}^{avg}$	0.8997	0.8985	0.8972	0.8857	0.8729

Continued on next page

Table C.5 – continued from previous page

Component	Undamaged	Damage 1	Damage 2	Damage 3	Damage 4
$\phi^{avg}_{29,2}$	0.3614	0.3611	0.3607	0.3573	0.3142
$\phi^{avg}_{30,2}$	1.0000	1.0000	1.0000	1.0000	1.0000
$\phi^{avg}_{31,2}$	0.8442	0.8442	0.8441	0.8435	0.8358
$\phi^{avg}_{33,2}$	0.5081	0.5077	0.5073	0.5031	0.4512
$\phi^{avg}_{37,2}$	0.4716	0.4716	0.4715	0.4711	0.4653
$\phi^{avg}_{38,2}$	0.4995	0.4990	0.4984	0.4930	0.4674
$\phi^{avg}_{39,2}$	0.1225	0.1221	0.1218	0.1186	0.0831
$\phi^{avg}_{40,2}$	0.2229	0.2225	0.2220	0.2179	0.1669
$\phi^{avg}_{41,2}$	0.2628	0.2625	0.2622	0.2593	0.2414
$\phi^{avg}_{43,2}$	0.3481	0.3477	0.3471	0.3426	0.2864
$\phi^{avg}_{44,2}$	0.4713	0.4708	0.4703	0.4650	0.4420
$\phi^{avg}_{45,2}$	0.4491	0.4487	0.4481	0.4434	0.4181
$\phi^{avg}_{5,3}$	0.2348	0.2349	0.2350	0.2372	0.2404
$\phi^{avg}_{9,3}$	-0.2360	-0.2365	-0.2367	-0.2424	-0.2530
$\phi^{avg}_{11,3}$	-0.0054	-0.0062	-0.0072	-0.0200	-0.0502
$\phi^{avg}_{12,3}$	0.3947	0.3946	0.3943	0.3920	0.3845
$\phi^{avg}_{13,3}$	0.2962	0.2953	0.2941	0.2788	0.2385
$\phi^{avg}_{17,3}$	0.5130	0.5128	0.5123	0.5079	0.4949
$\phi^{avg}_{23,3}$	0.5312	0.5306	0.5296	0.5182	0.4825
$\phi^{avg}_{24,3}$	0.5992	0.5991	0.5987	0.5966	0.5797
$\phi^{avg}_{25,3}$	0.0775	0.0786	0.0800	0.1011	0.1285
$\phi^{avg}_{27,3}$	0.8629	0.8625	0.8620	0.8557	0.8472
$\phi^{avg}_{28,3}$	-0.3362	-0.3346	-0.3326	-0.3039	-0.2731
$\phi^{avg}_{29,3}$	0.8621	0.8618	0.8613	0.8555	0.8554
$\phi^{avg}_{30,3}$	-0.5980	-0.5994	-0.6007	-0.6265	-0.5784
$\phi^{avg}_{31,3}$	-0.6150	-0.6161	-0.6171	-0.6378	-0.5772
$\phi^{avg}_{33,3}$	0.7810	0.7805	0.7801	0.7726	0.7916
$\phi^{avg}_{37,3}$	-0.3835	-0.3841	-0.3846	-0.3960	-0.3569
$\phi^{avg}_{38,3}$	0.5743	0.5743	0.5743	0.5753	0.5702
$\phi^{avg}_{39,3}$	0.4851	0.4856	0.4861	0.4954	0.5017
$\phi^{avg}_{40,3}$	1.0000	1.0000	1.0000	1.0000	1.0000
$\phi^{avg}_{41,3}$	0.4369	0.4370	0.4366	0.4360	0.4296
$\phi^{avg}_{43,3}$	0.8190	0.8189	0.8187	0.8173	0.8385
$\phi^{avg}_{44,3}$	0.6345	0.6345	0.6344	0.6340	0.6214
$\phi^{avg}_{45,3}$	0.5501	0.5502	0.5501	0.5510	0.5468
$\phi^{avg}_{5,4}$	-0.0947	-0.0937	-0.0929	-0.0823	-0.0824

Continued on next page

Table C.5 – continued from previous page

Component	Undamaged	Damage 1	Damage 2	Damage 3	Damage 4
$\phi_{9,4}^{avg}$	0.4373	0.4335	0.4305	0.3905	0.3869
$\phi_{11,4}^{avg}$	0.9485	0.9421	0.9372	0.8708	0.8624
$\phi_{12,4}^{avg}$	0.3122	0.3106	0.3094	0.2933	0.2888
$\phi_{13,4}^{avg}$	0.8653	0.8619	0.8593	0.8253	0.8196
$\phi_{17,4}^{avg}$	0.4178	0.4163	0.4152	0.4002	0.3949
$\phi_{23,4}^{avg}$	0.2287	0.2317	0.2341	0.2683	0.2702
$\phi_{24,4}^{avg}$	-0.5395	-0.5322	-0.5264	-0.4456	-0.4366
$\phi_{25,4}^{avg}$	-0.8149	-0.8162	-0.8175	-0.8339	-0.8338
$\phi_{27,4}^{avg}$	0.1351	0.1372	0.1389	0.1644	0.1648
$\phi_{28,4}^{avg}$	-0.1506	-0.1610	-0.1696	-0.2893	-0.3035
$\phi_{29,4}^{avg}$	0.1498	0.1510	0.1524	0.1701	0.1702
$\phi_{30,4}^{avg}$	0.6314	0.6348	0.6382	0.6837	0.6898
$\phi_{31,4}^{avg}$	1.0000	1.0000	1.0000	1.0000	1.0000
$\phi_{33,4}^{avg}$	0.4275	0.4274	0.4274	0.4281	0.4261
$\phi_{37,4}^{avg}$	0.7034	0.7025	0.7016	0.6897	0.6882
$\phi_{38,4}^{avg}$	0.2389	0.2372	0.2357	0.2165	0.2111
$\phi_{39,4}^{avg}$	-0.9119	-0.9063	-0.9020	-0.8413	-0.8327
$\phi_{40,4}^{avg}$	0.0956	0.0952	0.0950	0.0930	0.0907
$\phi_{41,4}^{avg}$	0.0731	0.0738	0.0743	0.0819	0.0802
$\phi_{43,4}^{avg}$	0.4147	0.4129	0.4113	0.3904	0.3860
$\phi_{44,4}^{avg}$	0.4148	0.4123	0.4102	0.3820	0.3749
$\phi_{45,4}^{avg}$	0.0868	0.0867	0.0867	0.0862	0.0832
$\phi_{5,5}^{avg}$	-0.3096	-0.3068	-0.3042	-0.2854	-0.2793
$\phi_{9,5}^{avg}$	0.8665	0.8609	0.8565	0.8242	0.8151
$\phi_{11,5}^{avg}$	1.0000	1.0000	1.0000	1.0000	1.0000
$\phi_{12,5}^{avg}$	0.0027	0.0070	0.0111	0.0404	0.0501
$\phi_{13,5}^{avg}$	0.0974	0.1066	0.1132	0.1635	0.1765
$\phi_{17,5}^{avg}$	-0.0941	-0.0884	-0.0831	-0.0441	-0.0318
$\phi_{23,5}^{avg}$	-0.8899	-0.8817	-0.8751	-0.8231	-0.8100
$\phi_{24,5}^{avg}$	-0.9185	-0.9209	-0.9227	-0.9353	-0.9369
$\phi_{25,5}^{avg}$	0.7378	0.7305	0.7249	0.6786	0.6666
$\phi_{27,5}^{avg}$	0.1192	0.1160	0.1128	0.0877	0.0852
$\phi_{28,5}^{avg}$	0.8354	0.8428	0.8502	0.9034	0.9145
$\phi_{29,5}^{avg}$	0.3437	0.3392	0.3350	0.3027	0.2976
$\phi_{30,5}^{avg}$	0.0773	0.0704	0.0644	0.0191	0.0125
$\phi_{31,5}^{avg}$	-0.7547	-0.7465	-0.7397	-0.6838	-0.6754

Continued on next page

Table C.5 – continued from previous page

Component	Undamaged	Damage 1	Damage 2	Damage 3	Damage 4
$\phi^{avg}_{33,5}$	0.3047	0.3037	0.3011	0.2832	0.2790
$\phi^{avg}_{37,5}$	-0.7792	-0.7685	-0.7594	-0.6866	-0.6760
$\phi^{avg}_{38,5}$	0.1744	0.1753	0.1775	0.1927	0.1992
$\phi^{avg}_{39,5}$	-0.0243	-0.0354	-0.0449	-0.1180	-0.1347
$\phi^{avg}_{40,5}$	0.6406	0.6379	0.6323	0.5900	0.5817
$\phi^{avg}_{41,5}$	-0.3861	-0.3807	-0.3759	-0.3409	-0.3300
$\phi^{avg}_{43,5}$	0.1219	0.1252	0.1270	0.1426	0.1426
$\phi^{avg}_{44,5}$	0.1290	0.1321	0.1354	0.1611	0.1698
$\phi^{avg}_{45,5}$	-0.0992	-0.0979	-0.0955	-0.0785	-0.0715
$\phi^{avg}_{5,6}$	-0.4700	-0.4704	-0.4706	-0.4719	-0.5026
$\phi^{avg}_{9,6}$	0.8965	0.8970	0.8973	0.8996	0.8998
$\phi^{avg}_{11,6}$	0.2707	0.2717	0.2725	0.2770	0.2481
$\phi^{avg}_{12,6}$	-0.5724	-0.5725	-0.5726	-0.5729	-0.6373
$\phi^{avg}_{13,6}$	-0.7487	-0.7485	-0.7483	-0.7470	-0.7604
$\phi^{avg}_{17,6}$	-0.6586	-0.6590	-0.6593	-0.6610	-0.7333
$\phi^{avg}_{23,6}$	-0.6967	-0.6984	-0.6997	-0.7072	-0.7184
$\phi^{avg}_{24,6}$	0.3739	0.3718	0.3700	0.3606	0.3369
$\phi^{avg}_{25,6}$	-0.0154	-0.0134	-0.0115	-0.0018	0.0343
$\phi^{avg}_{27,6}$	0.3148	0.3158	0.3165	0.3207	0.2868
$\phi^{avg}_{28,6}$	-0.9785	-0.9791	-0.9794	-0.9813	-0.9927
$\phi^{avg}_{29,6}$	0.2406	0.2431	0.2449	0.2554	0.2660
$\phi^{avg}_{30,6}$	-0.5228	-0.5103	-0.5006	-0.4481	-0.4258
$\phi^{avg}_{31,6}$	0.6983	0.6903	0.6837	0.6489	0.6852
$\phi^{avg}_{33,6}$	0.4766	0.4780	0.4790	0.4842	0.5609
$\phi^{avg}_{37,6}$	0.9453	0.9305	0.9187	0.8557	0.8601
$\phi^{avg}_{38,6}$	-0.2061	-0.2066	-0.2070	-0.2089	-0.2816
$\phi^{avg}_{39,6}$	1.0000	1.0000	1.0000	1.0000	1.0000
$\phi^{avg}_{40,6}$	0.1702	0.1763	0.1810	0.2064	0.2916
$\phi^{avg}_{41,6}$	-0.7330	-0.7335	-0.7340	-0.7362	-0.7859
$\phi^{avg}_{43,6}$	0.6140	0.6098	0.6064	0.5882	0.6752
$\phi^{avg}_{44,6}$	0.0042	0.0023	0.0009	-0.0067	-0.0928
$\phi^{avg}_{45,6}$	-0.2973	-0.2981	-0.2986	-0.3016	-0.3747
$\phi^{avg}_{5,7}$	-0.3482	-0.3456	-0.3439	-0.3289	-0.2921
$\phi^{avg}_{9,7}$	0.1231	0.1228	0.1227	0.1197	0.0659
$\phi^{avg}_{11,7}$	-0.5846	-0.5797	-0.5766	-0.5496	-0.5279
$\phi^{avg}_{12,7}$	-0.7023	-0.6972	-0.6940	-0.6652	-0.6068

Continued on next page

Table C.5 – continued from previous page

Component	Undamaged	Damage 1	Damage 2	Damage 3	Damage 4
$\phi^{avg}_{13,7}$	-0.2324	-0.2325	-0.2325	-0.2316	-0.1707
$\phi^{avg}_{17,7}$	-0.5340	-0.5307	-0.5286	-0.5096	-0.4646
$\phi^{avg}_{23,7}$	0.5540	0.5483	0.5448	0.5139	0.4942
$\phi^{avg}_{24,7}$	0.3509	0.3505	0.3504	0.3473	0.2817
$\phi^{avg}_{25,7}$	-0.7849	-0.7823	-0.7808	-0.7654	-0.6907
$\phi^{avg}_{27,7}$	-0.2184	-0.2155	-0.2136	-0.1971	-0.1925
$\phi^{avg}_{28,7}$	0.1999	0.1911	0.1858	0.1380	0.1189
$\phi^{avg}_{29,7}$	0.0846	0.0850	0.0852	0.0892	0.0849
$\phi^{avg}_{30,7}$	0.8478	0.8631	0.8726	0.9604	1.0000
$\phi^{avg}_{31,7}$	-0.0380	-0.0438	-0.0474	-0.0810	-0.1213
$\phi^{avg}_{33,7}$	0.6481	0.6447	0.6426	0.6235	0.5818
$\phi^{avg}_{37,7}$	-0.8223	-0.8372	-0.8463	-0.9304	-0.9778
$\phi^{avg}_{38,7}$	-0.4387	-0.4367	-0.4355	-0.4244	-0.4068
$\phi^{avg}_{39,7}$	-0.3448	-0.3402	-0.3374	-0.3131	-0.3190
$\phi^{avg}_{40,7}$	1.0000	1.0000	1.0000	1.0000	0.9660
$\phi^{avg}_{41,7}$	-0.4920	-0.4887	-0.4866	-0.4677	-0.4134
$\phi^{avg}_{43,7}$	0.2662	0.2580	0.2528	0.2055	0.1613
$\phi^{avg}_{44,7}$	0.0141	0.0120	0.0106	-0.0023	-0.0384
$\phi^{avg}_{45,7}$	-0.5154	-0.5118	-0.5095	-0.4892	-0.4649
$\phi^{avg}_{5,8}$	0.1709	0.1773	0.1879	0.2630	0.2000
$\phi^{avg}_{9,8}$	0.8248	0.8217	0.8171	0.5776	0.6612
$\phi^{avg}_{11,8}$	0.6297	0.6434	0.6654	0.7514	0.7171
$\phi^{avg}_{12,8}$	0.4412	0.4538	0.4743	0.5975	0.5218
$\phi^{avg}_{13,8}$	-0.9404	-0.9387	-0.9363	-0.6814	-0.7172
$\phi^{avg}_{17,8}$	0.3723	0.3792	0.3905	0.4368	0.3885
$\phi^{avg}_{23,8}$	-0.4157	-0.4330	-0.4604	-0.6468	-0.6358
$\phi^{avg}_{24,8}$	1.0000	1.0000	1.0000	0.7418	0.7608
$\phi^{avg}_{25,8}$	-0.7365	-0.7327	-0.7261	-0.4441	-0.5003
$\phi^{avg}_{27,8}$	0.0569	0.0631	0.0731	0.1727	0.2303
$\phi^{avg}_{28,8}$	-0.1530	-0.1773	-0.2161	-0.5718	-0.5945
$\phi^{avg}_{29,8}$	-0.2401	-0.2427	-0.2473	-0.2258	-0.1759
$\phi^{avg}_{30,8}$	0.7610	0.7849	0.8222	1.0000	1.0000
$\phi^{avg}_{31,8}$	-0.0420	-0.0433	-0.0455	-0.0788	-0.1050
$\phi^{avg}_{33,8}$	-0.4659	-0.4748	-0.4891	-0.5426	-0.5267
$\phi^{avg}_{37,8}$	-0.7837	-0.8058	-0.8403	-0.9773	-0.9395
$\phi^{avg}_{38,8}$	0.2696	0.2747	0.2830	0.3181	0.3371

Continued on next page

Table C.5 – continued from previous page

Component	Undamaged	Damage 1	Damage 2	Damage 3	Damage 4
$\phi^{avg}_{39,8}$	0.2039	0.2210	0.2478	0.4674	0.5152
$\phi^{avg}_{40,8}$	-0.3343	-0.3395	-0.3482	-0.3882	-0.3900
$\phi^{avg}_{41,8}$	0.1265	0.1347	0.1481	0.2670	0.1848
$\phi^{avg}_{43,8}$	-0.4976	-0.5120	-0.5350	-0.6636	-0.6880
$\phi^{avg}_{44,8}$	0.2117	0.2085	0.2036	0.0978	0.1902
$\phi^{avg}_{45,8}$	0.6325	0.6416	0.6563	0.6691	0.6418

TABLE C.6: Standard deviations of the measured mode shape components for all cases of damage where the experimental substructure represented member 31

Component	Undamaged	Damage 1	Damage 2	Damage 3	Damage 4
$\sigma_{5,1}$	0.0001	0.0001	0.0001	0.0001	0.0003
$\sigma_{9,1}$	0.0001	0.0001	0.0001	0.0002	0.0005
$\sigma_{11,1}$	0.0001	0.0001	0.0002	0.0003	0.0007
$\sigma_{12,1}$	0.0001	0.0001	0.0002	0.0002	0.0002
$\sigma_{13,1}$	0.0001	0.0002	0.0003	0.0003	0.0008
$\sigma_{17,1}$	0.0001	0.0001	0.0002	0.0002	0.0002
$\sigma_{23,1}$	0.0002	0.0001	0.0002	0.0003	0.0006
$\sigma_{24,1}$	0.0001	0.0001	0.0001	0.0007	0.0003
$\sigma_{25,1}$	0.0002	0.0001	0.0002	0.0028	0.0013
$\sigma_{27,1}$	0.0001	0.0001	0.0002	0.0007	0.0002
$\sigma_{28,1}$	0.0002	0.0002	0.0003	0.0039	0.0020
$\sigma_{29,1}$	0.0001	0.0001	0.0001	0.0005	0.0003
$\sigma_{30,1}$	0.0002	0.0002	0.0002	0.0070	0.0020
$\sigma_{31,1}$	0.0001	0.0001	0.0003	0.0048	0.0014
$\sigma_{33,1}$	0.0001	0.0001	0.0002	0.0009	0.0004
$\sigma_{37,1}$	0.0001	0.0001	0.0002	0.0025	0.0007
$\sigma_{38,1}$	0.0001	0.0001	0.0001	0.0006	0.0006
$\sigma_{39,1}$	0.0001	0.0001	0.0001	0.0015	0.0006
$\sigma_{40,1}$	0.0002	0.0001	0.0001	0.0011	0.0006
$\sigma_{41,1}$	0.0001	0.0001	0.0001	0.0001	0.0002
$\sigma_{43,1}$	0.0001	0.0001	0.0003	0.0010	0.0006
$\sigma_{44,1}$	0.0001	0.0001	0.0002	0.0006	0.0006
$\sigma_{45,1}$	0.0001	0.0001	0.0001	0.0004	0.0004

Continued on next page

Table C.6 – continued from previous page

Component	Undamaged	Damage 1	Damage 2	Damage 3	Damage 4
$\sigma_{5,2}$	0.0000	0.0000	0.0000	0.0005	0.0001
$\sigma_{9,2}$	0.0000	0.0000	0.0001	0.0008	0.0001
$\sigma_{11,2}$	0.0000	0.0000	0.0001	0.0012	0.0001
$\sigma_{12,2}$	0.0001	0.0000	0.0001	0.0003	0.0001
$\sigma_{13,2}$	0.0001	0.0000	0.0001	0.0012	0.0001
$\sigma_{17,2}$	0.0001	0.0001	0.0001	0.0003	0.0001
$\sigma_{23,2}$	0.0001	0.0001	0.0001	0.0006	0.0000
$\sigma_{24,2}$	0.0001	0.0001	0.0001	0.0004	0.0001
$\sigma_{25,2}$	0.0000	0.0001	0.0001	0.0023	0.0002
$\sigma_{27,2}$	0.0001	0.0001	0.0001	0.0004	0.0001
$\sigma_{28,2}$	0.0001	0.0001	0.0002	0.0031	0.0002
$\sigma_{29,2}$	0.0001	0.0001	0.0001	0.0003	0.0001
$\sigma_{30,2}$	0.0000	0.0001	0.0001	0.0052	0.0005
$\sigma_{31,2}$	0.0000	0.0001	0.0001	0.0040	0.0004
$\sigma_{33,2}$	0.0001	0.0001	0.0001	0.0002	0.0001
$\sigma_{37,2}$	0.0000	0.0001	0.0001	0.0022	0.0002
$\sigma_{38,2}$	0.0000	0.0000	0.0001	0.0009	0.0001
$\sigma_{39,2}$	0.0000	0.0001	0.0001	0.0014	0.0002
$\sigma_{40,2}$	0.0001	0.0001	0.0001	0.0014	0.0002
$\sigma_{41,2}$	0.0000	0.0000	0.0001	0.0005	0.0001
$\sigma_{43,2}$	0.0001	0.0001	0.0001	0.0011	0.0002
$\sigma_{44,2}$	0.0000	0.0001	0.0001	0.0009	0.0001
$\sigma_{45,2}$	0.0000	0.0000	0.0001	0.0008	0.0001
$\sigma_{5,3}$	0.0001	0.0001	0.0002	0.0001	0.0001
$\sigma_{9,3}$	0.0002	0.0001	0.0003	0.0003	0.0002
$\sigma_{11,3}$	0.0002	0.0002	0.0005	0.0006	0.0006
$\sigma_{12,3}$	0.0001	0.0002	0.0004	0.0001	0.0002
$\sigma_{13,3}$	0.0002	0.0002	0.0005	0.0008	0.0007
$\sigma_{17,3}$	0.0001	0.0002	0.0003	0.0002	0.0003
$\sigma_{23,3}$	0.0002	0.0002	0.0002	0.0006	0.0006
$\sigma_{24,3}$	0.0001	0.0002	0.0003	0.0001	0.0001
$\sigma_{25,3}$	0.0003	0.0003	0.0006	0.0011	0.0011
$\sigma_{27,3}$	0.0001	0.0001	0.0002	0.0003	0.0003
$\sigma_{28,3}$	0.0004	0.0004	0.0007	0.0015	0.0016
$\sigma_{29,3}$	0.0001	0.0002	0.0002	0.0003	0.0003
$\sigma_{30,3}$	0.0002	0.0003	0.0006	0.0013	0.0013

Continued on next page

Table C.6 – continued from previous page

Component	Undamaged	Damage 1	Damage 2	Damage 3	Damage 4
$\sigma_{31,3}$	0.0002	0.0003	0.0005	0.0010	0.0011
$\sigma_{33,3}$	0.0001	0.0001	0.0004	0.0004	0.0004
$\sigma_{37,3}$	0.0002	0.0002	0.0003	0.0006	0.0006
$\sigma_{38,3}$	0.0001	0.0001	0.0001	0.0001	0.0001
$\sigma_{39,3}$	0.0002	0.0002	0.0004	0.0005	0.0005
$\sigma_{40,3}$	0.0002	0.0002	0.0005	0.0001	0.0001
$\sigma_{41,3}$	0.0001	0.0002	0.0003	0.0000	0.0001
$\sigma_{43,3}$	0.0001	0.0002	0.0001	0.0001	0.0001
$\sigma_{44,3}$	0.0001	0.0001	0.0002	0.0000	0.0000
$\sigma_{45,3}$	0.0001	0.0001	0.0002	0.0001	0.0001
$\sigma_{5,4}$	0.0003	0.0003	0.0003	0.0006	0.0002
$\sigma_{9,4}$	0.0004	0.0004	0.0006	0.0021	0.0012
$\sigma_{11,4}$	0.0004	0.0003	0.0007	0.0031	0.0016
$\sigma_{12,4}$	0.0004	0.0004	0.0003	0.0005	0.0003
$\sigma_{13,4}$	0.0002	0.0001	0.0002	0.0011	0.0002
$\sigma_{17,4}$	0.0004	0.0005	0.0003	0.0003	0.0004
$\sigma_{23,4}$	0.0002	0.0003	0.0006	0.0026	0.0011
$\sigma_{24,4}$	0.0004	0.0003	0.0009	0.0046	0.0023
$\sigma_{25,4}$	0.0002	0.0002	0.0005	0.0022	0.0010
$\sigma_{27,4}$	0.0004	0.0003	0.0004	0.0020	0.0014
$\sigma_{28,4}$	0.0005	0.0006	0.0019	0.0082	0.0055
$\sigma_{29,4}$	0.0005	0.0002	0.0003	0.0016	0.0013
$\sigma_{30,4}$	0.0005	0.0007	0.0007	0.0039	0.0034
$\sigma_{31,4}$	0.0005	0.0002	0.0004	0.0013	0.0005
$\sigma_{33,4}$	0.0004	0.0002	0.0003	0.0008	0.0004
$\sigma_{37,4}$	0.0004	0.0001	0.0002	0.0001	0.0005
$\sigma_{38,4}$	0.0003	0.0004	0.0002	0.0008	0.0007
$\sigma_{39,4}$	0.0003	0.0002	0.0006	0.0028	0.0019
$\sigma_{40,4}$	0.0005	0.0004	0.0003	0.0002	0.0001
$\sigma_{41,4}$	0.0004	0.0003	0.0003	0.0007	0.0002
$\sigma_{43,4}$	0.0002	0.0003	0.0003	0.0007	0.0010
$\sigma_{44,4}$	0.0002	0.0003	0.0002	0.0012	0.0012
$\sigma_{45,4}$	0.0004	0.0005	0.0004	0.0003	0.0002
$\sigma_{5,5}$	0.0009	0.0001	0.0011	0.0017	0.0015
$\sigma_{9,5}$	0.0047	0.0001	0.0006	0.0015	0.0014
$\sigma_{11,5}$	0.0061	0.0001	0.0017	0.0047	0.0036

Continued on next page

Table C.6 – continued from previous page

Component	Undamaged	Damage 1	Damage 2	Damage 3	Damage 4
$\sigma_{12,5}$	0.0047	0.0002	0.0023	0.0050	0.0041
$\sigma_{13,5}$	0.0192	0.0003	0.0029	0.0092	0.0069
$\sigma_{17,5}$	0.0053	0.0002	0.0028	0.0063	0.0054
$\sigma_{23,5}$	0.0072	0.0002	0.0013	0.0051	0.0042
$\sigma_{24,5}$	0.0102	0.0002	0.0026	0.0062	0.0049
$\sigma_{25,5}$	0.0077	0.0001	0.0011	0.0052	0.0038
$\sigma_{27,5}$	0.0004	0.0002	0.0015	0.0037	0.0026
$\sigma_{28,5}$	0.0090	0.0005	0.0056	0.0124	0.0085
$\sigma_{29,5}$	0.0008	0.0002	0.0020	0.0040	0.0030
$\sigma_{30,5}$	0.0062	0.0004	0.0032	0.0071	0.0046
$\sigma_{31,5}$	0.0067	0.0002	0.0017	0.0070	0.0053
$\sigma_{33,5}$	0.0095	0.0003	0.0015	0.0015	0.0015
$\sigma_{37,5}$	0.0087	0.0003	0.0029	0.0096	0.0074
$\sigma_{38,5}$	0.0039	0.0002	0.0019	0.0034	0.0030
$\sigma_{39,5}$	0.0146	0.0004	0.0046	0.0128	0.0096
$\sigma_{40,5}$	0.0170	0.0004	0.0026	0.0044	0.0035
$\sigma_{41,5}$	0.0045	0.0002	0.0021	0.0042	0.0034
$\sigma_{43,5}$	0.0098	0.0002	0.0007	0.0035	0.0026
$\sigma_{44,5}$	0.0013	0.0002	0.0021	0.0052	0.0041
$\sigma_{45,5}$	0.0049	0.0002	0.0016	0.0024	0.0022
$\sigma_{5,6}$	0.0001	0.0001	0.0002	0.0013	0.0016
$\sigma_{9,6}$	0.0003	0.0001	0.0004	0.0023	0.0029
$\sigma_{11,6}$	0.0002	0.0002	0.0003	0.0015	0.0024
$\sigma_{12,6}$	0.0001	0.0001	0.0002	0.0013	0.0010
$\sigma_{13,6}$	0.0002	0.0001	0.0003	0.0013	0.0013
$\sigma_{17,6}$	0.0002	0.0001	0.0003	0.0017	0.0015
$\sigma_{23,6}$	0.0003	0.0002	0.0005	0.0029	0.0036
$\sigma_{24,6}$	0.0002	0.0001	0.0002	0.0011	0.0021
$\sigma_{25,6}$	0.0002	0.0001	0.0003	0.0018	0.0030
$\sigma_{27,6}$	0.0001	0.0001	0.0002	0.0015	0.0018
$\sigma_{28,6}$	0.0002	0.0002	0.0005	0.0024	0.0056
$\sigma_{29,6}$	0.0003	0.0001	0.0004	0.0025	0.0041
$\sigma_{30,6}$	0.0009	0.0004	0.0014	0.0091	0.0098
$\sigma_{31,6}$	0.0004	0.0002	0.0008	0.0053	0.0061
$\sigma_{33,6}$	0.0002	0.0001	0.0004	0.0021	0.0018
$\sigma_{37,6}$	0.0009	0.0004	0.0016	0.0102	0.0110

Continued on next page

Table C.6 – continued from previous page

Component	Undamaged	Damage 1	Damage 2	Damage 3	Damage 4
$\sigma_{38,6}$	0.0001	0.0001	0.0001	0.0008	0.0012
$\sigma_{39,6}$	0.0002	0.0001	0.0003	0.0021	0.0023
$\sigma_{40,6}$	0.0005	0.0002	0.0008	0.0053	0.0052
$\sigma_{41,6}$	0.0002	0.0001	0.0003	0.0020	0.0019
$\sigma_{43,6}$	0.0002	0.0001	0.0004	0.0022	0.0026
$\sigma_{44,6}$	0.0001	0.0001	0.0002	0.0015	0.0017
$\sigma_{45,6}$	0.0001	0.0001	0.0002	0.0012	0.0014
$\sigma_{5,7}$	0.0006	0.0004	0.0014	0.0010	0.0080
$\sigma_{9,7}$	0.0003	0.0003	0.0005	0.0003	0.0057
$\sigma_{11,7}$	0.0009	0.0005	0.0022	0.0016	0.0153
$\sigma_{12,7}$	0.0009	0.0006	0.0025	0.0019	0.0183
$\sigma_{13,7}$	0.0001	0.0001	0.0002	0.0002	0.0040
$\sigma_{17,7}$	0.0006	0.0004	0.0016	0.0013	0.0157
$\sigma_{23,7}$	0.0010	0.0006	0.0026	0.0018	0.0189
$\sigma_{24,7}$	0.0001	0.0001	0.0002	0.0005	0.0193
$\sigma_{25,7}$	0.0004	0.0005	0.0014	0.0013	0.0181
$\sigma_{27,7}$	0.0006	0.0003	0.0014	0.0010	0.0105
$\sigma_{28,7}$	0.0017	0.0011	0.0043	0.0027	0.0183
$\sigma_{29,7}$	0.0002	0.0003	0.0003	0.0001	0.0036
$\sigma_{30,7}$	0.0027	0.0020	0.0074	0.0048	0.0375
$\sigma_{31,7}$	0.0010	0.0008	0.0029	0.0022	0.0297
$\sigma_{33,7}$	0.0003	0.0004	0.0017	0.0012	0.0162
$\sigma_{37,7}$	0.0026	0.0018	0.0072	0.0048	0.0491
$\sigma_{38,7}$	0.0004	0.0003	0.0009	0.0007	0.0144
$\sigma_{39,7}$	0.0008	0.0005	0.0021	0.0013	0.0149
$\sigma_{40,7}$	0.0002	0.0001	0.0002	0.0002	0.0041
$\sigma_{41,7}$	0.0006	0.0005	0.0017	0.0012	0.0116
$\sigma_{43,7}$	0.0014	0.0011	0.0042	0.0029	0.0268
$\sigma_{44,7}$	0.0002	0.0004	0.0012	0.0008	0.0032
$\sigma_{45,7}$	0.0006	0.0005	0.0018	0.0012	0.0146
$\sigma_{5,8}$	0.0003	0.0006	0.0012	0.0022	0.0013
$\sigma_{9,8}$	0.0011	0.0019	0.0040	0.0085	0.0041
$\sigma_{11,8}$	0.0005	0.0008	0.0015	0.0016	0.0025
$\sigma_{12,8}$	0.0006	0.0010	0.0020	0.0033	0.0020
$\sigma_{13,8}$	0.0011	0.0018	0.0041	0.0094	0.0034
$\sigma_{17,8}$	0.0002	0.0004	0.0006	0.0012	0.0023

Continued on next page

Table C.6 – continued from previous page

Component	Undamaged	Damage 1	Damage 2	Damage 3	Damage 4
$\sigma_{23,8}$	0.0010	0.0016	0.0033	0.0047	0.0024
$\sigma_{24,8}$	0.0011	0.0017	0.0039	0.0100	0.0051
$\sigma_{25,8}$	0.0010	0.0018	0.0040	0.0108	0.0062
$\sigma_{27,8}$	0.0004	0.0007	0.0016	0.0030	0.0019
$\sigma_{28,8}$	0.0019	0.0030	0.0063	0.0097	0.0054
$\sigma_{29,8}$	0.0001	0.0002	0.0001	0.0014	0.0021
$\sigma_{30,8}$	0.0012	0.0017	0.0036	0.0026	0.0027
$\sigma_{31,8}$	0.0001	0.0001	0.0002	0.0014	0.0048
$\sigma_{33,8}$	0.0002	0.0004	0.0008	0.0012	0.0016
$\sigma_{37,8}$	0.0010	0.0015	0.0031	0.0013	0.0058
$\sigma_{38,8}$	0.0001	0.0003	0.0005	0.0009	0.0019
$\sigma_{39,8}$	0.0011	0.0019	0.0039	0.0057	0.0040
$\sigma_{40,8}$	0.0001	0.0001	0.0003	0.0016	0.0035
$\sigma_{41,8}$	0.0005	0.0010	0.0019	0.0036	0.0018
$\sigma_{43,8}$	0.0006	0.0010	0.0022	0.0030	0.0020
$\sigma_{44,8}$	0.0005	0.0008	0.0017	0.0036	0.0023
$\sigma_{45,8}$	0.0001	0.0002	0.0002	0.0006	0.0012

APPENDIX D: SUPPLEMENTAL MATLAB/C++ CODES

This appendix provides representative MATLAB and C++ scripts utilized for structural identification in this dissertation. Section C.1 provides representative scripts for the problems presented in Chapter 4 and Section C.2 provides a representative script for structural identification of a multiple degree-of-freedom system model.

D.1 MATLAB C++ Code Generation For Two Spring Identification

The following MATLAB script generates the C++ code utilized for the identification of the rotational end restraints at a fixed internal axial force for the numerical verification of the methodology presented in Chapter 4. The script also parses the results returned from the nonlinear constraint solver for subsequent analysis and plotting of the feasible solution space.

```
user=char(getenv('USERNAME'));

%kA = 0.70, kB=0.30, kC=1, kD=1; gamT=180, gamR=11.5;
freq=[[17.8291431915000,...
            40.2369941688000,...
       70.0496328254000,...
      108.577487984000]];
nfreq=3;
freq=freq(1:nfreq);
randmoff=[-0.02;+0.05;-0.04;0]'; %
freq=freq+randmoff(1:nfreq);
N=581;                                  %Units: kN
E=200e6;                                %Units: kPa
d=0.065;                                %Units: m (diameter)
I=pi/64*d^4;                            %Units: m^4
L=5;                                    %Units: m
A=pi*(d/2)^2;
rho=7.850;
nu=0.29;  %Poisson Ratio
G=E/(2*(1+nu));
ky=6*(1+nu)/(7+6*nu); %Shear factor for circular cross secton
kGA=G*A*ky;
EI=E*I;
syms w kA kB kC kD;
```

```
kC=1;
kD=1;
gamT=180;
gamR=11.5;
tol=0.05;
for k=1:length(freq)
        for j=1:2
                if j==1
                        w=2*pi*(freq(k)-tol*(-1)^(k+1));
                else
                        w=2*pi*(freq(k)+tol*(-1)^(k+1));
                end
                a=EI*(1+(N/(kGA)));
                b=-N+(EI*rho*w^2)/(ky*G)+rho*I*w^2+(N*rho*I*w^2)/(kGA);
                c=-rho*A*w^2+(rho^2*I*w^4)/(ky*G);
                d=w^2*rho*I-kGA;
                e=(EI*rho*w^2)/(ky*G)+kGA;
                alp=sqrt((b+sqrt(b^2-4*a*c))/(2*a))*L;
                beta=sqrt((-b+sqrt(b^2-4*a*c))/(2*a))*L;
                Ma=0;Mb=0;Ja=0;Jb=0;
MTRX=sym(zeros(4,4));
MTRX(:,1)=[alp^2*(e*L^2 - a*alp^2)*(kA - 1);...
-(alp*(e*L^2 - a*alp^2)*(EI*gamR*kA - Ja*L*w^2 + Ja*L*kA*w^2))/EI ;...
-beta^2*(e*L^2 + a*beta^2)*(kA - 1);...
-(beta*(e*L^2 + a*beta^2)*(EI*gamR*kA - Ja*L*w^2 + Ja*L*kA*w^2))/EI];
MTRX(:,2)=[-alp*(e*L^2 - a*alp^2)*(EI*alp*cos(alp) - EI*alp*kB*cos(alp) + EI*gamR*kB*sin(
    alp) - Jb*L*w^2*sin(alp) + Jb*L*kB*w^2*sin(alp));...
alp*(e*L^2 - a*alp^2)*(EI*gamR*kB*cos(alp) - EI*alp*sin(alp) + EI*alp*kB*sin(alp) - Jb*L*w
    ^2*cos(alp) + Jb*L*kB*w^2*cos(alp));...
beta*(e*L^2 + a*beta^2)*(EI*beta*cosh(beta) - EI*beta*kB*cosh(beta) + EI*gamR*kB*sinh(beta
    ) - Jb*L*w^2*sinh(beta) + Jb*L*kB*w^2*sinh(beta));...
beta*(e*L^2 + a*beta^2)*(EI*beta*sinh(beta) + EI*gamR*kB*cosh(beta) - EI*beta*kB*sinh(beta
    ) - Jb*L*w^2*cosh(beta) + Jb*L*kB*w^2*cosh(beta))];%*exp(-bet);
MTRX(:,3)=[-d*(EI*gamT*kC - L^3*Ma*w^2 + L^3*Ma*kC*w^2);...
-alp*(kC - 1)*(L^2*N*d + L^2*d*kGA + L^2*e*kGA - a*alp^2*kGA);...
-d*(EI*gamT*kC - L^3*Ma*w^2 + L^3*Ma*kC*w^2);...
-beta*(kC - 1)*(L^2*N*d + L^2*d*kGA + L^2*e*kGA + a*beta^2*kGA)];
MTRX(:,4)=[L^2*alp*d*kGA*sin(alp) - a*alp^3*kGA*sin(alp) + L^2*alp*e*kGA*sin(alp) + a*alp
    ^3*kD*kGA*sin(alp) + L^3*Mb*d*w^2*cos(alp) - EI*d*gamT*kD*cos(alp) + L^2*N*alp*d*sin(
    alp) - L^2*N*alp*d*kD*sin(alp) - L^2*alp*d*kD*kGA*sin(alp) - L^2*alp*e*kD*kGA*sin(alp)
     - L^3*Mb*d*kD*w^2*cos(alp);...
a*alp^3*kGA*cos(alp) - L^2*alp*d*kGA*cos(alp) - L^2*alp*e*kGA*cos(alp) - a*alp^3*kD*kGA*
    cos(alp) + L^3*Mb*d*w^2*sin(alp) - EI*d*gamT*kD*sin(alp) - L^2*N*alp*d*cos(alp) + L^2*
    N*alp*d*kD*cos(alp) + L^2*alp*d*kD*kGA*cos(alp) + L^2*alp*e*kD*kGA*cos(alp) - L^3*Mb*d
    *kD*w^2*sin(alp);...
a*beta^3*kD*kGA*sinh(beta) - L^2*beta*d*kGA*sinh(beta) - L^2*beta*e*kGA*sinh(beta) - a*
    beta^3*kGA*sinh(beta) + L^3*Mb*d*w^2*cosh(beta) - EI*d*gamT*kD*cosh(beta) - L^2*N*beta
    *d*sinh(beta) + L^2*N*beta*d*kD*sinh(beta) + L^2*beta*d*kD*kGA*sinh(beta) + L^2*beta*e
    *kD*kGA*sinh(beta) - L^3*Mb*d*kD*w^2*cosh(beta);
a*beta^3*kD*kGA*cosh(beta) - L^2*beta*d*kGA*cosh(beta) - L^2*beta*e*kGA*cosh(beta) - a*
    beta^3*kGA*cosh(beta) + L^3*Mb*d*w^2*sinh(beta) - EI*d*gamT*kD*sinh(beta) - L^2*N*beta
    *d*cosh(beta) + L^2*N*beta*d*kD*cosh(beta) + L^2*beta*d*kD*kGA*cosh(beta) + L^2*beta*e
    *kD*kGA*cosh(beta) - L^3*Mb*d*kD*w^2*sinh(beta)];
MTRX(:,1)=-MTRX(:,1);
eq = simplify(det(MTRX.'));
eq=vpa(eq,50);
eqs{j,k}=eq;
end
end

vars={'kA', 'kB'};
%vars={'kB','kC','kD'};
varstring='';
for k=1:numel(vars)
if k==1
varstring=sprintf([vars{k}]);
else
varstring=sprintf([varstring,',',vars{k}]);
```

```
77  end
78  end
79  prec=0.0005;
80  precb=0.0005;
81  LB=[0,0];
82  UB=[1,1];
83
84  for k=1:numel(eqs)
85  Cfun=ccode(eqs{k});
86  func{k}=Cfun(7:end-1);
87  end
88
89  func{end+1}='kA-kB';
90  cons=repmat({'>=0','<0','<=0','>0'},1,numel(freq));
91  cons{end+1}='<0';
92  cons{end+1}='>=0';
93  CtcIn=[];
94  CtcOut=[];
95  cnt=1;
96  for k=1:2:numel(func)*2
97  CtcIn{cnt}=strcat('c',num2str(k));
98  CtcOut{cnt}=strcat('c',num2str(k+1));
99  cnt=cnt+1;
100 end
101
102 filename=strcat('SiviaCableTest_kakb');
103 Results=strcat('TwoSprings_example',num2str(numel(freq)),'freqs_tol',num2str(tol),'_prec',
        num2str(prec),'_precb',num2str(precb),'.txt');
104 fid=fopen(strcat(filename,'.cpp'),'w+');
105 fprintf(fid,'#include "ibex.h"\n\nusing namespace std;\nusing namespace ibex;\n');
106 fprintf(fid,'int main() {\n');
107 fprintf(fid,sprintf(['Variable ',varstring,';\n']));
108
109 %Define functions
110 for k=1:numel(func)
111 fprintf(fid,sprintf(['Function f',num2str(k),'(',varstring,',',func{k},');\n']));
112 end
113
114 %Define constraints
115 for k=1:numel(func)
116 fprintf(fid,sprintf(['NumConstraint c',num2str(1+2*(k-1)),'(',varstring,',f',num2str(k),'(
        ',varstring,')',cons{1+2*(k-1)},');\n']));
117 fprintf(fid,sprintf(['NumConstraint c',num2str(2+2*(k-1)),'(',varstring,',f',num2str(k),'(
        ',varstring,')',cons{2+2*(k-1)},');\n']));
118 end
119
120 %Define functions for inner contraction
121 for k=1:numel(CtcIn)
122 fprintf(fid,sprintf(['CtcHC4 in',num2str(k),'(',CtcIn{k},');\n']));
123 end
124
125 %Define functions for out contraction
126 for k=1:numel(CtcOut)
127 fprintf(fid,sprintf(['CtcHC4 out',num2str(k),'(',CtcOut{k},');\n']));
128 end
129
130 if mod(numel(CtcIn)/2,1)==0
131 %Define Union of Contractors
132 for k=1:numel(CtcIn)/2
133 fprintf(fid,sprintf(['CtcUnion inside',num2str(k),'(in',num2str(1+2*(k-1)),',in',num2str
        (2+2*(k-1)),');\n']));
134 end
135
136 for k=1:numel(CtcIn)/2-1
137 fprintf(fid,sprintf(['CtcUnion inside',num2str(k+numel(freq)),'(inside',num2str(1+2*(k-1))
        ,',inside',num2str(2+2*(k-1)),');\n']));
138 end
139
```

```
%Define Intersection of Contractors
for k=1:numel(CtcOut)/2
fprintf(fid,sprintf(['CtcCompo outside',num2str(k),'(out',num2str(1+2*(k-1)),',out',num2str(2+2*(k-1)),');\n']));
end
for k=1:numel(CtcOut)/2-1
fprintf(fid,sprintf(['CtcCompo outside',num2str(k+numel(freq)),'(outside',num2str(1+2*(k-1)),',outside',num2str(2+2*(k-1)),');\n']));
end
else
for k=1:numel(CtcIn)/2
fprintf(fid,sprintf(['CtcUnion inside',num2str(k),'(in',num2str(1+2*(k-1)),',in',num2str(2+2*(k-1)),');\n']));
end
fprintf(fid,sprintf(['CtcUnion inside',num2str(k+1),'(inside1',',in',num2str(2+2*(k-1)+1),');\n']));
k=k+1;
for k=2:numel(CtcIn)/2
fprintf(fid,sprintf(['CtcUnion inside',num2str(numel(freq)+k),'(inside',num2str(2*(k-1)),',inside',num2str(1+2*(k-1)),');\n']));
end

%Define Intersection of Contractors
for k=1:numel(CtcIn)/2
fprintf(fid,sprintf(['CtcCompo outside',num2str(k),'(out',num2str(1+2*(k-1)),',out',num2str(2+2*(k-1)),');\n']));
end
fprintf(fid,sprintf(['CtcCompo outside',num2str(k+1),'(outside1',',out',num2str(2+2*(k-1)+1),');\n']));
k=k+1;
for k=2:numel(CtcIn)/2
fprintf(fid,sprintf(['CtcCompo outside',num2str(numel(freq)+k),'(outside',num2str(2*(k-1)),',outside',num2str(1+2*(k-1)),');\n']));
end

end

%Define Composition of Contractors
fprintf(fid,sprintf(['CtcFixPoint fix1(outside',num2str(numel(freq)+k),',',num2str(prec),');\n']));
fprintf(fid,sprintf(['CtcFixPoint fix2(inside',num2str(numel(freq)+k),',',num2str(prec),');\n']));
%Define the precision contractor
fprintf(fid,sprintf(['PdcDiameterLT prec(',num2str(precb),');\n']));
fprintf(fid,sprintf(['CtcEmpty boundary(prec);\n']));
%Push contractor to an array
fprintf(fid,sprintf(['Array<Ctc> ctc(fix2,fix1,boundary);\n']));
fprintf(fid,sprintf(['RoundRobin lf(',num2str(prec),',0.6);\n']));
fprintf(fid,sprintf(['CellStack stack;\n']));
fprintf(fid,sprintf(['Paver p(ctc,lf,stack);\n']));
fprintf(fid,sprintf(['p.trace = 0;\n']));
fprintf(fid,sprintf(['p.timeout = 25000;\n']));
fprintf(fid,sprintf(['p.ctc_loop = false;\n\n']));
%Define Parameter bounds
fprintf(fid,sprintf(['IntervalVector box(',num2str(numel(vars)),');\n']));
for k=1:numel(vars)
fprintf(fid,sprintf(['box[',num2str(k-1),']=Interval(',num2str(LB(k)),',',num2str(UB(k)),');\n\n']));
end

%Run the paver
fprintf(fid,sprintf(['SubPaving* paving=p.pave(box);\n']));
fprintf(fid,sprintf(['for (int i=0; i<3; i++) {\n',...
'for (std::vector<std::pair<IntervalVector,IntervalVector> >::const_iterator it=paving[i].traces.begin(); it!=paving[i].traces.end(); it++) {\n',...
'IntervalVector *boxes;\n',...
'int size=it->first.diff(it->second,boxes);\n',...
'for (int j=0; j<size; j++) {\n',...
```

```
'cout << "',num2str(N),' "<< boxes[j][0].lb() << " " << boxes[j][0].ub() << " " <<\n',...
'boxes[j][1].lb() << " " << boxes[j][1].ub() << " " << i << endl;\n',...
'}\n}\n}\n']));
fclose(fid);
movefile(strcat(pwd,'/',filename,'.cpp'),strcat('/home/',user,'/Ibex/ibex-2.1.17/examples/'));

unix(sprintf(['export PREFIX=/usr/local;',...
'export PKG_CONFIG_PATH=$PREFIX/share/pkgconfig;',...
'export LD_LIBRARY_PATH=/usr/local/lib;',...
'cd /home/',user,'/Ibex/ibex-2.1.17/examples;',...
'make ',filename]))

unix(sprintf(['export PREFIX=/usr/local;',...
'export PKG_CONFIG_PATH=$PREFIX/share/pkgconfig;',...
'export LD_LIBRARY_PATH=/usr/local/lib;',...
'cd /home/',user,'/Ibex/ibex-2.1.17/examples;',...
'./',filename, '| tee /home/',user,'/Ibex/ibex-2.1.17/examples/',Results]))
copyfile(strcat('/home/',user,'/Ibex/ibex-2.1.17/examples/',Results),pwd);

end

% Data processing and plotting
fid=fopen(Results);
D=textscan(fid,'%f');
fclose(fid);
data=reshape(cell2mat(D),6,numel(D{1,1})/6)';
N=data(:,1);
Low=data(:,[2,4]);
High=data(:,[3,5]);
Color=data(:,6);

StaticVar=1; %Chooses variable for x axis in each subplot
DynVars=setdiff(1:size(High,2),StaticVar);
if size(High,2)==4
params={'$k_A$','$k_B$','$k_C$','$k_D$'};
elseif size(High,2)==2
params={'$k_A$','$k_B$'};
end
% Inner subpaving (solutions)
C0=find(Color==0);
j=C0;
count=1;
for k=DynVars
patch([Low(j,StaticVar) High(j,StaticVar) High(j,StaticVar) Low(j,StaticVar) Low(j,StaticVar)]', [Low(j,k) Low(j,k) High(j,k) High(j,k) Low(j,k)]',...
[Low(j,k) Low(j,k) High(j,k) High(j,k) Low(j,k)]'*0,'FaceColor',[0 1 0],'FaceAlpha',1,'EdgeColor',[0 0 0],'EdgeAlpha',1)
hold on
%         axis square
xlabel(params(StaticVar),'interpreter','latex','FontSize',22)
ylabel(params(k),'interpreter','latex','FontSize',22)
set(gca,'FontSize',8)
count=count+1;
box on
grid on
end
% Boundary (potential solutions)
C1=find(Color==1);
j=C1;
count=1;
for k=DynVars
patch([Low(j,StaticVar) High(j,StaticVar) High(j,StaticVar) Low(j,StaticVar) Low(j,StaticVar)]', [Low(j,k) Low(j,k) High(j,k) High(j,k) Low(j,k)]',...
[Low(j,k) Low(j,k) High(j,k) High(j,k) Low(j,k)]'*0,'FaceColor',[1 0 0],'FaceAlpha',1,'EdgeColor',[0 0 0],'EdgeAlpha',1)
hold on
%         axis square
```

```
xlabel(params(StaticVar),'interpreter','latex','FontSize',22)
ylabel(params(k),'interpreter','latex','FontSize',22)
set(gca,'FontSize',8)
count=count+1;
box on
grid on
end
% Outer Contractor (not solutions)
C2=find(Color==2);
j=C2;
count=1;
for k=DynVars
patch([Low(j,StaticVar) High(j,StaticVar) High(j,StaticVar) Low(j,StaticVar) Low(j,
    StaticVar)]', [Low(j,k) Low(j,k) High(j,k) High(j,k) Low(j,k)]',...
[Low(j,k) Low(j,k) High(j,k) High(j,k) Low(j,k)]'*0,'FaceColor',[0 1 1],'FaceAlpha',1,'
    EdgeColor',[0 0 0],'EdgeAlpha',1)
hold on
%         axis square
xlabel(params(StaticVar),'interpreter','latex','FontSize',22)
ylabel(params(k),'interpreter','latex','FontSize',22)
set(gca,'FontSize',22)
count=count+1;
box on
grid on
end
```

The above MATLAB script generated the following C++ code, which defines the constraint equations developed as well as the composition of contractors employed for subpaving the parameter space.

```
#include "ibex.h"

using namespace std;
using namespace ibex;
int main() {
        Variable kA,kB;
        Function f1(kA,kB, kA*-1.123385573341135E10-kB*(kA*2.562902221510882E7
            +1.123385573340688E10)+1.143810708972797E12);
        Function f2(kA,kB, kA*-1.125918229988777E10-kB*(kA*2.586783730978182E7
            +1.125918229989676E10)+1.166842677499912E12);
        Function f3(kA,kB, kA*2.239168911698834E11-kB*(kA*5.92329177389296E8
            -2.239168911699298E11)-2.085038955774528E13);
        Function f4(kA,kB, kA*2.22159237380887E11-kB*(kA*5.93120113528449E8
            -2.221592373807488E11)-2.039895057611793E13);
        Function f5(kA,kB, kA*-5.435619672260873E12+kB*(kA*3.149248219638995E10
            -5.435619672267313E12)+4.702992125007383E14);
        Function f6(kA,kB, kA*-5.457954953561l2E12+kB*(kA*3.156040390950529E10
            -5.457954953554662E12)+4.742289561492746E14);
        Function f7(kA,kB, kA*1.4606446399818E14-kB*(kA*1.116218282054587E12
            -1.460644639916379E14)-1.216461597349127E16);
        Function f8(kA,kB, kA*1.45220539720831E14-kB*(kA*1.11194682931245E12
            -1.452205397143123E14)-1.204088281700873E16);
        Function f9(kA,kB, kA*-4.041181335085064E15+kB*(kA*3.561391266084E13
            -4.041181340398488E15)+3.263257393110684E17);
        Function f10(kA,kB, kA*-4.06807890680237E15+kB*(kA*3.578377942536746E13
            -4.068078899007777E15)+3.298811594057201E17);
        Function f11(kA,kB, kA*1.141570158886043E17-kB*(kA*1.092920107109161E15
            -1.141570158886043E17)-9.058589151069867E18);
        Function f12(kA,kB, kA*1.136241175512789E17-kB*(kA*1.089110659657806E15
            -1.136241175512789E17)-8.992665769568559E18);
```

```
19      Function f13(kA,kB, kA*-3.216447413194726E18+kB*(kA*3.253294336590439E16
            -3.216447413194726E18)+2.514868744281297E20);
20      Function f14(kA,kB, kA*-3.232497462081738E18+kB*(kA*3.265685660202877E16
            -3.232497462081738E18)+2.533870470580463E20);
21      Function f15(kA,kB, kA*9.093700820202279E19-kB*(kA*9.542591931392956E17
            -9.093700820202279E19)-7.054950461797738E21);
22      Function f16(kA,kB, kA*9.069013833158766E19-kB*(kA*9.522510080308711E17
            -9.069013833158766E19)-7.026627383463862E21);
23      Function f17(kA,kB,kA-kB);
24      NumConstraint c1(kA,kB,f1(kA,kB)>=0);
25      NumConstraint c2(kA,kB,f1(kA,kB)<0);
26      NumConstraint c3(kA,kB,f2(kA,kB)<=0);
27      NumConstraint c4(kA,kB,f2(kA,kB)>0);
28      NumConstraint c5(kA,kB,f3(kA,kB)>=0);
29      NumConstraint c6(kA,kB,f3(kA,kB)<0);
30      NumConstraint c7(kA,kB,f4(kA,kB)<=0);
31      NumConstraint c8(kA,kB,f4(kA,kB)>0);
32      NumConstraint c9(kA,kB,f5(kA,kB)>=0);
33      NumConstraint c10(kA,kB,f5(kA,kB)<0);
34      NumConstraint c11(kA,kB,f6(kA,kB)<=0);
35      NumConstraint c12(kA,kB,f6(kA,kB)>0);
36      NumConstraint c13(kA,kB,f7(kA,kB)>=0);
37      NumConstraint c14(kA,kB,f7(kA,kB)<0);
38      NumConstraint c15(kA,kB,f8(kA,kB)<=0);
39      NumConstraint c16(kA,kB,f8(kA,kB)>0);
40      NumConstraint c17(kA,kB,f9(kA,kB)>=0);
41      NumConstraint c18(kA,kB,f9(kA,kB)<0);
42      NumConstraint c19(kA,kB,f10(kA,kB)<=0);
43      NumConstraint c20(kA,kB,f10(kA,kB)>0);
44      NumConstraint c21(kA,kB,f11(kA,kB)>=0);
45      NumConstraint c22(kA,kB,f11(kA,kB)<0);
46      NumConstraint c23(kA,kB,f12(kA,kB)<=0);
47      NumConstraint c24(kA,kB,f12(kA,kB)>0);
48      NumConstraint c25(kA,kB,f13(kA,kB)>=0);
49      NumConstraint c26(kA,kB,f13(kA,kB)<0);
50      NumConstraint c27(kA,kB,f14(kA,kB)<=0);
51      NumConstraint c28(kA,kB,f14(kA,kB)>0);
52      NumConstraint c29(kA,kB,f15(kA,kB)>=0);
53      NumConstraint c30(kA,kB,f15(kA,kB)<0);
54      NumConstraint c31(kA,kB,f16(kA,kB)<=0);
55      NumConstraint c32(kA,kB,f16(kA,kB)>0);
56      NumConstraint c33(kA,kB,f17(kA,kB)<0);
57      NumConstraint c34(kA,kB,f17(kA,kB)>=0);
58      CtcHC4 in1(c1);
59      CtcHC4 in2(c3);
60      CtcHC4 in3(c5);
61      CtcHC4 in4(c7);
62      CtcHC4 in5(c9);
63      CtcHC4 in6(c11);
64      CtcHC4 in7(c13);
65      CtcHC4 in8(c15);
66      CtcHC4 in9(c17);
67      CtcHC4 in10(c19);
68      CtcHC4 in11(c21);
69      CtcHC4 in12(c23);
70      CtcHC4 in13(c25);
71      CtcHC4 in14(c27);
72      CtcHC4 in15(c29);
73      CtcHC4 in16(c31);
74      CtcHC4 in17(c33);
75      CtcHC4 out1(c2);
76      CtcHC4 out2(c4);
77      CtcHC4 out3(c6);
78      CtcHC4 out4(c8);
79      CtcHC4 out5(c10);
80      CtcHC4 out6(c12);
81      CtcHC4 out7(c14);
82      CtcHC4 out8(c16);
```

```
83          CtcHC4 out9(c18);
84          CtcHC4 out10(c20);
85          CtcHC4 out11(c22);
86          CtcHC4 out12(c24);
87          CtcHC4 out13(c26);
88          CtcHC4 out14(c28);
89          CtcHC4 out15(c30);
90          CtcHC4 out16(c32);
91          CtcHC4 out17(c34);
92          CtcUnion inside1(in1,in2);
93          CtcUnion inside2(in3,in4);
94          CtcUnion inside3(in5,in6);
95          CtcUnion inside4(in7,in8);
96          CtcUnion inside5(in9,in10);
97          CtcUnion inside6(in11,in12);
98          CtcUnion inside7(in13,in14);
99          CtcUnion inside8(in15,in16);
100         CtcUnion inside9(inside1,in17);
101         CtcUnion inside10(inside2,inside3);
102         CtcUnion inside11(inside4,inside5);
103         CtcUnion inside12(inside6,inside7);
104         CtcUnion inside13(inside8,inside9);
105         CtcUnion inside14(inside10,inside11);
106         CtcUnion inside15(inside12,inside13);
107         CtcUnion inside16(inside14,inside15);
108         CtcCompo outside1(out1,out2);
109         CtcCompo outside2(out3,out4);
110         CtcCompo outside3(out5,out6);
111         CtcCompo outside4(out7,out8);
112         CtcCompo outside5(out9,out10);
113         CtcCompo outside6(out11,out12);
114         CtcCompo outside7(out13,out14);
115         CtcCompo outside8(out15,out16);
116         CtcCompo outside9(outside1,out17);
117         CtcCompo outside10(outside2,outside3);
118         CtcCompo outside11(outside4,outside5);
119         CtcCompo outside12(outside6,outside7);
120         CtcCompo outside13(outside8,outside9);
121         CtcCompo outside14(outside10,outside11);
122         CtcCompo outside15(outside12,outside13);
123         CtcCompo outside16(outside14,outside15);
124         CtcFixPoint fix1(outside16,0.1);
125         CtcFixPoint fix2(inside16,0.1);
126         PdcDiameterLT prec(0.1);
127         Array<Ctc> ctc(fix2,fix1);
128         RoundRobin lf(0.1,0.6);
129         CellStack stack;
130         Paver p(ctc,lf,stack);
131         p.trace = 0;
132         p.timeout = 25000;
133         p.ctc_loop = false;
134
135         IntervalVector box(2);
136         box[0]=Interval(0,100);
137
138         box[1]=Interval(0,100);
139
140         SubPaving* paving=p.pave(box);
141         for (int i=0; i<1; i++) {
142                 for (std::vector<std::pair<IntervalVector,IntervalVector> >::
                        const_iterator it=paving[i].traces.begin(); it!=paving[i].traces.end()
                        ; it++) {
143                         IntervalVector *boxes;
144                         int size=it->first.diff(it->second,boxes);
145                         for (int j=0; j<size; j++) {
146                                 cout << "585.85 "<< boxes[j][0].lb() << " " << boxes[j
                                        ][0].ub() << " " <<
147                                 boxes[j][1].lb() << " " << boxes[j][1].ub() << " " << i <<
```

```
                                        endl;
148                                 }
149                             }
150                         }
151 }
```

D.2 MATLAB Script For Three DOF Example

The following MATLAB script develops the input file for structural identification of the three degree-of-freedom system model presented in Chapters 3 and 6.

```
1  clear
2  load('data3DOF.mat');
3  sind=[1]; % unmeasured degree-of-freedom u_1
4  pf=1;     % scalar for standard deviation
5  % Compiling the eigeninformation from the data file
6  DLam(1,:)=(([mean(data(1:3:45))-pf*std(data(1:3:45)),mean(data(1:3:45))+pf*std(data
       (1:3:45))])*2*pi).^2;
7  DLam(2,:)=(([mean(data(2:3:45))-pf*std(data(2:3:45)),mean(data(2:3:45))+pf*std(data
       (2:3:45))])*2*pi).^2;
8  DLam(3,:)=(([mean(data(3:3:45))-pf*std(data(3:3:45)),mean(data(3:3:45))+pf*std(data
       (3:3:45))])*2*pi).^2;
9  Xmin=([mean(data(46:9:180))-pf*pf2*std(data(46:9:180)),mean(data(49:9:180))-pf*pf2*std(
       data(49:9:180)),mean(data(52:9:180))-pf*pf2*std(data(52:9:180));...
10 mean(data(47:9:180))-pf*pf2*std(data(47:9:180)),mean(data(50:9:180))-pf*pf2*std(data
       (50:9:180)),mean(data(53:9:180))-pf*pf2*std(data(53:9:180));...
11 mean(data(48:9:180))-pf*pf2*std(data(48:9:180)),mean(data(51:9:180))-pf*pf2*std(data
       (51:9:180)),mean(data(54:9:180))-pf*pf2*std(data(54:9:180))]);
12 Xmax=([mean(data(46:9:180))+pf*pf2*std(data(46:9:180)),mean(data(49:9:180))+pf*pf2*std(
       data(49:9:180)),mean(data(52:9:180))+pf*pf2*std(data(52:9:180));...
13 mean(data(47:9:180))+pf*pf2*std(data(47:9:180)),mean(data(50:9:180))+pf*pf2*std(data
       (50:9:180)),mean(data(53:9:180))+pf*pf2*std(data(53:9:180));...
14 mean(data(48:9:180))+pf*pf2*std(data(48:9:180)),mean(data(51:9:180))+pf*pf2*std(data
       (51:9:180)),mean(data(54:9:180))+pf*pf2*std(data(54:9:180))]);
15
16 precision='0.01';
17 uname=getenv('USERNAME');
18 fscale=1;
19
20 k1=1; k2=1; k3=1;
21 M=diag([1 1 1]);
22 K=[k1+k2 -k2      0;...
23 -k2    k2+k3 -k3;...
24 0    -k3     k3]*2000;
25 LB=[0 0 0]; %Permissible LB
26 UB=[3 3 3]; %Permissible UB
27
28
29 [X,Lam]=eig(K,M);
30
31 for k=1:3
32 m=max(abs(X(:,k)));
33 X(:,k)=X(:,k)./m*1;
34 end
35 OUTPUT(:,1)=sqrt(diag(Lam))/2/pi;
36
37
38 filename=['3DOF_',num2str(sind),'sind_',num2str(pf),'std'];
39 k=2;    % number of modes to include
40 modesin=k;
41 % Initialize input file for IBEX
```

```
fid=fopen(strcat(filename,'.bch'),'w+');
fprintf(fid,'Variables\n\n');

fprintf(fid,strcat('k1 in [',num2str(LB(1)),',',num2str(UB(1)),'];\n'));
fprintf(fid,strcat('k2 in [',num2str(LB(2)),',',num2str(UB(2)),'];\n'));
fprintf(fid,strcat('k3 in [',num2str(LB(3)),',',num2str(UB(3)),'];\n'));

syms k1 k2 k3
K=[k1+k2 -k2 0;...
-k2 k2+k3 -k3;...
0 -k3 k3]*2000;

syms X11 X12 X13
syms X21 X22 X23
syms X31 X32 X33
Xsym=[X11 X12 X13;...
X21 X22 X23;...
X31 X32 X33];

sinc=setdiff(1:length(M(:,1)),sind);    %included sens
Xs=Xsym;

% Normalize the "Measured Data"
for kk=1:modesin
[localmax,I]=max(abs(X(sinc,kk)));
X(:,kk)=sign(X(sinc(I),kk))*X(:,kk)/localmax*fscale;
end
OUTPUT(:,2:4)=X;
for kk=2:4
[localmax,I]=max(abs(OUTPUT(sinc,kk)));
OUTPUT(:,kk)=sign(OUTPUT(sinc(I),kk))*OUTPUT(:,kk)/localmax;
end

for kk=1:modesin
for jj=1:length(sind)
fprintf(fid,strcat(char(Xs(sind(jj),kk)),' in [-10,10];\n'));
end
end

fprintf(fid,'\nConstraints\n');

syms L1 L2 L3 L4 L5 L6
SLam=diag([L1,L2,L3]);
CON=M*Xs(:,1:k)*SLam(1:k,1:k)-K*Xs(:,1:k);
unknowns=[k1 k2 k3 Xs(sind,1:modesin)];
CON=NewConditioning(CON,unknowns,3);
SCON=Xs(:,1:k).'*M*Xs(:,1:k);
SCON2=Xs(:,1:k).'*K*Xs(:,1:k);
SCON=NewConditioning(SCON,unknowns,3);
SCON2=NewConditioning(SCON2,unknowns,3);
CONS='';

for k=1:length(CON(:,1))
for j=1:length(CON(1,:))
temp=char(CON(k,j));
for jj=1:modesin
temp=strrep(temp,['L',num2str(jj)],['[',num2str(DLam(jj,1)),',',num2str(DLam(jj,2)),']']);
end
for jj=1:modesin
for kk=sinc
temp=strrep(temp,['X',num2str(kk),num2str(jj)],...
['[',num2str(Xmin(kk,jj)),',',num2str(Xmax(kk,jj)),']']);
end
end
fprintf(fid,strcat(temp,'=0;\n'));
end
end
```

```
110
111 %if ~isempty(sind)
112 for k=2:length(SCON(:,1))
113 for j=1:k-1
114 temp=char(SCON(k,j));
115 for jj=1:modesin
116 for kk=sinc
117 temp=strrep(temp,['X',num2str(kk),num2str(jj)],...
118 ['[',num2str(Xmin(kk,jj)),',',num2str(Xmax(kk,jj)),']']);
119 end
120 end
121 fprintf(fid,strcat(temp,'=0;\n'));
122 end
123 end
124 %end
125
126 %if ~isempty(sind)
127 for k=1:length(SCON2(:,1))
128 for j=1:size(SCON2,1)
129 if j~=k
130 temp=char(SCON2(k,j));
131 for jj=1:modesin
132 for kk=sinc
133 temp=strrep(temp,['X',num2str(kk),num2str(jj)],...
134 ['[',num2str(Xmin(kk,jj)),',',num2str(Xmax(kk,jj)),']']);
135 end
136 end
137 fprintf(fid,strcat(temp,'=0;\n'));
138 end
139 end
140 %end
141 end
142 if ~isempty(sind)
143 for k=1:length(SCON2(:,1))
144 temp=char(SCON2(k,k)/SCON(k,k));
145 for jj=1:modesin
146 for kk=sinc
147 temp=strrep(temp,['X',num2str(kk),num2str(jj)],...
148 ['[',num2str(Xmin(kk,jj)),',',num2str(Xmax(kk,jj)),']']);
149 end
150 end
151 fprintf(fid,strcat(temp,'=','[',num2str(DLam(k,1)),',',num2str(DLam(k,2)),']',';\n'));
152 end
153 end
154
155 %Eigenvalue Constraint
156 syms l
157 for k=1:modesin
158 tempA = det(K-SLam(k,k)*M);
159 CFS=coeffs(tempA); %Condition polynomial by normalizing leading term
160 temp=char(subs(tempA/CFS(1),1,SLam(k,k)));
161 temp=strrep(temp,['L',num2str(k)],['[',num2str(DLam(k,1)),',',num2str(DLam(k,2)),']']);
162 fprintf(fid,strcat(temp,'=0;\n'));
163 end
164 fprintf(fid,'end');
165 fclose(fid);
166 % Characterize parameter space by subpaving
167 unix(sprintf(['export PREFIX=/usr/local;',...
168 'export PKG_CONFIG_PATH=$PREFIX/share/pkgconfig;',...
169 'export LD_LIBRARY_PATH=/usr/local/lib;',...
170 'cd /home/',uname,'/Ibex/ibex-2.1.17/examples;',...
171 './defaultsolver ',pwd,'/',filename,'.bch ',precision,' 150000 | tee ',pwd,'/',filename,'_
    ',precision,'_subpaving.txt']))
172 % Contract to the interval hull of the parameter space
173 unix(sprintf(['export PREFIX=/usr/local;',...
174 'export PKG_CONFIG_PATH=$PREFIX/share/pkgconfig;',...
175 'export LD_LIBRARY_PATH=/usr/local/lib;',...
176 'cd /home/',uname,'/Ibex/ibex-2.1.17_mod/examples;',...
```

```
'./defaultsolver_polytope    ',pwd,'/',filename,'.bch 0.0000000 | tee ',pwd,'/',filename,'
    _hull.txt']))

% Reading/Processing the Results
lfont=16;
afont=14;
fid=fopen(strcat(filename,'_',precision,'_defaultsolver.txt'));
fidh=fopen([filename,'_hull.txt']);
nvars=3+modesin*numel(sind);
cstr=repmat('%f64 %*2c %f64 %*5c',1,nvars-1);
Ch=textscan(fidh,strcat('%*s %*s %*s %*s %*f %*s %*s %*s %*1c %*2c',cstr,'%f64 %*2c %f64
    %*2c'),'headerlines',1);
C=textscan(fid,strcat('%*s %*f %*s %*f %*2c',cstr,'%f64 %*2c %f64 %*2c'),'headerlines',1);

clear Low High
% Solutions for the subpaving
Low=double([C{1:2:end}]);
High=double([C{2:2:end}]);
% Solutions for the interval hull
Lowh=double([Ch{1:2:end}]);
Highh=double([Ch{2:2:end}]);
Lowh=Lowh(end,:);        % Last contraction of the hull
Highh=Highh(end,:);      clear
```

The above MATLAB script generated the following input file for the nonlinear solver. The uncertain variables and their domains are defined first, followed by the constraint equations employed.

```
Variables

k1 in [0,3];
k2 in [0,3];
k3 in [0,3];
X11 in [-10,10];
X12 in [-10,10];

Constraints
(-2000*X11)*k1 + ([389.0624,406.7765]*X11 + (2000*[-0.5989,-0.58572] - 2000*X11)*k2)=0;
(-2000*X12)*k1 + ([3054.4725,3193.5433]*X12 + (2000*[0.32505,0.33237] - 2000*X12)*k2)=0;
(2000*X11 - 2000*[-0.5989,-0.58572])*k2 + ([389.0624,406.7765]*[-0.5989,-0.58572] +
    (2000*[-0.74682,-0.73038] - 2000*[-0.5989,-0.58572])*k3)=0;
(2000*X12 - 2000*[0.32505,0.33237])*k2 + ([3054.4725,3193.5433]*[0.32505,0.33237] +
    (2000*[-0.5989,-0.58572] - 2000*[0.32505,0.33237])*k3)=0;
(2000*[-0.5989,-0.58572] - 2000*[-0.74682,-0.73038])*k3 +
    [389.0624,406.7765]*[-0.74682,-0.73038]=0;
(2000*[0.32505,0.33237] - 2000*[-0.5989,-0.58572])*k3 +
    [3054.4725,3193.5433]*[-0.5989,-0.58572]=0;
X12*X11 + ([-0.5989,-0.58572]*[0.32505,0.33237] + [-0.74682,-0.73038]*[-0.5989,-0.58572])
    =0;
(2000*X11*X12)*k1 + ((X12*(2000*X11 - 2000*[-0.5989,-0.58572]) - [0.32505,0.33237]*(2000*
    X11 - 2000*[-0.5989,-0.58572]))*k2 + ([0.32505,0.33237]*(2000*[-0.5989,-0.58572] -
    2000*[-0.74682,-0.73038]) - [-0.5989,-0.58572]*(2000*[-0.5989,-0.58572] -
    2000*[-0.74682,-0.73038]))*k3)=0;
(2000*X11*X12)*k1 + ((X11*(2000*X12 - 2000*[0.32505,0.33237]) - [-0.5989,-0.58572]*(2000*
    X12 - 2000*[0.32505,0.33237]))*k2 + ([-0.5989,-0.58572]*(2000*[0.32505,0.33237] -
    2000*[-0.5989,-0.58572]) - [-0.74682,-0.73038]*(2000*[0.32505,0.33237] -
    2000*[-0.5989,-0.58572]))*k3)=0;
((2000*X11^2)*k1 + ((X11*(2000*X11 - 2000*[-0.5989,-0.58572]) - [-0.5989,-0.58572]*(2000*
    X11 - 2000*[-0.5989,-0.58572]))*k2 + ([-0.5989,-0.58572]*(2000*[-0.5989,-0.58572] -
    2000*[-0.74682,-0.73038]) - [-0.74682,-0.73038]*(2000*[-0.5989,-0.58572] -
    2000*[-0.74682,-0.73038]))*k3))/(X11^2 + ([-0.5989,-0.58572]^2 +
```

```
    [-0.74682,-0.73038]^2))=[389.0624,406.7765];
((2000*X12^2)*k1 + ((X12*(2000*X12 - 2000*[0.32505,0.33237]) - [0.32505,0.33237]*(2000*X12
     - 2000*[0.32505,0.33237]))*k2 + ([0.32505,0.33237]*(2000*[0.32505,0.33237] -
    2000*[-0.5989,-0.58572]) - [-0.5989,-0.58572]*(2000*[0.32505,0.33237] -
    2000*[-0.5989,-0.58572]))*k3))/(X12^2 + ([0.32505,0.33237]^2 + [-0.5989,-0.58572]^2))
    =[3054.4725,3193.5433];
([389.0624,406.7765]^2*k1)/4000000 + ([389.0624,406.7765]^2*k2)/2000000 +
    ([389.0624,406.7765]^2*k3)/2000000 - [389.0624,406.7765]^3/8000000000 -
    ([389.0624,406.7765]*k1*k2)/2000 - ([389.0624,406.7765]*k1*k3)/1000 -
    (3*[389.0624,406.7765]*k2*k3)/2000 + k1*k2*k3=0;
([3054.4725,3193.5433]^2*k1)/4000000 + ([3054.4725,3193.5433]^2*k2)/2000000 +
    ([3054.4725,3193.5433]^2*k3)/2000000 - [3054.4725,3193.5433]^3/8000000000 -
    ([3054.4725,3193.5433]*k1*k2)/2000 - ([3054.4725,3193.5433]*k1*k3)/1000 -
    (3*[3054.4725,3193.5433]*k2*k3)/2000 + k1*k2*k3=0;
end
```